

# **Seismic Protection of Structures Using Passive Control System**

A thesis  
Submitted in partial fulfilment  
of the requirements for the degree of

Doctor of Philosophy

in the  
Department of Civil Engineering  
University of Canterbury

By  
**Nagui William Bishay-Girges**

**University of Canterbury  
Christchurch, New Zealand**

**2004**



TA  
660  
.F3  
.B622  
S  
2004

## Abstract

There is a relationship between inelastic deformation and energy dissipation in structures that are subjected to earthquake ground motions. Thus, if seismic energy dissipation can be achieved by means of a separate non-load bearing supplementary damping system, the load bearing structure can remain elastic with continuing serviceability following the design level earthquake.

This research was carried out to investigate the advantages of using added damping in structures. The control system consists of passive friction dampers called ring spring dampers installed in the ground floor of the structure using a tendon to transmit the forces to the other parts of the structure. The ring springs dampers are friction devices consisting of inner and outer ring elements assembled to form a spring stack. External load applied to the spring produces sliding action across mating ring interfaces. The damping forces generated by the dampers and transferred in the supplemental system to the structure by the tendon and horizontal links oppose the internal loads. A four storey-two bay steel frame structure was used in the study.

Experimental and analytical studies to investigate the effectiveness of a supplemental control system are presented. The model was subjected to a series of earthquake simulations on the shaking table in the Structural Laboratory of the Civil Engineering Department, at the University of Canterbury. The earthquake simulation tests have been performed on the structure both with and without the supplemental control system. The earthquake simulations were a series of gradually increasing intensity replications of two commonly used earthquake records. This thesis includes detailed description of the structural model, the supplemental control system, the ring springs dampers and the data obtained during the testing.

Analyses were then carried out on a twelve storey framed structure to investigate the possible tendon arrangements and the size and type of dampers required to control the response of a real building. Guidelines for determining the appropriateness of including a supplemental damping system have been investigated.

The main features of the supplemental control system adopted in this research are:

- It is a passive control system with extreme reliability and having no dependence on external power sources to effect the control action. These power sources may not be available during a major earthquake.
- Ring springs are steel friction devices capable of absorbing large amounts of input energy. No liquid leakage can occur and minimal maintenance is required for the ring spring dampers.
- With a damper-tendon system, the distribution of the dampers throughout the structure is not so critical. Only one or two dampers are used to produce the damping forces needed, and forces are then transferred to the rest of the building by the tendon system.
- It is a relatively inexpensive control system with a long useful life.

## Acknowledgments

This research was carried out in the Civil Engineering Department of the University of Canterbury.

I wish to express my sincere gratitude to Dr Athol. J. Carr and Dr. Peter Moss for their invaluable advice and encouragement as supervisors of the project.

I wish to thank my family (my brother and sister) for their support and prayers, and also the soul of my late mother who prays for me in front of God in His Kingdom.

Finally, I would like to give my deep thanks and praises to my God and my Lord – Jesus Christ, and to my Holy Mother Virgin St. Mary.

## Table of Contents

<b>Abstract.....</b>	<b>i</b>
<b>Acknowledgments .....</b>	<b>ii</b>
<b>Table of Contents.....</b>	<b>iii</b>
<b>List of Symbols.....</b>	<b>x</b>
<b>Chapter 1 Introduction.....</b>	<b>1</b>
1.1 General.....	1
1.2 Passive Structural Control.....	2
1.2.1 Seismic Base Isolation .....	2
1.2.2 Supplemental Damping.....	2
1.3 Objectives and Scope of the Research .....	3
1.4 Organisation of the Thesis .....	5
<b>Chapter 2 Seismic Control Systems .....</b>	<b>6</b>
2.1 Introduction.....	6
2.2 Seismic Isolation.....	9
2.2.1 Characteristic of Seismic Isolation Systems .....	9
2.2.2 Dissipation Mechanisms .....	9
2.2.2.1 Hysteretic Dampers.....	9
2.2.2.1.1 Lead-Extrusion Dampers .....	10
2.2.2.1.2 Lead-Rubber Bearing (LRB) .....	11
2.2.2.2 Viscous Dampers .....	13
2.2.2.3 Frictional Dampers.....	15
2.3 Control Systems Other Than Base Isolation .....	16
2.3.1 Definitions .....	16
2.3.1.1 Passive Control .....	16
2.3.1.2 Active Control.....	16
2.3.1.3 Semi-Active Control .....	16
2.4 Passive Control Systems .....	18
2.4.1 Metallic Yield Dampers.....	18
2.4.2 Friction Dampers .....	20
2.4.3 Viscoelastic Dampers .....	21
2.4.4 Viscous Fluid Dampers.....	22

2.4.5 Tuned Mass Dampers .....	23
2.4.6 Tuned Liquid Dampers .....	25
2.4.7 Ring Spring Dampers.....	25
2.5 Active Control Systems .....	26
2.6 Semi-Active Control Systems.....	28
2.6.1 Controllable Fluid Dampers.....	28
2.6.1.1 Electrorheological Dampers.....	29
2.6.1.2 Magnetorheological Dampers.....	29
2.6.1.3 Large Scale Seismic MR Fluid Damper .....	30
2.6.2 Semi-Active Stiffness Damper .....	31
2.7 Summary .....	32
<b>Chapter 3 Amount of Supplemental Damping and Placement Strategies for Dampers .....</b>	<b>33</b>
3.1 Introduction.....	33
3.2 Amount of the Supplemental Damping .....	33
3.3 Response Spectra with Several Levels of Damping .....	34
3.4 Distribution of Dampers from Previous Research .....	38
3.4.1 Structure with Supplemental Lead Dampers .....	38
3.4.2 Structure with Supplemental Viscoelastic Dampers.....	39
3.4.2.1 Three-Storey Building .....	41
3.4.2.2 Ten-Story Building .....	41
3.5 Optimal Damper Placement.....	43
3.5.1 Transfer Matrix Formulation .....	43
3.5.2 The Sequential Search Algorithm (SSA).....	47
3.6 Toggle-Brace Damper System.....	48
3.6.1 Toggle-Brace Theory .....	48
3.6.2 Forces in Toggle-Brace Systems .....	51
3.6.3 Applications .....	53
3.7 Scissor-Jack-Damper Theory.....	53
3.8 Damper -Tendon Supplemental Control System .....	56
3.9 Seismic Shear and Overturning Moments on Structures .....	56
3.10 Load Balancing Solution.....	58
3.10.1 Tendon Layout for Multi-Storey Frame .....	59

3.10.2 Straight Tendon.....	62
3.11 Concept Development of the Supplemental Control System .....	64
3.12 Concept Validation .....	64
3.13 Damper Type .....	65
3.14 Fields of Applications for Ring Springs in Mechanical Engineering .....	66
3.15 Comparison between Single and Double Tendon System.....	66
3.16 The Benefits of the Damper-Tendon System.....	67
<b>Chapter 4 Ring Springs.....</b>	<b>68</b>
4.1 Introduction.....	68
4.2 Details of Construction .....	70
4.2.1 Single-Acting Ring Spring.....	71
4.2.2 Pre-load .....	72
4.2.3 Double-Acting Ring Spring .....	72
4.3 Characteristics of Ring Springs .....	73
4.3.1 Linear Characteristic.....	73
4.3.2 Overloaded-Safe in Blocked Position.....	73
4.3.3 Effect of the Number of Rings.....	74
4.3.4 Temperature Independence.....	74
4.4 Force-Travel Relationship .....	75
4.4.1 Behaviour in the Absence of Friction.....	75
4.4.2 Friction Forces under Load .....	75
4.4.3 Friction Forces on Load Removal .....	76
4.4.4 Complete Force-Travel Diagram .....	77
4.5 Ring Spring Hysteresis Relationship .....	77
4.5.1 Double-Acting Hysteresis .....	78
4.6 Ring Spring Stiffness Equations .....	79
4.7 Number of Elements .....	81
4.8 Test Devices .....	84
4.9 Components of the Test Devices .....	86
4.10 Damper Size.....	87
4.10.1 Ring Spring Hysteresis .....	88
4.10.2 The Properties of the Damper for Different Earthquake Excitations .....	89

4.11 Experimental Testing of the Ring Spring Devices .....	90
<b>Chapter 5 Structural Model for Experimental Tests and the Supplemental Control System .....</b>	<b>94</b>
5.1 Introduction.....	94
5.2 Frame Configuration .....	94
5.3 Frame Members .....	96
5.3.1 Mass .....	97
5.3.2 Ingots .....	97
5.3.3 Top Plates .....	97
5.4 Beam Connections .....	99
5.5 Mass Connections .....	100
5.6 Joints, Fuses and Connection Details.....	100
5.6.1 Beam-Column and Mid-Span Joints.....	100
5.6.2 Beam Fuses .....	104
5.6.3 Column Base Fuses and Connections .....	106
5.7 Hinge Joint Fuse Stress-Relief Annealing .....	107
5.8 Results on Joint Specimens Tests .....	109
5.9 Results of the Hinge Joints Tests .....	111
5.10 Determination of the Joint Stiffness .....	113
5.11 Supplemental Control System.....	117
5.11.1 Tendon Profile .....	118
5.11.2 Layout of the System.....	118
5.12 Damper Connections.....	122
5.13 Tendon Connections .....	124
<b>Chapter 6 Experimental Investigation.....</b>	<b>127</b>
6.1 Introduction.....	127
6.2 Test Set-up .....	127
6.2.1 Shaking Table .....	127
6.2.2 Instrumentation .....	129
6.2.2.1 Displacements and Interstorey Drifts.....	129
6.2.2.2 Floor Accelerations .....	132
6.2.2.3 Data Logger .....	133
6.3 Free Vibration Tests.....	133

6.3.1 Free Vibration Tests without the Supplemental Control System.....	135
6.3.2 Free Vibration Tests with the Supplemental Control System.....	137
6.4 Computer Model .....	138
6.4.1 Elements.....	138
6.4.2 Nodes .....	139
6.4.3 Member Elastic Properties .....	139
6.4.4 Earthquake Excitations .....	139
6.5 Comparison between Experimental and Analytical Free Vibration .....	140
6.5.1 Free Vibration without the Supplemental Control System.....	140
6.5.2 Free Vibration with the Supplemental Control System .....	141
6.5.3 Experimental and Analytical Time History Comparisons .....	142
6.6 Floor Acceleration .....	144
6.7 Horizontal Members in the Supplemental Control System .....	147
6.8 Effect of Increasing the Stiffness of the Structure Due to Adding the Supplemental Control System.....	149
<b>Chapter 7 Experimental Results.....</b>	<b>151</b>
7.1 Introduction.....	151
7.2 Experimental Procedure.....	151
7.3 El Centro Shaking Table Excitation .....	153
7.3.1 Displacement of the Structure with El Centro 50%.....	153
7.3.2 Interstorey Drift with El Centro 50% .....	154
7.3.3 Displacement and Interstorey Drift Ratios .....	155
7.3.4 Displacement of the Structure with EL Centro 100% .....	156
7.3.5 Interstorey Drift with El Centro 100% .....	157
7.3.6 Displacement and Interstorey Drift Ratios .....	158
7.3.7 Displacement of the Structure with El Centro 120%.....	159
7.3.8 Interstorey Drift of the Structure with El Centro 120%.....	160
7.3.9 Displacement and Interstorey Drift Ratios .....	161
7.4 TAFT- Shaking Table Excitation.....	162
7.4.1 Displacement of the Structure with TAFT 80% .....	162
7.4.2 Interstorey Drift of the Structure with TAFT 80% .....	163
7.4.3 Displacement and Interstorey Ratios .....	164
7.4.4 Displacement of the Structure with TAFT 100% .....	165

7.4.5 Interstorey Drift of the Structure with TAFT 100% .....	166
7.4.6 Displacement and Interstorey Drift Ratios .....	167
7.4.7 Displacement of the Structure with TAFT 120% .....	168
7.4.8 Interstorey Drift of the Structure with TAFT 120% .....	169
7.4.9 Displacement and Interstorey Drift Ratios .....	170
7.5 Conclusion .....	171
<b>Chapter 8 Design Considerations of Structures with Supplemental Damping Control Systems .....</b>	<b>173</b>
8.1 Introduction.....	173
8.2 Total Damping .....	173
8.2.1 Inherent Viscous Damping .....	174
8.2.2 Hysteretic Damping .....	174
8.2.3 Damping due the Supplemental Control System.....	175
8.2.3.1 Target Displacement .....	178
8.2.3.2 Structural Demand .....	179
8.3 Design Verification.....	180
8.4 Example .....	184
8.4.1 Amount of Damping .....	184
8.4.2 Force in the Damper.....	185
8.4.3 Shape of the Tendon .....	187
8.5 Time-History Analysis of the Structure Using Ring Spring Damper and a Single Tendon .....	189
8.5.1 Tendon Properties .....	190
8.5.2 Draped Tendon .....	191
8.5.3 Equivalent Straight Tendon .....	194
8.5.4 Straight Tendon to the Top of the Structure .....	196
8.6 Double Tendons .....	198
8.6.1 Double Draped Tendons .....	199
8.6.2 Double Straight Tendons .....	201
8.7 Discussion .....	203
8.8 Tendon Flexibility.....	204
8.9 Viscous Fluid Dampers.....	205
8.9.1 Operation of Viscous Dampers.....	205

8.9.2 Size of Fluid Dampers .....	206
8.9.2.1 Low Capacity Viscous Fluid Dampers (10 Kip to 30 Kip output) ....	206
8.9.2.2 High Capacity Viscous Fluid Dampers (100 Kip to 2000 Kip output) .....	207
8.9.3 Structural Response with Viscous Fluid dampers (Dashpots).....	208
8.10 Lead Shear Dampers .....	210
8.10.1 Lead Damper Hysteresis .....	210
8.10.2 Time History Analysis with the Lead-Shear Dampers .....	211
8.11 General Comparison between Ring Spring, Viscous Fluid and Lead Shear Dampers .....	212
8.12 Summary .....	213
<b>Chapter 9 Conclusions and Recommendations.....</b>	<b>214</b>
9.1 Summary .....	214
9.2 Conclusions.....	216
9.3 Main Contributions of This Research .....	217
9.4 Recommendations for Further Research.....	218
<b>REFERENCES .....</b>	<b>220</b>
<b>Appendix A.....</b>	<b>226</b>
<b>Appendix B .....</b>	<b>244</b>
<b>Appendix C .....</b>	<b>250</b>
<b>Appendix D .....</b>	<b>255</b>

## List of Symbols

$A$	= effective cross section area of ring
$A_p$	= area of piston
$A_0$	= area of orifices
$B_l$	= spectral amplification factor
$C$	= damping coefficient, or = amplitude of vibration
$C_0$	= discharge constant
$c_d$	= structural demand
$c_{\text{sup}}$	= capacity of the supplemental damping system
$c_{st}$	= coefficient represents lateral force resisted by the structure
$D_1$	= outer diameter of rings
$d_1$	= inner diameter of rings
$D_2$	= outer diameter of the guide
$d_2$	= inner diameter of the guide
$E$	= Young's modulus
$F$	= tendon force, or = spring end force
$F_D$	= force in damper
$F_i$	= storey shear at level i
$F_0$	= storey shear at base of structure
$F_y$	= yield force
$F_p$	= plastic force
$g$	= ground acceleration
$G_e$	= element weight
$h$	= storey height
$H$	= total height of the structure
$h_e$	= element height, or
$H_{\text{eff}}$	= effective height
$I$	= moment of inertia
$I_i$	= interstorey drift of level i
$k$	= stiffness
$k_x$	= stiffness of tendon
$k_r$	= stiffness of one element
$k_0$	= elastic ring spring stiffness
$k_i$	= increasing ring spring stiffness
$k_d$	= decreasing ring spring stiffness
$k_1$	= ring spring stiffness between $k_i$ and $k_d$
$L_i$	= length of tendon segment i

$L_D$	= total length of elements in damper
$m$	= mass
$m_e$	= effective mass
$M$	= moment
$M_y$	= yield moment
$M_p$	= plastic moment
$n$	= number of elements
$N$	= radial force
$p$	= point force of tendon
$p_{cr}$	= critical load
$S$	= plastic section modulus
$S_e$	= spring travel for one element
$S_{total}$	= total spring travel
$S_a$	= pseudo spectral acceleration
$S_d$	= spectral displacement
$S_v$	= pseudo spectral velocity
$T$	= natural period
$T_{eff}$	= effective period
$r$	= post-yield stiffness degrading factor
$r_L$	= lower stiffness factor
$r_s$	= steep stiffness factor
$R$	= friction force
$[R]$	= coefficient matrix
$e$	= eccentricity, or = number of elements
$x$	= displacement, or = length of fuse
$x_{max}$	= target displacement
$\dot{x}$	= velocity
$\ddot{x}$	= acceleration
$X$	= Fourier transforms
$X_d$	= total displacement in damper
$X_y$	= elastic displacement
$\ddot{X}_0$	= Fourier transform of the ground acceleration
$y$	= resultant shear force
$Y$	= Fourier transforms
$\dot{u}$	= velocity
$w$	= distributed load per unit length
$W_e$	= energy absorption
$W_T$	= total weight of the structure
$V_b$	= base shear
$Z$	= elastic section modulus
$\zeta$	= fraction of critical damping

$\zeta_0$	= inherent viscous damping
$\zeta_{hy}$	= hysteresis damping
$\zeta_{sup}$	= damping due to supplemental control system
$\zeta_{Total}$	= total damping
$\varepsilon_\alpha$	= normalized damping coefficient
$\theta$	= joint rotation, or = phase angle
$\theta_D$	= angle of damper
$\theta_i$	= angle of inclination of the $i^{th}$ floor tendon
$\theta_{max}$	= design limit structural drift
$\omega$	= natural circular frequency
$\omega_d$	= damped natural circular frequency
$\alpha$	= tape angle of ring spring, or = damper power factor
$\beta$	= angle of derivation of tendon profile
$\mu$	= coefficient of friction
$\sigma$	= ring hoop stress
$\phi$	= curvature
$\phi_y$	= yield curvature
$\rho$	= density of fluid
$\Delta_{fuse}$	= fuse displacement
$\Delta_i$	= displacement at level i
$\Delta p$	= pressure differential
$\Delta_Y$	= yield displacement
$\Delta_u$	= ultimate displacement

## Chapter 1

### Introduction

#### **1.1 General**

The damage caused to buildings by recent earthquakes has demonstrated the need for a seismic design methodology that is performance-based whereby the post-earthquake damage state of the structure is considered. Conventional seismic resistant design is based on the ductile design philosophy in which seismic energy is dissipated in predefined plastic hinge zones. The criteria for the seismic design of ductile structures set by many countries have been that buildings should be able to resist moderate earthquake without collapse but perhaps with some structural and non-structural damage. To satisfy these design criteria, structures should be designed to have:

- Adequate strength and stiffness to satisfy the serviceability limit states when responding to moderate earthquakes with insignificant damage.
- Adequate strength, stiffness and ductility to satisfy the ultimate limit states when responding to severe earthquakes with repairable damage.

The design codes require that ductile structures be the subject of “capacity design”. In the capacity design of structures, appropriate regions of the primary seismic-resisting structural systems are chosen and carefully designed and detailed for adequate strength and ductility. This design approach while being attractive for a life preservation point-of-view, suffers from the inability to avoid damage in strong earthquakes. This damage may be so severe that post-earthquake serviceability cannot be maintained and replacement of the structure is necessary. Even if the damage is modest, the structure may be required to be taken out of service while inspection and/or repairs are undertaken. For structures such as hospitals, fire stations, civil defence centres, schools, bridges etc. this down-time is quite untenable from a community perspective: such structures should remain functional after a severe earthquake. Therefore, an alternative approach to ductile deformation is sought to prevent structural damage while accommodating large displacements due to the lateral loading.

Structural control is an alternative seismic energy dissipation approach that can be achieved by means of separate non-load bearing supplementary damping systems. This ensures continued post-earthquake serviceability by keeping the primary gravity load-bearing structure behaving in a largely elastic manner.

As pointed out in the foreword to the Proceedings of the First World Conference on Structural Control, “.... Structural control has distinctive features that govern the direction of research” in this area [51]. Several of these features are pre-eminent. First, civil engineering structures are anchored and, thus, are statically stable. The addition of purely active control carries with it the possibility of destabilization and is thus

suspect. This is contrast to space structures which, when deployed, require active control for stability. Further, environmental disturbances that are associated with civil engineering structures, for example wind and earthquakes, are highly uncertain with respect to magnitude and arrival times, while the characteristics of mechanical loads are fairly well documented [51].

## **1.2 Passive Structural Control**

Passive structural control uses passive mechanism to reduce the response of the structure in that no input energy is required to operate the devices. Passive structural control approach utilises two methods: seismic base isolation and supplemental damping.

### **1.2.1 Seismic Base Isolation**

Seismic base isolation is a design strategy that reduces the level of deformation which a structure undergoes during an earthquake by moving the period of the structure away from the predominant period of the ground motion and by increasing the equivalent damping level of the structure by hysteretic behaviour of the isolation devices. This can be achieved by introducing a flexible energy-absorbing connection, usually at the foundation level, between the structure and the ground [48]. The advantages of seismic isolation can be summarised as follows:

1) The benefits of seismically isolating structures include:

- Simpler design procedures;
- Use of non-ductile forms or components in the structural system;
- Construction economies;
- Greater protection against earthquake induced damage;
- Confinement of damage to a readily replaceable element.

2) For seismically isolated structures subjected to earthquakes possessing response spectra whose spectral accelerations reduce at longer periods (similar to that of El-Centro 1940 N-S), the inertia forces and interstorey drifts of multi-storey structures can be considerably reduced. For earthquakes greater than the design level, seismic isolation buildings show fewer plastic hinges and much lower ductility demands when compared with conventional ductile design structures.

### **1.2.2 Supplemental Damping**

Providing additional damping (to augment the damping inherent in a structural system), can be beneficial in limiting the maximum response of a structure during a seismic disturbance. This constitutes the basic concept of supplemental damping, which involves controlling structural response by increasing system damping. This is achieved by incorporating suitable damping devices within a structure. Many damping devices have been proposed and studied for applications for seismic

mitigation of building damage. Some of the major damping devices in use include viscous dampers, hysteretic dampers, tuned mass dampers, etc....Figure (2-1).

The advantages of using mechanical dissipators in supplemental damping systems have been reported as follows [7]:

- 1- supplemental damping, by increasing the system damping, primarily reduces the inertia loads induced in the structural systems; this effect may provide:
  - Increased protection of the structural system since member loads are reduced.
  - A reduction in inelastic deformation sustained by the structure since some of the input energy is dissipated by the mechanical dissipators.
  - Increased capability of the structure to resist subsequent earthquakes as inelastic deformation of the structure's primary load carrying system is reduced.
  - A reduction in non-structural damage since the maximum response of the structure is reduced.
- 2- The mechanical dissipators employed in supplemental damping schemes, can be simple, inexpensive, and exhibit reliable and repeatable characteristics. The devices dissipate a portion of the input seismic energy; hence can reduce the energy that the structure is required to absorb through inelastic deformation.

### **1.3 Objectives and Scope of the Research**

This research study largely investigates added damping as a passive means of controlling structural deformation and concentrates on the use of a type of double-acting friction device known as a ring spring. The ring springs are friction devices capable of absorbing large amounts of input energy and are constructed of steel materials. The reasons for choosing this type of device in this research are that they are passive control devices with extreme reliability, no dependence on external power sources which may not be available during major earthquakes to effect the control action. No leakage of liquid can occur and minimal maintenance is required for the ring spring dampers.

The principal objectives of investigating the performance of the supplemental control system are:

- Develop strategies for adding damping to reduce the seismic response of structures.
- Evaluate the effectiveness of ring spring dampers in reducing the response of structures under ground motion excitations

- Investigate the performance of the supplemental control system in providing and transferring the damping forces throughout the structure.
- Investigate the experimental and analytical response characteristics of a model steel structure with and without ring spring dampers.
- To study the design steps for a supplemental control system including tendon layout for different types of dampers.
- To investigate the satisfactory layout for the tendons and for the sizes of the devices which need to be used in real buildings.
- To develop a design approach for structures with a supplemental control system.

To achieve these objectives, the following tasks were undertaken:

- 1- Review different types of supplemental control systems (passive, active and semi-active).
- 2- An existing 4 storey-2 bay steel frame structure [11] was available as a prototype structure for the experimental verification of the behaviour of damping system.
- 3- Establish the appropriate size of the ring spring dampers to be used in the experimental work.
- 4- Establish the properties of the dampers and the model structure to be tested on the shaking table.
- 5- Investigate the analysis of the structure with and without the dampers under earthquake excitation.
- 6- Perform shake table tests of the structure with and without the dampers.
- 7- Assess the response of the structure from the experimental results.
- 8- Investigate the effects of different damper-tendon systems in reducing the response of the structure under different earthquakes excitations.
- 9- Analyse a prototype building using different types of damper-tendon systems to assess the advantages and disadvantages of each arrangement.
- 10- Develop a design strategy for reducing the response of structures using added damping system.

## 1.4 Organisation of the Thesis

The organisation of the thesis reflects the work done to achieve the above-mentioned objectives. First, several types of structural control systems are detailed in chapter 2. Passive, active and semi-active control systems are discussed to show how they work and the advantages and disadvantages of each system. Chapter 3 details the placement strategies for dampers and how the distribution of dampers throughout the structure effects the response of the structures. The required amount of supplement damping to achieve a reasonable reduction in the response of structures is discussed.

Chapter 4 details the basic characteristics and the dynamic behaviour of passive ring spring dampers which were adopted in this research. Details of construction of single and double acting ring spring dampers are shown. The components of the test devices used in the experimental tests and their hysteresis loops under tension and compression loads are presented. Chapter 5 presents details of the four storey steel frame model used in the experimental study. Tests on the inelastic beam and column connection joints of the structure in preparing the structure for the experimental work are described. The description of the damper-tendon system using a straight tendon configuration, horizontal links and the damper connections are presented.

Chapter 6 describes the dynamic experimental tests of the test structure. Free vibration tests were carried out to determine the fundamental period and the critical damping ratio of the structure with and without the supplemental control system. Different levels of shaking were carried out to obtain the effect of the supplement control system in reducing the response of the structure. In Chapter 7, shaking table experimental results on the frame structure model with and without the supplemental control system are presented. This section shows the effectiveness of the supplemental control system in reducing the response of the structure.

Chapter 8 presents guidelines for determining the appropriateness of including a supplemental control system in a structure. The steps include determination of the shape of the tendon, damper size and the force-displacement hysteresis loop values of the ring spring dampers. A reinforced concrete twelve storey–two bay frame structure is analysed to investigate the system layout and the size of the dampers which may be used in real buildings. The effect of using different damper-tendon systems in reducing the response of the structure was investigated. Comparison between ring spring and viscous fluid dampers are made to show that the ring spring dampers have a smaller length and diameter than do the equivalent viscous dampers which are required to get the same reduction of the structure response. This chapter leads to the development of an appropriate design approach for the added damping system for structures.

In chapter 9, the conclusions drawn from this work and the recommendations for future research are presented.

## Chapter 2

### Seismic Control Systems

#### **2.1 Introduction**

In conventional seismic design, acceptable performance of a structure during earthquake shaking is based on the lateral force resisting system being able to absorb and dissipate energy in a stable manner for a large number of cycles. Energy dissipation occurs in specially detailed ductile plastic hinge regions of beams and in column bases. These members also form part of the gravity load carrying system. Plastic hinges are regions of concentrated damage in the gravity frame, which is hopefully reliable. Nevertheless, this design approach is acceptable on economic considerations provided structural collapse is prevented and life safety is ensured.

Situations exist in which the conventional design approach is not applicable. When a structure must remain functional after an earthquake, as in the case of important structures (hospitals, police stations, etc.), the conventional design approach is inappropriate. For such cases, the structure may be designed with sufficient strength so that inelastic action is either prevented or is minimal, an approach that is very costly. Moreover, in such structures, special precautions need to be taken in safeguarding against damage or failure of important secondary systems, which are needed for continuing serviceability.

Moreover, a large number of older structures have insufficient lateral strength and lack the detailing required for fully ductile behaviour. Seismic retrofitting of these structures is necessary and may be achieved by conventional seismic design, although often at significant cost and with undesirable disruption of architectural features and use of the building during the period taken for the retrofitting.

Alternative design procedures have been developed which incorporate earthquake protective systems in the structure. These systems may take the form of seismic isolation systems or supplemental energy dissipation devices.

During a seismic event, a finite quantity of energy is input into a structure. This input energy is transformed into both kinetic and potential strain energy which must be either absorbed or dissipated through heat or damage. If there were no damping action, vibrations would exist for all time. However, there is always some level of inherent damping which withdraws energy from the system and therefore reduces the amplitude of vibration until motion ceases. The structural performance can be improved if a portion of the input energy can be absorbed, not by the structure itself, but by some type of supplemental devices. This is made clear by considering the conservation of energy relationship [25]:

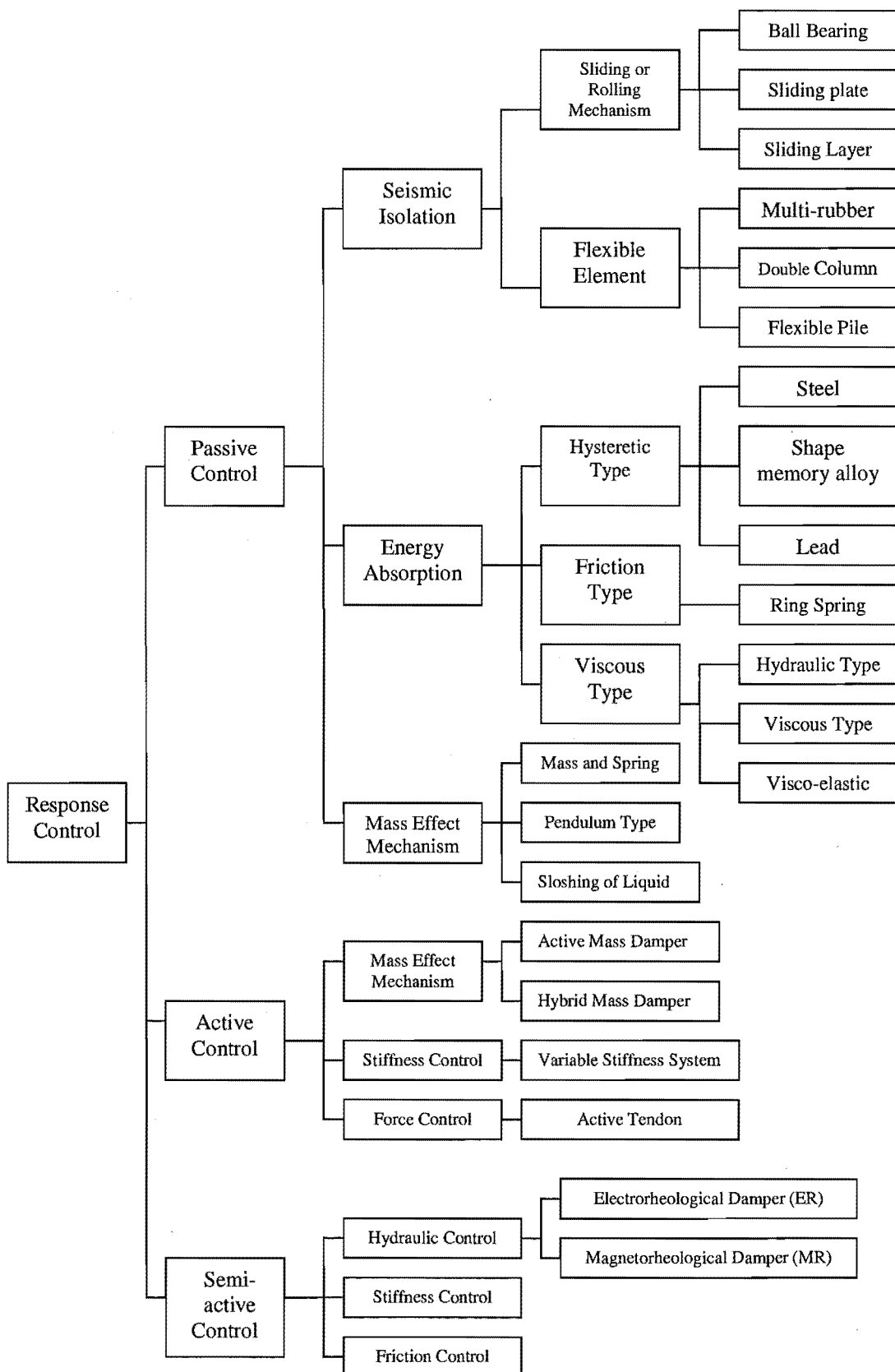


Fig (2-1) Classification of response control system

$$E = E_k + E_s + E_h + E_d$$

2-1

where:

$E$  is the absolute energy input from the earthquake motion

$E_k$  is the absolute kinetic energy

$E_s$  is the recoverable elastic strain energy

$E_h$  is the irrecoverable energy dissipation by the structural system through inelastic or other forms of action, usually implying damage to the structure.

$E_d$  is the energy dissipated by both the natural damping in the structure and supplemental damping devices.

The absolute energy input  $E$ , represents the work done by the total base shear force at the foundation on the ground (foundation) displacement. It thus contains the effect of the inertia forces of the structure.

In the conventional design approach, acceptable structural performance is accomplished by the occurrence of inelastic deformations. This has the direct effect of increasing energy  $E_h$ . It also has an indirect effect. The occurrence of inelastic deformations results in softening of the structural system which itself modifies the absolute input energy.

The technique of seismic isolation accomplishes the same task by the introduction, at the foundation of a structure, of a system which is characterized by flexibility and energy absorption capacity. The flexibility alone, typically expressed by a period of the order of 2 seconds, is sufficient to reflect a major portion of the earthquake energy so that inelastic action does not occur.

Energy dissipation in the isolation system is then useful in limiting the displacement response and in avoiding resonance. However, in earthquakes rich in long period components it is not possible to provide sufficient flexibility for the reflection of the earthquake energy. In this case, energy absorption plays an important role.

Modern seismic isolation systems incorporate energy dissipating mechanisms. Examples are lead plugs in elastomeric bearings, yielding mild steel dampers and viscous fluid dampers.

Another approach to improving earthquake response performance and damage control is that of supplemental energy dissipation systems. In these systems, mechanical devices are incorporated into the frame of the structure and dissipate energy throughout the height of the structure. One such method is by overcoming the friction produced by sliding action across ring interfaces in the ring spring device that is used in the research report herein. Such a device is described in the chapter 4.

In general, the addition of an energy dissipation system will result in a reduction in drift, therefore, a reduction of damage (due to energy dissipation) and decrease in the total force exerted on the structure. Reduction of both drift and total lateral force may be achieved only when deformations are reduced to levels below the elastic limit.

## 2.2 Seismic Isolation

Seismic isolation is a response control technique that aims to protect structures during earthquakes. This is essentially achieved by isolating the structure from ground disturbances. For over a century, efforts have been made to develop systems that minimise structural damage during earthquakes. The first seismic isolation system developed consists of supporting a structure on layers of logs, each layer positioned orthogonally. However, it was not until 1909 that an earthquake-resistant design was patented; this design proposed separating a building from its foundation by a layer of talc [49].

### 2.2.1 Characteristic of Seismic Isolation Systems

Principally, a seismic isolation system incorporates a mechanism that introduces both flexibility and damping into a structural system. Flexibility is incorporated within the system to lengthen its fundamental period. This action shifts the fundamental period of the system away from the dominant earthquake energy region, thus significantly reducing the inertia forces induced in the structure. Damping devices are also incorporated within the system; their purpose being to dissipate earthquake energy and resist excessive horizontal displacements at the base of the structure.

Although seismic isolation systems may be either passively, actively or semi-actively controlled, few known applications employ active or semi-active control. Passive control on the other hand, has been widely used in practice.

### 2.2.2 Dissipation Mechanisms

Practical seismic isolation systems also require dissipative elements that absorb the seismic input energy and limit excessive base deflections. These elements can be classified into the following three categories: hysteretic dampers, viscous dampers and friction dampers [7].

#### 2.2.2.1 Hysteretic Dampers

Hysteretic dampers provide damping by utilising the deformation properties of materials, such as, steel or lead. These dampers generally exhibit displacement-dependent characteristics. Extensive research has been undertaken on the use of steel as a hysteretic damping material and has also concentrated on the property of lead to recrystallize at ambient temperatures. This has resulted in the development of the lead extrusion dampers and the lead-rubber bearing (LRB).

### 2.2.2.1.1 Lead-Extrusion Dampers

A device which acts as a hysteretic damper by utilising the yield property of lead is shown in Figure (2-1). The reasons for choosing lead as the material for extrusion dampers and lead rubber bearings are [46]:

First, in shear the lead yields at the relatively low stress of 10 MPa and behaves approximately as an elastic-plastic solid. Second, at room temperature when lead is plastically deformed it is being “hot worked” and the mechanical properties of the lead are being continuously restored by interrelated processes of recovery, recrystallization and grain growth which are occurring simultaneously. Plastic deformation of lead at 20°C is equivalent to plastically deforming iron or steel at a temperature of greater than 450°C. Therefore, lead has good fatigue properties during cycling at plastic strains. Third, because of its use in batteries, lead is readily available at the high purity of 99.9 percent required for its mechanical properties to be predictable.

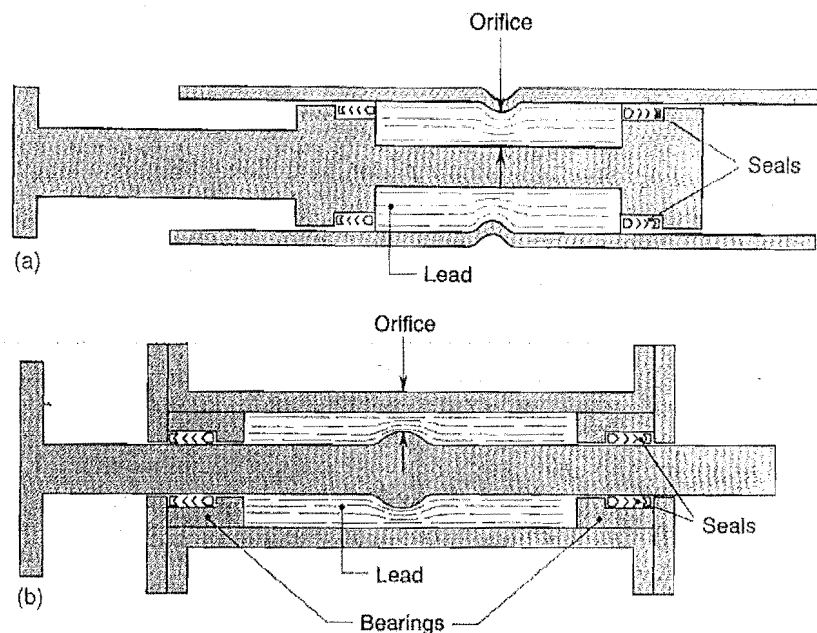


Fig (2-1) Longitudinal section of lead-extrusion damper [48].

The lead extrusion damper consists of a thick-walled tube co-axial with a shaft which carries two pistons. There is constriction on the tube between the pistons, and the space between the pistons is filled with lead. The lead is separated from the tube by a thin layer of lubricant kept in place by hydraulic seals around the pistons. The central shaft extends beyond one end of the tube. During operation, axial loads are applied with one attachment point at the protruding end of the central shaft and the other at the far end of the tube. The damper is fixed between a point on the structure and a point on the foundation, which move relative to one another during an earthquake. As the attachment points move to and from the pistons move along the tube and the captive lead is forced to extrude back and forth through the orifice formed by the constriction in the tube.

Since extrusion is a process of plastic deformation, work is done and very little energy is stored elastically, as the lead is forced through the orifice during structural deformation. Thus during an earthquake such a device, by absorbing energy, limits the build-up of destructive oscillations in a typical structure [48]. The successful operation of the hysteretic damper depends on the use of a material, in this case lead, which recovers and recrystallises rapidly at the operation temperature, so that the force required to extrude it is practically the same on each successive cycle. If the extruded material had a recrystallisation temperature much over the operating temperature, it would work-harden and be subject to low-cycle fatigue. Moreover, such materials typically have much higher stresses, which would present very severe problems for containment, piston sealing and lubrication in a cyclic extrusion device.

A hysteretic damper which operates on this same principle but has different construction details is shown in Figure (2-1b). Here the extrusion orifice is formed by bulge on the central shaft rather than by a constriction in the outer tube. The central shaft is located by bearings which also serve to hold the lead in place. As the shaft moves relative to the tube, the lead must extrude through the orifice formed between the bulge and the tube.

The lead-extrusion damper has the following properties [48]:

- It is almost a pure ‘Coulomb damper’ in that its force-displacement hysteresis loop is nearly rectangular and is practically rate-independent at earthquake-like frequencies.
- Because the interrelated processes of recovery, recrystallisation and grain growth occur during and after the extrusion of the lead, the energy absorber is not affected by work hardening or fatigue, but instead the lead returns to its original undeformed state.
- The higher the temperature, the more rapidly the lead will recover and recrystallise, thereby regaining its plasticity.

The lead-extrusion damper has been used in New Zealand in three bridges and to provide damping for one ten-storey building mounted on flexible piles [48].

#### **2.2.2.1.2 Lead-Rubber Bearing (LRB)**

Lead-rubber hysteretic bearings provide in a single unit the combination of vertical load support, horizontal flexibility and energy absorbing capacity required for the base isolation of structures from earthquake attack. The lead-rubber hysteretic bearing is a laminated elastomeric bearing of the type used in bridge structures, with a lead plug located down its centre axis (Figure 2-2).

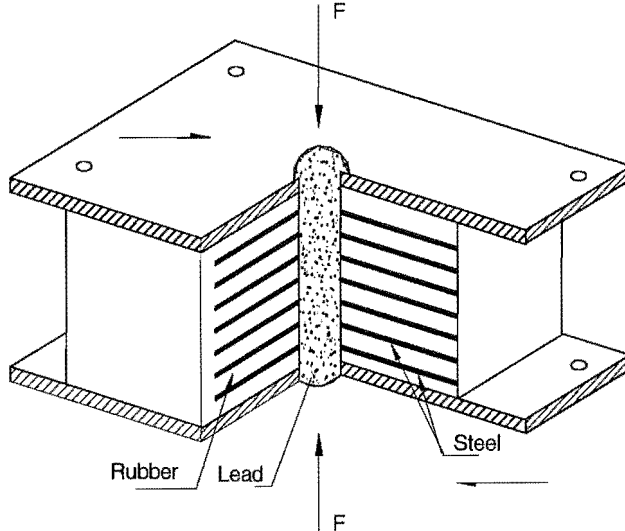


Fig (2-2) Lead-rubber hysteretic bearing

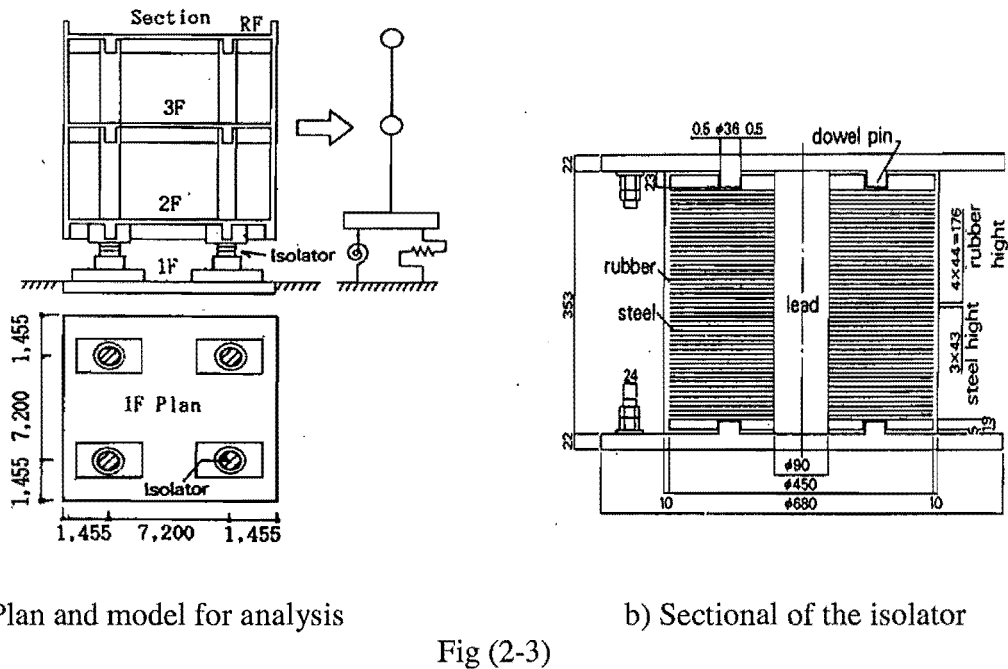
The normal elastomeric bearing consists of alternate layers of rubber sheets cemented or vulcanized to steel plates. The elastomeric bearing supports the weight of the structure, provides an elastic restoring force and in the case of bridges allows the bridge to expand thermally without causing excessive forces in the structure.

The elastomeric bearing is readily converted into a lead-rubber hysteretic bearing by placing a lead plug down its centre. The hole for the lead plug can be machined through the bearing after manufacture or the hole can be made in the steel plates and rubber sheets before they are assembled. The lead is cast into the hole or machined into a plug before being pressed into the hole. When the elastomeric bearing is deformed horizontally, the lead insert is forced by the interlocking steel plates to deform over its whole volume in pure shear [46].

The lead-rubber hysteretic bearing provides a solution to the problem of base isolating structures in that one unit provides the three functions of vertical support, horizontal flexibility via the rubber, and hysteretic damping by the plastic deformation of the lead.

An example of using lead-rubber bearing was present by Hirasawa [44]. The building was a three-storey reinforced framed structure with four base isolators between foundation and first floor as shown in Figure (2-3a). The building vertical load was 85 ton per one isolator. The vertical stiffness is nearly rigid and the horizontal support is flexible and the energy absorbing capacity is large.

The isolator's diameter and height was 45 cm and 35 cm respectively, the lead plug diameter was 9 cm, and these were 43 layers of 3 mm thick steel and 44 layers of 4 mm thick rubber. The isolators were mounted in the building using dowel pins to avoid tensile stress in the isolator. The section of the isolator is shown in Figure (2-3b).



a) Plan and model for analysis

b) Sectional of the isolator

Fig (2-3)

The building was first constructed as a non-isolated structure and the isolators were installed six months later. The forced vibration test and earthquake observations were carried out in two states. The results of the analysis are summarised as follows:

- 1- The base isolation system reduced the maximum shear force and acceleration to one third to one fifth as compared with the non-isolated system.
- 2- The maximum deflections of the base isolated building were about three times of that of the non-isolated building, but the interstorey deflections of the superstructure were small because the displacement was concentrated at the isolator. The maximum shear strain of the isolator was about 30% and the isolator had a great reserve of power considering the results of the loading test.

### 2.2.2.2 Viscous Dampers

Generally, viscous dampers use either a liquid medium or semi-solid possessing visco-elastic characteristics. The damping force of these devices is normally a function of velocity. In Japan, two test buildings, base-isolated and the other on conventional foundations were constructed side by side. The buildings were full-sized three-storey reinforced concrete structures, the dimensions and construction method of the superstructures being exactly the same for both buildings. The base-isolation system consisted of six rubber bearings and twelve oil dampers. The rubber bearing are shown in Figure (2-4), it has eighteen layers of 6.7 mm thick rubber and seventeen 3.0 mm thick steel plates.

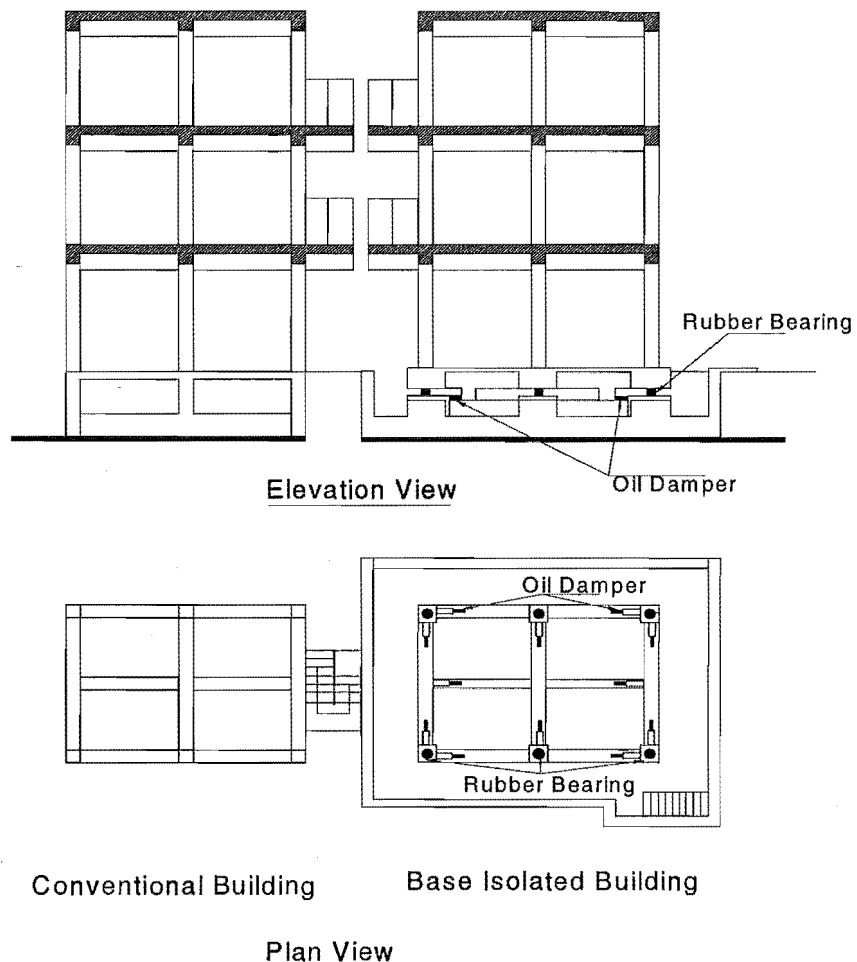


Fig (2-4) Plan and Elevation of test buildings

Site tests have been carried out, as well as, observation of thirty earthquakes that occurred throughout a one year period. One of most powerful earthquakes was recorded during the earthquake of February 6, 1987 (magnitude 6.7). The peak accelerations at the roof of the base-isolated building were from 1/5.7 to 1/4.9 of the values at the roof of the conventional building. On the other hand, the conventional building amplified the input ground acceleration by three to six times. Therefore the earthquake response of the base-isolated building is about 1/6 to 1/3 of the ordinary building on an average.

Since viscous dampers are velocity dependent devices, they can be effective over both large and small displacements. This has advantages where isolation from ambient ground noise is also a requirement. A disadvantage in their use for seismic protection of buildings is that under service loadings (such as wind loads) the structure will drift, hence, the system requires wind stabilisers. Maintenance requirements may also present problems, especially if the devices are left unused for a long period of time before being called into action during a major earthquake.

### 2.2.2.3 Frictional Dampers

Frictional damper is a dissipative mechanism that is reliant on relative motion between contacting surfaces. A practical example of a sliding bearing seismic isolation system has been implemented in Japan [45]. The system is essentially composed of sliding bearings, bearing plates and horizontal springs as shown in Figure (2-5).

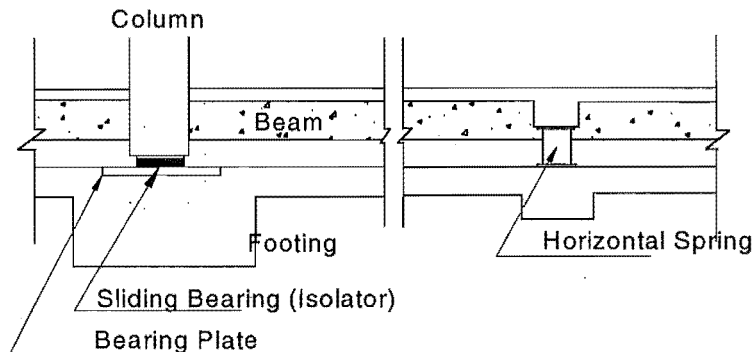


Fig (2-5) General composition of the system

Sliding bearings and bearing plates support the vertical load of a superstructure and reduce the horizontal seismic force by sliding during severe earthquake motion. Horizontal springs restrain the sliding displacement with a weak lateral stiffness. They sustain no long-term vertical load. The horizontal spring is a cylindrical column made of a rubber block with steel attachment plates at both ends. Both end plates are fixed to the first floor and foundation respectively. The spring deforms laterally in shear and has a restraining effect against the horizontal sliding displacement. It also works as a vertical restraint connecting the upper and lower structures. Each sliding bearing plate is made of stainless-steel with a smoothly finished flat surface. It supports the vertical compressive load transmitted through the sliding bearing and also provides a sliding surface.

The behaviour of the isolation devices under earthquake motions is drawn schematically in Figure (2-6). The advantages of this system include:

- For any given dynamic input the structure should not resonate since the frictional sliding mechanism does not have a defined natural period;
- The superstructure is stably supported since the bearings do not deform excessively due to the sliding action;
- The transmitted horizontal input force to the supported structure is limited to the value of the friction force.

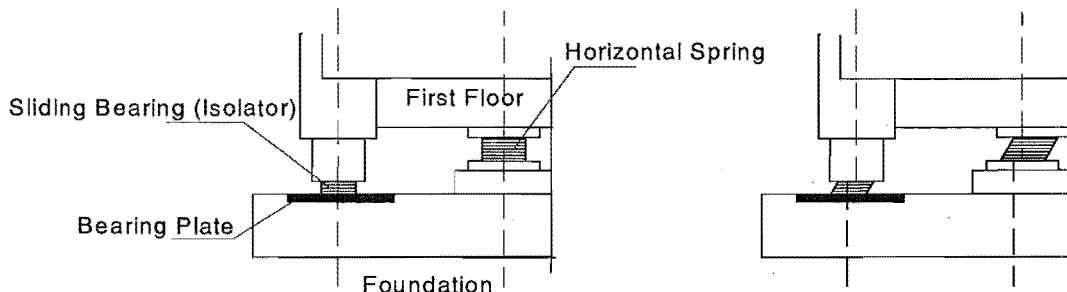


Fig (2-6) Behaviour of Isolation.

## **2.3 Control Systems Other Than Base Isolation**

### **2.3.1 Definitions**

#### **2.3.1.1 Passive Control**

Passive control may be incorporated in the initial design of the structure, by the addition of viscoelastic material to the structure, by the use of dampers, or by the use of tuned mass dampers. Initial design may use a tapered distribution of mass and stiffness, or use techniques of base isolation, where the support for the lowest floor is deliberately made very flexible, thereby reducing the transmission of forces into the upper storeys. Passive control has four main advantages:

- It requires no external power source in order to operate.
- It is usually relatively inexpensive.
- It is inherently stable
- It works during a major earthquake as well as in minor earthquakes.

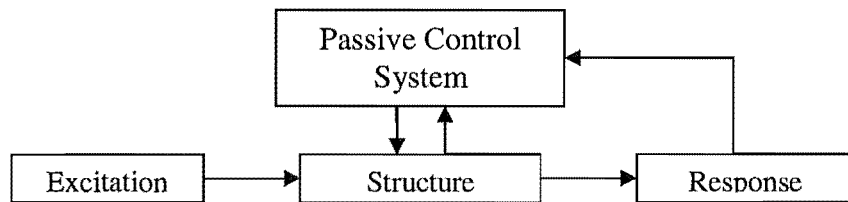
Passive control systems prevail in engineering practice due to their simplicity and the low cost of installing and maintaining them. A common feature of all passive control systems is that they reduce the dynamic response of the structures by absorbing and dissipating vibration energy (see Figure 2-7a). Some examples of the passive control systems are discussed in section (2-4).

#### **2.3.1.2 Active Control**

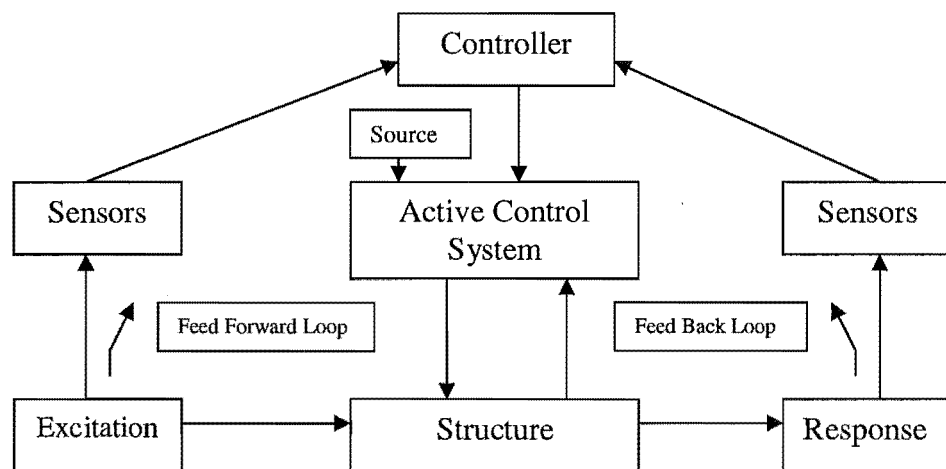
An active control system is one in which an external power source controls actuators that apply forces to the structure in a prescribed manner. These forces can be used to both add and dissipate energy in the structure. In an active feedback control system, the signals sent to the control actuators are a function of the response of the system measured with physical sensors (mechanical, electrical, and etc.), Figure (2-7b). Section (2-5) discusses this type of control system.

#### **2.3.1.3 Semi-Active Control**

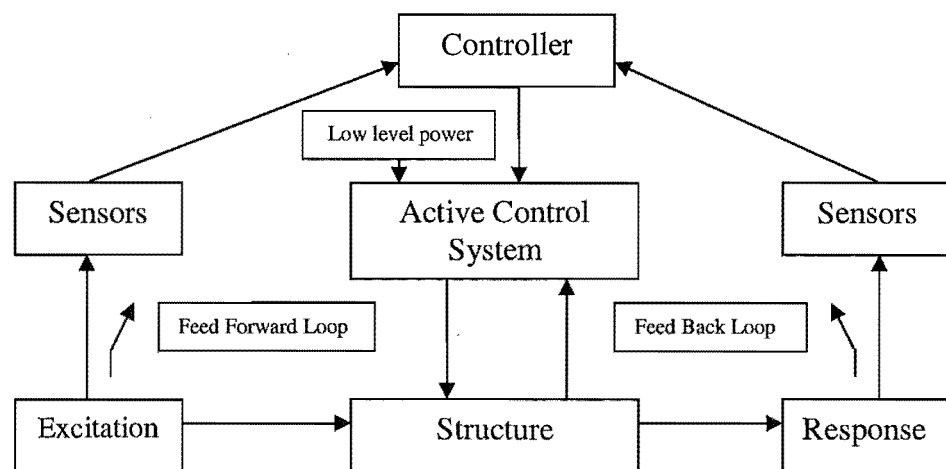
Semi-active control systems are a class of active control systems for which the external energy requirements are orders of magnitude smaller than typical active control systems. Typically, semi-active control devices do not add mechanical energy to the structural system including the structure and the control actuators; therefore bounded-input bounded-output stability is guaranteed, (Figure 2-7c).



a) Passive Control System



b) Active Control System



c) Semi-active Control System

Fig (2-7) Block diagram of structural control systems [47].

## 2.4 Passive Control Systems

All vibrating structures dissipate energy due to internal stressing, friction, cracking, plastic deformations, etc. The larger the energy dissipation capacity, the smaller the amplitudes of vibration. Some structures have very low damping of the order of 1% of critical viscous damping and consequently experience large amplitudes of vibration even for moderately small earthquakes.

Passive energy dissipation systems encompass a range of materials and devices for enhancing damping, stiffness and strength, and can be used both for natural hazard mitigation and in rehabilitation of aging or deficient structures.

In general, they are all characterized by a capacity to enhance energy dissipation in the structural systems in which they are installed. They may be achieved either by conversion of kinetic energy to heat, or by transferring of energy among vibrating modes. The first method includes devices that operate on principles such as frictional sliding, yielding of metals, phase transformation in metals, deformation of viscoelastic solids or fluids, and fluids passing through confined orifices.

### 2.4.1 Metallic Yield Dampers

One of the effective mechanisms for the dissipation of energy input into a structure from earthquakes is through inelastic deformation of metals. In traditional steel structures, a seismic design relies upon the post-yield ductility of structural members to provide the required energy dissipation. The idea of utilizing added metallic energy dissipators within a structure to absorb a large portion of the seismic energy began with conceptual and experimental work. Several of these devices use mild steel plates with triangular or X-shapes so that yielding is spread almost uniformly throughout the material. A typical X-shaped plate damper or ADAS (added damping and stiffness) device is shown in Figure (2-8).

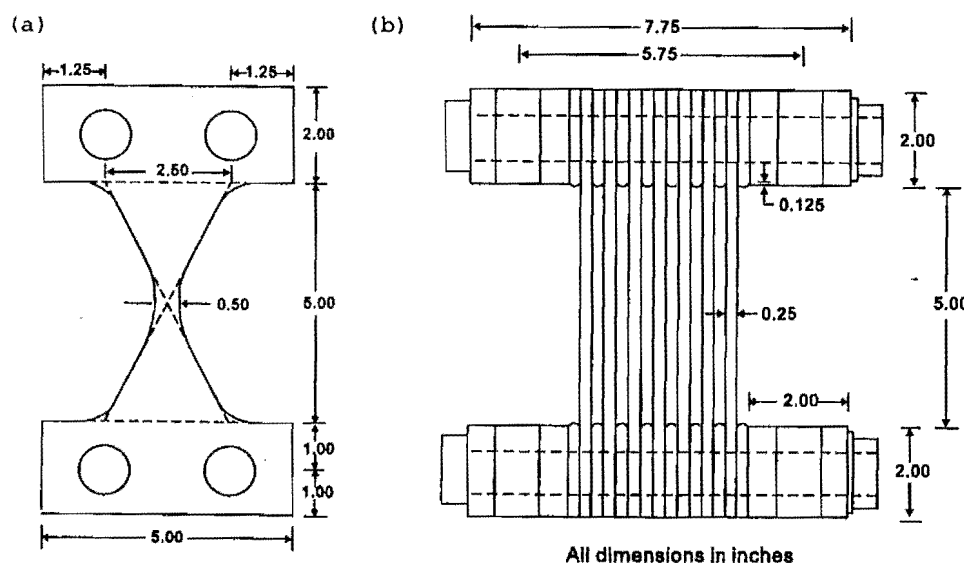


Fig (2-8) ADAS device [30].

Another configuration of a steel yielding device, used mostly in Japan and USA, is shown in Figure (2-9). An unbonded brace is a bracing member consisting of a core steel plate encased in a concrete-filled steel tube. A special coating is provided between the core plate and concrete in order to reduce friction. The core steel plate provides stable energy dissipation by yielding under reversed axial loading, while the surrounding concrete-filled steel tube resists compression buckling.

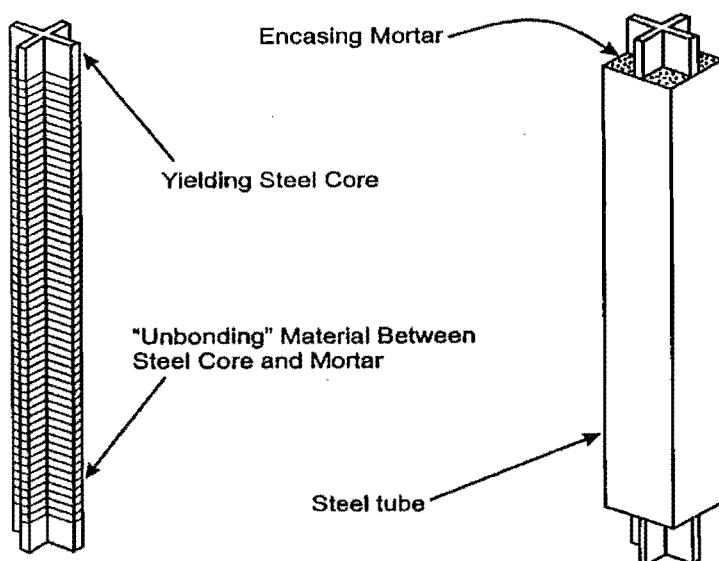


Fig (2-9) unbonded brace [30].

Some characteristics of ADAS devices are:

- ADAS devices installed in building frames are able to increase the stiffness, strength and energy dissipation capacity of structure. It is often desired that the ADAS devices will remain elastic under wind and yield under major earthquakes.
- The ADAS device has excellent ductility without fatigue problems and exhibits stable behaviour without any sign of pinching and degradation of the hysteresis loops.
- Yield forces and yield displacements of ADAS elements can be readily varied throughout the height of a structure to improve the distribution of ductility.
- The behaviour is not significantly affected by frequency and the number applied load cycles

## 2.4.2 Friction Dampers

Friction provides an excellent mechanism for energy dissipation, and has been used for many years in automotive brakes to dissipate kinetic energy of motion. In structural engineering, a wide variety of devices have been proposed and developed, differing in mechanical complexity and sliding materials,

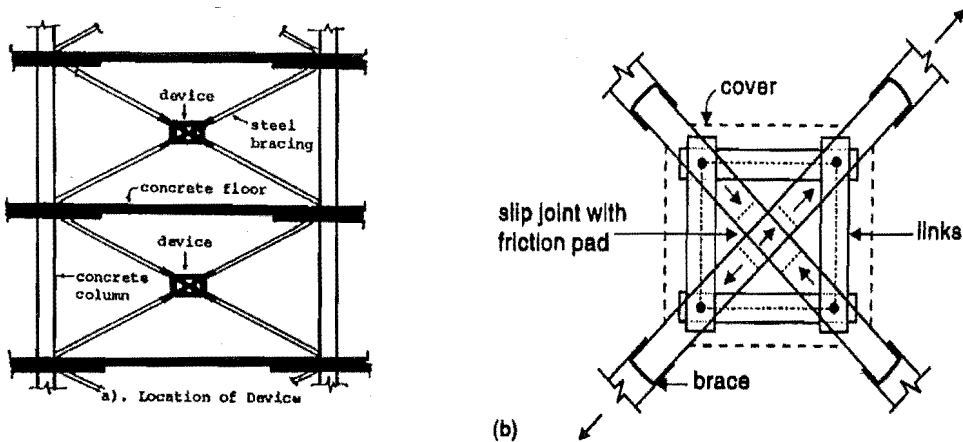


Fig (2-10) X-braced friction damper [51].

The device shown in Figure (2-10) is one of these damper elements utilizing the friction principle, which can be installed in a structure in an X-braced frame as is shown in Figure [51]. The dampers are designed not to slip during wind storms or moderate earthquakes. However, under severe loading conditions, the devices slip at a predetermined optimum load before yielding occurs in the primary structural members.

Most friction devices utilize sliding interfaces consisting of steel on steel, brass on steel, or graphite impregnated bronze on stainless steel. Composition of the interface is of great importance for insuring longevity of operation of the devices. Low carbon alloy steels, for example, corrode and their interface properties will change with time. Moreover, brass or bronze promotes additional corrosion when it is in contact with low carbon steels. Only steels with the high chromium content do not appear to suffer additional corrosion in contact with brass or steel.

At present, most macroscopic hysteretic models for friction dampers are obtained from tests and are assumed to be Coulomb friction devices with a constant coefficient of friction. Some care is needed in adopting one of these models in the response analysis and design of structures with friction dampers. Additionally, long-term behaviour and durability of these devices, particularly after long periods of inactivity, have been adequately addressed [51].

Some characteristics of friction dampers are:

- The dissipated energy increases in proportion with displacement. Further, the damping ratio also increases within a certain range of excitation level.
- The dampers show stiffening characteristics at their initial stages and show only strengthening afterwards. Stiffening and strengthening effects are almost unaffected by frequency.
- The hysteretic behaviour of the dampers provides the main contribution to the reduction of the structural response.

### 2.4.3 Viscoelastic Dampers

Viscoelastic (VE) materials used in structural applications are copolymers or glassy substances which dissipate energy when subjected to shear deformation. A typical VE damper, which consists of VE layers bonded with steel plates, is shown in Fig (2-11). When mounted in a structure, shear deformation and hence energy dissipation takes place when the structural vibration induces relative motion between the outer steel flanges and the centre plate.

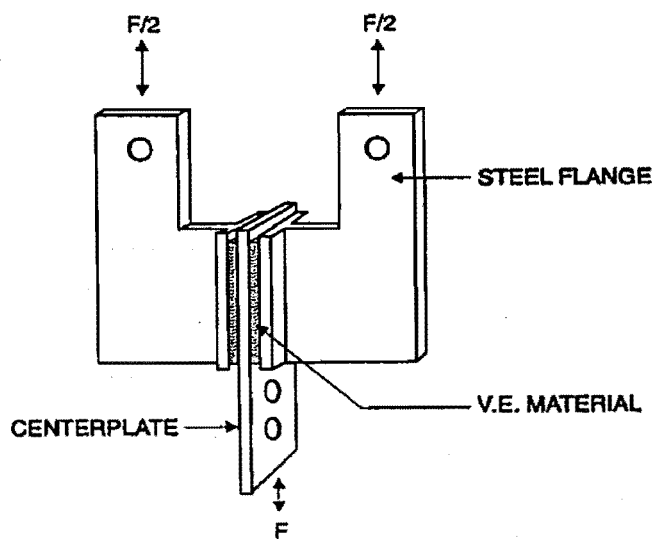


Fig (2-11) Typical VE damper configuration [31].

A viscoelastic material is linear over a wide range of strain provided the temperature is constant. At large strain, there is a considerable self-heating due to the large amount of energy being dissipated. The heat generated changes the mechanical properties of the material, and the overall behaviour is nonlinear.

The addition of viscoelastic dampers to a reinforced concrete structure can dissipate energy at the early stages of cracking of the reinforced concrete elements and can reduce the development of damage to the members.

Some characteristics of viscoelastic dampers are:

- They have no threshold or activation force level, thus they dissipate energy for all levels of earthquake excitation and wind even while the structure remains elastic or at the early stages of cracking
- They can be manufactured to add significant damping to building frames for improved structural response. The hysteretic characteristics of dampers are functions of shear strain level, excitation frequency, damping material type, thickness and temperature.
- They make a substantial contribution to the initial stiffness of the structure. While the stiffening effect may lead to better control of lateral deformations, the same stiffening may lead to larger seismically induced forces from the input ground motions.

#### 2.4.4 Viscous Fluid Dampers

The viscous fluid (VF) devices developed recently include viscous walls and VF dampers. The viscous wall consists of a plate moving in a thin steel case filled with highly VF. The VF damper, widely used in the military and aerospace industry for many years, has recently been adapted for structural applications in civil engineering.

A VF cylindrical device contains compressible silicon oil which is forced to flow via the action of a stainless steel piston rod with a bronze head. The head includes a state-of-the-art fluidic control orifice design with a passive bimetallic thermostat to compensate for temperature changes. In addition, an accumulator is provided to compensate for the change in volume due to rod positioning. The damper construction detail is shown in Figure (2-12).

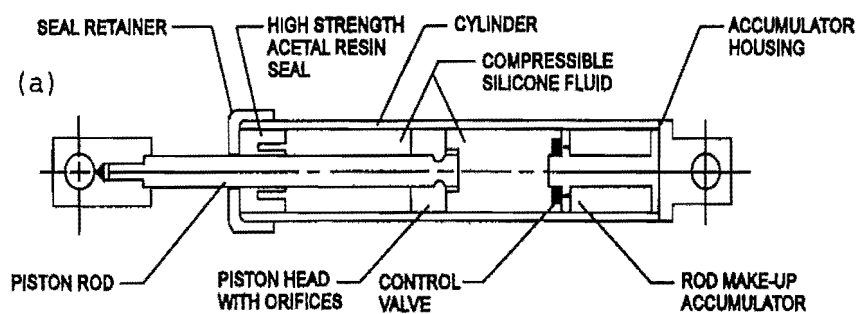


Fig (2-12) Viscous liquid damper [24]

The main characteristic of the damper is the “viscous” behaviour where the force is proportional to the velocity.

### 2.4.5 Tuned Mass Dampers

The objective of incorporating a tuned mass damper into a structure is basically the same as that with other energy dissipation devices discussed above, to reduce the energy dissipation demand on the primary structural members under the action of external forces. This reduction is accomplished by transferring some of the structural vibration energy to the tuned mass damper (TMD) which, in its simplest form, consists of an auxiliary mass-spring-dashpot system anchored or attached to the main structure.

A number of practical considerations must be observed in the engineering design of a TMD system. First and foremost is the amount of added mass that can be practically placed in the building. The TMD travel relative to the building is an important design parameter. A large movement often needs to be accommodated for a reasonable reduction of response of the building. Another major technique associated with a sliding mass arrangement is to provide a low-friction bearing surface so that the mass can respond to the building movement at low levels of excitation. This becomes more critical when TMD functions are used as an additional damper to improve occupant comfort. Finally, cost is an issue which must be addressed in the evaluation of a TMD for a specified application. Involved in the cost estimation are:

- Design and system engineering.
- Mass damper supporting system and accessories, e.g., pressure balanced support bearings for a sliding mass damper.
- Enclosure of space occupied by the entire TMD system.
- Roof elevator access and hoisting capacity during installation.
- Maintenance and operational costs.

Most of the TMD applications have been made for the mitigation of wind motion [24]. Under earthquake-type loading, TMDs are not as effective as for wind-type loading due to the frequency band width of an earthquake excitation being not only wider than that of wind load but also richer in high frequency content so that high modes of a building structure are usually excited and the first mode representation of the structure is not adequate. In terms of TMD configurations, there is a large variety of possible arrangements as indicated in Figure (2-13).

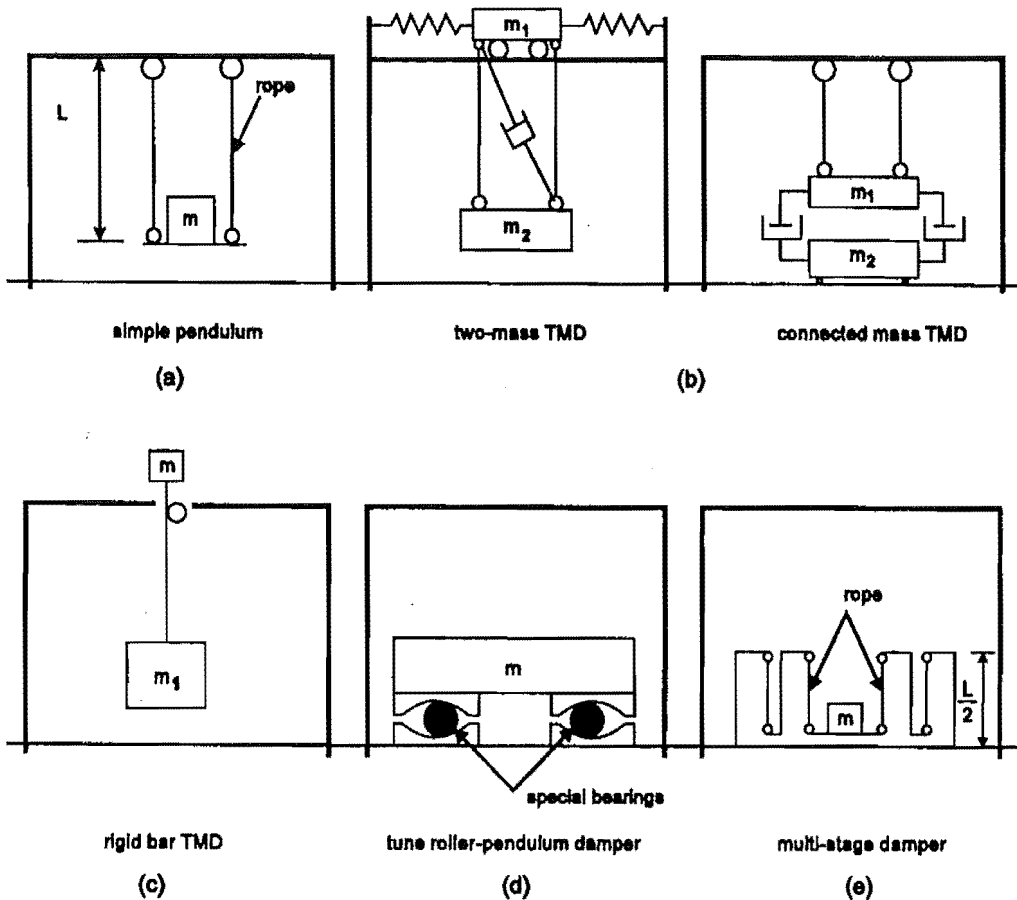


Fig (2-13) Various forms of TMD [24]

For a simple pendulum, the arm length often requires a large space to match the resonant frequency of the structure. In order to be flexible in selecting the pendulum length, one may modify this basic pendulum in such a way that the pendulum period depends on both the pendulum length and mass. For example, the pendulum arm can be designed as a rigid bar with counterweights or a two-mass damper can be used, with one mass sliding on the building floor and the other acting as a pendulum as shown in Figures (2-13 b, c). Their natural frequencies can be flexibly adjusted to tune with the structural frequency in these cases. However, these arrangements are much more difficult to implement than a simple pendulum, especially when their masses increase. In addition, the pendulum period is elongated by the participation of the counterweight, which diminishes the effectiveness of the TMD system. The practical application of such arrangements could be limited for the above reasons.

Alternative solutions for space-limited applications include the turned roller pendulum damper (TRD), as shown in Figures (2-13 d, e). The height of the TRD equipment is smaller or comparable with that of a simple pendulum TMD even when the predominant natural frequency of a building is lower than 0.2-0.25Hz [24]. The multi-stage pendulum can even produce a lower natural frequency within a practical size. A two-stage pendulum can reduce the vertical space requirement to  $\frac{1}{2}$  while taking the same horizontal space.

#### **2.4.6 Tuned Liquid Dampers**

Similar in concept to a TMD, the tuned liquid damper (TLD) and tuned liquid column damper impart indirect damping to the system and thus improve structural performance. A TLD absorbs structural energy by means of viscous actions of the fluid and wave breaking. In a tuned liquid column damper, energy is dissipated by the passage of liquid through an orifice with inherent head loss characteristics.

Tuned liquid dampers operate on the same basic principles as tuned mass dampers. Due to the simple physical concepts on which the restoring force is provided in TLDs, no activation mechanism is required. Therefore, maintenance cost is minimized. Additionally, the mechanism activating a TMD must be set to a certain threshold level of excitation, while TLD systems are at all times active, avoiding problems due to an inadequate activation system.

Although the mathematical theory involved in accurately describing motion of a fluid in the container may be quite complicated, the hardware requirements are simple and installation requirements are minimal. Each damper, in general, consists of a tank with several shallow layers of water. In comparison with TMDs, the advantages associated with TLDs include low initial cost and the ease of frequency tuning. Maintenance of the system is practically nonexistent. Due to simplicity of the installation, they may be used in existing buildings.

#### **2.4.7 Ring Spring Dampers**

A new passive energy dissipater for seismic study based on a self-centring friction mechanism is the ring spring. Ring springs are frictional devices consisting of inner and outer rings that have tapered mating surfaces as. As the spring column is loaded in compression or tension, the axial displacement is accompanied by sliding of the rings on the conical friction surfaces. The outer rings are subjected to circumferential tension (hoop stress), and the inner rings experience compression. The ring spring damper has had much use in a wide range of industrial, defence and civilian applications. The dampers are used in many industrial applications including steel mills and process treatment industries, as well as heavy duty material handling systems such as cranes. Military applications include shock absorption devices on missile and gun recoil systems. These have been also suggested as energy dissipation devices for base isolation of building by Hill [7].

Ring spring are employed in the mechanical engineering sector when high kinetic energy must be absorbed and damped or when springs of relatively compact dimensions are required for high forces. The passive control technique using ring spring dampers is the subject matter and attracted attention for this study because it is a simple, yet highly effective means of reducing seismic loads experienced by structures during earthquakes, no dependence on external power sources, no leakage of liquid can occur minimal maintenance is required for the ring spring dampers. Details of the ring spring dampers are shown in Chapter 4.

## 2.5 Active Control Systems

In structural engineering, active structural control is an area of research in which the motion of a structure is controlled or modified by means of the action of a control system through an external energy supply.

An active structural control system has the basic configuration as shown schematically in Figure (2-14). It consists of:

- 1- Sensors located about the structure to measure either external excitations, or structural response variables, or both.
- 2- Devices to process the measured information and to compute necessary control forces needed, based on a given control algorithm.
- 3- Actuators, usually powered by external energy sources, to produce the required forces.

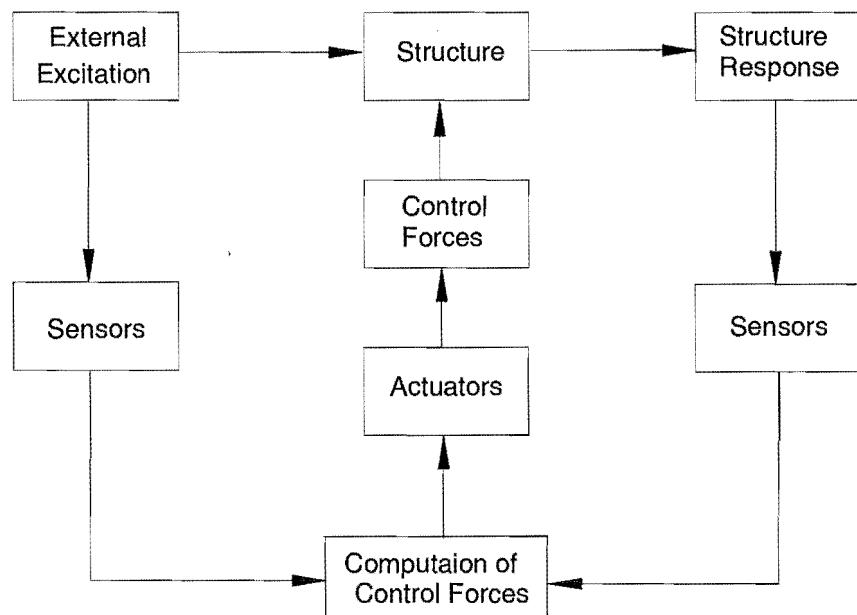


Fig (2-14) Schematic diagram of active control [22].

When only the structural response variables are measured, the control configuration is referred to as closed-loop control since the structural response is continually monitored and this information is used to make continual corrections to the applied control forces. An open-loop control results when the control forces are regulated only by the measured external excitation. In the case where the information on both the response quantities and excitation are utilized for control design, the term closed-open-loop control is used in the literature.

The base task is to determine a control strategy that uses the measured structural responses to calculate an appropriate control signal to send to the actuator that will

enhance structural safety and serviceability. Figure (2-15) shows a control system of the tall building using an active mass damper (AMD). For this control system, a small auxiliary mass is installed on one of the upper floors of the building, and an actuator is connected between the auxiliary mass and the structure. Responses and excitation at key locations on the building are measured and sent to the control computer. The computer processes the response according to the control algorithm and sends an appropriate signal to the AMD actuator. The actuator then reacts against the auxiliary mass, applying inertial control forces to the structure to reduce the structural responses in the desired manner.

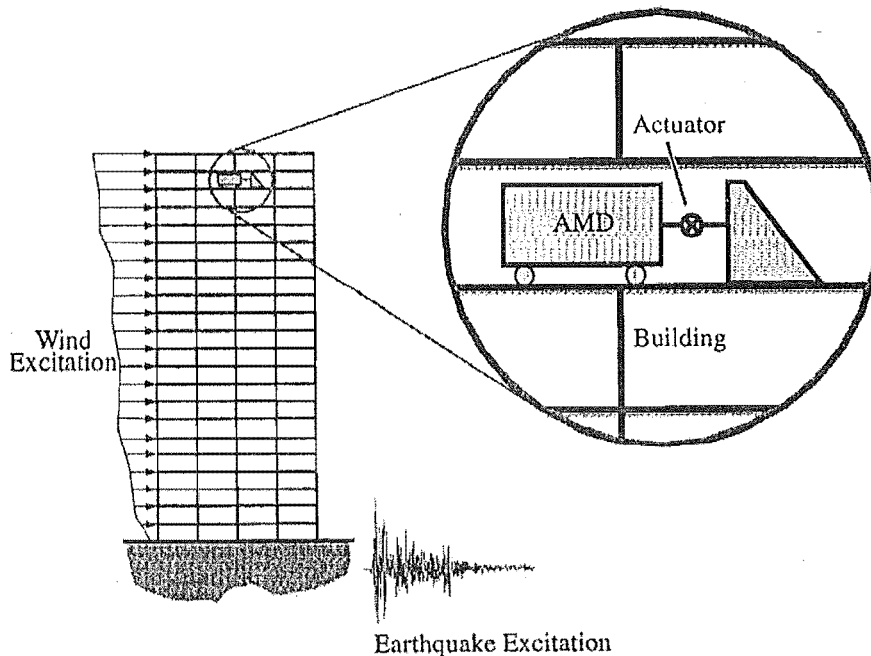


Fig (2-15) Concept of the AMD control system [48].

The first full-scale application of active control to a building was accomplished by the Kajima Corporation in 1989 [48]. The building is an 11-storey building in Tokyo, Japan, having a total floor area of  $423 m^2$ . A control system was installed, consisting of two AMDs. The primary AMD is used for transverse motion and has a mass of 4 tons, while the secondary AMD has a mass of 1 ton and is employed to reduce torsional motion. The role of the active system is to reduce building vibration under strong winds and moderate earthquake excitations and consequently to increase the comfort of occupants of the building.

Although more than a decade has passed since construction of the building, a number of serious challenges remain to be solved before feedback control technology can gain general acceptance by the engineering and construction professions at large [30]. The challenges include:

- Reduction of capital cost and maintenance.
- Eliminating reliance on external power.
- Increasing system reliability and robustness.
- Gaining acceptance of non-traditional technology.

The advantages associated with active control systems are:

- Enhanced effectiveness in response control; only limited by the capacity of the control systems.
- Relative insensitivity to site conditions and ground motion.

Since active control devices require external energy for their operation, it is imperative that the power supply remains uninterrupted throughout a severe seismic disturbance to maintain structural integrity and performance. This is a major factor limiting widespread use of active control in protecting engineering systems from earthquake damage. Other disadvantageous features include maintenance requirements as well as the large power requirement.

Generally, active control systems are more costly and less reliable (due to their complexity) than passive control systems.

## **2.6 Semi-Active Control Systems**

Semi-active control systems have only very recently been considered for structural control applications. A semi-active control system generally originates from a passive control system which has been subsequently modified to allow for adjustment of its mechanical properties. For example, supplemental energy dissipation devices which dissipate energy through shearing of viscous fluid, passage of fluids through orifices, and sliding friction have been modified to behave in a semi-active manner. The mechanical properties of these systems may be adjusted based on feedback from the excitation and/or from the measured response. As in an active control system, a controller monitors the feedback measurements and generates an appropriate command signal for the semi-active devices. As in a passive control system, however, the control forces are developed as a result of the motion of the structure itself. The control forces are developed through appropriate (based on a pre-determined control algorithm) adjustment of the mechanical properties of the semi-active control system.

Furthermore, the control forces in many semi-active control systems primarily act to oppose the motion of the structural system and therefore promote the global stability of the structure. Semi-active control systems generally require only small amounts of external power for operation.

### **2.6.1 Controllable Fluid Dampers**

Most of the semi-active control devices have employed some electrically controlled valves or mechanisms. Such mechanical components can be problematic in terms of reliability and maintenance. Another class of semi-active devices uses controllable fluids. The advantage of controllable fluid devices is that they contain no moving parts other than the piston, which makes them more reliable.

The essential characteristic of controllable fluids is their ability to reversibly change from a free-flowing, linear viscous fluid to a semisolid with controllable yield

strength in milliseconds when exposed to an electric (for ER Fluids) or magnetic (for MR fluids) fields. Two such fluids that are viable contenders for development of controllable dampers are:

1. Electrorheological (ER) fluids
2. Magnetorheological (MR) fluids.

### **2.6.1.1 Electrorheological Dampers**

An Electrorheological (ER) damper typically consists of a hydraulic cylinder containing micron-sized dielectric particles suspended within a fluid (usually oil). In the response to a strong electric field, the particles polarize and become aligned, thus offering an increased resistance to flow. By varying the electric field, the dynamic behaviour of an ER damper can be modulated.

### **2.6.1.2 Magnetorheological Dampers**

Magnetorheological (MR) dampers are essentially magnetic analogs of ER dampers; the behaviour of the two types of dampers is very similar except that control effect is governed by the application of an electric field in one case and by a magnetic field in the other. MR dampers typically consist of a hydraulic cylinder containing micron-sized, magnetically polarized particles suspended in a fluid. MR fluid behaviour is controlled by subjecting the fluid to a magnetic field. In the absence of a magnetic field, the MR fluid behaves as a semi-solid.

Summary of properties of ER and MR fluids are given in Table (2-1) below [30].

Table (2-1)

<b>Property</b>	<b>ER Fluids</b>	<b>MR Fluids</b>
Max. yield stress	2-5 kPa	50-100 kPa
Passive viscosity	0.1-1.0 Pa-s	0.1-1.0 Pa-s
Operable temp. range	+10 to 90 °c	-50 to 150 °c
Stability	Cannot tolerate impurities	Unaffected by impurities
Response time	milliseconds	milliseconds
Density	1-2 g/cm <sup>3</sup>	3-4 g/cm <sup>3</sup>
Max. energy density	0.001 Joules/ cm <sup>3</sup>	0.1 Joules/ cm <sup>3</sup>
Power supply	2000 – 5000 V	2 – 25 V

Several of the key differences between the ER and MR fluids are:

- 1- The MR fluids have a maximum field-induced yield strength that is 20 to 50 times larger than that of ER fluids.
- 2- The MR fluids may be operated directly from low-voltage power supplies.
- 3- The MR fluids are less sensitive to contaminants and extremes in temperature

The maximum strength of a given ER fluid is generally limited by the electric field breakdown strength of the carrier liquid. Operational temperature ranges for most ER fluids are generally limited to +10 to 90°C.

ER fluids are quite sensitive to the presence of contaminants, particularly water, small amounts can have a profound influence on the strength of the fluid and the amount of electric power needed to energize the fluid. This sensitivity has a large impact on the types of surfactants and additives that may be used to stabilize the suspension.

MR fluids exhibit yield strength of 50-100 kPa for an applied magnetic field. The ultimate strength of MR fluids is limited by magnetic saturation. Operation temperatures for MR fluids easily span -50 to 150°C. MR fluids are not sensitive to contaminants or impurities.

#### 2.6.1.3 Large Scale Seismic MR Fluid Damper

To prove the scalability of MR fluid technology to devices of the appropriate size for civil engineering applications, a large scale MR fluid damper, shown in Figure (2-16), has been designed and built [31].

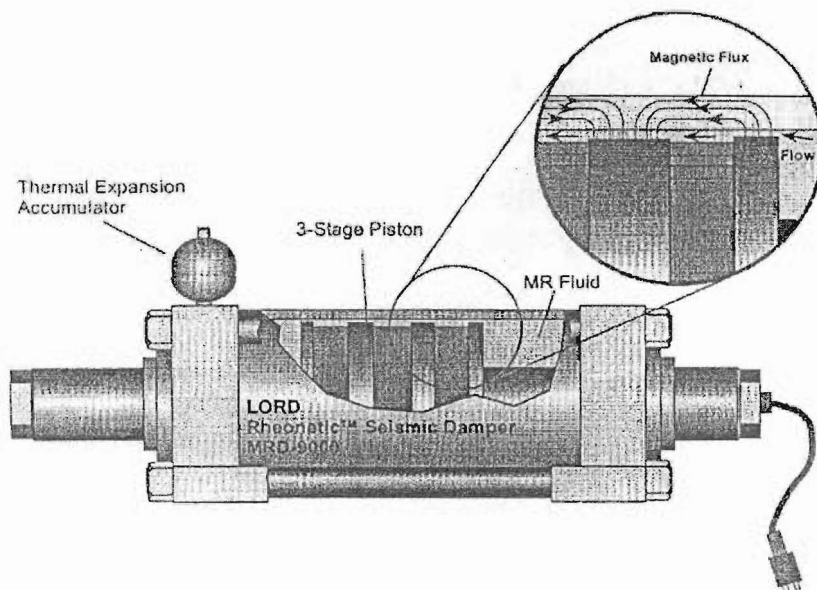


Fig (2-16) Schematic of the large-scale 20-ton MR fluid damper [31].

The damper uses a particularly simple geometry in which the outer cylindrical housing is part of the magnetic circuit. The effective fluid orifice is the entire annular space between the piston outside diameter and the inside of the damper cylinder housing. Movement of the piston causes fluid to flow through this entire annular region. The damper is double-ended i.e., the piston is supported by a shaft at both ends. This arrangement has an advantage in that a rod-volume compensator does not need to be incorporated into the damper, although a small pressurized accumulator is provided to accommodate thermal expansion of the fluid. The damper has an inside diameter of 20.3 cm and a stroke of  $\pm 8$  cm. The electromagnetic coils are wired in three sections on the piston. This result in four effective valve regions as the fluid flows past the piston. The coils contain a total of about 1.5 km of copper wire. The complete damper is approximately 1m long, has a mass of 250 kg, and contains approximately 6 litres of MR fluid. The amount of fluid energized by the magnetic field at given instant is approximately  $90 \text{ cm}^3$ . A summary of the design parameters for the large-scale 20-ton MR damper is given in Table (2-2).

Table (2-2) Design parameters for the large scale 20-ton MR damper [31]

Stroke	$\pm 8$ cm
Cylinder bore (ID)	20.32 cm
Max. input power	$\leq 50$ W
Max. force (nominal)	200,000 N
Effective axial pole length	8.4 cm
Coils	3x1050 turns
Apparent fluid $\eta$	1.3 Pa-s
Fluid $\tau_0$ max	62 kPa
Gap	2 mm
Active fluid volume	$\approx 90 \text{ cm}^3$
Wire	16 gauge
Coil resistance	3x7.3 ohms

## 2.6.2 Semi-Active Stiffness Damper

Various types of control laws have been proposed for on-off semi-active dampers [32]. A semi-active stiffness damper consists of a cylinder-piston system with a valve in the bypass pipe connecting two sides of the cylinder. When the valve is closed, the damper serves as a stiffness element in which the stiffness is provided by the bulk modulus of the fluid. When the valve is open, the piston is free to move and the hydraulic damper provides only a small damping without stiffness.

With the resetting control mode, the valve is always closed; hence the energy is stored in the damper system in terms of the potential energy. At appropriate time instants,

the valve is pulsed to open and close quickly. At that moment, the piston of the damper is at the position referred to as the resetting piston, and the energy stored in the damper system is released and converted into heat energy. Immediately after resetting, the damper system does not exert force on the structure. Hence, by pulsing the valve at appropriate time instants, energy can be drawn from the vibrating structure to reduce the response.

Hunt [52] has investigated the efficacy of semi-active control systems using non-linear structural models and realistic suites of earthquake records representing extremes of seismic excitations. A statistical assessment of control architecture was developed and he examined the distribution of a constant maximum actuator authority for structures. The research presents the tradeoffs between control law, architecture type, non-linear effects, and seismic input characteristics for semi-active control in structures.

## 2.7 Summary

Several types of active, semi-active and passive structural control systems are outlined in the chapter and the way in which they work is described to show the advantages and disadvantages of each system. An active control system is one in which an external power source controls actuators that apply forces to the structure in a prescribed manner. The disadvantage is that the required power supply may not be available during a major earthquake due to damage to the electrical power supply system that the algorithms for the control system for the large earthquake are still in the development stage. Semi-active control systems are a class of active control systems for which the external energy requirements are orders of magnitude smaller than typical active control systems as the power is used only to control the behaviour of the passive devices. Passive control systems prevail in engineering practice due to their simplicity, reliability and the low cost of installing and maintaining them. Passive structural control is, in general, grouped into two approaches: seismic base isolation and supplemental damping. Seismic isolation is achieved by isolating the structure from the ground excitation earthquake by moving the period of the structure away from the predominant period of the ground motion and by increasing the equivalent damping level of the structure by hysteretic behaviour of the isolation devices. Providing additional damping constitutes the basic concept of the supplemental damping method, which involves controlling structural response by increasing the system damping. The mechanical dissipaters employed in supplemental damping schemes, can be simple, inexpensive, and exhibit reliable and repeatable characteristics. Adding damping in structures is the approach considered in this research.

This thesis has focused on added damping in structures by using passive control system. One type of a passive control damper is a ring spring damper. Ring spring dampers do not depend on external power sources to effect the control action. They are constructed of only steel materials in which no liquid leakage is possible and no refilling or other maintenance is needed. Details of the ring spring dampers are discussed in Chapter 4.

## Chapter 3

### Amount of Supplemental Damping and Placement Strategies for Dampers

#### 3.1 Introduction

There are several techniques which can be used to mitigate the effects of earthquake ground motions on the response of buildings. Passive and active structural response devices and schemes are being considered to control the structural response. For some structures, energy dissipation devices such as viscous dampers, viscoelastic dampers, friction dampers, and yielding devices have been considered and installed as energy dissipaters to reduce the structural response and energy dissipation demand on the structural members. It is well known that the installation of an energy dissipation device or a damper will cause a reduction in the response. Some response quantities will be reduced more than others. The damping capacity of a device (rated damping force of the device), and where and how many are placed in a structure will have a significant effect on the ability of the design to reduce the response and to achieve the desired design objectives. In the absence of a better rationale, it may be convenient to distribute the dampers uniformly in all storeys of a building. However, such a distribution may not be the most effective or economical arrangement.

In considering supplemental damping to a structure, providing 10% to 20% supplemental damping reduces the response significantly for most structures. Providing more damping is difficult to justify from a cost-benefit perspective [39].

#### 3.2 Amount of the Supplemental Damping

The design of structures with supplemental control systems is, in general, an iterative process for which the design and analysis of the structure without the supplemental damping system should first be carried out. The required effective damping ratio to achieve the targeted response reduction is of primary concern. In general, increasing damping in a structure reduces the earthquake demand forces and deformations. The amount of the reduction varies, depending on the inherent mass, stiffness and damping characteristics of the basic structure, on the amplitude, frequency content, and duration characteristics of the earthquake motion the structure is expected to experience, and the amount of supplemental damping provided.

Damping can reduce the dynamic amplification of the response which is commonly referred to in terms of a Dynamic Amplification Factor (DAF). For elastic steady-state response at the resonant condition,  $DAF = 1/(2\zeta)$  where  $\zeta$  is the equivalent viscous damping ratio. From this it follows that for steady-state motion, the motion in resonance with the structures, and for  $\zeta = 0.05$ , the DAF is equal to 10.

Providing 10% to 20% supplemental damping reduces the response significantly for most structures. Providing more damping increases the cost of the structure and the provision of even 50% damping in a structure does not ensure minimal performance [39]. Figure (3-1) shows the effect of increasing damping on the structural response based on steady-state excitations.

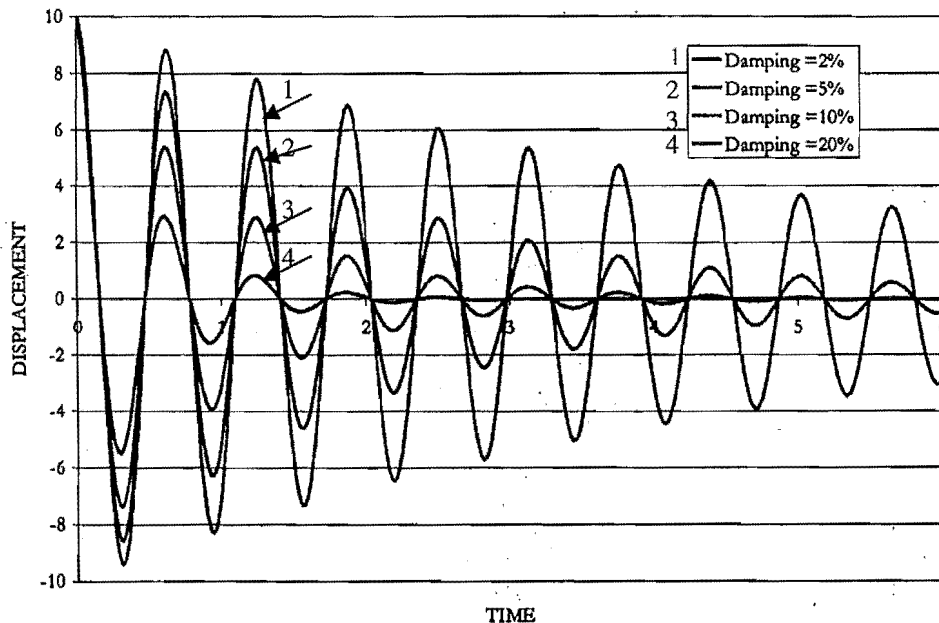


Fig (3-1) Effect of increasing damping on free vibration response.

Earthquake ground motions are not steady-state excitation. They do not contain nearly enough cycles of motion to produce a steady-state response. Thus the steady-state resonant condition provides an estimate of the upper bound for the DAF for earthquake excitation.

### 3.3 Response Spectra with Several Levels of Damping

Response spectra are derived from the response of a single degree of freedom system subjected to an earthquake ground acceleration motion. The maximum absolute value of the displacement of the mass is obtained from

$$x_{\max} = S_d = \frac{1}{\omega} S_v = \frac{1}{\omega^2} S_a \quad 3-1$$

where  $S_v$  is the Pseudo Spectral Velocity and can be obtained from

$$S_v = \left[ \int_0^t \ddot{x}_g e^{-\zeta \omega(t-\tau)} \sin \omega_D(t-\tau) dt \right]_{\max} \quad 3-2$$

and  $S_d$  is the Spectral Displacement and  $S_a$  is the Pseudo Spectral Acceleration. The Pseudo Spectral Velocity is the maximum value of the term in Equation 3-2, which is an integration of acceleration with respect to time and therefore has the units of velocity.

The period used in the calculation of the model response is that of the structure in undamped free vibration. The response spectra are shown below with several levels of damping 0%, 2%, 5%, 10%, 20%, 30%, 40%, and 50% of critical viscous damping to El-Centro and Pacoima Dam accelerograms in Figures(3-2 and 3-3) respectively.

In these figures, it can be readily seen that a significant decrease in response occurs by adding a further 15% percent damping. It is generally assumed 5% damping is inherent in the structure. Typically, the amplitude decrease in going from 5 to 20 percent damping is greater than that realized in going from 20 to 50 percent. A decision regarding the amount of supplemental damping to be provided in a structure should be based on the structure's desired response performance characteristics and cost. Providing 15 percent supplemental damping was a target used in the experimental tests to give a significant reduction in the structural response and a suitable size of the ring spring dampers attached to the frame.

It should be noted that the decrease in response amplitude with increasing damping is highly dependent on the nature of the applied excitations.

### El Centro ground acceleration

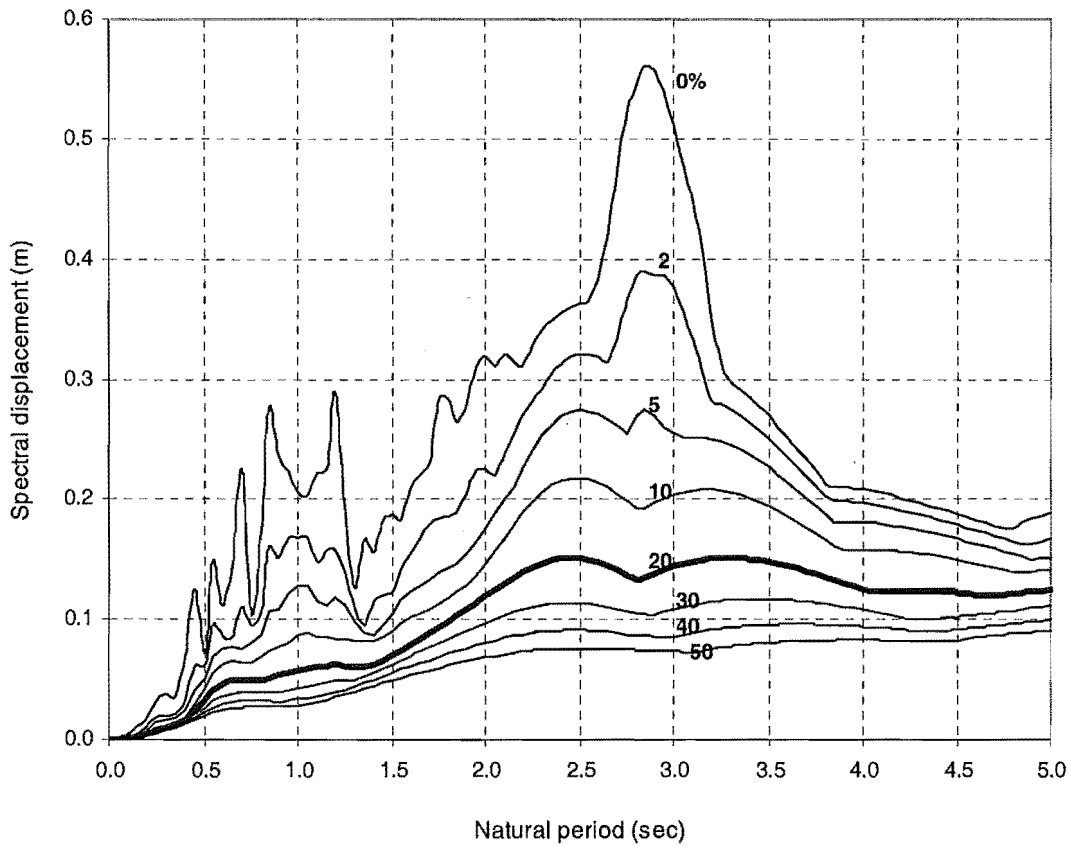


Figure (3-2a) Displacement Response Spectrum

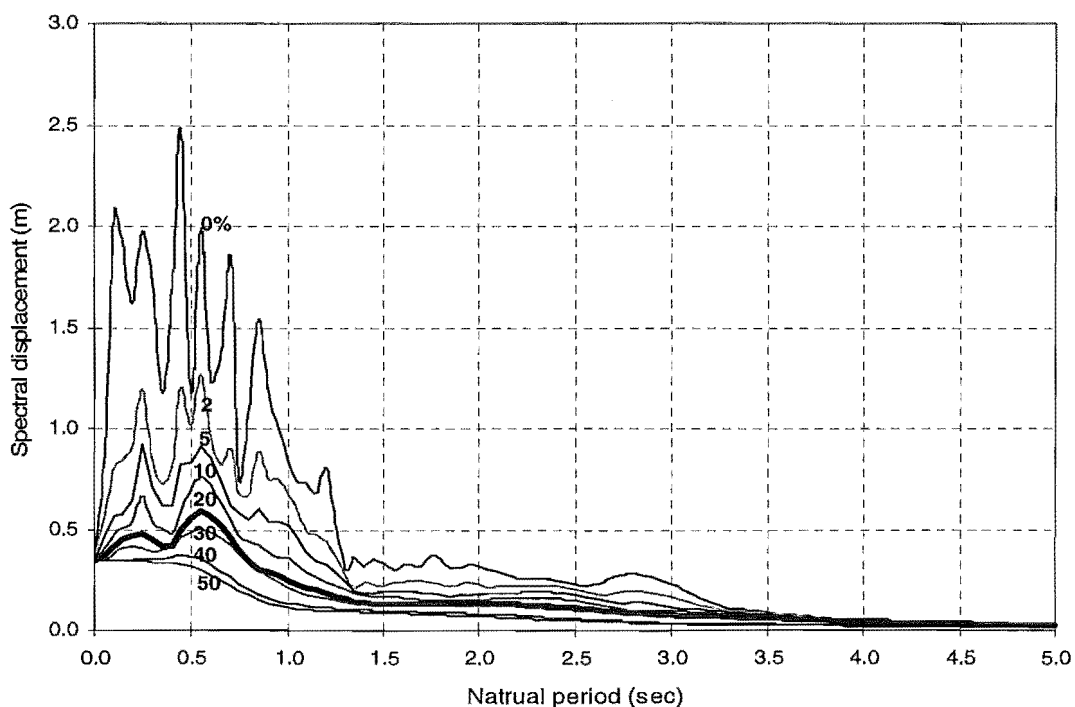


Figure (3-2b) Pseudo Acceleration Response Spectrum

### Pacoima Dam ground acceleration

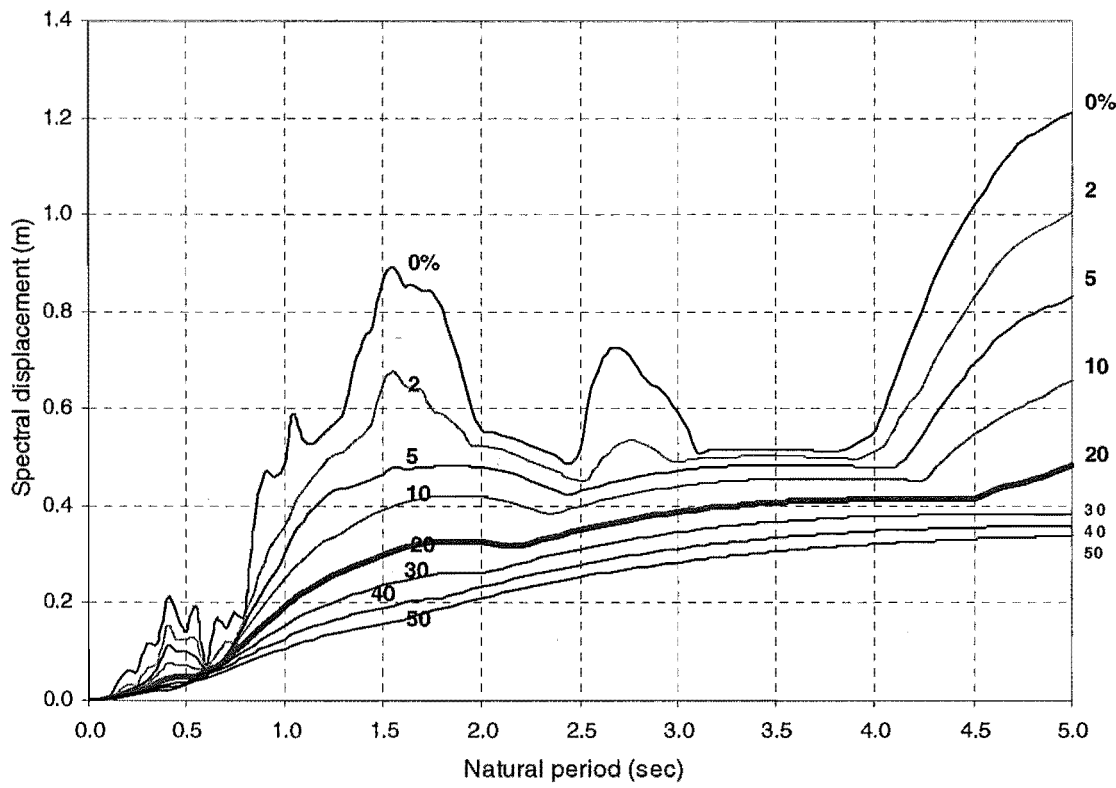


Fig (3-3a) Displacement Response Spectrum

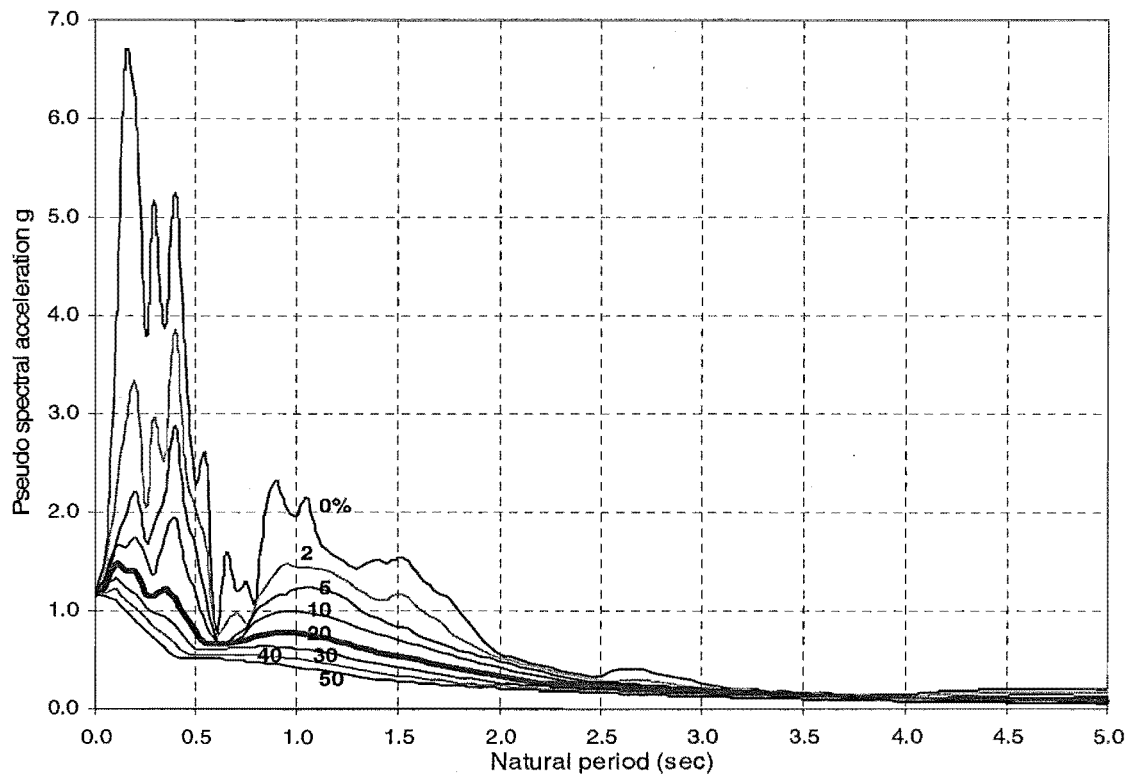


Fig (3-3b) Pseudo Acceleration Response Spectrum

### 3.4 Distribution of Dampers from Previous Research

#### 3.4.1 Structure with Supplemental Lead Dampers

A previous study by Lin [21] used supplemental lead dampers in a 12 storey-3 bay frame. Four different placements of the supplemental dampers were examined. These were: only one damper at the first floor, one damper every third level, one damper every second level, and one damper for every level, as shown in Figure (3-4). The total numbers of dampers for these four types of distribution is 1, 4, 6 and 12 respectively. The results are shown in Table (3-1). The peak roof displacement and the peak interstorey drift were used as parameters for comparison. The results of all cases were then compared with those of the original structure without the extra dampers.

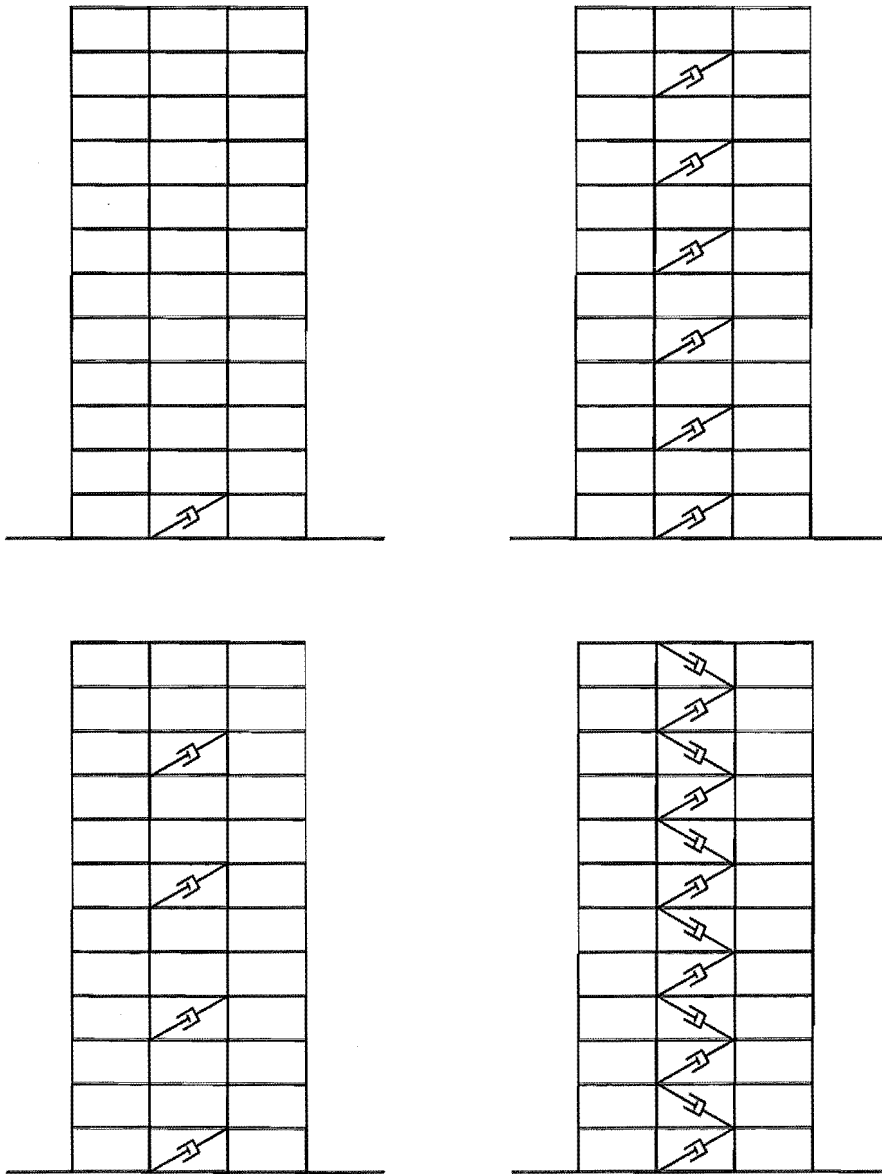


Fig (3-4) Four types of placement of the supplemental dampers in the structure [21].

Table (3-1) Comparison of the peak interstory drift for the structure with different number of dampers under El Centro 1940 NZS4203 compatible earthquake[21].

	Peak Roof Displacement (cm)	Peak Interstory Drift (cm)
Original structure without damper	25.49 (0%)	3.8 (0%)
One damper only	24.91 (Reduced by 2%)	3.78 (Reduced by 0.4%)
One damper every third storey	19.0 (Reduced by 25%)	2.66 (Reduced by 29%)
One damper every second storey	17.48 (Reduced by 31%)	2.33 (Reduced by 38%)
One damper every storey	15.26 (Reduced by 40%)	1.99 (Reduced by 47%)

It can be seen that only one damper at the first level is not beneficial as the reduction of the response caused by the supplemental dampers is negligible. This means that additional damping caused by merely one damper is quite small in a multi-story structure. Where dampers are placed at every third level (4 dampers for the structure), the effect of the supplemental dampers becomes significant and as the number of dampers increases from 4 to 12, the response of the structure is reduced further.

Based on the above observation, it was concluded that a uniform placement of the dampers throughout the structure is better than the case where dampers are placed at only some storeys; however there is the cost of the extra dampers to be balanced against the decrease in the response.

### 3.4.2 Structure with Supplemental Viscoelastic Dampers

Another study has been made of the effects of changing the distribution of added viscoelastic dampers on the seismic response on the behaviour of tall buildings. The study reported in [27] considered the response of the structures with several different damper distributions.

The system considered are shear buildings with three-and ten-storeys, and include systems A1, A2, A3 and A4, as shown in Figure (3-5), and systems B1, B2, B3, B4 and B5, presented in Figure (3-6). Systems A1 and B1 represent ‘original’ structures without any added dampers, the other systems have added dampers placed in different storeys as shown in Figure(3-5) and (3-6). In particular, systems A2 and B2 are structures with added dampers in all storeys, whereas systems A4 and B5 only have one damper installed in the first storey.

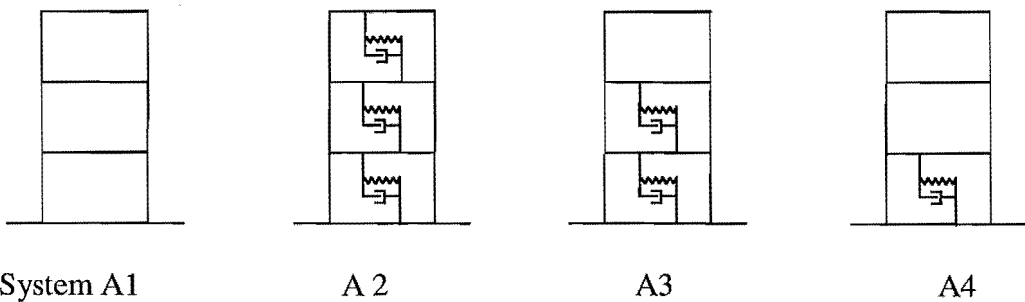


Fig (3-5) Three-storey systems considered [27].

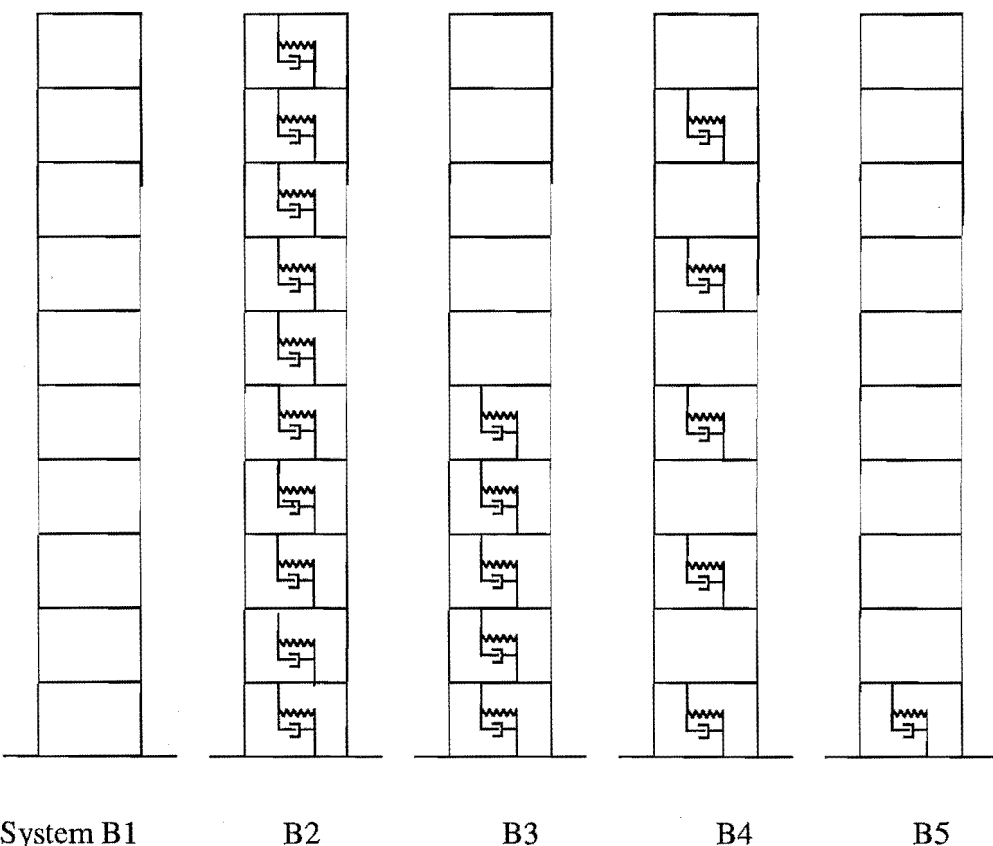


Fig (3-6) Ten-storey systems considered [27].

### 3.4.2.1 Three-Storey Building

Figure (3-7) presents the normalized maximum responses for the systems shown in Figure (3-5) (three-storey building). These results suggest that system A4, the first-storey damped case, may be effectively used to mitigate the earthquake response of short buildings such as this three-storey structure. Involving a one-storey installation only, this case will be particularly attractive for practical applications [27].

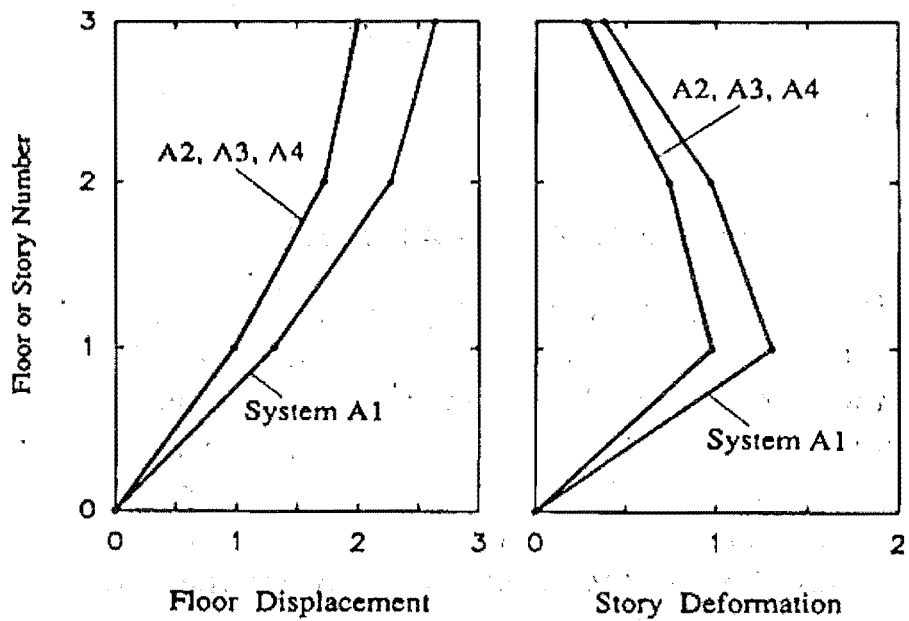


Figure (3-7)

### 3.4.2.2 Ten-Story Building

Maximum normalized responses for the ten-storey buildings considered are shown in Figure (3-8). It is apparent that the solutions of Figure (3-7) generally follow the trends of those of Figure (3-8). However, a comparison of Figures (3-7) and (3-8), reveals that the first storey damped case (system B5) is less effective for the ten-storey building than for the three-storey structure (system A4), indicating that the response of tall building is generally more sensitive than that of short buildings to changes in the distribution of the added dampers. This further suggests that the first-storey damped case is not particularly suitable for tall structures. In taller buildings the higher modes of free-vibration have a greater contribution to the displacements than they do in shorter buildings.

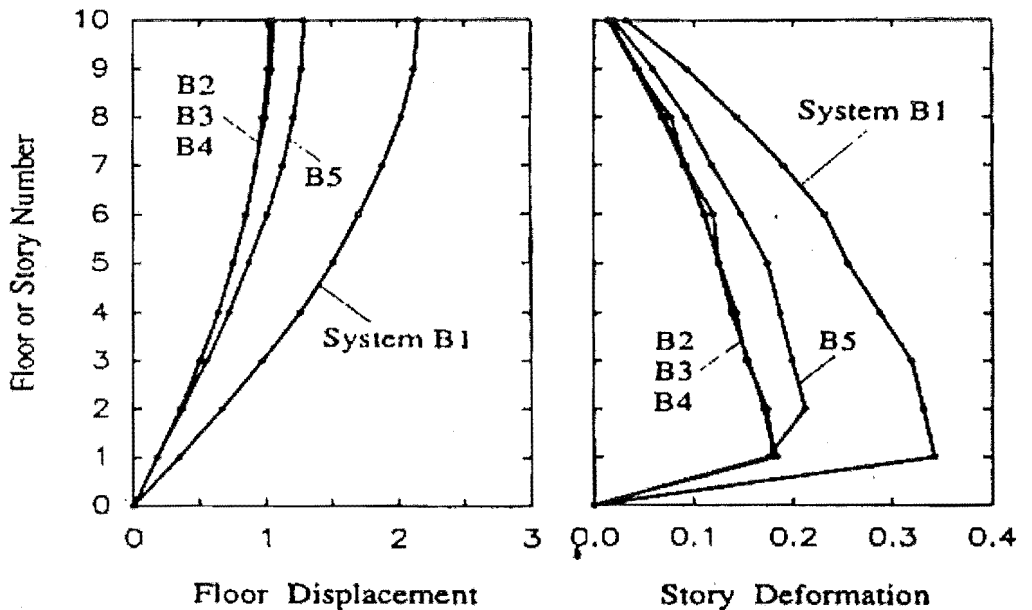


Fig (3-8)

The response reductions achieved for the ten-storey building using system B3 (five storeys damped) are almost the same as those obtained for system B2 (all storeys damped), and this indicates that the earthquake response of a tall structure may be effectively reduced by adding dampers to the storeys in the lower half of the building.

A comparison of Figs (3-7), (3-8), reveals that the response reductions are more significant for the ten-storey building than for the three-storey structure. Figure (3-7) shows that the displacements for the three-storey structure are reduced by about 25% by the added dampers, whereas such reductions are observed in Fig (3-8) to be about 50% for the ten-storey system.

An examination has been made of the seismic response of simple building systems with added dampers. Adding dampers to all storeys of a building is not necessarily the most economical design. For short buildings, the first storey-damped case effectively reduces the response. Involving a first-storey installation only, it could also be an efficient retrofitting solution. For tall structures, the first-story damped case was found to be ineffective. However, the solutions reported herein suggest that the response of a tall building may be effectively reduced by damping the lower half of the structure [27].

Another damper placement strategy is discussed for modelling a structure as a uniform shear beam. The optimal locations of the dampers are found to conform to the pattern of distribution which will result in maximizing the first mode's damping ratios as shown in section 3.5.

### 3.5 Optimal Damper Placement

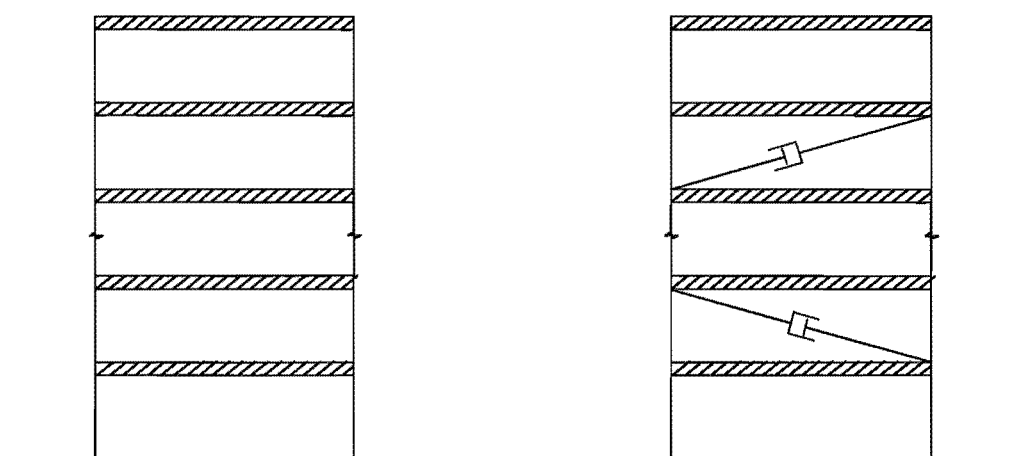
The optimal location of the dampers is found to conform to the pattern of distribution that maximizes the first mode damping ratio. In another approach, a sequential optimization is proposed in which a performance index is maximized at each step to determine the optimal location of a damper in the sequence. The basic idea is to place each viscous damper at a location experiencing the largest relative displacement and velocity between the damper's attachment points.

There are, however, some limitations associated with the procedure. First, the uncontrolled modes of the structure are used to find the optimal locations, and these locations are found all at once without considering the effect of the added controllers on the mode shapes. In fact, the addition of a damper will alter the mode shapes of free vibration and thus change the optimal locations for the remaining controllers. A sequential procedure, in which the optimal locations are found one by one adding controllers sequentially, is more appropriate [26].

In what follows, a sequential procedure for optimal damper placement is proposed that determines the optimal location index by solving the random seismic response of a structure using the transfer matrix method. The best position for the first damper is found from the uncontrolled free vibration response to be the storey with the maximum interstorey drift. After adding a damper to that location, the procedure is repeated by taking into account the added stiffness and damping of the first damper to determine the optimal location of the next controller. This process is repeated until the required numbers of dampers are placed in the structure.

#### 3.5.1 Transfer Matrix Formulation

The transfer matrix method has been used as a convenient way of finding the dynamic characteristics and response of chainlike systems. It is adopted for finding the controllability index because it can be easily formulated. Figure (3-9), shows the structural model used in an N-storey shear-type building [26].



Typical shear-type building

Shear type building with dampers

Fig (3-9)

The structural model used in an N-storey shear-type building, as shown in Fig (3-9),

$x_j$  and  $y_{j-1}$  are the displacement of the  $j^{\text{th}}$  floor and the resultant shear force in the columns of the  $j^{\text{th}}$  floor unit, respectively.

The equation of motion and the force displacement relationship of the  $j^{\text{th}}$  floor are:

$$y_j = y_{j-1} + m_j \ddot{x}_j \quad 3-3$$

$$y_{j-1} = k_j(x_j - x_{j-1}) + c_j(\dot{x}_j - \dot{x}_{j-1}) \quad 3-4$$

where  $m_j$ ,  $k_j$  and  $c_j$  are the mass, stiffness and damping of the  $j^{\text{th}}$  floor, respectively. In the frequency domain, we have

$$Y_j = Y_{j-1} - m_j \omega^2 X_j \quad 3-5$$

$$Y_{j-1} = (k_j + i c_j \omega) X_j - (k_j + i c_j \omega) X_{j-1} \quad 3-6$$

where  $X$  and  $Y$  are the Fourier transforms of  $x$  and  $y$ . Therefore:

$$\begin{pmatrix} X_j \\ Y_j \end{pmatrix} = \begin{bmatrix} 1 & 1/(k_j + i c_j \omega) \\ -m_j \omega^2 & 1 - m_j \omega^2 / (k_j + i c_j \omega) \end{bmatrix} \begin{pmatrix} X_{j-1} \\ Y_{j-1} \end{pmatrix} \quad 3-7$$

This can be written in matrix form as

$$Z_j = T_j Z_{j-1} \quad 3-8$$

The transfer relationship between the ground acceleration and the first-storey displacement becomes:

$$\begin{pmatrix} X_1 \\ Y_1 \end{pmatrix} = \begin{bmatrix} 1/\omega^2 & 1/(k_1 + i c_1 \omega) \\ -m_1 & 1 - m_1 \omega^2 / (k_1 + i c_1 \omega) \end{bmatrix} \begin{pmatrix} \ddot{X}_0 \\ \ddot{Y}_0 \end{pmatrix} \quad 3-9$$

or

$$Z_1 = T_1 Z_0 \quad 3-10$$

where  $\ddot{X}_0$  is the Fourier transform of the ground acceleration. The relation between  $Z_L$  and  $Z_0$  is given by

$$Z_L = T_L T_{L-1} \dots T_1 Z_0 \quad 3-11$$

where  $Z_L$  is the value of  $Z$  at  $L^{\text{th}}$  level.

To find the response at any floor, we need to use the boundary conditions at the ground (the ground acceleration) and at the top (zero shear force). The response  $x_j$  and  $y_j$  are the impulse response functions, and their Fourier transforms, represented by  $Z_j = \begin{pmatrix} X_j \\ Y_j \end{pmatrix}$  which are the frequency response functions. Thus, the boundary conditions at the top and at the base of the building are, respectively

$$\begin{aligned} Z_N &= \begin{pmatrix} X_N \\ 0 \end{pmatrix} \\ Z_0 &= \begin{pmatrix} 1 \\ Y_0 \end{pmatrix} \end{aligned} \quad 3-12$$

Substituting (3-12) into (3-11), we have

$$\begin{pmatrix} X_N \\ 0 \end{pmatrix} = \begin{bmatrix} b_{11} & b_{12} \\ b_{21} & b_{22} \end{bmatrix} \begin{pmatrix} 1 \\ Y_0 \end{pmatrix} = B \begin{pmatrix} 1 \\ Y_0 \end{pmatrix} \quad 3-13$$

where matrix B is the product of all transfer matrices. We now have

$$\begin{aligned} Y_0 &= \frac{-b_{21}}{b_{22}} \\ X_N &= b_{11} - \left( \frac{b_{12}b_{21}}{b_{22}} \right) \end{aligned} \quad 3-14$$

With this transfer matrix formulation, one can proceed [26] to find the statistics of the response due to an earthquake excitation. It has often been assumed that the strong shaking portion of a typical earthquake accelegram is a stationary process, as is the corresponding structural response. Consequently, the earthquake ground acceleration has often been modelled as a stationary stochastic process with a zero mean and a power spectral density function  $\phi(\omega)$ :

$$\phi(\omega) = \frac{1 + 4\zeta_g^2 (\frac{\omega}{\omega_g})^2}{\left[ 1 - \left( \frac{\omega}{\omega_g} \right)^2 \right]^2 + 4\zeta_g^2 \left( \frac{\omega}{\omega_g} \right)^2} S^2 \quad 3-15$$

where  $\omega_g$ ,  $\zeta_g$  and S are the frequency, damping and duration parameters that depend on the intensities and characteristics of earthquakes in a particular geological location.

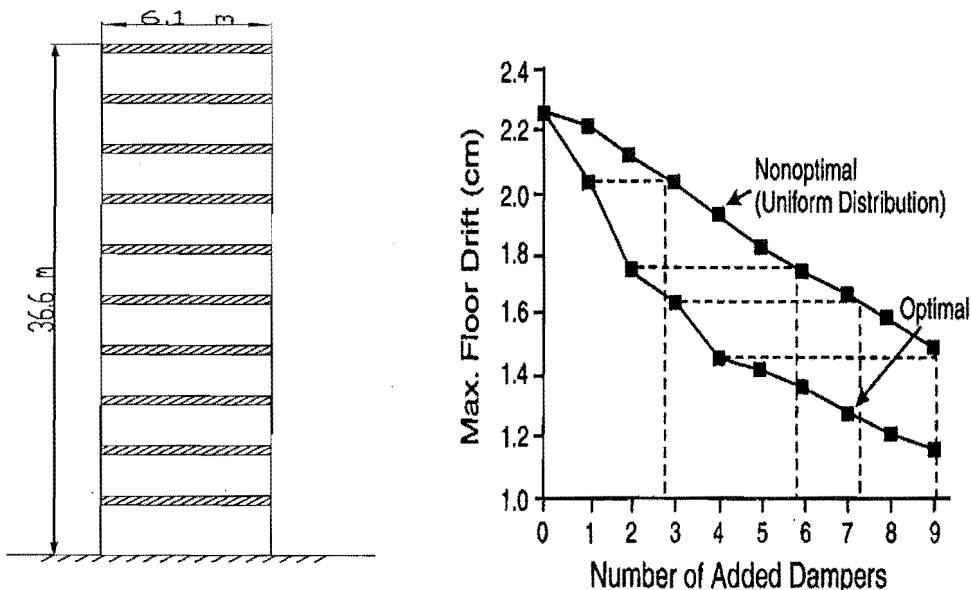
Using this characterization, the mean square response  $\sigma_m^2$  of the structure at every floor can be found by:

$$\sigma_m^2 = \int_{-\infty}^{+\infty} |Z_m|^2 \phi(\omega) d\omega, \quad m = 1, 2, \dots, N \quad 3-16$$

Since dampers are placed between neighboring floors, the mean square values of interstorey drifts are used as optimal location indices.

Once the optimal location indices are found, the optimal location of the first damper is determined as the storey with the maximum index value. Adding one damper to the storey means an increase in stiffness and equivalent viscous damping. Therefore, to find the best location of the next damper, the response is recalculated accounting for the increased stiffness and damping coefficient due to the addition of the first damper. The response is repeated until the last damper has been added to the structure.

The advantage of adding dampers at optimal locations can be shown by estimating the number of dampers that can be saved to achieve the same effect as compared with non optimal placement. For example, consider a 10-storey steel frame structure [26], as shown in Figure (3-10), with the parameter values shown in Table (3-2). Figure (3-10) shows the maximum storey drifts plotted against the number of identical dampers added at optimal locations and at a uniform distribution (non optimal) locations [26].



Configuration of  
10 storey structure

Floor drifts as a function of the number of  
dampers

Figure (3-10)

It is seen, for example, that the same storey drift of approximately 1.45 cm can be achieved by using four optimal located dampers as compared with nine uniformly spaced dampers.

Table (3-2) Parameter values of a 10-storey structure [26]

Floor	Mass (kg x 1000)	Stiffness (kN/cm)	Damping (kN.s/cm)
10	0.207	164.5	1.44
9	0.207	164.5	1.44
8	0.207	286.6	1.98
7	0.207	286.6	1.98
6	0.207	421.7	2.91
5	0.207	421.7	2.91
4	0.207	540.1	3.73
3	0.207	540.1	3.73
2	0.207	687.1	4.76
1	0.207	687.1	4.76

### 3.5.2 The Sequential Search Algorithm (SSA)

Alternative approach base on seismic input demand on structure was presented by Garacia [62]. In this method, a simplification to the Sequential Search Algorithm (SSA) was proposed so that the resulting procedure can be easily integrated into conventional design procedures used by practicing engineers dealing with damper added to structures.

The seismic random response of the bare structure (i.e., the structure without any added dampers) is obtained using the transfer matrix method. Mean square values of interstorey drifts are calculated and used as optimal location indices. The greatest optimal location index indicates the optimal placement of the first damper. The stiffness and damping of the added damper are incorporated into the mathematical model of the structure and new optimal location indices are calculated. The second damper is then placed at the storey where the revised optimal location index is a maximum. The procedure is repeated until all necessary dampers have been placed in the structure. All dampers are assumed to have the same size. The modal strain energy method is used to develop simple equations relating the number and size of the dampers and the equivalent damping ratio [62].

Since all dampers have the same size, the SSA is more practical than other optimization methods, which usually lead to a different damper size at each storey. If the damper size is constrained, then the number of dampers can be adjusted. If, for other reasons, the number of dampers is subjected to limitations, then the damper size can be conveniently selected. Moreover, the SSA is not limited to damper configurations of equally sized dampers. The effect of two equal dampers placed at the same storey is equivalent to the effect of one damper whose size is twice the size of the original dampers and placed at the same storey. Therefore, by limiting the number of dampers sizes can be controlled [62].

### 3.6 Toggle-Brace Damper System

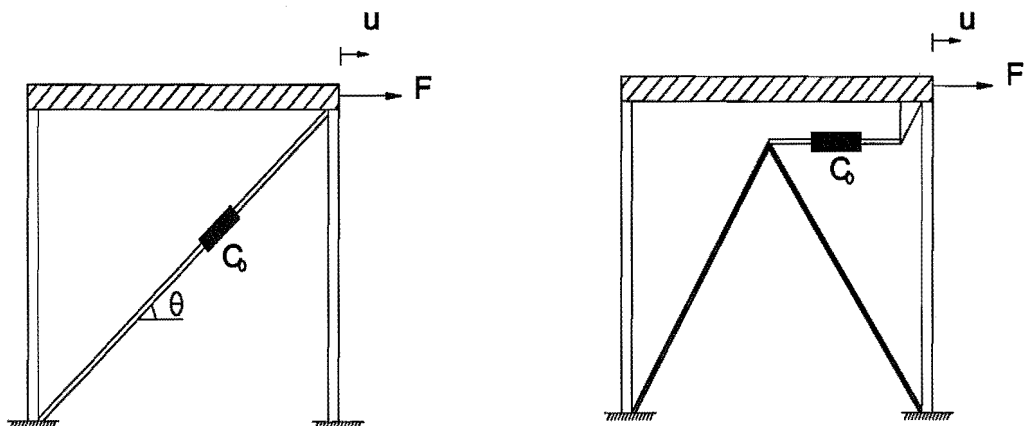
Toggle-brace-damper systems represent novel energy dissipation systems that operate on the principle of magnification of small damper forces in shallow trusses and the delivery of the magnified forces to the structural frame. Diagonal brace and chevron brace configurations have been used for the delivery of forces from energy dissipation devices to the structures frame. The use of these configurations is apparently based on the experience of engineers with bracing systems in steel construction and the fact that experimental research studies utilized these two configurations for energy dissipation systems [60].

It is generally recognized that stiff structural systems respond to dynamic excitation with small drifts and small interstorey velocities. This fact, coupled with the practice of implementing damping devices either as diagonal elements or as horizontal elements on top of chevron bracing, leads to device displacements that are less than or equal to the drift. This, in turn, results in the requirement for substantial forces in the damping devices for effective energy dissipation.

In recent research [60], three novel configurations of energy dissipation devices which are based on the toggle mechanism and which result in device displacements that are larger than the structural drift are discussed. The amount of magnification depends on the geometry of the toggle braces and can be significant; however, practical values of the magnification are in the range of 2 to 5. As the result of the energy dissipation devices displacement magnification, the required device force is reduced by the same amount, leading to highly effective systems that are eminently suitable for stiff structural systems.

#### 3.6.1 Toggle-Brace Theory

Consider the diagonal and chevron brace configurations, in which the displacement of the energy dissipation devices is either equal to (case of chevron brace) or less than (case of diagonal brace) the drift to the storey at which the devices are installed (Figure 3-11).



a) Diagonal brace configuration

b) Chevron brace configuration

Fig (3-11) Illustration of diagonal and chevron brace configuration of single storey structure with fluid linear viscous devices [60].

The damper relative displacement can be calculated from the following equation:

$$u_D = f \cdot u \quad 3-17$$

where

$u_D$  = damper relative displacement along the axis of the damper.

$f$  = magnification factor.

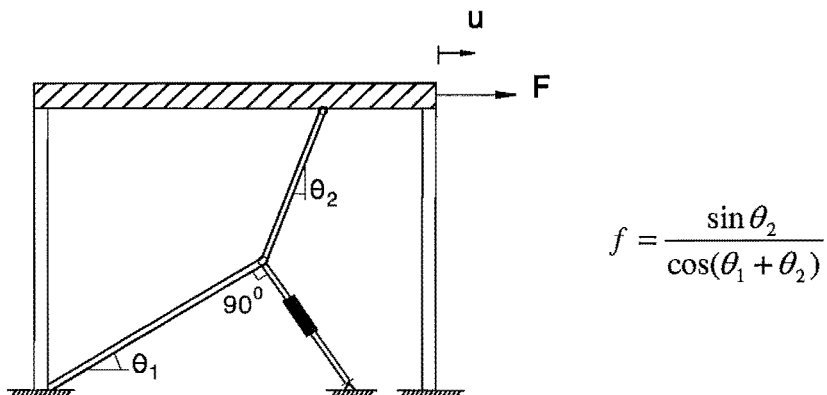
$u$  = interstorey drift.

For the chevron brace configuration,  $f = 1.0$ , whereas for the diagonal configuration,  $f = \cos \theta$ , where  $\theta$  = angle of inclination of the damper.

Similarly, the force along the axis of the damper  $F_D$  is related to the horizontal component of force,  $F$  exerted by the damper on the frame.

$$F = f \cdot F_D \quad 3-18$$

The significance of the configuration of the energy dissipation system is evident in the effect of the magnification factor on the damping ratio [60]. Fig (3-12) illustrates the configuration utilizing shallow trusses to magnify the effect of the structural drifts on the damper displacement and to magnify the small damper force and deliver it to the structural frame. Expressions for the magnification factor under conditions of small rotations are given. It is of interest to note in this figure that, if the same damper that provided the damping ratio of 5% in the chevron configuration is used in the toggle-membrane configurations, the damping ratio would have been between 30% and 50% of critical damping [60].



a) Lower Toggle

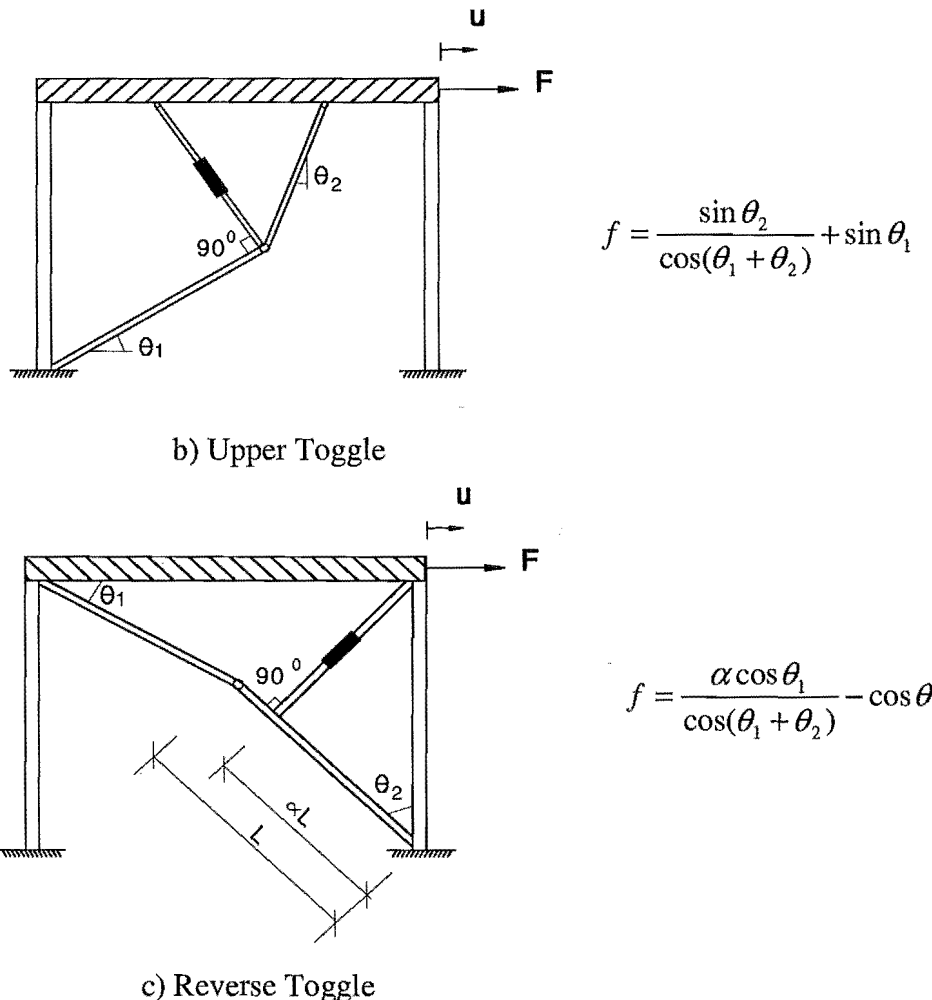


Fig (3-12) Illustration of toggle-brace-damper configurations.

Such performance is achieved with the selection of magnification factors in the range of 2.5 to 3.0 that is, the displacement of the damper is 2.5 to 3.0 times the interstorey drift. This itself represents a desirable feature when the interstorey drift is small, such as in seismic applications in stiff structural systems or for wind load applications. For such applications of small drift, fluid viscous dampers require special detailing that increases their size and, accordingly, their cost. Moreover, when drifts are small, the required damping forces are large, leading to further increase in the cost of the energy dissipation system. Therefore, the utilization of configurations with a large magnification factor, such as in these toggle-brace-damper systems, may lead to significant cost savings [60]. Table (3-3) shows the magnification factor  $f$  for different values of  $\theta_1$  and  $\theta_2$ .

Table (3-3) magnification factor

$\theta_1$	$\theta_2$	$f$		
		Case (a)	Case (b)	Case (c)
30	20	0.5	1.03	0.02
20	30	0.78	1.12	0.15
40	30	1.47	2.11	0.69
50	30	2.9	3.7	1.78

### 3.6.2 Forces in Toggle-Brace Systems

The determination of forces in the toggle-brace system is needed for the assessment of the safety of the toggles and for establishing the relation between the force in the damper and the horizontal component of force that acts on the structure. Fig (3-13) shows a one-storey frame with the three toggle systems. It should be noted that the frame is a mechanism so that force  $F$  represents the component of the inertia force that is balanced by forces supplied by the damping system.

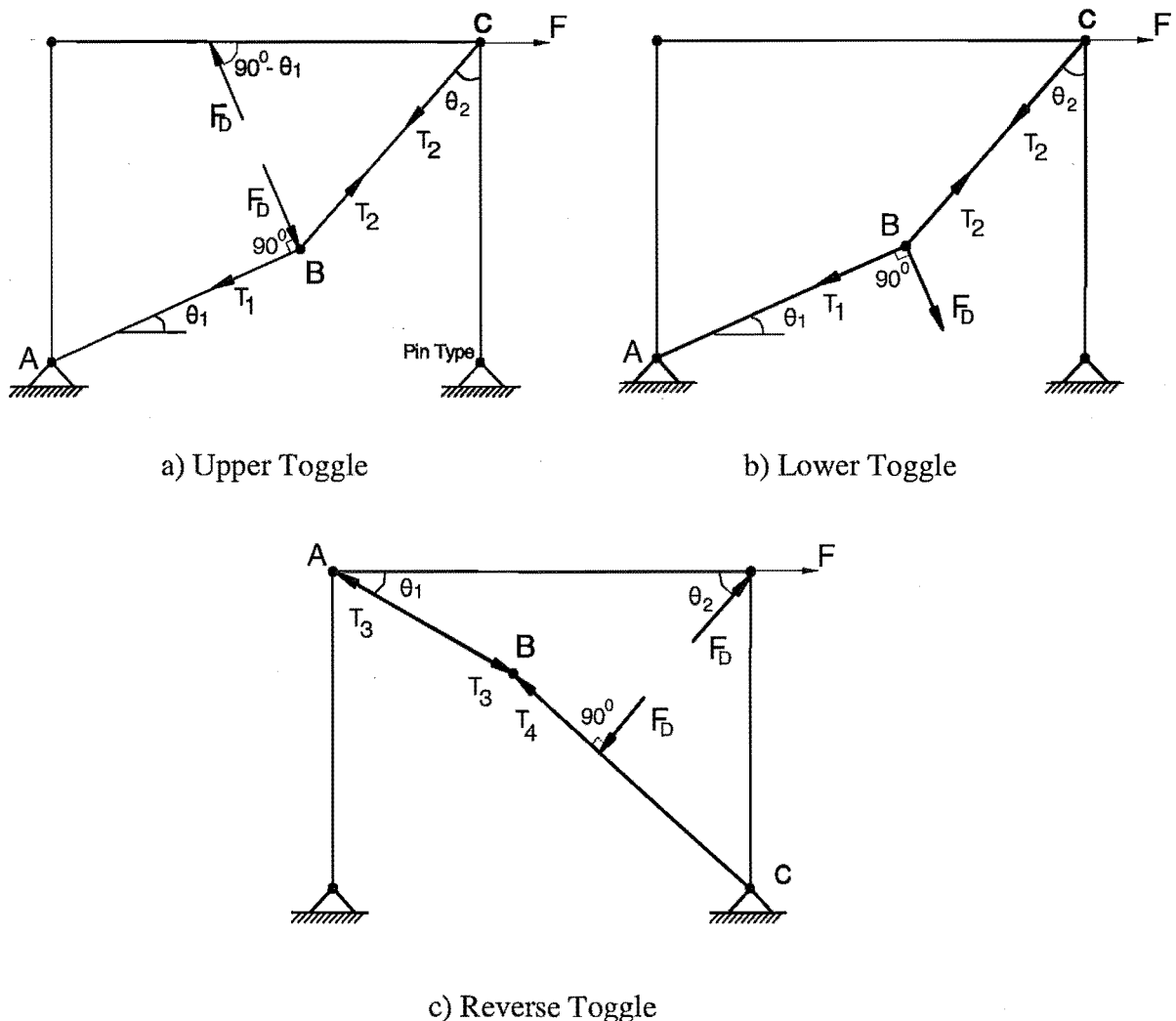


Fig (3-13) Forces acting on frame and toggle system

Simple equilibrium results in the following axial forces in the toggle:

$$T_1 = F_D \cdot \tan(\theta_1 + \theta_2) \quad 3-19$$

$$T_2 = \frac{F_D}{\cos(\theta_1 + \theta_2)} \quad 3-20$$

$$T_3 = \frac{\alpha \cdot F_D}{\cos(\theta_1 + \theta_2)} \quad 3-21$$

$$T_4 = \alpha \cdot F_D \cdot \tan(\theta_1 + \theta_2) \quad 3-22$$

The forces  $T_1$  and  $T_2$  are tensile, whereas forces  $T_3$  and  $T_4$  are compressive for force  $F$  acting as shown in Figure (3-13). Horizontal equilibrium of the beam results in the relation between the force  $F$  and the damper force  $F_D$ . It is easily confirmed that this relation is described in equation (3-18), with  $f$  given in Figure (3-12). That is, the magnification factor is given by:

$$f = \frac{F}{F_D} = \frac{u_D}{u} \quad 3-23$$

Equation (3-23) leads to the expected results  $F_D \cdot u_D = F \cdot u$ , which denotes the correctness of the analyses.

A steel model structure shown in Figure (3-14) was constructed for the purpose of testing the toggle-brace systems [60].

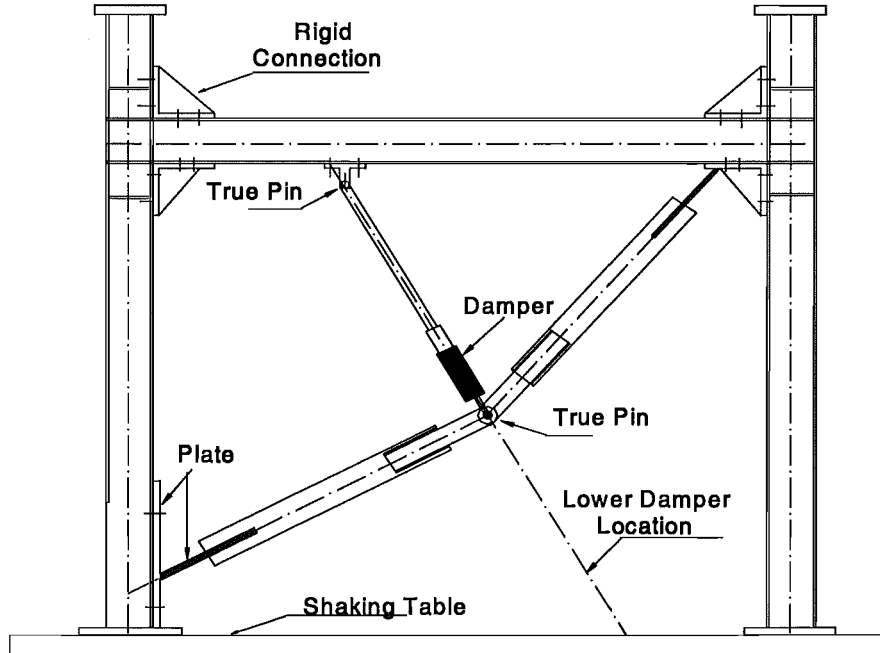


Fig (3-14) Tested toggle brace-damper configuration [60].

The results of the study reveal the following [60]:

- 1- The addition of the damping system causes an increase in the fundamental frequency of the model structure. Part of this increase in frequency is caused by deformations in the toggle system due to frame action on lateral movement, and part due to deformations caused by the damper force.
- 2- A substantial increase in the damping ratio of the frame with the toggle systems.

### **3.6.3 Applications**

Three buildings in the United States have been designed with toggle-brace-damper systems [60]. They are the 37-storey Yerba Buena Tower in San Francisco, the 37-storey Millenium Place in Boston and another 38-storey building in Boston. The first two utilize reverse toggle systems, whereas the third utilizes a modified lower toggle system. The modification consists of installing the damper at an angle other than  $90^{\circ}$  with respect to the lower toggle so that the two toggles and the damper directly connect to the beam-to-column joints. The installation with the connections of the toggles and dampers directly to the beam-to-column joints eliminates additional bending in the beams and provides for easy and reliable calculation of the magnification factor. Interestingly, all three applications are for the reduction of wind-induced vibrations.

The Toggle-brace-damper systems are suitable for applications with small structural drifts, as may be the case in applications of seismic hazard mitigation in stiff structures and in applications of wind response reduction [60].

### **3.7 Scissor-Jack-Damper Theory**

Scissor-jack damper energy dissipation systems offer a further opportunity to apply damping systems. As for the toggle-brace-damper system that preceded its development, the scissor-jack damper system utilizes shallow trusses to magnify the damper displacement for a given interstorey drift, and to magnify the damper force output delivered to the structural frame. Moreover, the scissor jack damping system can be configured to allow for open space because of its compactness and near-vertical installation, a feature that is often desired for architectural purposes [61].

The scissor-jack-damper system is best explained by first reviewing the conventional diagonal and chevron brace configurations, in which the displacement of the energy dissipation devices is either less than or equal to the drift of the storey at which the devices are installed. Figure (3-15) illustrates the scissor-jack-damper as implemented in a single-storey frame.

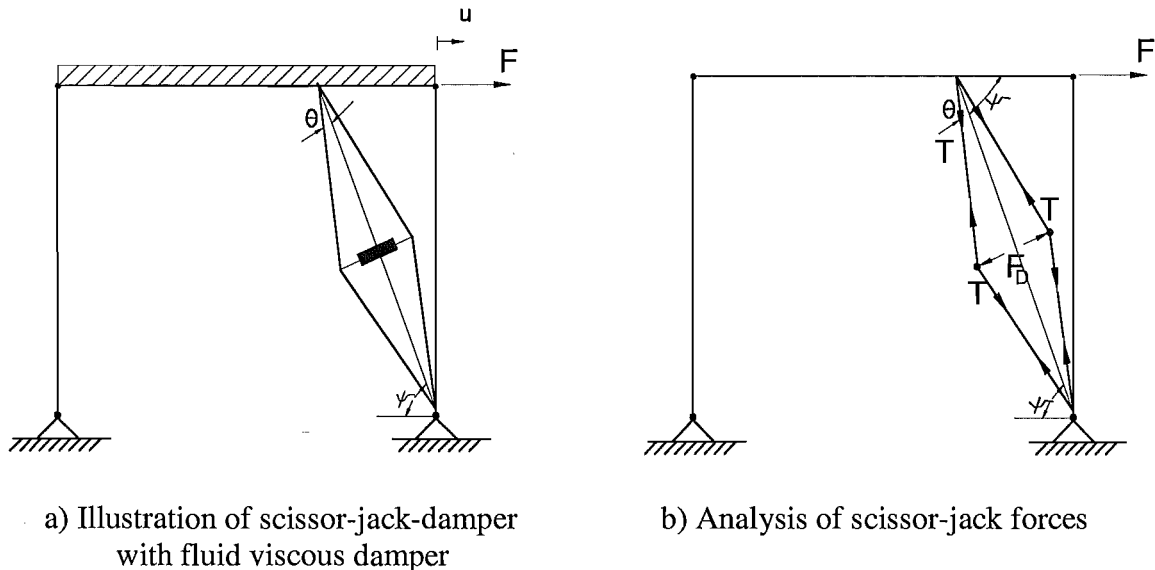


Fig (3-15) Scissor-jack-damper implemented in a single-storey frame

The scissor-jack damping system may be installed in a variety of configurations as show in Figure (3-16).

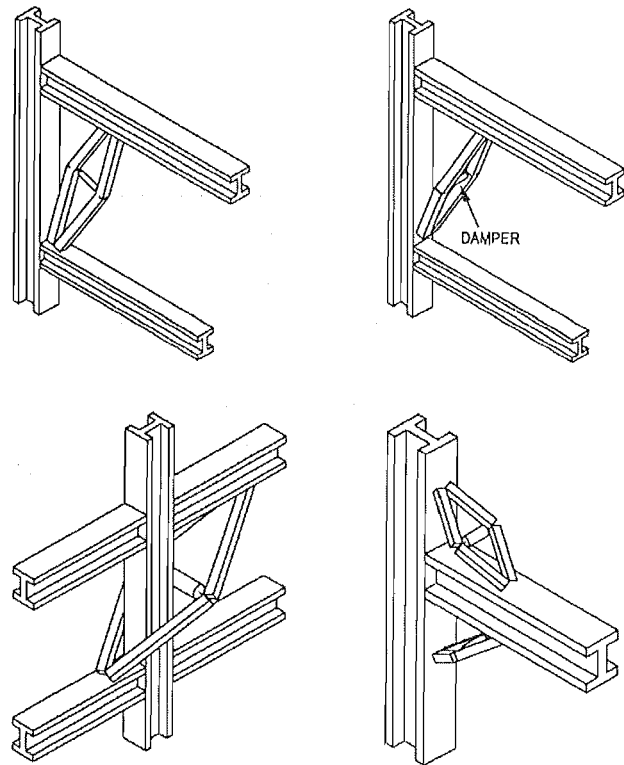


Fig (3-16) Possible installation configuration of a scissor-jack damping system [61].

The forces that act on the scissor-jack and on the single-storey frame are shown in Figure (3-15b). It should be noted that the force  $F$  represents the component of the inertia force that is balanced by forces from the damping system. Considering equilibrium in the configuration reveals the forces that develop in the scissor-braces as:

$$T = \frac{1}{2 \sin \theta} \cdot F_D \quad 3-24$$

where  $T$  and  $F_D$  denote the forces in the brace and damper, respectively. The forces  $T$  are greater than the force  $F_D$  by a factor of  $1/2 \sin \theta$  due to the shallow truss configuration of the scissor-braces [61]. The resultant of the horizontal component of forces  $T$  equals  $F$ , that is,

$$F = 2T \cos \theta \cdot \cos \psi \quad 3-25$$

The magnification factor can be written as:

$$f = \frac{F}{F_D} = \frac{2T \cos \theta \cdot \cos \psi}{F_D} = \frac{\cos \psi}{\tan \theta} \quad 3-26$$

The scissor-jack-damper system tested in a frame connected to a strong floor and subjected to an imposed displacement history is shown in Figure 3-17. The model structure was previously utilized for testing of the toggle-brace-damper system [61]. Table (3-4) shows the magnification factor  $f$  for different values of  $\psi$  and  $\theta$ .

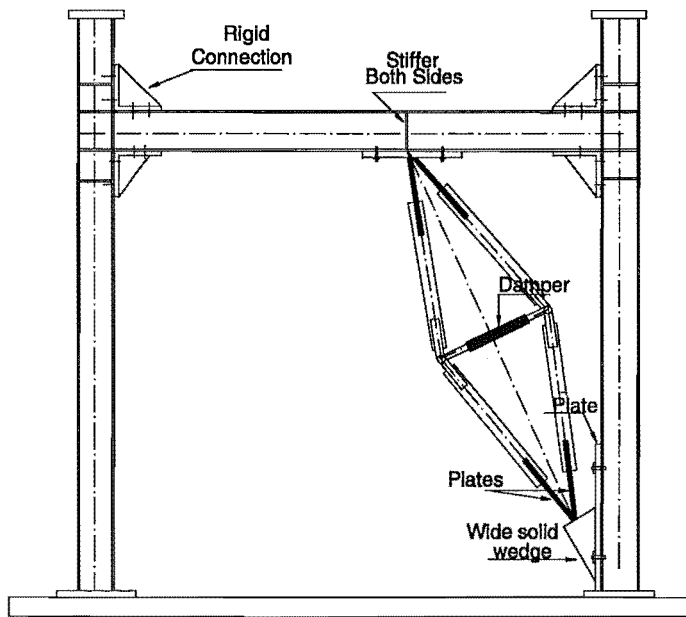


Table (3-4) magnification factor

$\psi$	$\theta$	$f$
30	10	5.06
40	20	2.11
50	30	1.12

Fig (3-17) Tested scissor-jack-damper configuration

The following conclusions can be made [61]:

- 1- The results demonstrate that the scissor-jack system operates as an effective damping system. Drifts are substantially reduced. The damped structure undergoes less than half the undamped drift. The reduction in displacement response is the combined result of stiffening of the structure and of increased damping.
- 2- There is considerable increase in the effective stiffness of the frame when significant damping forces develop. Recorded response of the frame shows 60 percent increase in effective stiffness which corresponds to about 25 percent increase in frequency. This increase in frequency is the result of viscoelastic behaviour caused by frame and energy dissipation deformations.

### **3.8 Damper -Tendon Supplemental Control System**

The main objective of this section is to present a concept for the placement of dampers which create damping forces and the transfer of these forces throughout the structure by using tendon elements. The approach is firstly contrasted with the concept of loading balancing that is presently used by designers and advocated in FEMA 273/274 [35], [36], and by Pekcan & Mander [12-15]. The damper-tendon system can be thought of as an extension to a conventional bracing system in building structures. The load-path is implicitly defined by the damper braces so as to reduce the storey shear demand on the structure. Apart from the desired load path, the benefits of added damping can be identified as a function of the damper properties and the interstorey deformations and velocities. The configuration for the proposed concept, which is originally introduced by Pekcan [13], is based on notions of load-balancing and uses a combination of damper and tendon characteristics. The system has a direct effect in balancing the lateral load demands on the structure.

The supplemental damping devices for the seismic protection of building structures are most commonly implemented in the form of interstorey bracing. A load balancing Damper-Tendon system for providing this bracing and damping is discussed in the following section.

### **3.9 Seismic Shear and Overturning Moments on Structures**

Seismic design concepts require consideration of two basic principles: i) visualization of the general nature of the deflected shape of the structure under dynamic loads as a function of a dominant response parameter, and, ii) understanding and being able to identify the continuous load path followed by the lateral forces. Any design should then proceed in a way to oppose or negate the undesired effects of the ground motion (deformation, forces,...etc.) imposed on the structural system.

Earthquake ground motions are time dependent and create inertia or lateral forces by shaking the structure back and forth. The deformation of the structure at any instant of

time is a function of the mass, stiffness and damping of the structure and of the characteristics of the ground motion. However, what is of more concern in seismic design are the maximum response quantities observed during ground shaking. Therefore, the maximum forces and deformations can be idealized with the equivalent lateral forces shown in Figure (3-18). This is similar to saying horizontal forces induced by the ground motion and transmitted to the structure cause a set of inter-storey drifts  $\Delta_i$ . This in turn corresponds to an equivalent set of storey forces  $F_i$  that act upon the structure to cause the same deformations. A general seismic design approach is to develop these numerically so that they best represent the maximum ground motion as well as structural characteristics. This kind of representation of seismically induced forces allows one to determine the storey shear force distribution and overturning moments at the peak structural response as shown in Figure (3-18).

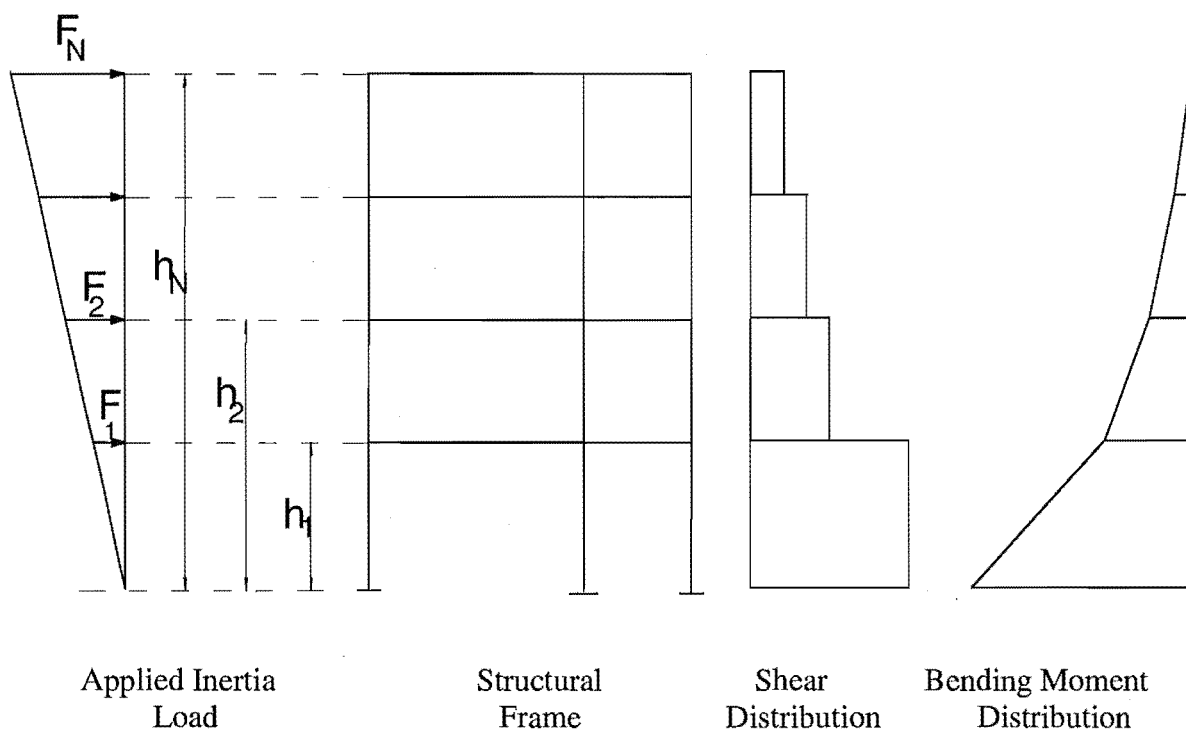


Fig (3-18) Seismic shear and overturning moment impose on structural frames.

The storey shear ( $\Sigma F_i$ ) of the equivalent static system shown in Figure (3-18) can be readily determined from the horizontal force equilibrium requirements. Similarly, the externally applied overturning moments ( $F_i h_i$ ) are resisted by the structure due to moment action, cantilever shear wall action, or braced-truss action. This observation might be the first step in determining a realistic load path followed by the externally applied seismic loads.

### 3.10 Load Balancing Solution

Consider the design of a pre-stressed concrete beam. Using post-tensioning along with a draped parabolic tendon profile, it is possible to balance gravity loads as shown in Figure (3-19). If the tendon profile has a draped parabolic profile similar to the moment diagram, then the gravity loads are balanced and deflections removed when the product of the tendon force F and the maximum eccentricity e is equal to the maximum bending moment.

$$Fe = \frac{wl^2}{8} \quad 3-27$$

where  $F$  = Tendon Forces

$l$  = length of the beam

$w$  = Distributed load per unit length

$e$  = maximum eccentricity of tendon

Alternatively, if it is not possible to use a draped tendon profile, deflections can be minimized by using a harped profile as shown in Figure (3-19). In this case the deflections are due to the difference between the parabolic shape of the gravity moment diagram and the piece-wise linear shape of the harped tendon profile (this is the shaded region in Figure (3-19)). The harped tendon profile provides point forces where the tendon suddenly changes direction; the point force (P) being equal to:

$$P = F \sin \beta \quad 3-28$$

where  $\beta$  = angle of deviation of the tendon profile.

The concept of load balancing is widely used in post-tensioned prestressed concrete design. The proposed load balancing supplemental system adopted in this research is a system composed of two major components: tendons with high axial stiffness and a supplementary damping system (damper). The Damper-Tendon system is discussed in detail in this research.

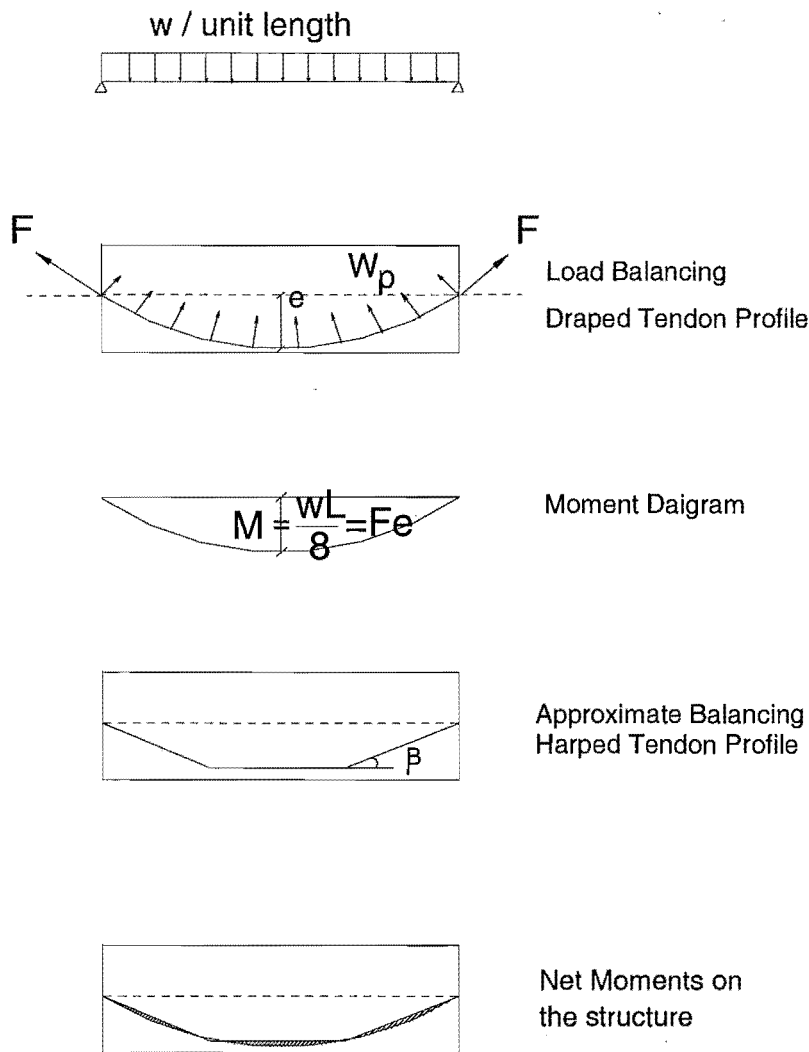


Fig (3-19) Pre-stressed concrete beam analogy with load balancing tendon

### 3.10.1 Tendon Layout for Multi-Storey Frame

The horizontal force equilibrium at a floor level (Figure 3-20) assuming rigid beam and column elements can be written as [13]:

$$F_{Ti} \cos \theta_i = \sum_{j=i+1}^N F_j \quad i = 0, \dots, N-1 \quad 3-29$$

in which  $F_{Ti}$  are the Forces in the Tendon at the  $i^{th}$  level and  $\theta_i$  is the angle of inclination of the  $i^{th}$  floor Tendon and  $F_j$  is the horizontal lateral load or storey shear at level  $i$ .

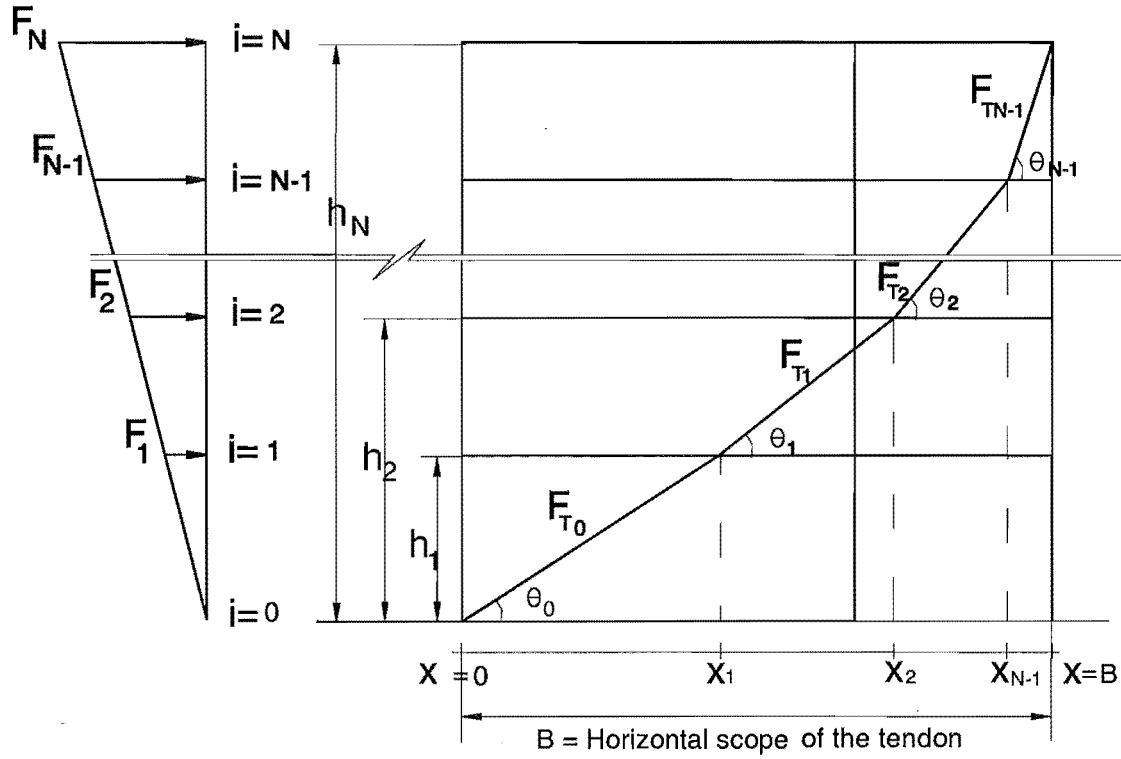


Fig (3-20) Determination of tendon layout

Similarly, vertical force equilibrium at each floor level can be written as

$$F_{Ti} \sin \theta_i = F_{Ti+1} \sin \theta_{i+1} \quad i = 0, \dots, N-2 \quad 3-30$$

Equation (3-30) can be written as

$$\frac{F_{Ti} \cos \theta_i}{F_{Ti+1} \cos \theta_{i+1}} = \frac{\tan \theta_{i+1}}{\tan \theta_i} = \frac{h_{i+2}(x_{i+2} - x_{i+1})}{h_{i+1}(x_{i+1} - x_i)} \quad 3-31$$

Substituting Equation (3-29) into Equation (3-31) gives:

$$\frac{h_{i+1}}{h_{i+2}} R_{i,i+1} = \frac{x_{i+1} - x_i}{x_{i+2} - x_{i+1}} \quad i = 0, \dots, N-2 \quad 3-32$$

in which  $h_{i+1}$  = storey height between level  $i$  and  $i+1$ , and

$$R_{i,i+1} = \sum_{j=i+1} F_j / \sum_{j=i+2} F_j \quad 3-33$$

is the ratio of the storey shear at the  $i^{th}$  to that at  $i+1^{th}$  level.

Equation (3-32) defines a system of  $N-1$  simultaneous equations with  $N-1$  unknowns,  $x_i$ :

$$\begin{aligned} x_0 - \left(\frac{h_1}{h_2} R_{0,1} + 1\right)x_1 + \frac{h_1}{h_2} R_{0,1} x_2 &= 0 \\ x_1 - \left(\frac{h_2}{h_3} R_{1,2} + 1\right)x_2 + \frac{h_2}{h_3} R_{1,2} x_3 &= 0 \\ &\vdots & 3-34 \\ &\vdots \\ x_{N-3} - \left(\frac{h_{N-2}}{h_{N-1}} R_{N-3,N-2} + 1\right)x_{N-2} + \frac{h_{N-2}}{h_{N-1}} R_{N-3,N-2} x_{N-1} &= 0 \\ x_{N-2} - \left(\frac{h_{N-1}}{h_N} R_{N-2,N-1} + 1\right)x_{N-1} &= x_N \end{aligned}$$

where  $x_0 = 0$ , and  $x_N = B$ , the width of the tendon system in the structure.

Finally, the tendon layout can be determined by solving the tri-diagonal matrix equation defined by equation (3-35).

$$[R]\{x\} = \{D\} \quad 3-35$$

where  $[R]$  is the coefficient matrix determined by:-

$$[R] = \begin{bmatrix} -(R_{0,1} + 1) & R_{0,1} & 0 & 0 & 0 & 0 & 0 \\ 1 & -(R_{1,2} + 1) & R_{1,2} & 0 & 0 & 0 & 0 \\ 0 & 1 & -(R_{2,3} + 1) & R_{2,3} & 0 & 0 & 0 \\ 0 & 0 & 1 & . & . & 0 & 0 \\ 0 & 0 & 0 & 1 & . & . & 0 \\ 0 & 0 & 0 & 0 & 1 & . & 0 \\ 0 & 0 & 0 & 0 & 0 & 1 & -(R_{n-3,n-2} + 1) \\ 0 & 0 & 0 & 0 & 0 & 0 & (R_{n-3,n-2}) \\ 0 & 0 & 0 & 0 & 0 & 1 & -(R_{n-2,n-1} + 1) \end{bmatrix}_{n-1,n-1} \quad 3-36$$

where the diagonal  $= -(R_{i-1,i} + 1)$   
the above diagonal  $= (R_{i-1,i})$   
the below diagonal  $= 1$   
and  $i = 1, n-1$

$\{x\}^T = \{x_1, x_2, \dots, x_{n-1}\}$  is the unknown column vector of tendon coordinates,

$$\{D\}^T = \{0, \dots, -R_{n-2,n-1}B\}$$

where  $B$  is the width of the tendon layout of the structure.

The above derivation may be performed assuming an equivalent static lateral force applied to the frame structure. However, since the lateral deformations will only cause small angle changes, the lateral force distribution will in fact remain unchanged. The so-called load balancing tendon layout has the shape of the moment diagram scaled to the tendon's horizontal projected width. An example on this method is presented in chapter 8.

### 3.10.2 Straight Tendon

An approximate load balancing solution (the simplest approach to an equivalent harped tendon), can be employed in which the draped tendon system is replaced with a straight tendon as shown in Figure (3-21).

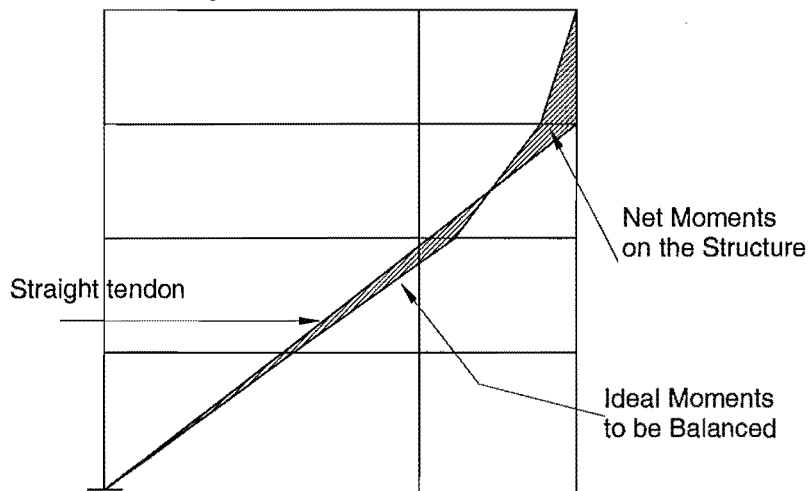


Fig (3-21) Straight tendon

It must be noted that the straight tendon layout does not provide damping forces at each storey. This approach is analogous to the approximate load balancing with harped tendons as mentioned previously for the laterally loaded beam. However, the net moments on the structure can be minimized by carefully selecting the tendon layout.

The damping forces are applied to structures by dampers which are preferably (but not necessarily) placed at the lower end of the tendon (at the ground floor of buildings). The tendon layout is designed to be in piecewise continuous segments that pass through holes located in the floors of the buildings. Typical details are shown schematically in Figure (3-22).

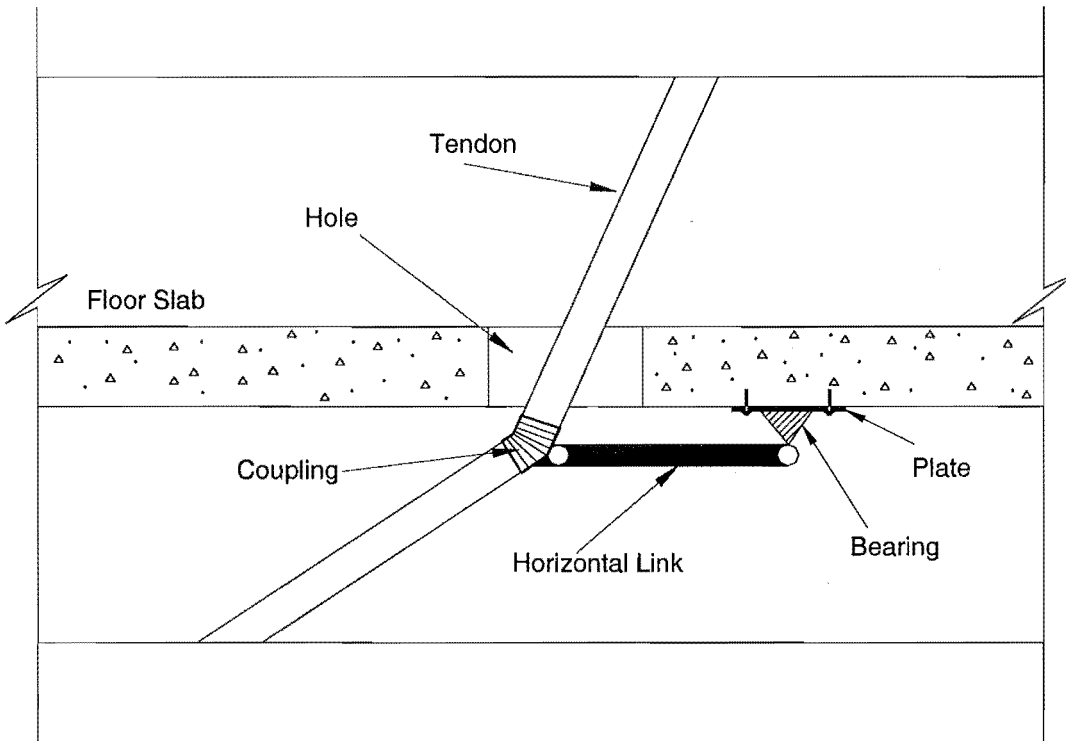


Figure (3-22) Tendon-floor slab details.

As can be seen from Figure (3-22), the damping forces are transferred in the horizontal direction by connecting the tendons via links to the floor slabs. The connection force has a horizontal component which must be resisted by the floor slab action.

In the case of the structure used in the experimental study, horizontal links are used to transfer the damping forces provided by the dampers to the floors. The horizontal links are modelled as spring members in the analytical analysis, and placed at the first and second floors to simulate the connection of the tendon to the floor slab the four storey frame. This is discussed in details in chapter 5. Significant forces will not be expected to be transferred by the horizontal links because the tendon is effectively straight from the base to the third floor anchorages. However, the links pick up the lateral inertia forces of the tendon and are also used to stabilize the tendon against buckling by reducing the effective unrestrained length.

### **3.11 Concept Development of the Supplemental Control System**

Much research has been done to date on the seismic design of new structures and the retrofit of existing structures. The objective of conventional approaches to seismic design is to improve the displacement capability either through the use of ductile detailing or the use of seismic isolation. More recently, researchers have sought to control seismic demands by using supplemental energy dissipation systems. Various types of devices, both active and passive, have been investigated both experimentally and analytically on models, as well as, on full-scale structures. As a result, an increasingly popular design and retrofit alternative is to incorporate supplemental energy dissipating devices to control structural deformations.

The alternative configuration proposed called the “load balancing damper-tendon system” which is designed to balance the earthquake forces on the structure by means of a draped tendon coupled with a supplemental damping system. This alternative approach, when properly designed, reduces the overturning moment demand as well as the storey shear demand on the structural elements. In most cases, it is economically more feasible because of the reduced number of devices needed in the supplemental damping system. Moreover, it provides optimal damping forces for the assumed vertical distribution of the inertial loads at each floor level. This approach can be applied to both relatively stiff structures as well as for flexible structures.

### **3.12 Concept Validation**

Dissipating seismic input energy can be achieved by means of specially designed non-structural elements or devices. The present study provides an alternative and potentially more economical solution that is based on the principles of passive control. The proposed seismic approach is intended to protect structures by introducing a tendon system with an energy dissipation device at the over end of the tendon.

For the purpose of validating the concept described above, a series of shaking table experiments were to be conducted on a model structure. The structural model shown in Figure (3-23), was constructed by Kao [11] and was subjected to unidirectional input ground motion on the shake table in the Structural Laboratory of the Civil Engineering Department, at the University of Canterbury. A prominent feature of this model building was the incorporation of special joint elements designed to form plastic hinges. These elements were designed to be able to be replaced with minimum effort and at a low cost. Descriptions of the building are presented in chapter 5. The shaking table tests were conducted on the model structure both with and without the supplemental control system which consisted of a damper and an approximate load-balancing straight tendon.

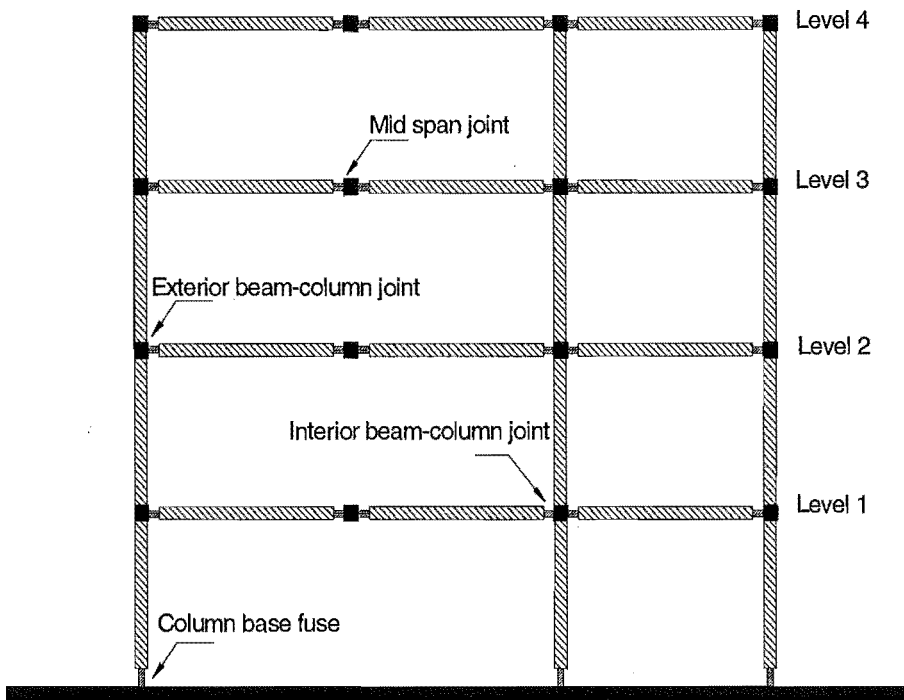


Fig (3-23) Elevation view of the test structure

### 3.13 Damper Type

Studies were carried out on Magneto-Rheological (MR) fluid dampers by researchers in Notre Dame University's Structural Dynamics and Control/Earthquake Engineering Laboratory. In the early stages of the present study, the author attempted to get commercially available devices from the Lord Corporation which produces this type of damper for the experimental tests because they might be available in sizes suitable for the experimental tests and the ability to change their properties. The Lord Corporation did not have a seismic damper available as they were still under development. The commercial devices that were available have a very small off-the shelf stroke and generate very small forces. Several of them could be used in parallel with mechanisms or levers to increase the force through mechanical advantage but would not be suitable for these seismic tests. Secondly, it was preferred to concentrate on passive devices. An alternative type of device, a ring spring damper was selected instead.

The ring spring damper investigated in the present study has had much use in a wide range of industrial, defence and civilian applications. The dampers are used in many industrial applications including steel mills and process treatment industries, as well as heavy duty material handling systems such as cranes. Military applications include shock absorption devices on missile and gun recoil systems.

### 3.14 Fields of Applications for Ring Springs in Mechanical Engineering

Ring spring are employed in the mechanical engineering sector when high kinetic energy must be absorbed and damped or when springs of relatively compact dimensions are required for high forces. The following examples illustrate the many application possibilities of ring spring in mechanical engineering: cranes, drill hammers, machine tools, lifts, landing gears, roller tables, locomotives, actuators, excavators, air brakes, and vehicle steering mechanisms.

The passive control technique using ring spring dampers, attracted attention for this study because it is a simple, yet highly effective means of reducing seismic loads experienced by structures during earthquakes. The proposed ring spring damper has the following advantages:

- The springs reduce the seismic displacements, thus avoiding damage in the structure.
- Suitably designed ring springs are capable of absorbing 60-70 percent of the input seismic energy with each cycle of vibration.

It was decided to use double acting devices working in compression and tension in the experimental tests to reduce the cost and to make them easy to attach to the tendon system. Single-acting dampers were modified to enable the application of seismic protection of building structures as described in chapter 5.

### 3.15 Comparison between Single and Double Tendon System

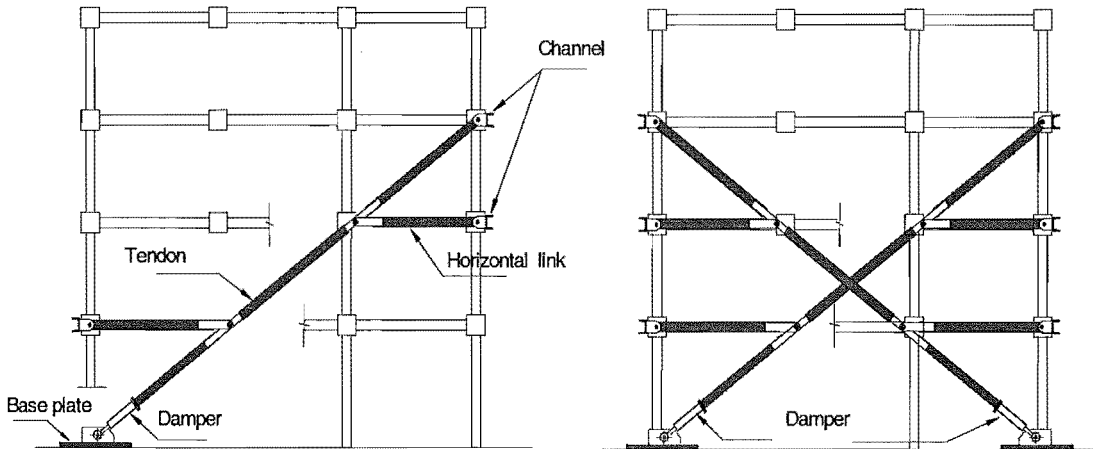


Fig (3-24) Supplemental control system with one frame of the test structure

Table (3-5) Number of elements when using single and double tendon system

Type of system	dampers	Channel sections	Horizontal links	Tendon	Base plate	Connections
Single tendon	1	3	2	1	1	7
Double tendon	2	6	4	2	2	14

From Figure (3-24) and Table (3-5) it can be seen that using a single tendon system in the supplemental control system leads to saving in both cost and ease of construction. The numbers of elements required for the supplemental system using single tendon is half of the elements and connections when using double tendon.

### **3.16 The Benefits of the Damper-Tendon System**

Many experimental and analytical studies have been undertaken on the investigation of various methods of control, that use either passive, semi-active and active energy dissipation devices. These studies have shown that seismic control of structures using supplemental energy dissipating systems is a viable alternative to the conventional practice of ductility-based toughening / strengthening and base isolation approaches.

Typically, control methods target reduced seismic demand via increased supplemental damping. This is achieved by dissipating input energy by means of specially designed non-structural elements or devices. The proposed damper-tendon system is composed of two major components, a tendon with high axial stiffness and a damper device located at the ground floor. The benefits of the damper-tendon system can be summarised as follows [13]:

1. The damper-tendon system approach is intended to reduce the response of the structures by introducing a tendon system throughout the structure and an effective type of energy dissipation device on the end of the tendon.
2. The damper-tendon system provides an alternative and potentially more economical solution than that based on the principles of base isolation.
3. A damper-tendon system is proposed in which the total design damper capacity is distributed along the height of the building in proportion to the design storey shears.
4. The damper-tendon solution reduces interstorey deformations within a structure through added damping.
5. The damping forces generated in the supplemental system are transferred to the floor slabs and oppose the inertial loads. The tendon layout is designed to counteract the inertial forces hence to reduce the overturning moments, thus a draped tendon results. However, a linear tendon profile may be used as a simplification of the lateral load balancing concept.
6. The load-balancing technique in the seismic design of building proved to be promising as the seismic response is reduced even by the approximate straight tendon solution.
7. High strength steel tendons can provide the lateral strength efficiently. In real prototype applications, shear forces can be safely transferred to the foundation level by the tendons.

## Chapter 4

### Ring Springs

#### **4.1 Introduction**

A new passive energy dissipater for seismic study based on a self-centring friction mechanism is the ring spring. Ring springs are frictional devices consisting of inner and outer rings that have tapered mating surfaces as shown in Figure (4-1). As the spring column is loaded in compression or tension, the axial displacement is accompanied by sliding of the rings on the conical friction surfaces. The outer rings are subjected to circumferential tension (hoop stress), and the inner rings experience compression.

This research project has concentrated on this type of energy dissipater for several reasons:

- Ring springs are totally passive dampers for extreme reliability, no dependence on external power sources to effect the control action which may not be available during major earthquakes.
- Ring spring dampers are constructed of steel materials. No liquid leakage and no refilling or maintenance of any of the parts is needed which are potential problems with viscous dampers.
- Ring spring devices are easy to install in structures thus saving time and materials. They do not require large building preparation to support the devices as in tuned or liquid mass dampers.
- Some of the other ways of adding supplemental damping to structures can be costly and involve major modifications to the structure as in a base isolation system. It is possible to secure a comparable degree of earthquake response mitigation with ring spring dampers located throughout a structure without having to isolate the building.
- Ring springs have powerful friction dampening.
- High spring work combined with low weight and volume.
- High capacity.
- Characteristic independent of loading rate.
- Simple and Compact design.

This chapter details the characteristics, the dynamic behaviour and the advantages of ring spring dampers. The details of the damper devices used in the experimental tests are also presented.

## Ring Springs



Fig (4-1) Prototype ring springs [33]

## 4.2 Details of Construction

Ring springs consist of a series of separate inner and outer ring elements with mating taper faces assembled in columnar form (Figure 4-2).

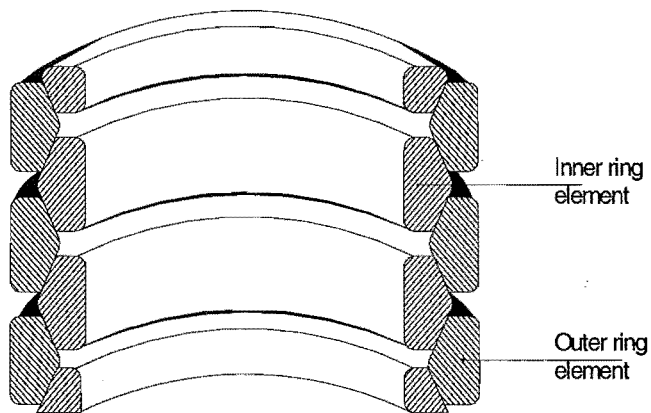


Fig (4-2) Section through ring springs

Under the application of an axial load, the wedge action of the taper faces causes the inner elements to radially contract and the outer elements to radially expand, allowing axial deflection (Figure 4-3). Sliding action between mating elements results in a large amount of energy being absorbed in overcoming the friction forces.

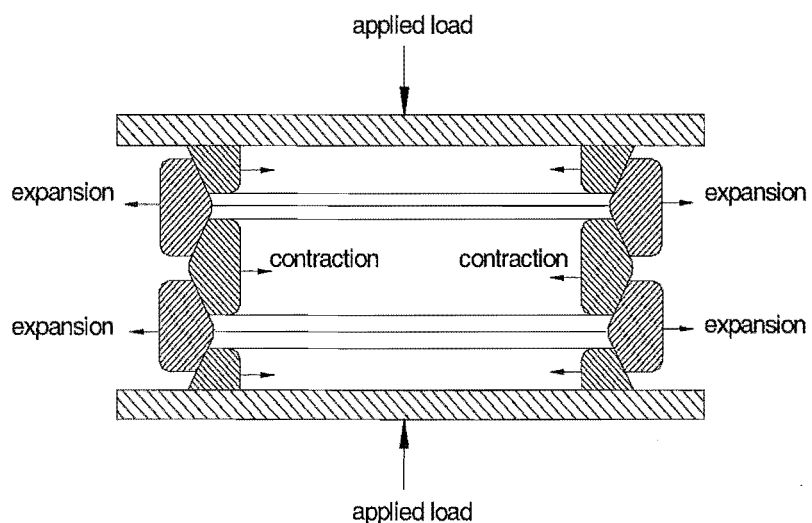


Fig (4-3) Loaded ring springs

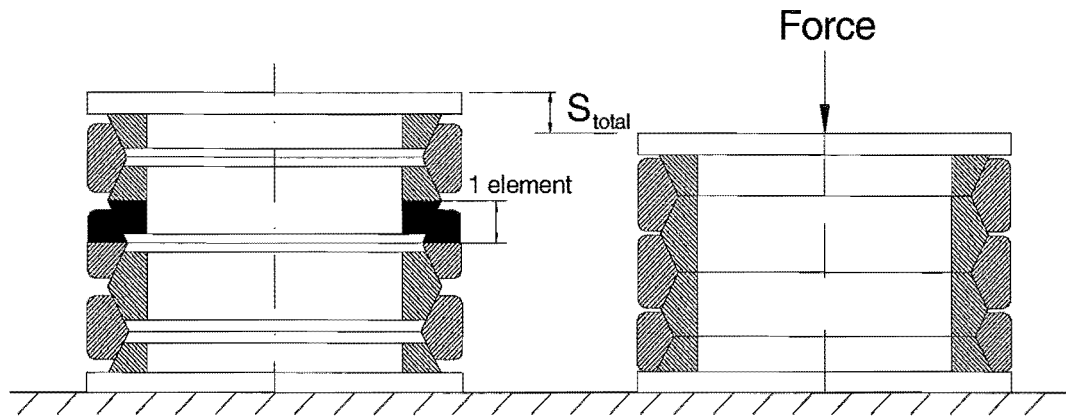


Fig (4-4) Deflection of a friction spring

One effective taper face i.e. one half inner ring and one half outer ring is defined as one element. This example is of a friction spring consisting of four outer rings, three inner rings and two half inner rings. As shown in Figure (4-4), this consists of eight elements. The figure shows the fully compacted device. This version of the device is not able to take tension forces.

#### 4.2.1 Single-Acting Ring Spring

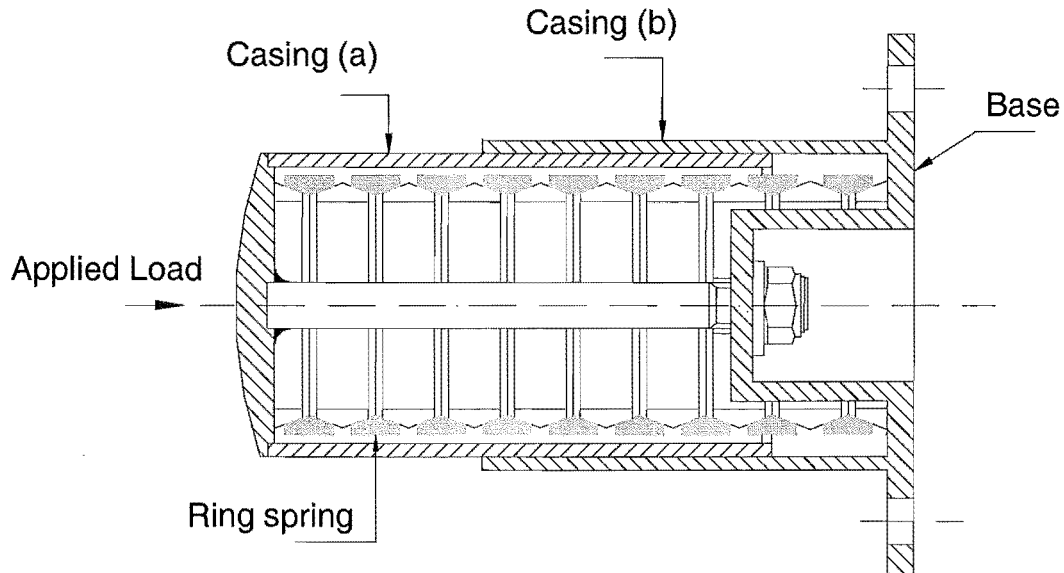


Fig (4-5) Single acting ring spring

Ring springs are used mainly in compression applications. Fig (4-5) shows a single acting ring spring damper, which is able to carry compression only. In this case the spring has to be pre-tensioned together with the casing components (a) and (b). The rings can neither be observed during pre-tensioning nor subsequently properly aligned. It can be shown that the casing (a) only moves under load while the casing (b) is fixed on the base plate. The nut is used to apply the pre-load which is needed to ensure that the spring column is aligned in the direction of the damper axis.

#### 4.2.2 Pre-load

Friction springs should be preloaded to 5 to 10% of their maximum forces in order to retain a spring column that is aligned in the direction of the axis. The friction springs should be installed in the casing as preloading spring cartridges and to hold the casing components together.

#### 4.2.3 Double-Acting Ring Spring

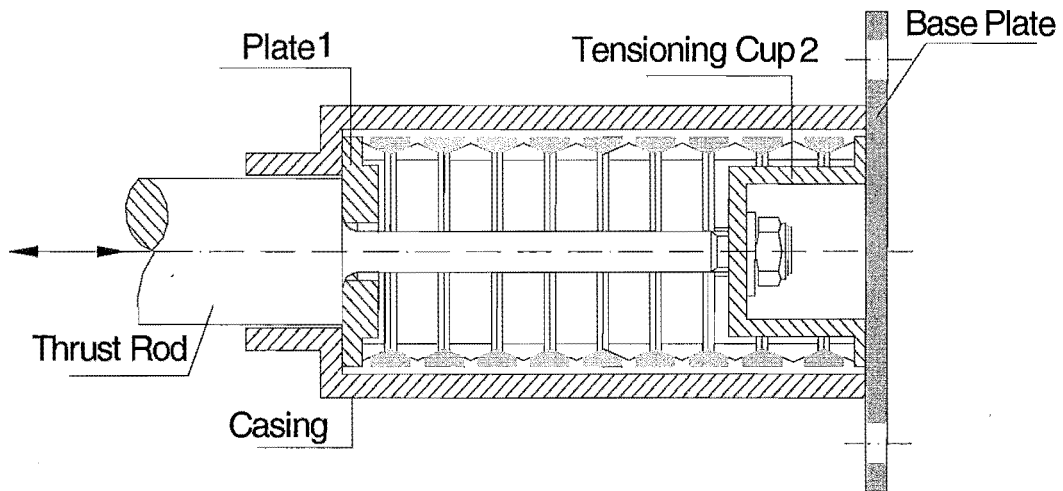


Fig (4-6) Double acting ring spring

To use the ring spring as a seismic energy dissipating device, it should act to resist the forces induced by earthquakes hazard in both the compression and the tension directions. A double acting spring arrangement is shown in its basic form in Figure (4-6).

Under loading in tension, plate (1) remains fixed, and the tensioning cup (2) moves. This is reversed when the damper is compressed. The two parts 1, 2 must be in

contact with both the shoulders in the casing and with the rod. By means of the nut on the tie and thrust rod a pre-load can be applied.

### 4.3 Characteristics of Ring Springs

#### 4.3.1 Linear Characteristic

Friction springs often serve as buffers, which have to absorb the kinetic energy of a moving mass. To protect the structural components one aims at the smallest possible forces in the end position. Often a high terminal force of a buffer is regarded as an advantage – but the contrary is the case: buffers should exhibit a maximum possible energy absorption capacity in conjunction with low forces.

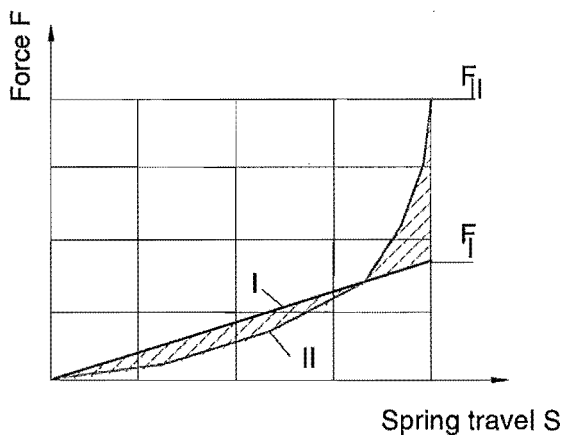


Fig (4-7) Linear I and non-linear II diagram at same energy absorption

Figure (4-7) shows, for comparison, two spring characteristic curves with the same spring work and same travel. As can be seen, the spring with a progressive characteristic II attains a much higher impact force than spring I with a linear characteristic. Although the progressive pattern of the spring characteristic may be quite desirable, such a characteristic is disadvantageous in any spring intended for use as a buffer as it required greater foundation forces.

#### 4.3.2 Overloaded-Safe in Blocked Position

Ring springs are generally designed to “block”, i.e. when the maximum spring travel is reached, the plane surfaces of the inner rings touch and form a rigid column as shown in Figure (4-4).

This ensures that the forces at blocking cannot be exceeded and the friction springs do not suffer any damage. In actual applications, however, such loading conditions

should be avoided because the spring is not effective in its “blocked” solid position. As a consequence, high peak forces may result which jeopardize the structural components due to the high acceleration that may be passed to the structure.

### 4.3.3 Effect of the Number of Rings

Friction springs are made up of similar inner and outer rings. By changing the number of elements any desired spring travel and hence any spring stiffness can be obtained. As can be seen from (Figure 4-8), the blocking force for different numbers of elements remains the same. The total spring displacement and hence stiffness depend on the number of elements used.

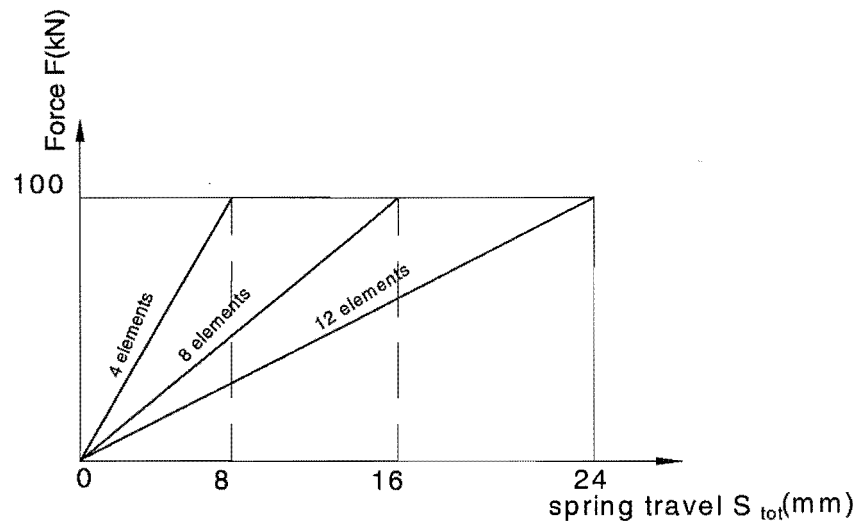


Fig (4-8) Influence of the number of elements on the spring characteristic for a typical ring spring damper

### 4.3.4 Temperature Independence

In spring or damping systems consisting of synthetic materials or employing the viscosity effect of a liquid, the force-travel diagram is influenced by temperature fluctuations and inherent temperature rises. The characteristic curve of a steel spring, however, remains independent of these factors within certain limits. Ring springs can be employed in the temperature range from  $-40^{\circ}\text{C}$  to  $+80^{\circ}\text{C}$  without the properties changing appreciably.

## 4.4 Force-Travel Relationship

The elastic property of any spring is uniquely determined by its characteristic curve, i.e. by the force-travel diagram indicating the pattern of the spring force  $F$  as a function of spring travel  $S_{total}$ . The characteristic force-travel relationship of the ring springs depends on whether loading or unloading is taking place and the different stages are described in the following sections.

### 4.4.1 Behaviour in the Absence of Friction

Assume there is no friction acting on the taper surfaces of the rings, then according to Hooke's law there is a linear relationship between spring travel  $S_{total}$  and force  $F_{elast}$  as the rings are deformed (Figure 4-9).

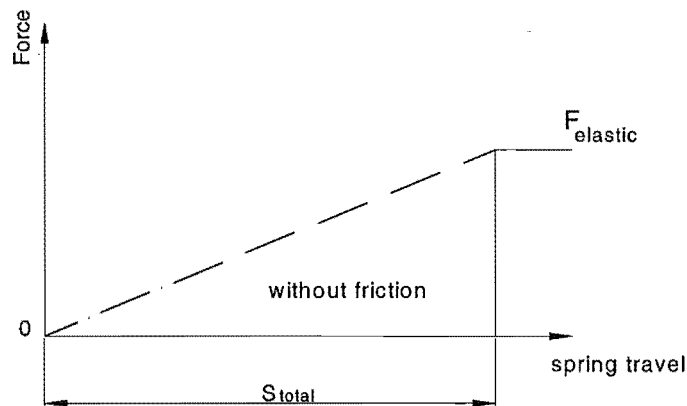


Fig (4-9) Force versus spring travel relationship in the absence of friction

### 4.4.2 Friction Forces under Load

The force  $F_{elast}$  is needed to expand the outer rings and simultaneously contract the inner rings. In addition, however, the friction forces acting on the taper surfaces have to be overcome. The friction force  $R_1$  is proportional to the force  $F_{elast}$ , so that the linear loading curve OF is obtained (Figure 4-10).

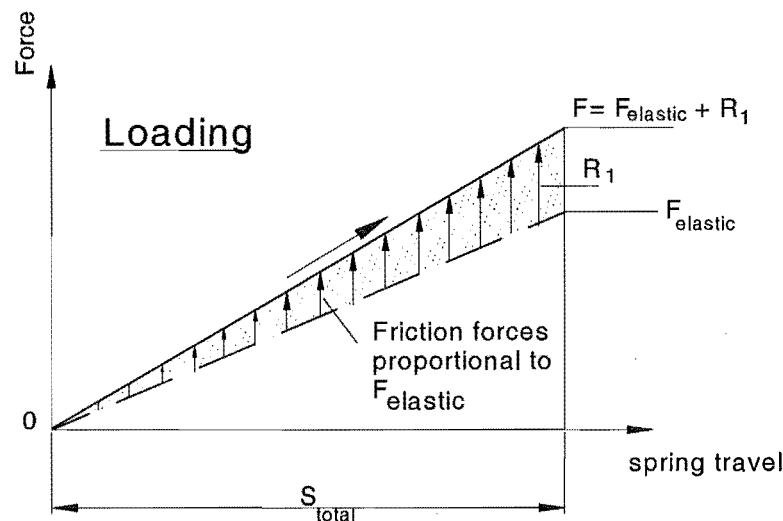


Fig (4-10) Friction forces once loading is applied

#### 4.4.3 Friction Forces on Load Removal

Since the friction force  $R_1$  occurs only when the rings are moved in the direction of loading, the force  $F$  can be reduced by the figure  $R_1$  to  $F_{elast}$  - with the result that the spring is decompressed because the peripheral stresses in the springs force apart the various spring elements with a force of only  $F_{elast}$  (Figure 4-11).

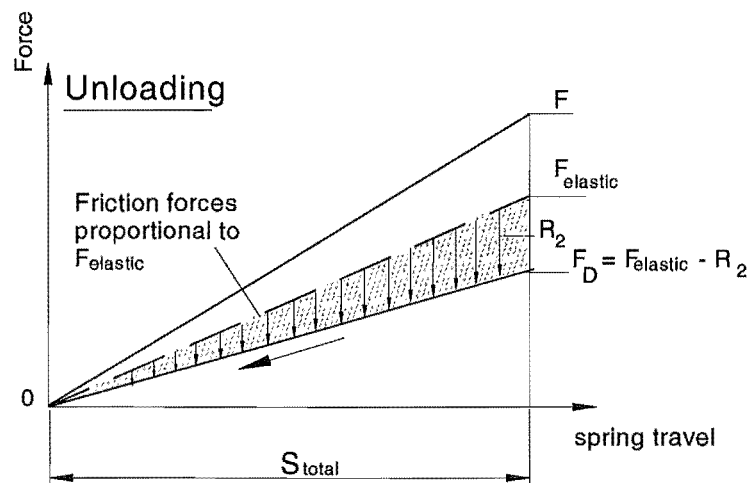


Fig (4-11) Braking friction forces on unloading

On decompression, braking friction forces  $R_2$  counteract the force  $F_{elast}$ , when the external load force is reduced to a value of  $F_D = F_{elast} - R_2$ .

The spring can decompress. The force  $F_D$  is about one-third of the maximum force  $F$ .

#### 4.4.4 Complete Force-Travel Diagram

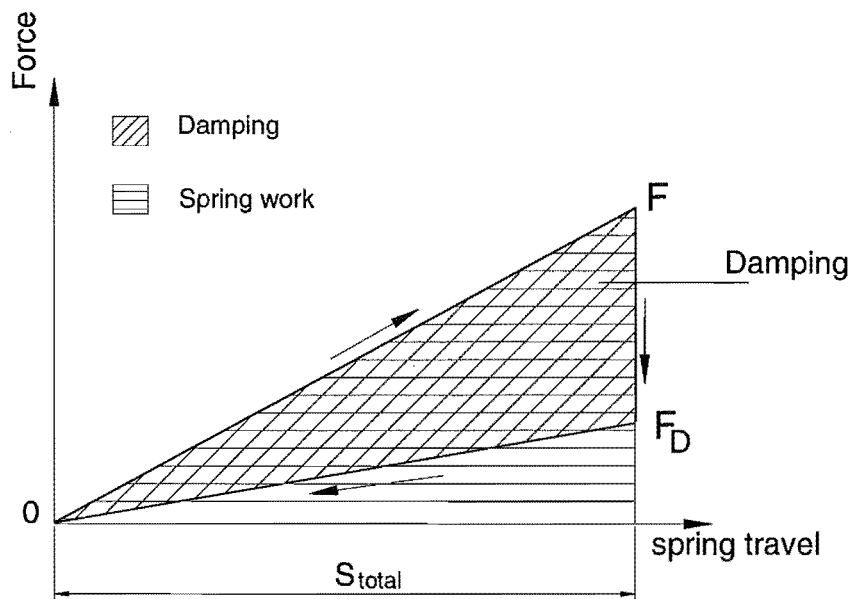


Fig (4-12) Force-travel diagram

Figure (4-12) shows the complete force-travel diagram of the ring spring. The closed diagram is to be interpreted clockwise. The area between the load curve OF and the abscissa (travel axis) is a criterion of the spring work absorbed, while the hatched hysteresis area represents the damping, i.e. the proportion of the energy converted into heat.

#### 4.5 Ring Spring Hysteresis Relationship

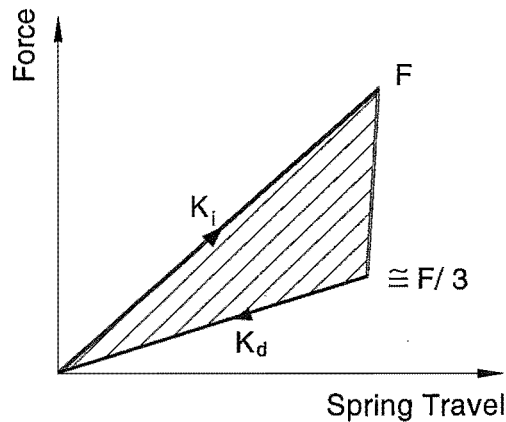


Figure (4-13) Ring spring hysteresis diagram

The area under the load-deflection diagram (Figure 4-13) corresponds to the work done or the input energy, while the hatched area within the loop is a measure of the

absorbed energy and represents effective damping. The lost energy amounts to 66% of the input work and is dissipated as heat due to friction at the spring interfaces.

These stiffnesses,  $K_i$  (ring spring stiffness when an increasing load is applied),  $K_d$  (ring spring stiffness when a decreasing load is applied), give rise to the general form of the ring spring hysteresis diagram as shown in Figure (4-13). As the axial load applied to the ring spring is increased, motion proceeds from the origin up to the slope  $K_i$ , when the axial load is reduced, motion proceeds down the slope  $K_d$ . This effect is the result of reversal of frictional force ( $\mu N$ ) acting at the element interfaces.

To ensure that the friction properties of ring springs remain reasonably constant for repeated load-unload cycling, it is essential that the elements be lubricated. Hence grease lubrication is provided during initial spring assembly. Lubricant selection directly affects the coefficient of friction  $\mu$ . The best compromise between energy absorption capability and requirement for spring recoil gives rise to practical ring springs with a taper angle,  $\alpha$  of between  $14^\circ$  to  $15^\circ$ , and coefficient of friction,  $\mu$  ranges between 0.09 - 0.12. Well lubricated ring spring assemblies do not require further lubrication for 100,000 load-unload cycles [7].

#### 4.5.1 Double-Acting Hysteresis

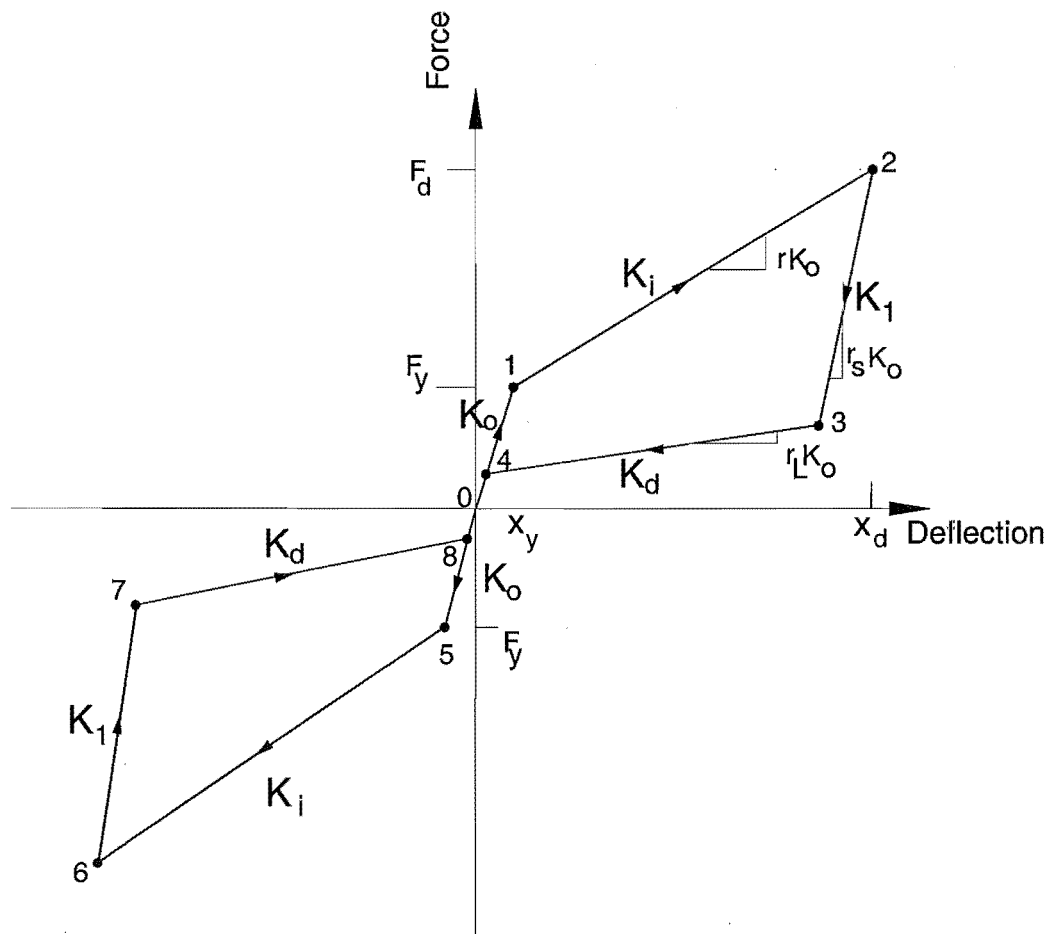


Fig (4-14) Force/deflection diagram for double acting ring spring

With reference to Figure (4-14), the hysteretic behaviour of the ring spring can be characterized by four different physical parameters [7]:

$k_o$  = elastic stiffness (from the origin to point 1)

$k_i$  = ring spring stiffness when an increasing load is applied (point 1 to point 2)

$k_1$  = ring spring stiffness between  $k_i$  and  $k_d$  (point 2 to point 3)

$k_d$  = ring spring stiffness when a decreasing load is applied (point 3 to point 4)

where:

$$k_i = r k_o$$

$$k_d = r_L k_o \quad (r_L \text{ is the lower unloading stiffness factor})$$

$$k_1 = r_s k_o \quad (r_s \text{ is the steeper unloading stiffness factor})$$

In applying load to a pre-loading system, sufficient force must be applied to the ring spring for motion to proceed along stiffness path from point 0 to point 1 Figure (4-14). That force is to overcome frictional resistance before sliding action within the ring spring commences. This gives rise to an elastic stiffness,  $k_o$  active between points 0-1. As load is increased, displacement continues between points 1-2. During the next phase of displacement unloading proceeds between points 2-3 and then continues along stiffness  $k_d$  to point 4, returning to the origin along stiffness  $k_o$ . This motion is repeated when the direction of the loading/unloading is reversed. Thus, motion proceeds around points 0-1, 1-2, 2-3, 3-4, 4-5, 5-6, 6-7, 7-8, and 8-0 for a complete load/unload cycle. The enclosed area represents the total energy absorbed for one full cycle.

The hysteresis diagram shown in Figure (4-14) shows that as displacement increases, the energy absorption per unit increase in displacement also increases. Hence, greater energy absorption is possible at larger displacements.  $k_o$  is the elastic stiffness of the spring.

#### 4.6 Ring Spring Stiffness Equations

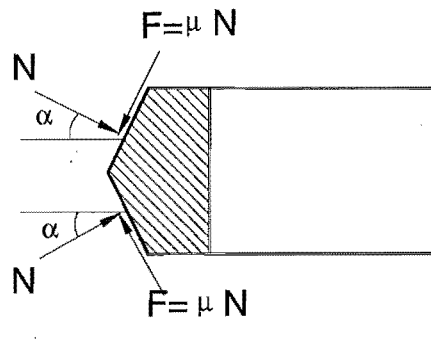


Fig (4-15) Inner ring element forces

For the case of an increasing compression load, the forces acting on an inner ring element are shown in Figure (4-15).

The total radial force acting on the ring element equals:

$$2(N \cos \alpha - F \sin \alpha) \quad 4-1$$

For increasing compressive force

$$P_i = \frac{N(\tan \alpha + \mu)}{(1 - \mu \tan \alpha)} \quad 4-2$$

$$N = \sigma \pi A \quad 4-3$$

where  $\sigma$  = ring hoop stress and  $A$  = effective cross sectional area of a ring. Therefore

$$P_i = \frac{\sigma \pi A (\tan \alpha + \mu)}{(1 - \mu \tan \alpha)} \quad 4-4$$

assuming inner and outer rings have the same effective area i.e.  $A = A_i = A_0$

For decreasing compressive force

$$P_d = \frac{\sigma \pi A (\tan \alpha - \mu)}{(1 + \mu \tan \alpha)} \quad 4-5$$

The total spring deflection

$$S_{total} = \frac{n\sigma(d_1 + d_2)}{2E \tan \alpha} \quad 4-6$$

The ring spring stiffness equation can be defined as follows [7]:

$$K_i = \frac{P_i}{S_{total}} = \left[ \frac{2\pi EA}{n(d_1 + d_2)} \cdot \frac{\tan \alpha (\tan \alpha + \mu)}{(1 - \mu \tan \alpha)} \right] \quad 4-7$$

$$K_d = \frac{P_d}{S_{total}} = \left[ \frac{2\pi EA}{n(d_1 + d_2)} \cdot \frac{\tan \alpha (\tan \alpha - \mu)}{(1 + \mu \tan \alpha)} \right] \quad 4-8$$

To determine the energy absorbed during the loading and unloading portions separately, the elastic stiffness of the ring spring,  $K_e$ , is obtained by setting  $\mu = 0$  in either equation 4-7 or 4-8. The elastic stiffness for the ring spring is given by equation 4-9.

$$K_e = \left[ \frac{2\pi EA}{n(d_1 + d_2)} \cdot \frac{\tan^2 \alpha}{1} \right] \quad 4-9$$

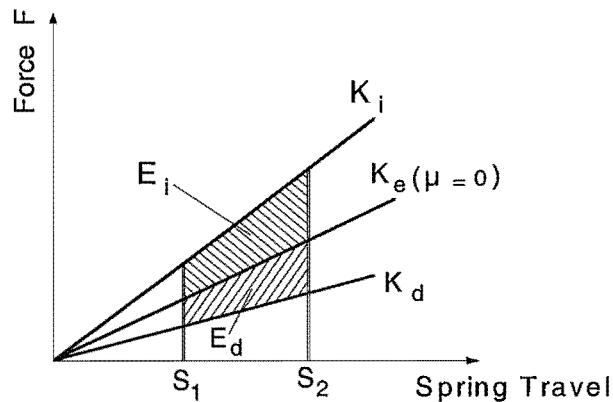


Fig (4-16) Energy absorption for loading and unloading

As shown in Figure (4-16), the area below  $K_i$  and above  $K_e$  represents the energy absorbed for spring loading,  $E_i$ , while the area below  $K_e$  and above  $K_d$  represents the energy absorbed for spring unloading  $E_d$ . Expressions for the energy absorbed by the enclosed areas  $E_i$  and  $E_d$  are [7]:

$$E_i = \frac{(K_i - K_e)(S_2^2 - S_1^2)}{2} \quad 4-10$$

$$E_d = \frac{(K_e - K_d)(S_2^2 - S_1^2)}{2} \quad 4-11$$

#### 4.7 Number of Elements

The choice of the ring spring size simultaneously determines the outer and inner guide diameters  $D_2, d_2$  and also the terminal force  $F$ . The necessary number of elements "e" is calculated from the required spring travel.

$$e = \frac{S_{tot}}{S_e} \quad 4-12$$

where:  $S_e$  is the spring travel for one element.

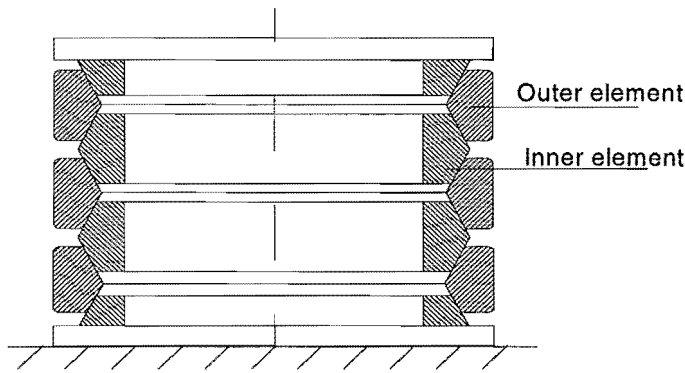


Fig (4-17) Standard layout of ring spring

The standard spring as shown in Figure (4-17) terminating with half inner rings exhibits the most favourable characteristics, an even number of elements "e" is selected as far as possible; the spring then consists of:

$$\text{Outer rings} = \frac{e}{2} \quad 4-13$$

$$\text{Inner rings} = \frac{e}{2} - 1 \quad 4-14$$

$$\text{Half inner rings} = 2 \quad 4-15$$

The un-compressed length  $L_o$  of the ring spring is calculated from:

$$L_o = e.h_e \quad 4-16$$

where  $h_e$  is the length of an element.

The total spring travel  $S_{tot}$  results from:

$$S_{tot} = e.s_e \quad 4-17$$

The following Table (4-1) comprises all springs being in series with blocking forces from 5 to 1800 kN

Table (4-1) Details of available ring spring [33].

Diagram		Dimensions					Guide		Weight
F (kN)	$s_e$ (mm)	$W_e$ (j)	$h_e$ (mm)	$D_1$ (mm)	$d_1$ (mm)	$b/2$ (mm)	$D_2$ (mm)	$d_2$ (mm)	$G_e$ (kg)
5	0.4	1.0	2.2	18.1	14.4	1.8	18.6	14.0	0.001
9	0.6	2.7	3.1	25.0	20.8	2.5	25.7	20.0	0.003
14	0.8	5.6	4.0	32.0	27.0	3.2	32.9	26.2	0.006
20	0.9	9.0	4.7	38.0	31.7	3.8	39.0	30.8	0.011
26	1.0	13.0	5.2	42.2	34.6	4.2	43.4	33.5	0.016
34	1.1	18.7	5.9	48.2	39.4	4.8	49.6	38.1	0.024
40	1.3	26.0	6.8	55.0	46.0	5.5	56.6	44.5	0.033
54	1.4	37.8	7.7	63.0	51.9	6.3	64.8	50.2	0.053
65	1.6	52.0	8.6	70.0	58.2	7.0	72.0	56.3	0.070
83	1.8	75.0	9.8	80.0	67.0	8.0	83.0	64.0	0.098
100	2.0	100.0	11.0	90.0	75.5	9.0	93.0	72.5	0.137
125	2.2	138.0	12.2	100.0	84.0	10.0	103.0	81.0	0.192
160	2.6	208.0	15.0	130.0	111.5	12.4	134.0	107.5	0.358
200	2.6	260.0	15.0	124.0	102.0	12.4	128.0	98.0	0.393
250	3.0	375.0	17.0	140.0	116.0	14.0	144.0	112.0	0.552
350	3.7	648.0	20.0	166.0	134.0	16.0	170.0	130.0	0.822
510	3.9	995.0	22.4	198.0	162.0	18.5	203.0	157.0	1.515
600	4.4	1320.0	23.4	194.0	155.0	19.0	199.0	150.0	1.061
720	4.4	1584.0	26.4	220.0	174.0	22.0	225.0	169.0	2.520
860	4.8	2064.0	25.8	262.0	208.0	21.0	268.0	202.0	3.315
1000	5.8	2900.0	35.8	300.0	250.0	30.0	306.0	245.0	5.410
1200	6.2	3720.0	38.2	320.0	263.0	32.0	326.0	258.0	6.950
1400	6.6	4620.0	41.6	350.0	288.0	35.0	356.0	283.0	8.950
1800	7.6	6840.0	47.6	400.0	330.0	40.0	407.0	324.0	13.35

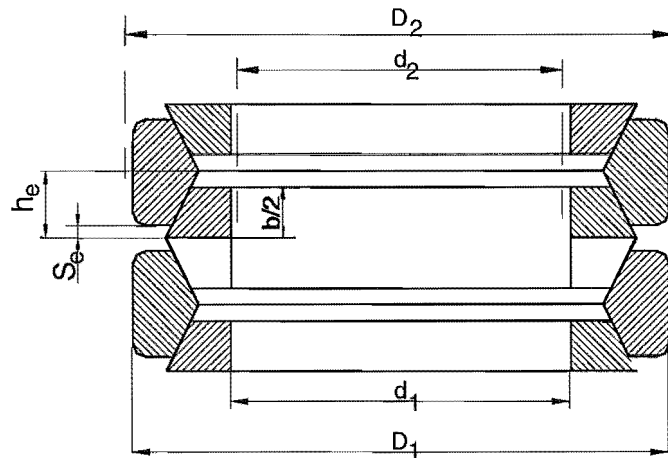


Fig (4-18) Dimensions of ring spring

- $F$  = spring end forces
- $S_e$  = spring travel for one element
- $W_e$  = energy absorption (work for one element)
- $h_e$  = element height
- $D_1, d_1$  = outer and inner diameter of the rings
- $D_2, d_2$  = outer and inner diameter of the guide components
- $b/2$  = half width of ring
- $G_e$  = element weight

#### 4.8 Test Devices

To determine the size of the dampers which were required for the experimental tests, analyses were carried out on the four storey test structure. The 15% of added damping to the structure was adopted for this research and used in the analyses. The structural analyses were carried out using the four-storey model structure to determine the size of the test devices. The analyses are based on comparing the roof displacement of the frame with a constant damping model to the roof displacement of the frame with a ring spring damper. By investigating the roof displacement, the size of the damper can be found so as to give the same roof deflection as that obtained when using the constant damping model.

The damping device used in the experimental tests in this research is a double acting ring spring device shown in Figure (4-19). They contain 84 ring spring elements (42 outer ring, 41 inner rings and 2 half inner rings). The number of the elements and the length of the dampers are determined from the steps of the design given in section 4.10. The blocking force capacity of the device is 5 kN, the height of each element  $h_e$  is 2.2mm and the spring travel for one element is 0.4mm.



Fig (4-19) Prototype ring spring devices used in the experimental tests.

#### 4.9 Components of the Test Devices

Table (4-2), shows the list of the components for the damper device with friction springs used in the tested device.

Table (4-2) Components of the damper device

Position	Quantity	Nomenclature
1	42	Outer ring
2	41	Inner ring
3	2	Half inner ring
4	0.03kg	Special grease
6	1	Draw cup
7	1	Piston
8	1	Bar
9	1	Preloaded part
10	1	Tube
11	1	Base plate
12	1	fillet weld 4.5
13	1	Socket head cup screw
14	3	Socket head cup screw
15	1	Rod end
16	1	Hexagon nut

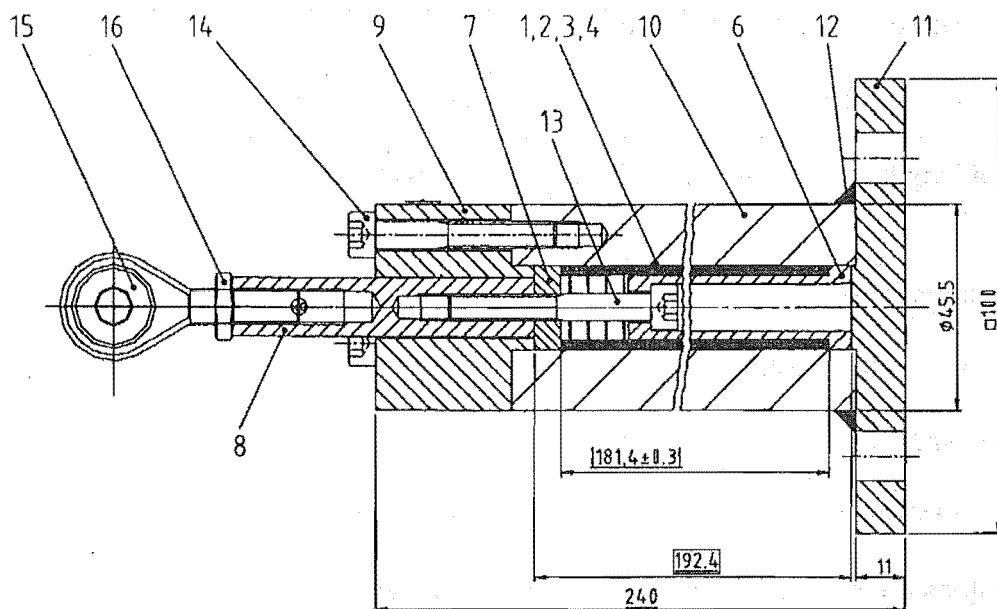


Fig (4-20) Ring spring device components

#### 4.10 Damper Size

To determine the numbers of the ring spring elements and the size of the damper which were required for the experimental tests, three time history analyses were carried out using the dynamic computer program RUAUMOKO [1]. The earthquake excitation records were El-Centro1940NS, modified Taft S69E, and Pacoima Dam ground accelerations (see section 6.4.4). The analytical model used is described in Chapter 5.

From the force-displacement relationship of the double acting ring spring, the maximum values of the forces and the displacements in both the tension and compression regions can be obtained. From Figure (4-21a), with the El-Centro ground acceleration as an example, the forces in the ring spring in tension and compression are 2.21 and 2.33 kN with 11.3 and 12.1mm displacements respectively. The properties of the damper can be calculated as follows:

The capacity of the damper = 5 kN.

The preload force in the spring = 10% of the capacity = 0.5 kN.

The stroke of one element = 0.4 mm

The length of one element = 2.2 mm (see Table 3-1).

a) In tension:

The spring stiffness =  $(2.21-0.5)/11.3 = 0.151 \text{ kN/mm}$

The total stroke =  $5/0.151 = 33.11 \text{ mm}$

The required numbers of the elements =  $33.11/0.4 = 83 \text{ element}$

The total length of the rings,  $L_0 = 83 \times 2.2 = 182.6 \text{ mm}$

b) In compression

The spring stiffness =  $(2.33-0.5)/12.1 = 0.151 \text{ kN/mm}$

The total stroke =  $5/0.151 = 33.11 \text{ mm}$

The required numbers of the elements =  $33.11/0.4 = 83 \text{ element}$

The total length of the rings,  $L_0 = 83 \times 2.2 = 182.6 \text{ mm}$

#### 4.10.1 Ring Spring Hysteresis

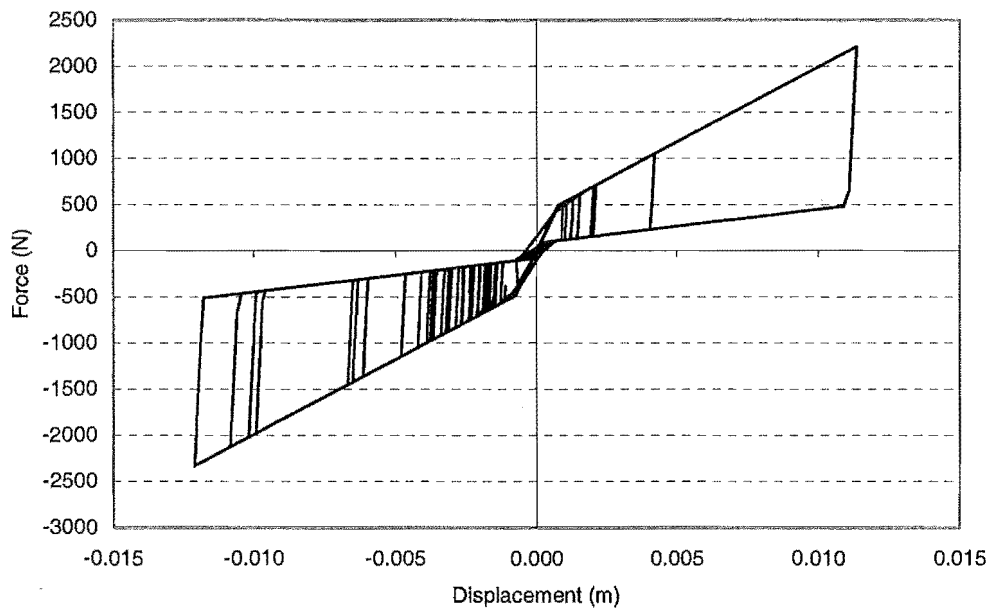


Fig (4-21a) Ring spring hysteresis for the El-Centro excitation.

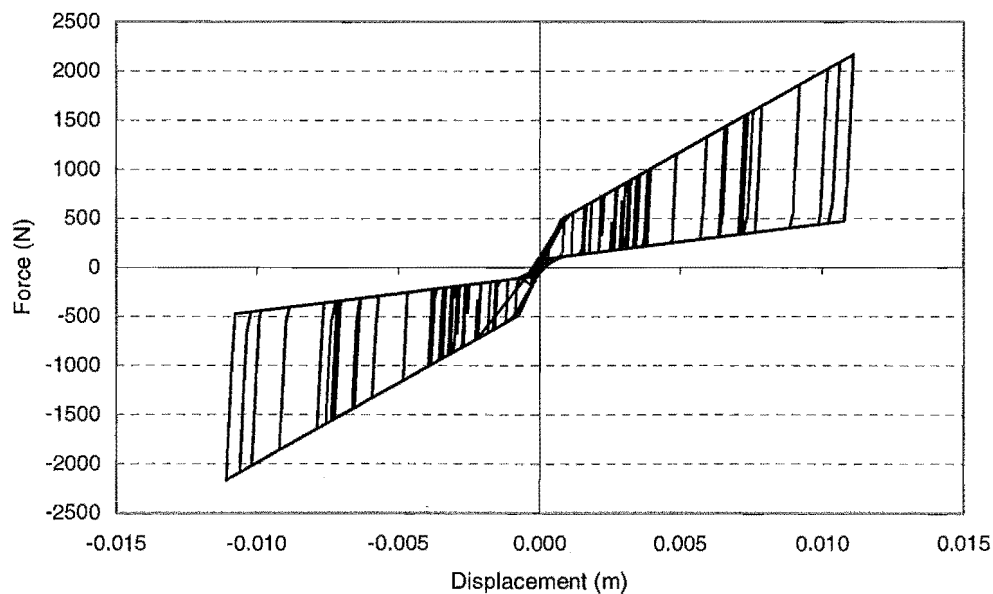


Fig (4-21b) Ring spring hysteresis for TAFT excitation.

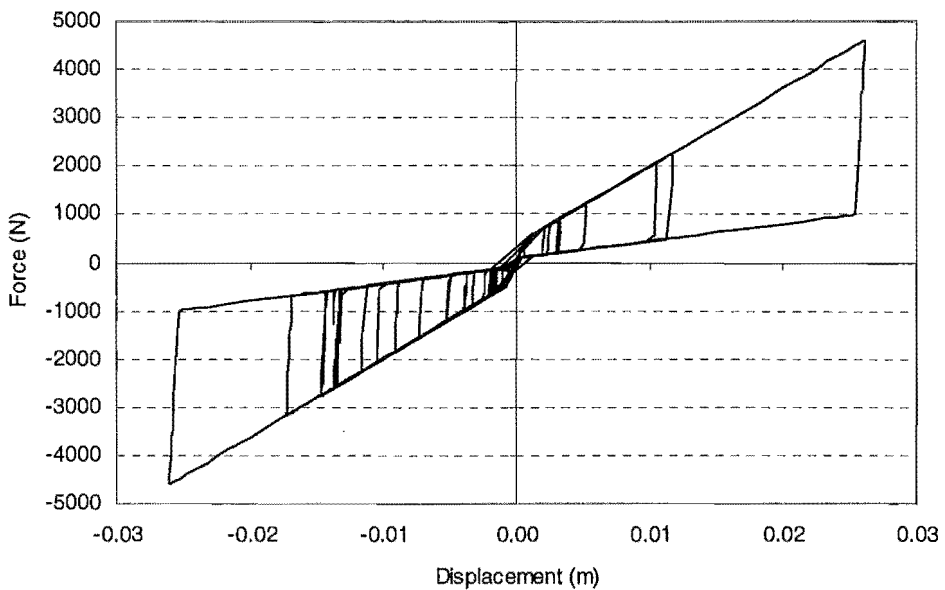


Fig (4-21c) Ring spring hysteresis for the Pacoima Dam excitation.

#### 4.10.2 The Properties of the Damper for Different Earthquake Excitations

The following table shows the forces and the displacements in the ring spring damper under the earthquake excitations in tension and compression and the number of the ring spring elements required.

Table (4-3)

Quake \\\diagdown	Forces (kN)		Displacement (mm)		Damper stiffness (kN/mm)		Number of elements	
	Tension	Comp.	Tension	Comp.	Tension	Comp.	Tension	Comp.
El-Centro	2.21	2.33	11.3	12.1	0.151	0.151	83	83
4203 Taft	2.17	2.17	11.1	11.1	0.150	0.150	84	84
Pacoima Dam	4.60	4.60	26.1	26.1	0.157	0.157	80	80

From the Table (4-3) it can be seen that:

- The most suitable numbers of elements is 84 elements.
- The damper stiffness is 0.15 kN/mm
- The capacity of the damper is 5 kN (the smallest size in Table 4-1).

#### 4.11 Experimental Testing of the Ring Spring Devices

Several tests were undertaken to determine the hysteresis characteristics of the ring spring devices. The devices were tested on a universal testing machine in the Structural Laboratory of the Civil Engineering Department, at the University of Canterbury.

Six tests covering the complete loading-unloading cycle in compression and tension region (three on each damper) were carried out on the two ring spring dampers on a universal testing machine as shown in Figure (4-24). The hysteresis characteristics of the devices can be observed from Figures (4-22, 23). The pre-load of the ring spring is about 10% of the maximum load equal to 0.5 kN. The pre-displacement is also about 10% of the total spring displacement and equals 3 mm.

The values of the hysteresis spring stiffness obtained from the tests on the dampers are shown in Table (4-4).

Table (4-4) Experimental ring spring characteristics.

##### Damper (1):

Stiffness ( $\times 10^6$ ) N/m	Test 1	Test 2	Test 3	Average
$k_o$	1.036	1.227	1.115	1.126
$k_i = (rk_o)$	0.158	0.169	0.172	0.17
$k_1 = (r_s k_o)$	3.61	3.41	3.95	3.65
$k_d = (r_L k_o)$	0.065	0.081	0.073	0.073

##### Damper (2):

Stiffness ( $\times 10^6$ ) N/m	Test 1	Test 2	Test 3	Average
$k_o$	1.119	1.065	1.12	1.101
$k_i = (rk_o)$	0.162	0.172	0.171	0.17
$k_1 = (r_s k_o)$	3.58	3.15	3.34	3.36
$k_d = (r_L k_o)$	0.083	0.082	0.068	0.077

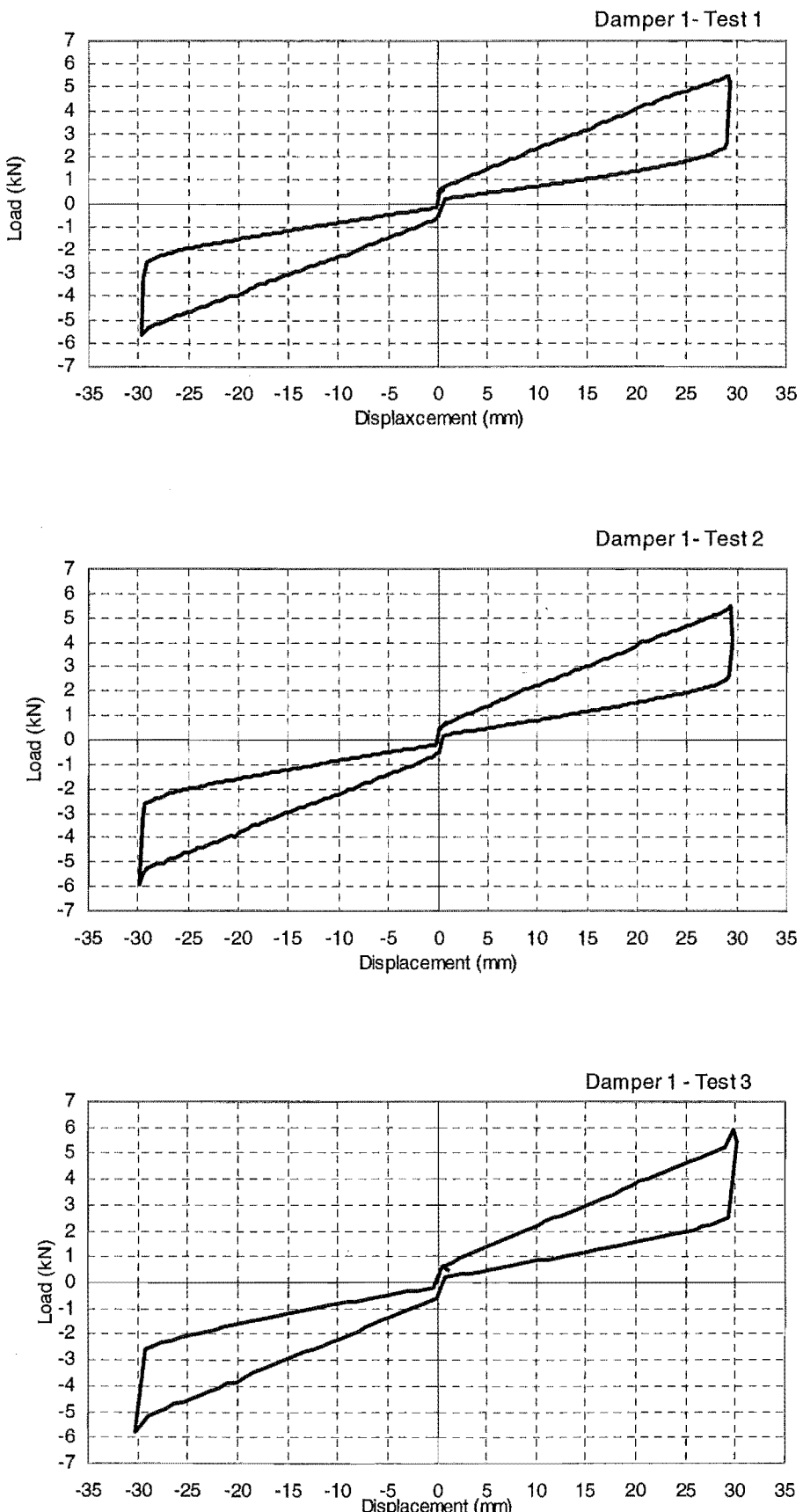


Fig (4-22) Experimental hysteresis diagrams of the ring spring device No. (1)

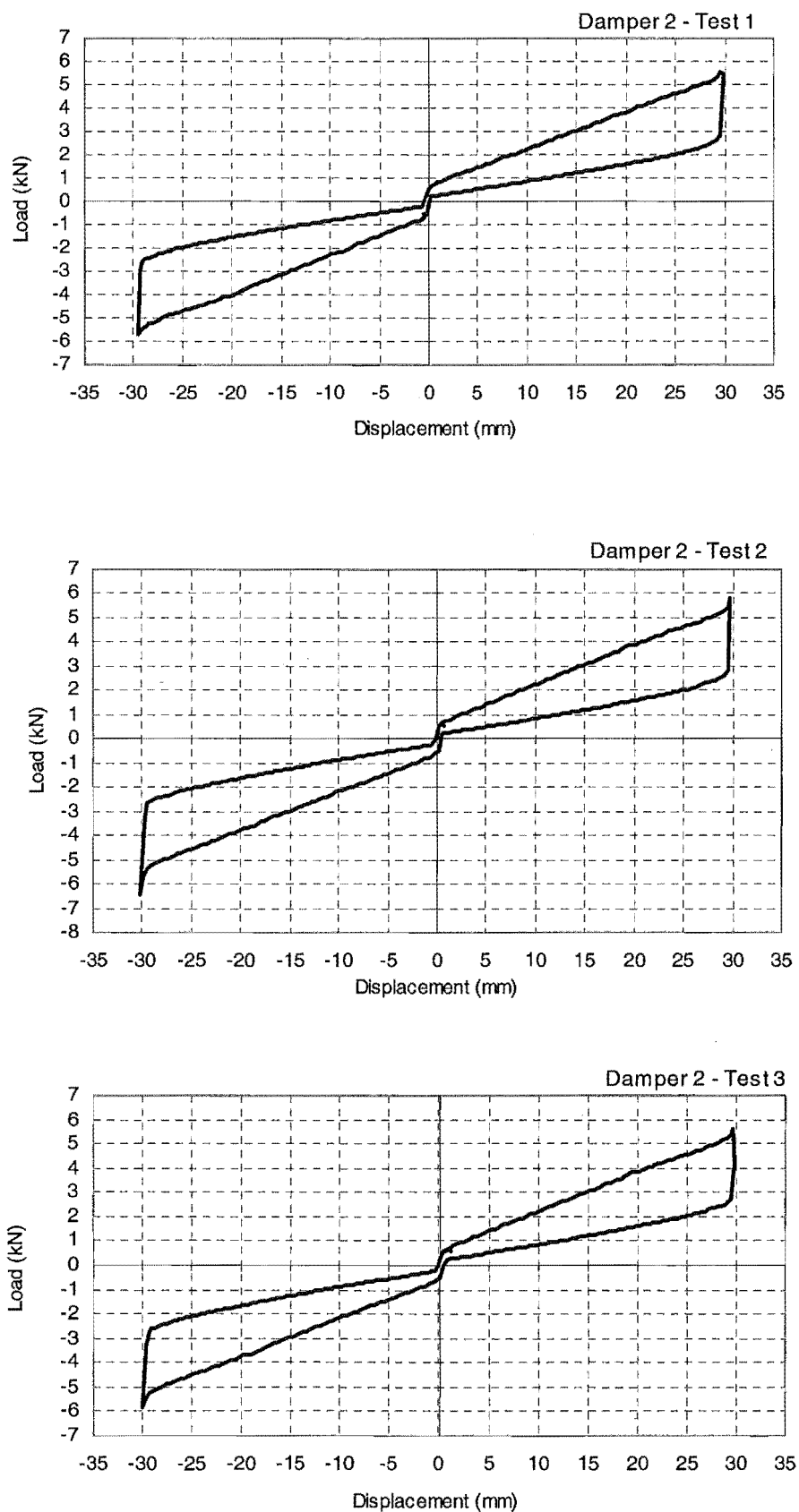


Fig (4-23) Experimental hysteresis diagrams of the ring spring device No. (2)

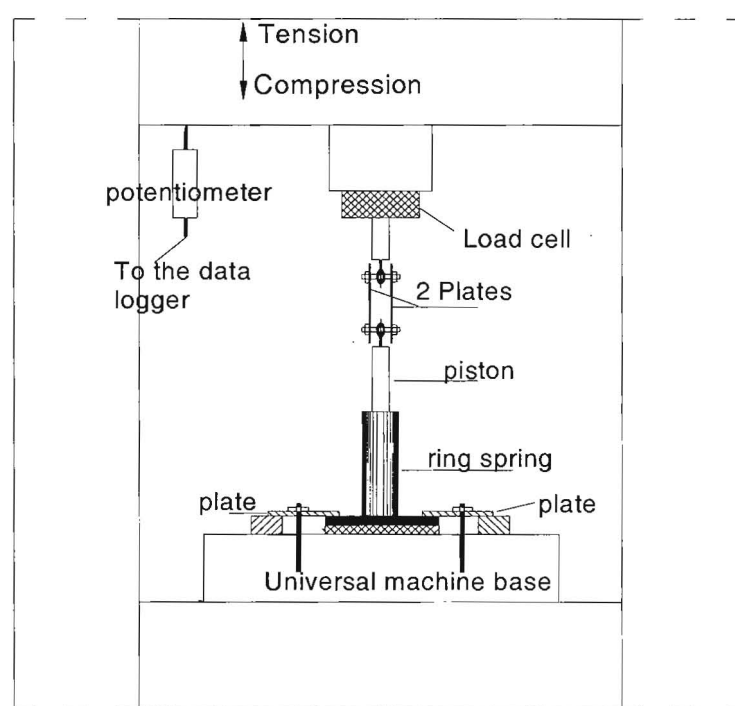
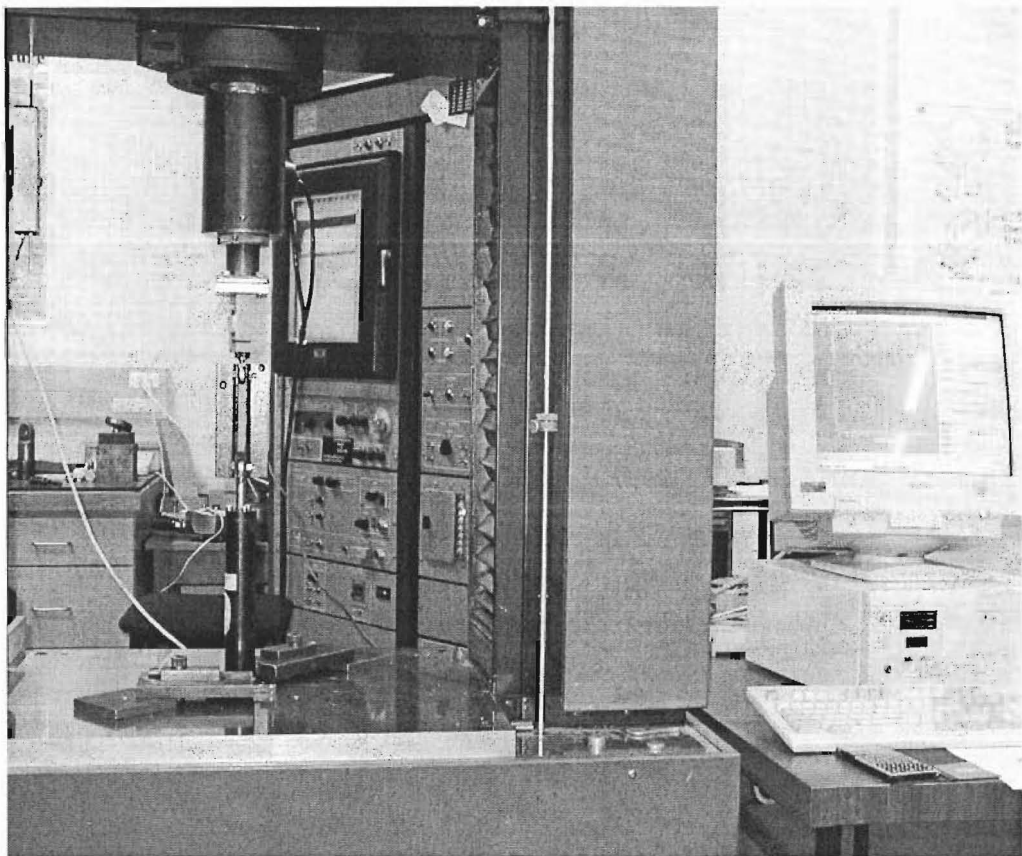


Fig (4-24) Set-up of the ring spring device on the universal testing machine.

## Chapter 5

### Structural Model for Experimental Tests and the Supplemental Control System

#### 5.1 Introduction

To mitigate the response of the structure during a seismic event, the damper-tendon system discussed in chapter 3 is proposed. The supplemental control system consists of ring spring devices (detailed in Chapter 4) to provide the damping forces and transfer them to the rest of the building by using a tendon system. The frame used to verify the usefulness of the effect of using ring spring in reducing the seismic response is an existing frame structure in the Structural Laboratory of the Civil Engineering Department, at the University of Canterbury [11]. An isometric drawing and a view of the assembled frame structure are shown in Figures (5-1) and (5-2) respectively. The description of the damper-tendon system with a straight tendon configuration, horizontal link elements, and the damper connections are presented in the following sections.

#### 5.2 Frame Configuration

The four storey steel frame is built using square hollow steel sections for the beam and column members. Flat bars are used for the beam-column joints and other connecting joints. The main feature of the structure is the incorporation of replaceable fuses located in the critical regions of the structure, i.e. plastic hinges [11]. The frame tries to model a typical four-storey reinforced concrete ductile frame building. Therefore, the fundamental natural period of free vibration of the frame was required to be within range of 0.4 second to 0.6 second to obtain similar response under earthquake excitation. For reinforced concrete members, the stiffness degrades after cracking especially in and around the critical regions where plastic hinges are expected to develop. Therefore, the stiffness of the fuses were designed to be much smaller than the rest of the frame.

The frame in the longitudinal direction, i.e. the earthquake loading direction, has two bays with different spans and one bay in the transverse direction. The overall length of the long span was 1.4 m whereas the short span was 0.7 m long. The overall dimensions of the frame are 2.1x 1.2 x 2.1 m as shown in Figure (5-1) and (5-3). A transverse beam is located at the mid-span of the long beam to induce a point load at mid-span of the long beam. The short bay is to show earthquake-dominated flexural plastic hinge response, while the long bay is to show gravity-dominated flexural plastic hinge response by having an extra point load induced by the transverse beam at the mid-span at each level. The point loads at the mid-spans of the long beams are to facilitate the formation of non-reversing plastic hinges, in which the plastic rotations only occur in one direction, i.e. in the positive direction at mid-span and the negative direction at the girder ends. Replaceable fuses were incorporated in the critical regions of the structure, at the beam end joints and mid-span joints of the long beams and the column bases, as shown in Figure (5-3) and discussed in section 5.6.

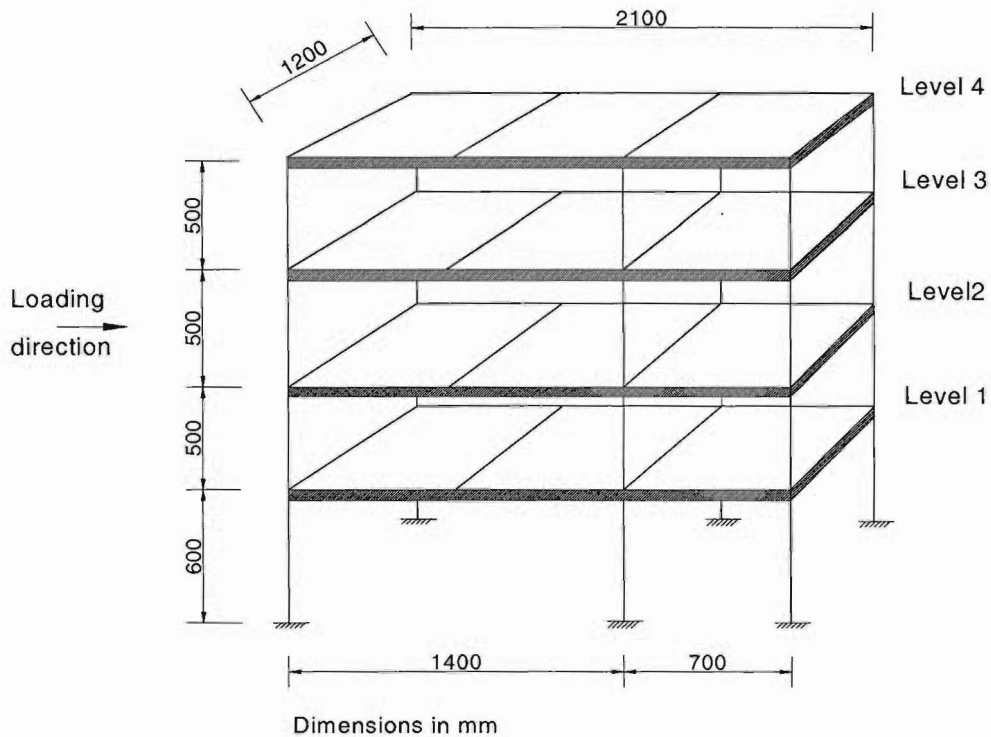


Fig (5-1) Outline drawing of the frame structure

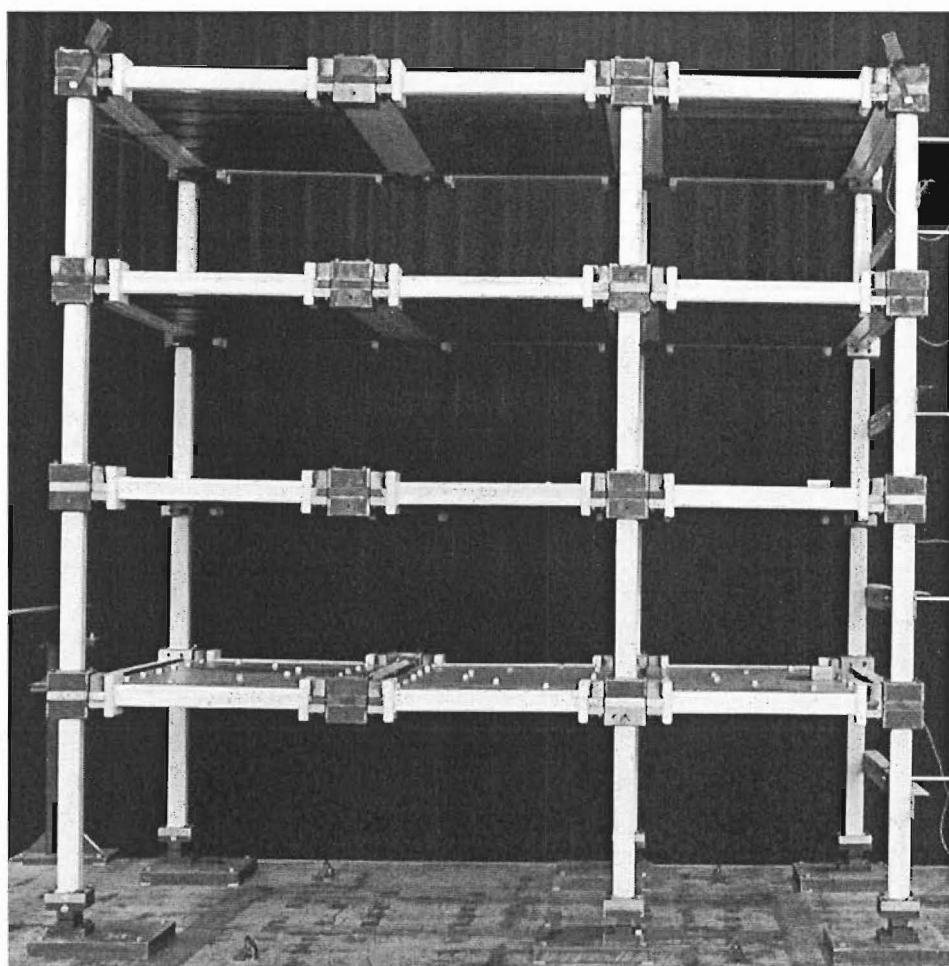


Fig (5-2) Assembled structure

### 5.3 Frame Members

In real structural members, the stiffness degrades especially in and around the critical regions, where plastic hinges are expected to develop. Therefore the stiffness of the fuses were designed to be much smaller than the rest of the frame which is built from rectangular hollow sections. Rectangular steel plate sections were selected for the fuses.

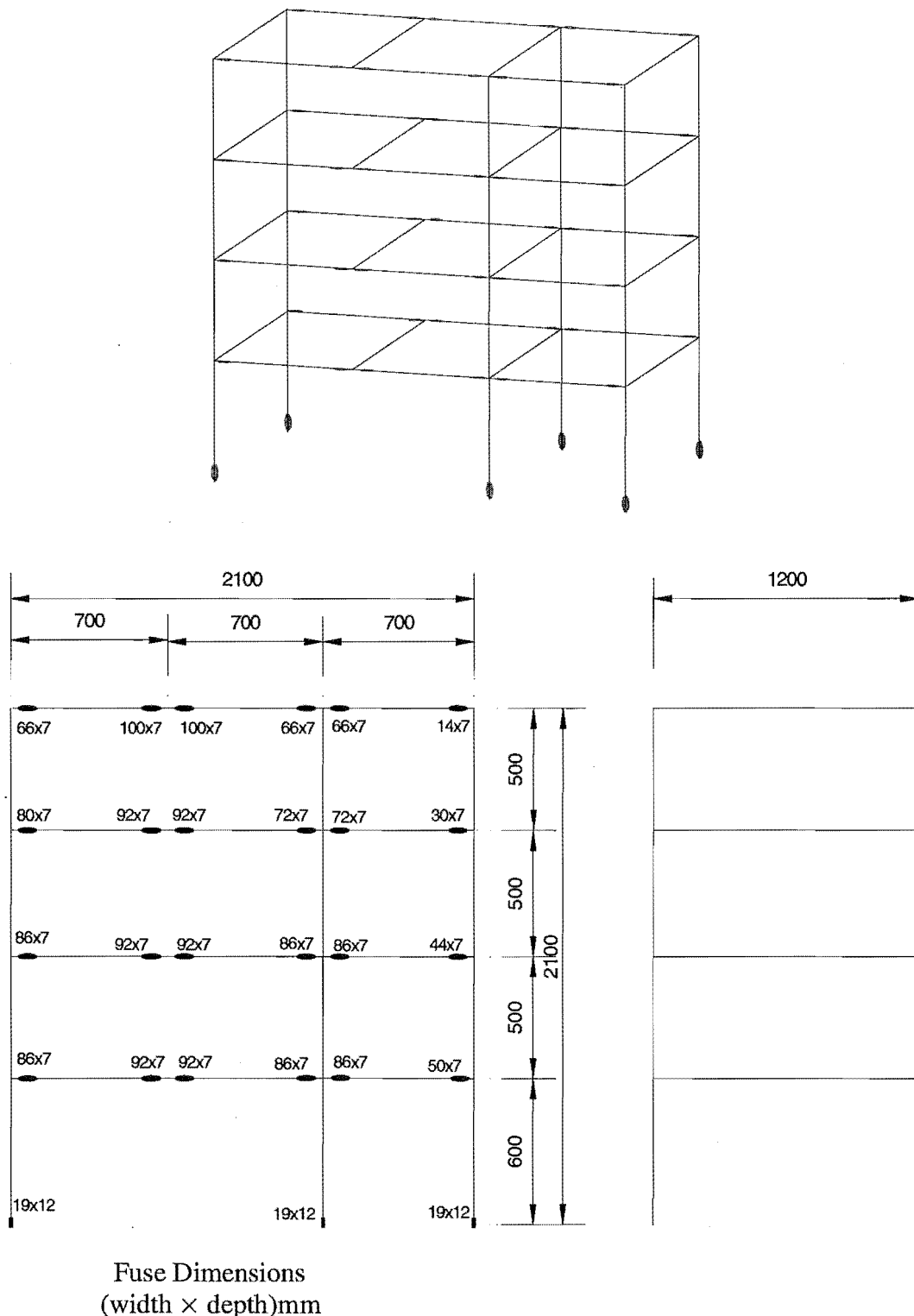


Fig (5-3) Elevations and end view of the frame

The fuse stiffness was designed to be a quarter of those of the beam and column members to give the right frame stiffness and the correct plastic hinge rotation. Fuses were located on the faces of the beam-column joints, at the column bases and at the mid-spans of the long beams. Figure (5-4) shows the fuse locations and dimensions.

### 5.3.1 Mass

In order to simulate the dead and live load of a real building, additional mass was added to the structure to give a natural period of free-vibration similar to that of a four storey frame. They act as uniformly distributed loads on the transverse beams, and are then transferred to the columns, or to the long beams as mid-span point loads. The additional mass consists of plates (ingots) and steel topping plates as shown in Figure (5-4). The total weight of the frame is 35.3 kN, the self weight of the steel column and beam members totals 8.6 kN and the additional added mass is 26.7 kN.

The mass was divided equally between each floor. The top level mass could have been reduced since the roof of a building usually has much less dead and live load when compared to that present at the lower levels. However, this aspect was not used to allow flexibility in future research, i.e. adding more storeys to the frame.

Additional mass to simulate dead and live loads was composed of 150 mm wide steel ingots and 2 mm thick steel plates. The 150 mm wide steel ingots model the precast concrete floor units in a reinforced concrete frame building, while the 2 mm thin plate models the cast-in-place reinforced concrete topping and acts as a rigid diaphragm carrying the floor inertia forces.

### 5.3.2 Ingots

For each of the three bays of the floor, 6 steel ingots are placed as shown in Figure (5-5a). Each strip consists of two ingots welded together to form a single unit. The top ingot is a 150 x 32 x 620 mm steel plate and the bottom one is 150 x 20 x 530 mm steel plate. The strips are placed with a 28mm gap between each other and a 14 mm clearance gap to the ends of the transverse beam.

### 5.3.3 Top Plates

The dimension of the topping plate is 1000 x 600 x 2 mm. For each bay of the floor, there is one plate bolted to the ingots. The plate and the ingots are arranged in a way that the centroid of each element coincides with the mid-depth of the fuses.

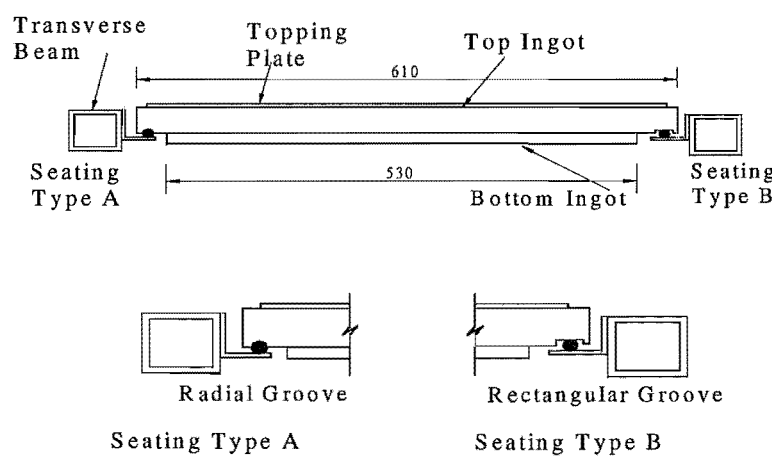


Fig (5-4) Elevation of mass layout

The top plates are to prevent lateral flexure in the transverse beams. If lateral flexure does occur in these beams, the ingot support is no-longer a straight knife-edge support and the frictional action between the bottom of the ingot and top of the knife-edge support on the beams adds up to an extra 7 % of equivalent viscous damping.

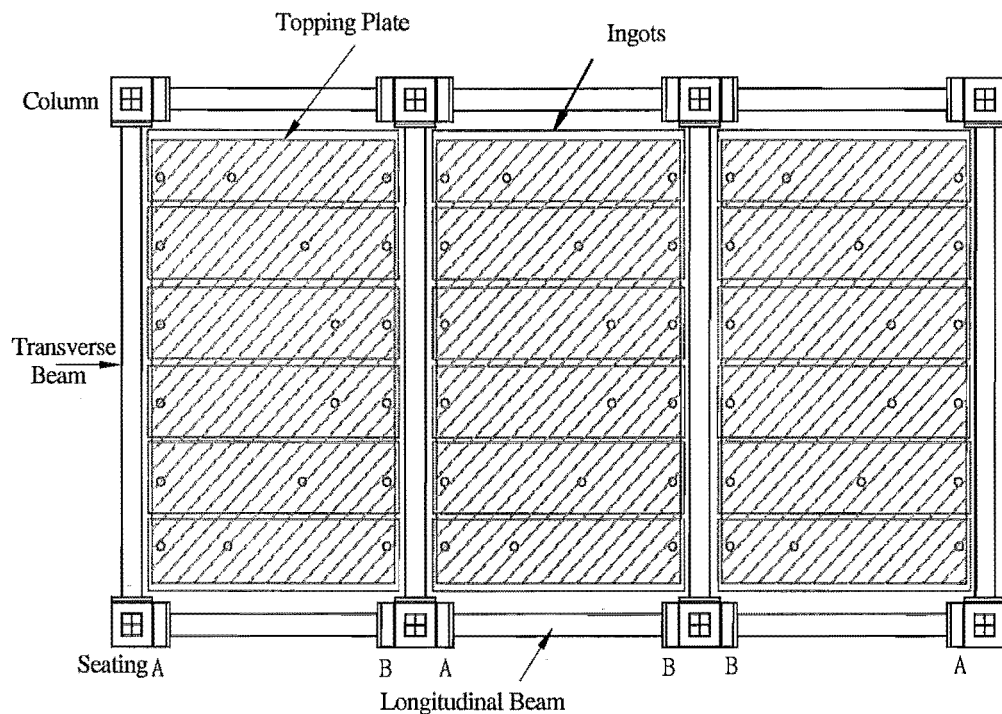


Fig (5-5a) Plan of mass layout

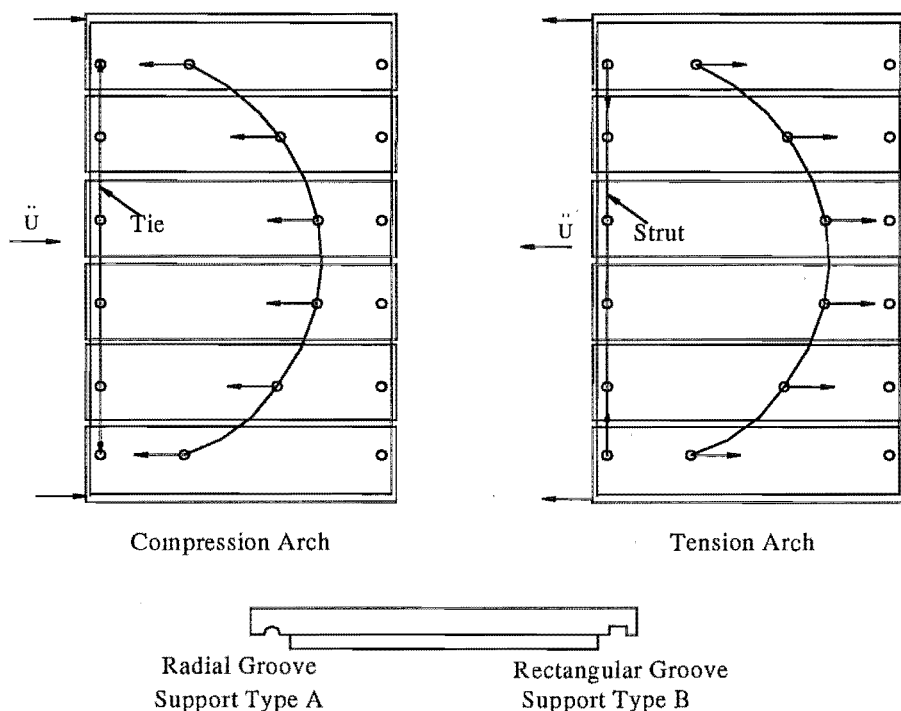


Fig (5-5b) Horizontal inertia force transfer mechanism through diaphragm.

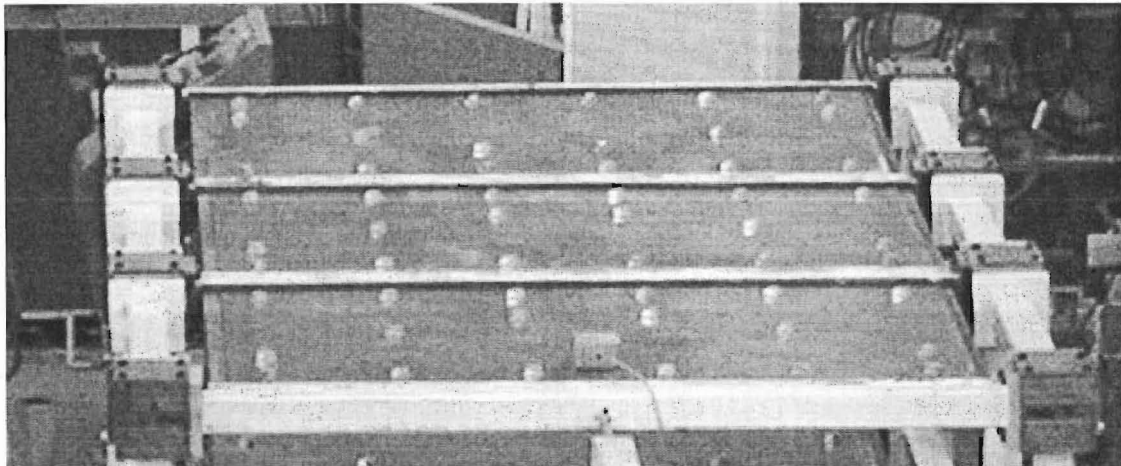


Fig (5-6a) Top view of the mass layout

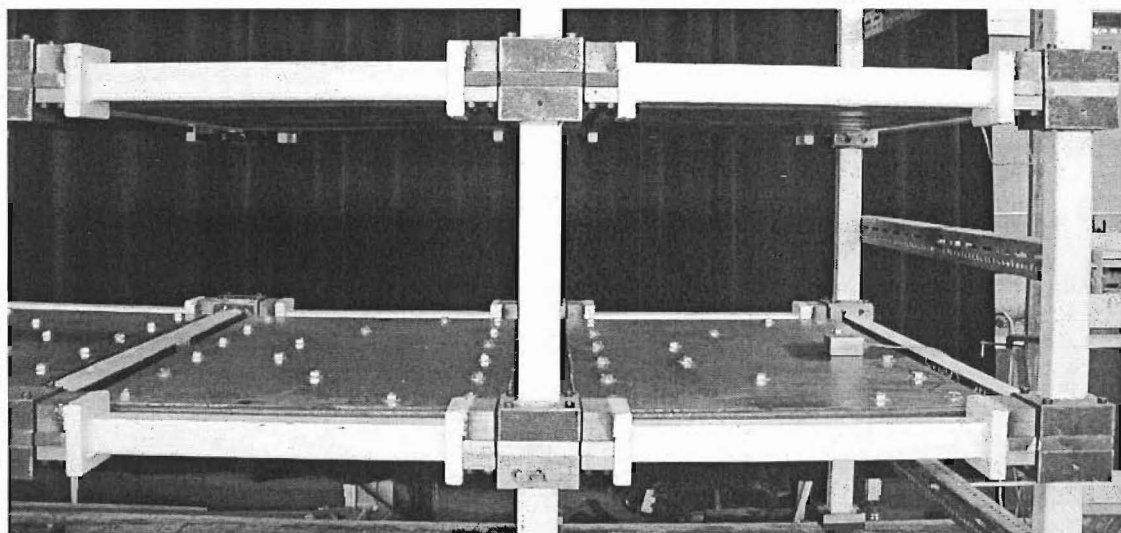


Fig (5-6b) Front view

#### 5.4 Beam Connections

To connect the ingots to the transverse beams, 50 x 50 x 3mm equal angle sections were welded to the beams to support the ingots. A 10 mm diameter steel rod was welded to the angle section to form a simply supported seating for the ingots.

There are two types of seating; Type A, which transfers both horizontal inertia forces and gravity loads, and Type B, which transfers only gravity loads, Figure (5-5). The shape of the groove, which is located on the lower end of the top ingot, differentiates the force transfer mechanism. Type A seating has a radial groove on the ingot and Type B seating has a rectangular groove. The radial groove enables inertia forces induced by earthquake loading and the gravity loading to be transferred to the transverse beam, while Type B seating prevents horizontal force been transferred and allows only vertical forces to be transferred to the beam (Figures 5-5 and 5-6).

## 5.5 Mass Connections

In a real frame building, the pre-cast floor usually has a reasonably stiff topping slab and it can usually be assumed to act as a rigid diaphragm to transfer inertia forces to the columns. Since the inertia force is transferred directly to the columns, no horizontal flexural bending acts in the transverse beams. It is unrealistic to allow the force to pass through the transverse beams as a distributed load (DL) before reaching the columns.

Cap screws that connect the ingots to the plate are arranged in a parabolic shape, i.e. the shape of the bending moment diagram under DL, to create an arch action to carry the inertia forces and to transfer them to the ends of the plate. Strut and tie mechanisms are also incorporated by arranging a row of cap screws parallel to the transverse beam at each end of the plate, to provide compression or tension forces to resist the force resulting from the arch action. The transverse beam is now subjected to two point loads at the ends, which are very close to the columns, instead of uniformly distributed loads along the span. Figure (5-5b) illustrates the above force transfer mechanism.

## 5.6 Joints, Fuses and Connection Details

### 5.6.1 Beam-Column and Mid-Span Joints

Every beam-column joint and mid-span joint consists of two steel blocks, i.e. top and bottom joint blocks, and a replaceable fuse plate in between. Columns were connected to the beam-column joints by 5mm fillet welds, at the top of the top blocks and at the bottom of the bottom blocks.

Figures (5-7, 8, 9) detail the interior and exterior beam-column connections and the mid-span connections respectively. Every replaceable fuse and longitudinal beam connection consists of an end plate, a free block, a block welded to the end plate and a fuse clamped by the blocks. The dimensions of the free block, welded block and end plate are 90 x 40 x 20 mm, 90 x 40 x 40 mm, and 100 x 100 x 20 mm respectively. The cap screws go through the free block and fuse, and are tapped to 20 mm depth in the welded block.

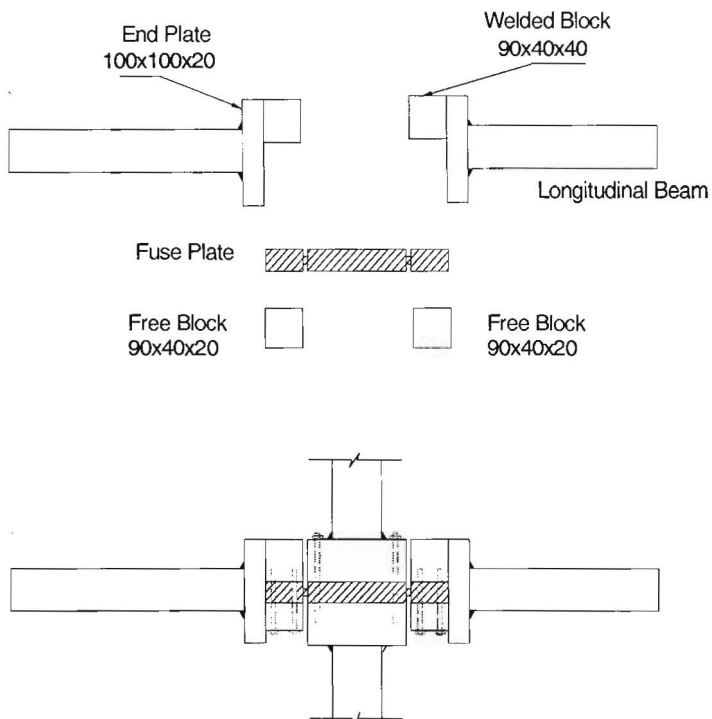


Fig (5-7a) Interior beam-column joint

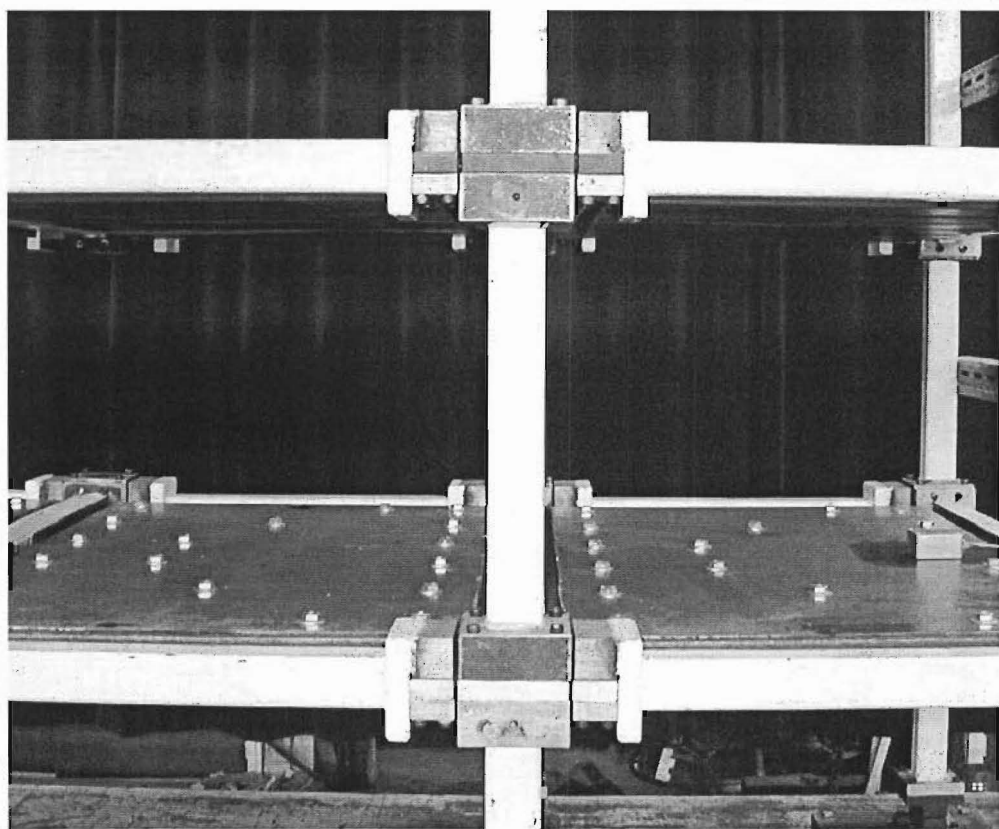


Fig (5-7b) Typical interior beam-column joint

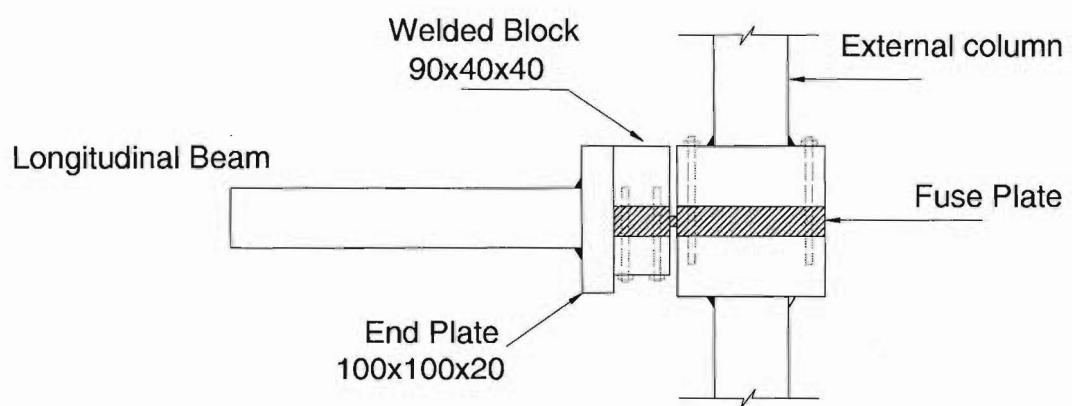


Fig (5-8a) Exterior beam-column joint

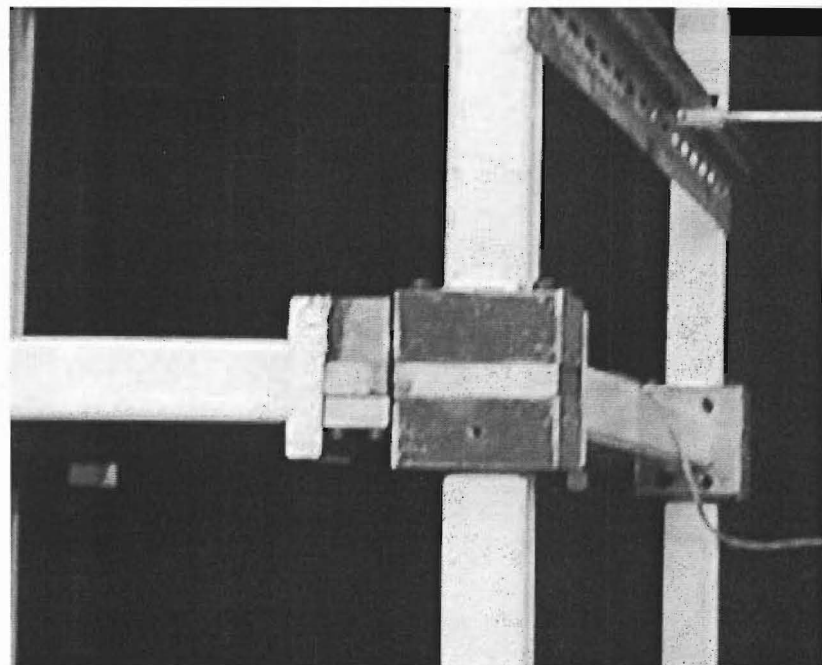


Fig (5-8b) Typical exterior beam-column joint

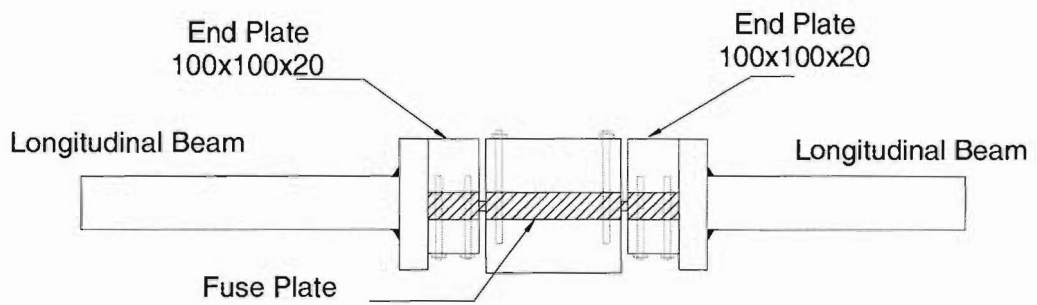


Fig (5-9a) Mid span joint

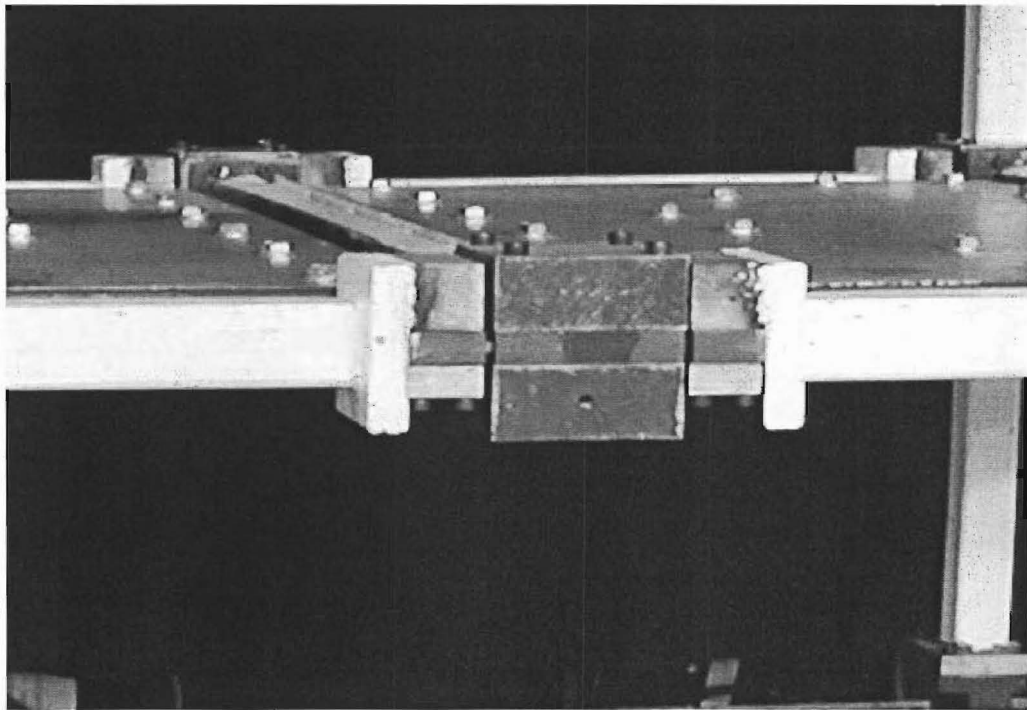


Fig (5-9b) Typical mid span joint

### 5.6.2 Beam Fuses

There are two types of the beam fuses; external and internal beam fuses (Figure 5-10). In the external beam fuse only one plastic hinge can form, while two plastic hinges can occur in the internal fuses. Figure (5-11) shows the mechanism of the inelastic deformation of the structure.

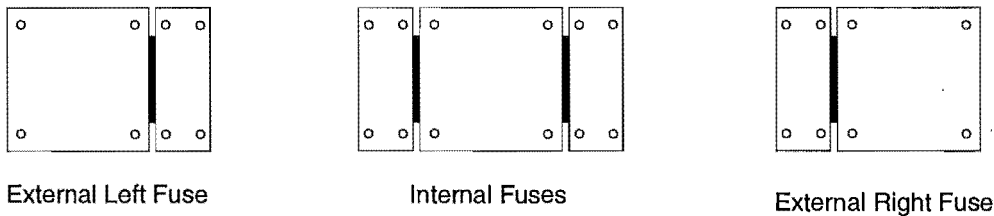


Fig (5-10) Fuse types

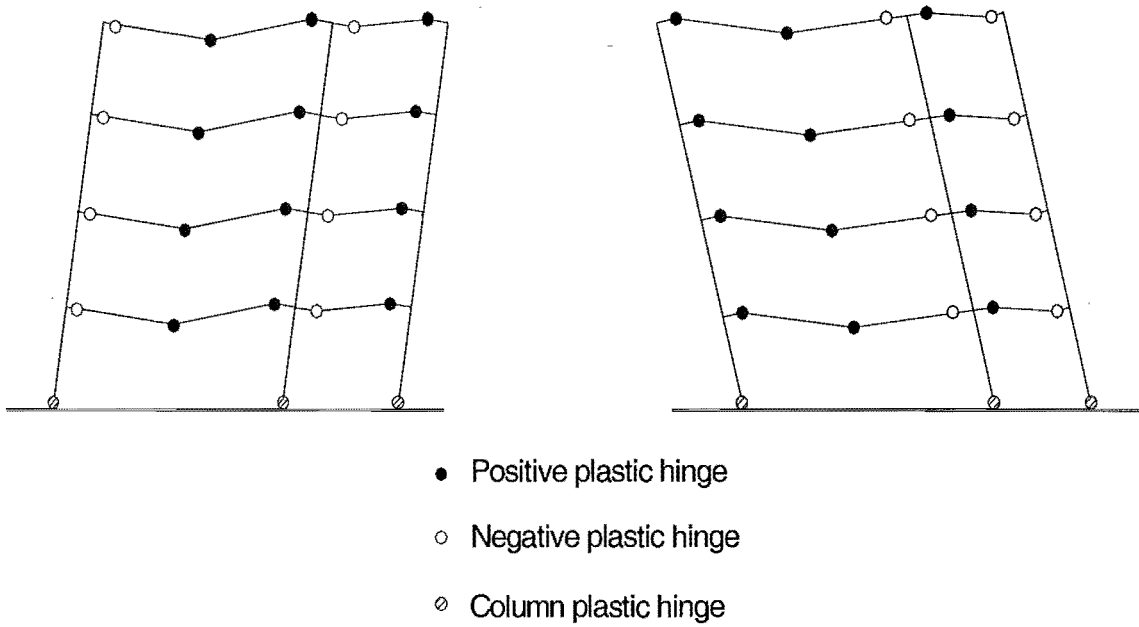


Fig (5-11) Mechanism of inelastic deformation for the frame structure

The fuse plates are made of 100 x 20 mm steel flat with a length of 145 mm for the external ones and a length of 190mm for the internal ones; Figure (5-12). Slots are made at the fuse location to reduce the section dimension to ensure that a plastic hinge will form at this location.

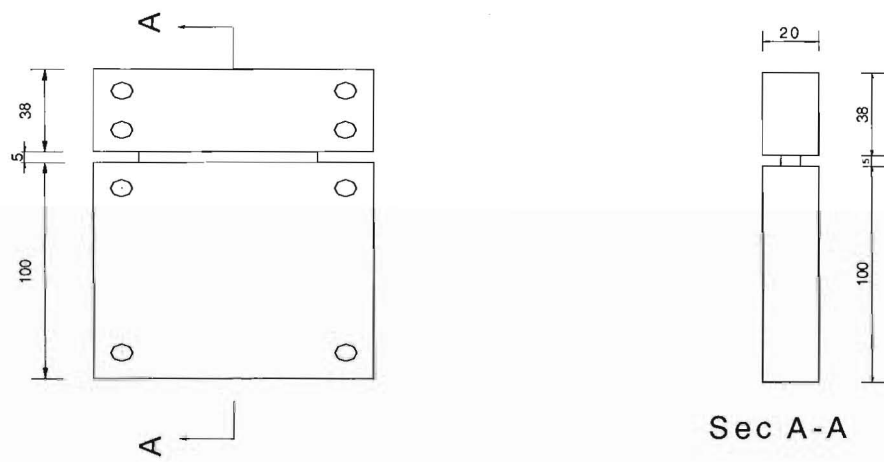
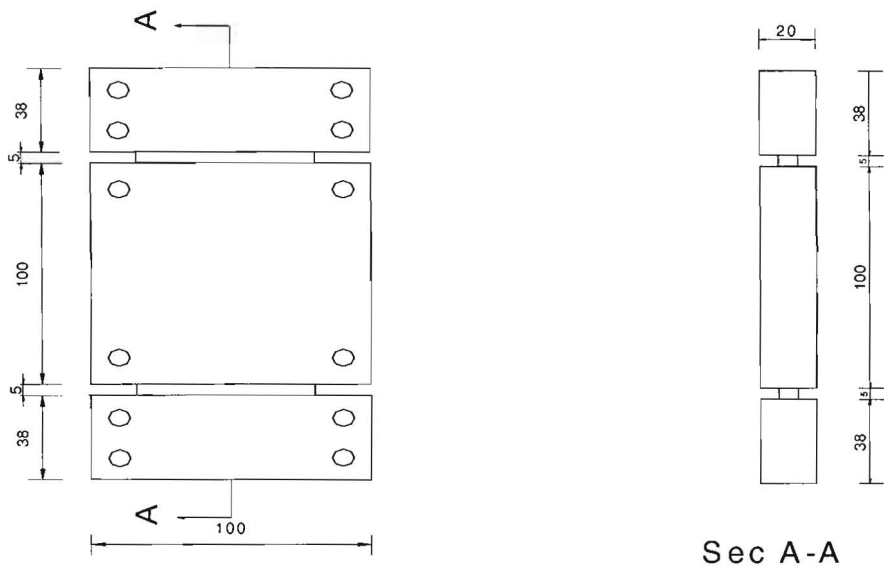


Fig (5-12a) Dimensions of the internal and external fuses

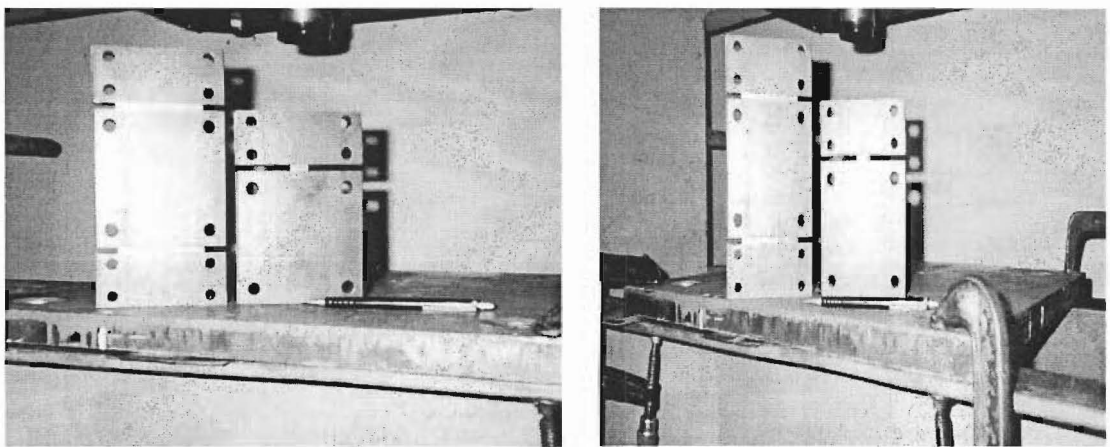


Fig (5-12b) Photographs of the fuses

### 5.6.3 Column Base Fuses and Connections

Column base fuses are made of steel blocks slotted at various locations to allow for connections and to reduce the section dimensions. This mechanism is based on the same principle as the beam fuses. The fuses are connected to the columns by 100 x 100 x 20mm plates welded to the bottom end of each column and connected to the shaking table by 300 x 300 x 40 mm plates (Figure 5-13).

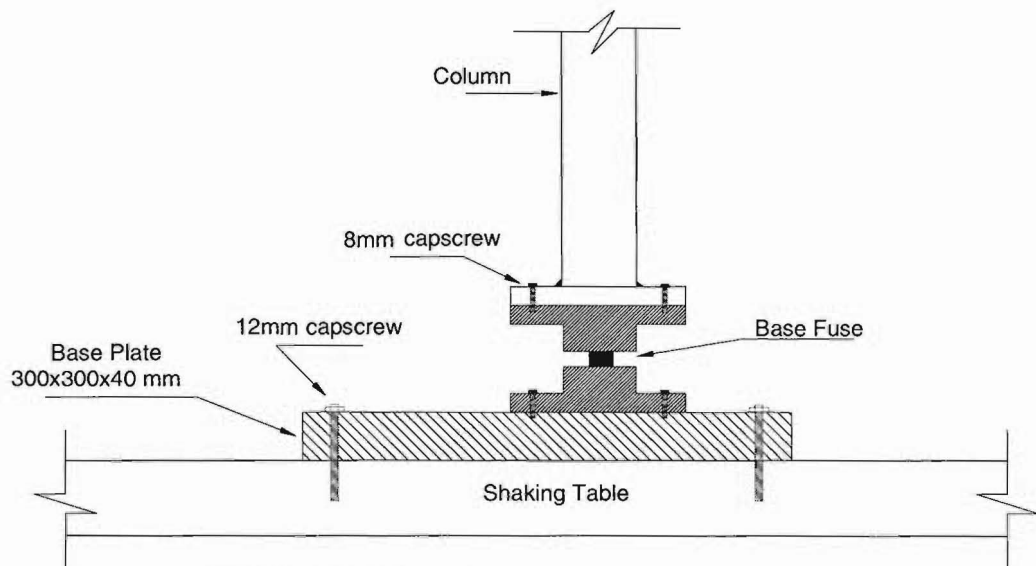


Fig (5-13a) Column base fuse and connections

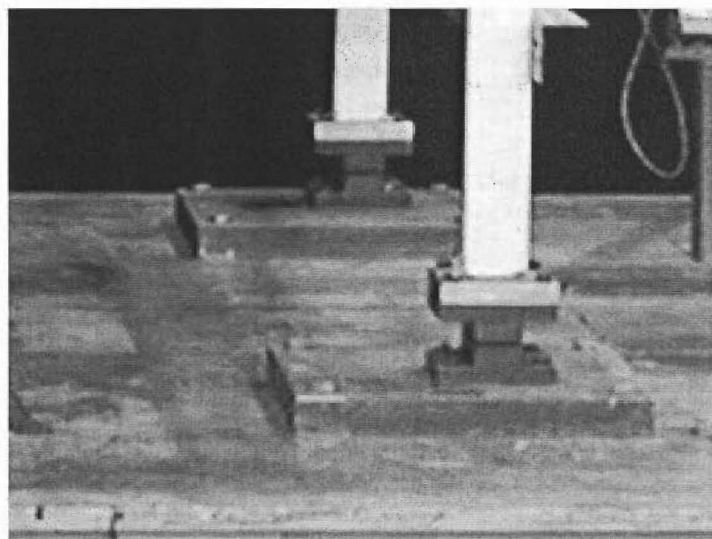


Fig (5-13b) Typical column base fuse

## 5.7 Hinge Joint Fuse Stress-Relief Annealing

Since the structural model has been used previously, the hinge joint fuses have been bent in flexure to beyond the yield level. It was important before using the frame in this research to machine and straighten the deformed fuses as shown in Figure (5-14).

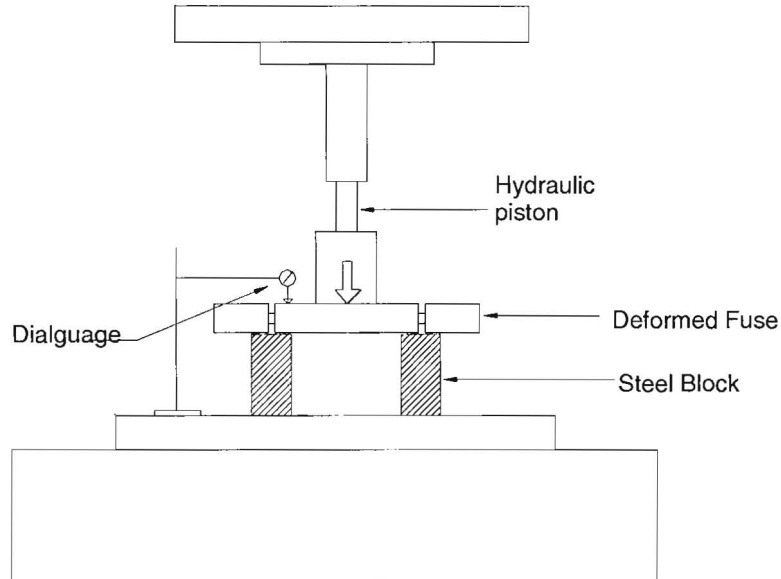


Fig (5-14a) Straightening of the deformed fuse

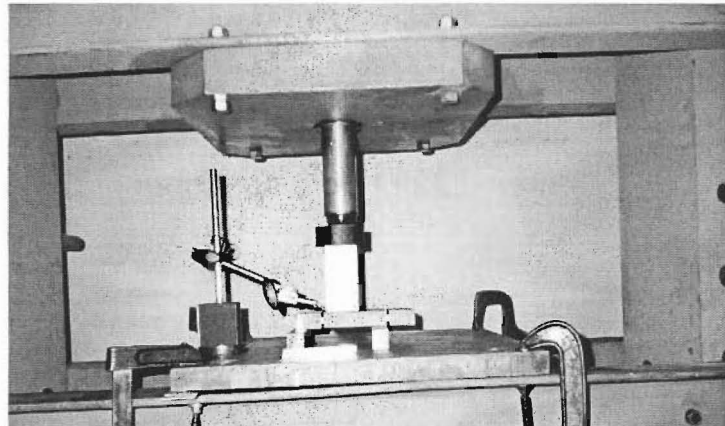


Fig (5-14) Typical straightening of the deformed fuse

When steel is machined or deformed plastically, stresses are induced in the cold-worked surfaces. These stresses may give rise to increased hardness which is likely to render continued working of the steel increasingly difficult. In addition the stresses may cause the steel to distort during the subsequent heat-treating operation and should therefore be eliminated. This can be done by a 1 to 2 hour stress-relief annealing process. For plain-carbon and low-alloy steels a temperature of 550-650°C is required

(Figure 5-15). This treatment will not cause any phase changes, but recrystallization may take place. In order that thermal stresses are not induced during cooling, the parts are allowed to cool slowly in the furnace to approximately 500°C after which they may be taken out and allowed to cool freely in air [34].

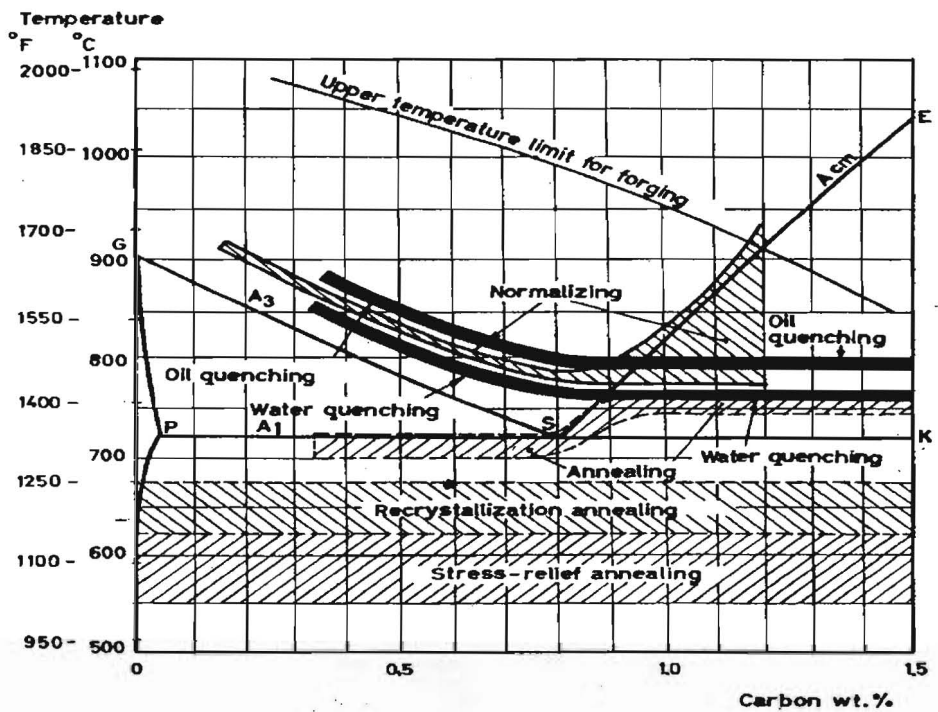


Fig (5-15) Temperature region for various heating operations [34].

All the fuses were treated to 600°C for 2 hours to relieve the stresses on their surfaces due to machining work (Figure 5-16).

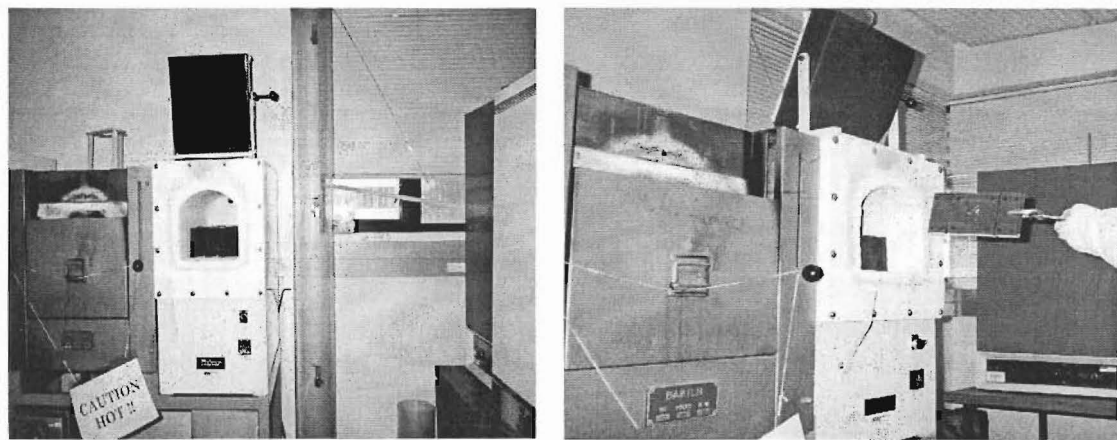


Fig (5-16) Photographs of the fuses heating

## 5.8 Results on Joint Specimens Tests

Quastic-static reverse cycle loading tests on a number of joint specimens were performed to determine the behaviour of the hinged joints subsequent to their heat treating and to check that the values of their stiffness have not been changed when compared with their known initial stiffness [11]. A diagram of the general test set-up is shown in Figure (5-17).

Each specimen tested was placed on a steel table with the column ends and the brackets for the load cells being clamped to the table surface. The beam was connected to two threaded steel rods, which acted as load cells. Calibration of both of the load cells was carried out using an Avery 100 kN Universal Testing machine, as well as hanging weights on one end of the rod. Two strain gauges were glued to the surface of each steel rod. A p3500 portable strain indicator was attached to measure strains and therefore, the applied load.

Since the maximum force required was small, the screw mechanism was used to apply forces. The forces were applied by screwing the nut on the rod against a bracket, which created a pulling action on the beam. Load cell actions were classified into positive and negative, according to the direction of loading.

A linear potentiometer was mounted on a box section to measure the overall beam displacement. A string was used to connect the potentiometer shaft to a bolt on the beam section at the intersection of the centrelines of the beam and the steel rods. The shaft of the potentiometer was set up to measure displacements in two opposite directions.

A digital voltmeter (DVM) was connected to the potentiometer to display voltage signals from the potentiometer during testing. The DVM was calibrated to give reading converted into displacement units. The strain indicator and DVM were connected to an XY plotter to give a graphical presentation of the load and displacement relationship during the test.

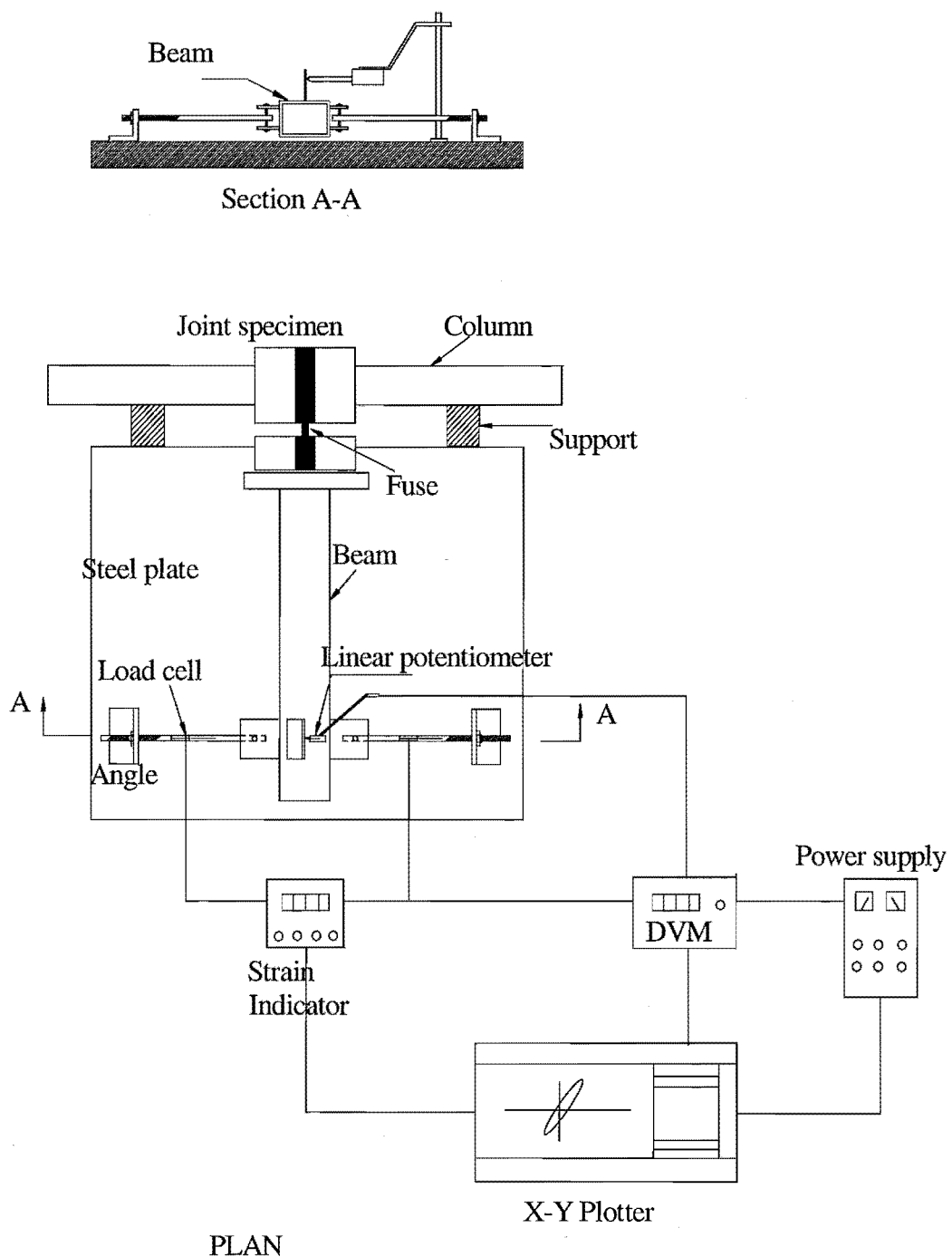


Fig (5-17) A diagram of the general test set-up for calibrating the fuses.

## 5.9 Results of the Hinge Joints Tests

Four tests were carried out in the elastic ranges on four different dimensioned beam joints as shown in Table (5-1). The elastic loads applied were equal to 0.75 of the yield forces to obtain the values of the  $(EI)_{eff}/(EI)$  ratio, where  $(EI)_{eff}$  is the effective flexural rigidity of the fuse and used instead of  $EI$  for all the fuses in the calculations and analyses in this study. The value of  $(EI)_{eff}$  can be calculated from Equation (5-2) in Section 5.10.

It can be observed that there is a comparatively small difference between the original and the experimental results obtained from the tests on the fuse hinge members [11].

Table (5-1) Beam joint stiffness

Fuse width (mm)	$(EI)_{eff}/(EI)$	
	Kao [11]	Experimental
30 x 7	0.44	0.45
66 x 7	0.38	0.39
86 x 7	0.32	0.33
100 x 7	0.36	0.35

The hysteretic responses of the (30x7), (86x7) and (100x7) mm fuses (hinge joints) are presented in Figures (5-18), (5-19) and (5-20) respectively.

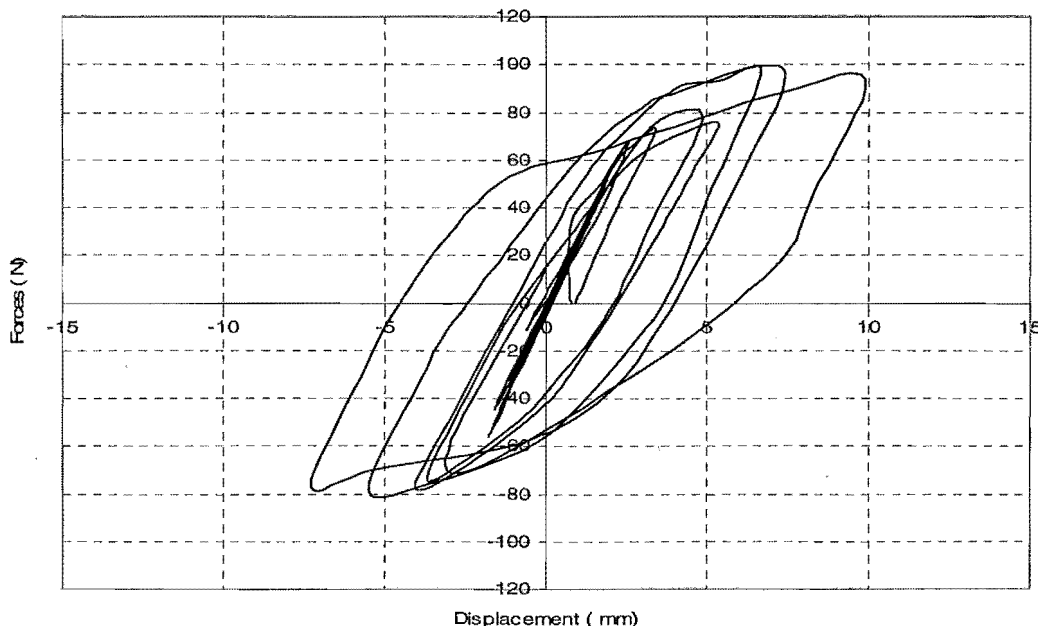


Fig (5-18) Hysteretic response of the (30x7) mm fuse

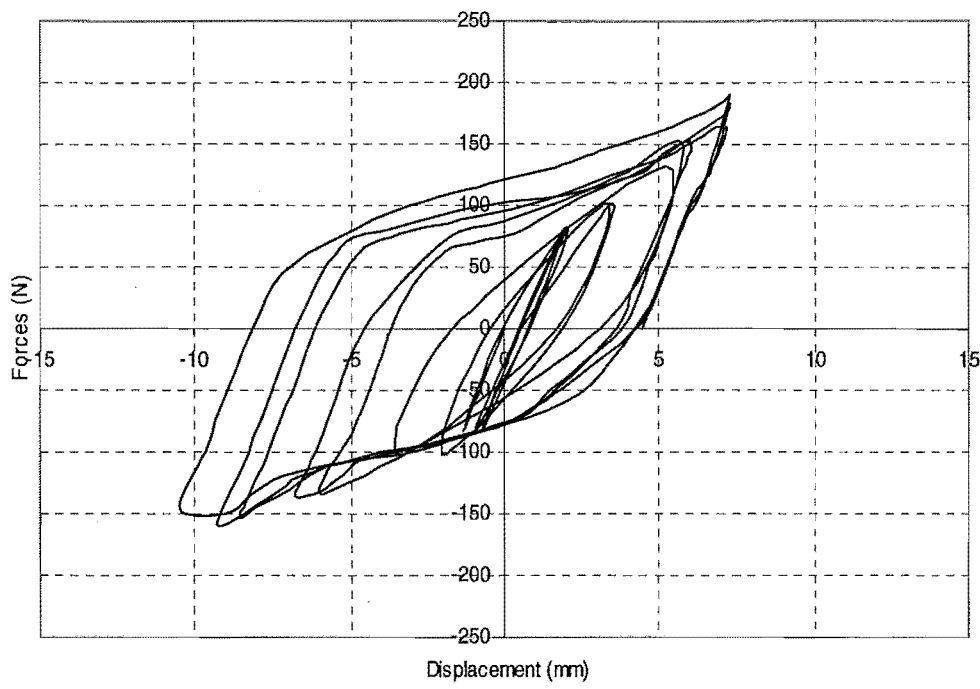


Fig (5-19) Hysteretic response of the (86x7) mm fuse.

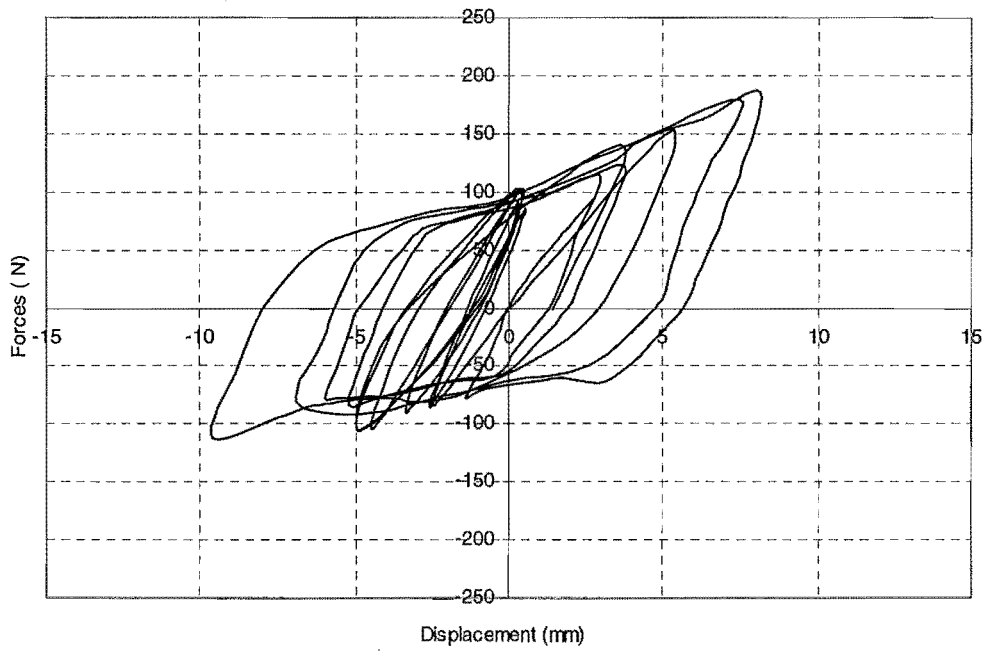


Fig (5-20) Hysteretic response of the (100x7) mm fuse

## 5.10 Determination of the Joint Stiffness

To investigate the stiffness of the fuse joints and compare the stiffness with the initial values from the original frame, a Staeger guage was used in the test to obtain the main source of the displacement. The Staeger guage is a portable, hand held gauge, and it measures displacement by measuring the distance between two 1.6mm diameter steel balls, which are punched into steel blocks. Two sets of steel balls were set up for measurement during the test in order to measure the net fuse rotation.

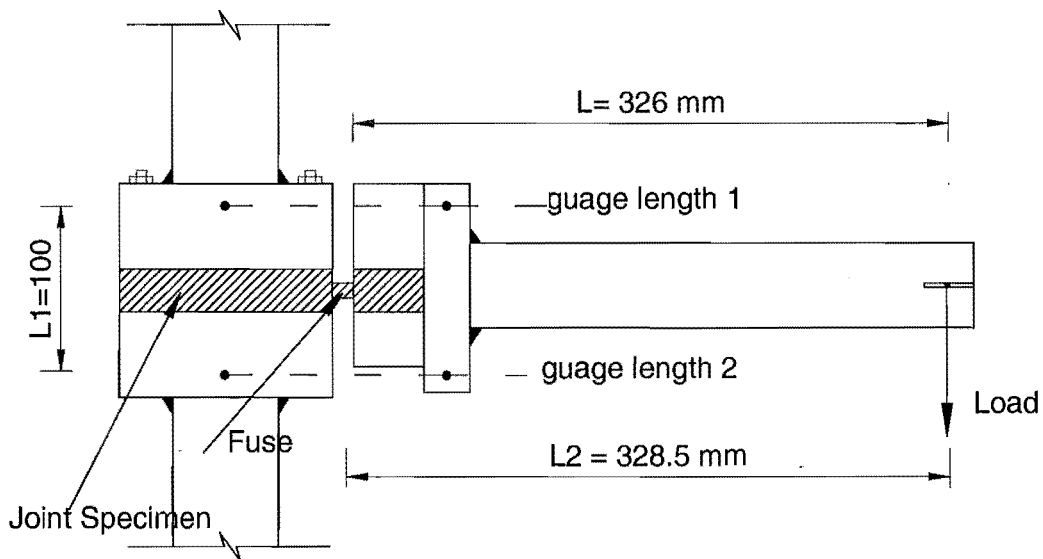


Fig (5-21) A diagram of the location of measuring sets.

The joint specimen was loaded to the peak load in the positive direction, and then in the negative direction. The maximum cyclic load applied to the specimen was 0.75 of the yield load of the fuse in order to study the stiffness of the connection detail. The values of the maximum applied forces were chosen to be equal to  $0.75 F_y$  to ensure the hinge joints remain elastic. For each step of the test, readings on the gauged lengths were taken.

The readings obtained from gauge lengths 1 and 2 were converted into the fuse displacement;  $\Delta_{\text{fuse}}$  by using the following equation assuming that the beam is very stiff relative to the flexibility of the hinge to compute flexural displacement of the cantilever

$$\Delta_{\text{fuse}} = \left( \frac{\Delta_1 - \Delta_2}{L_1} \right) L_2 \quad 5-1$$

where  $\Delta_{\text{fuse}}$  = Fuse displacement,

$\Delta_1$  = Displacement at gauge length 1,

$\Delta_2$  = Displacement at gauge length 2,

$L_1$  = Distance between gauge length 1 and 2,

$L_2$  = Distance between the loading point and the mid-span of the fuse.

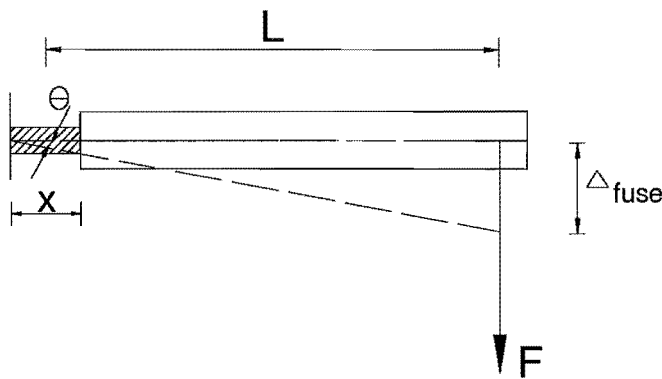


Fig (5-22) Beam joint curvature

Using the relationships from Figure (5-22),

$$\phi = \frac{M}{EI}; \quad \phi = \frac{\theta}{x}; \quad \theta = \frac{\Delta_{\text{fuse}}}{L}$$

where  $\phi$  is the curvature and  $\theta$  is the angle rotation across the fuse.

we can show that  $(EI)_{\text{eff}} = \frac{ML}{\Delta_{\text{fuse}}} x$  5-2

- where  $M$  = Moment at the fuse induced by the load
- $L$  = Distance from the loading point to the face of the joint
- $\Delta_{\text{fuse}}$  = Fuse displacement
- $x$  = Length of the fuse
- $I$  = Second moment of area of the fuse

$E_{\text{eff}}$  is used instead of  $E$  for all the fuses in the calculations and analysis, where  $(EI)_{\text{eff}}$  is the effective flexural rigidity of the fuse.

The  $(EI)_{\text{eff}} / (EI)$  ratio for the beam fuse sections tested are compared with the original values from the Kao design [11] in Table (5-1).

For the column base fuses, the flexural rigidity  $EI$  was used instead of the effective flexural rigidity,  $(EI)_{\text{eff}}$  due to the rigid design of the column fuses.

Table (5-2) Fuse Properties

Fuse Size (mm)	Z (mm <sup>3</sup> )	S (mm <sup>3</sup> )	$M_y$ (N.m)	$M_p$ (N.m)	Forces	
					$F_y$ (N)	$F_p$ (N)
30 x 7	245	367	66	100	94	142
66 x 7	539	808	146	219	444	667
86 x 7	702	1054	190	285	578	869
100 x 7	816	1225	221	332	673	1011

where:

$$Z = \text{elastic section modulus} = \frac{bh^2}{6}$$

$$S = \text{plastic section modulus} = \frac{bd^2}{4}$$

$$M_y = \text{Yield moment} = F_y \cdot Z$$

$$M_p = \text{Plastic moment} = F_y \cdot S$$

$$F_y = \text{Yield force at end of the cantilever}$$

$$F_p = \text{Plastic force at end of the cantilever}$$

A linear relationship between the  $(EI)_{eff}/(EI)$  ratio and the fuse width was assumed and the line of the best fit on the plot in Figure (5-23) was used to obtain suitable values for the analytical model of the structure joints.

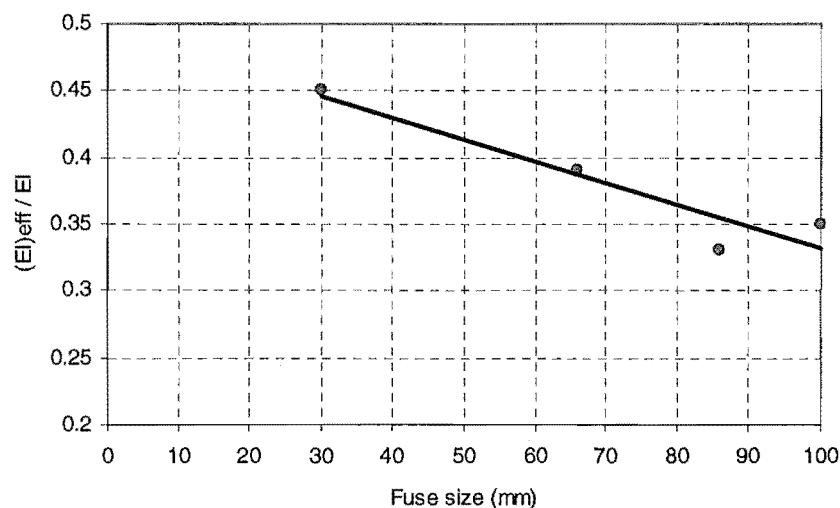


Fig (5-23) Linear stiffness relationship

The final values used for the  $(EI)_{eff} / (EI)$  ratios are shown in Table (5-3) based on Fig (5-23). Figure (5-24) shows the locations of the beam joints on the model of the frame structure and the sizes of the fuses used for each joint.

Table (5-3).

Fuse Width (mm)	$(EI)_{eff} / (EI)$ Ratio	
	Original [11]	Result values
14 x 7	0.45	0.47
30 x 7	0.43	0.44
44 x 7	0.41	0.40
66 x 7	0.38	0.385
72 x 7	0.37	0.375
80 x 7	0.36	0.36
86 x 7	0.35	0.35
92 x 7	0.34	0.345
100 x 7	0.33	0.33

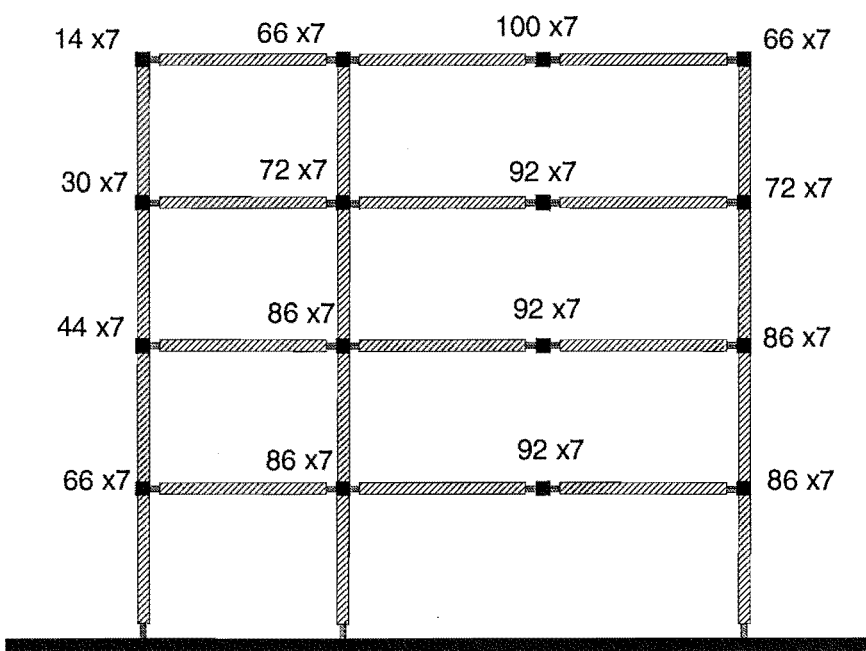


Fig (5-24) Location and dimension of the beam joints fuses

### 5.11 Supplemental Control System

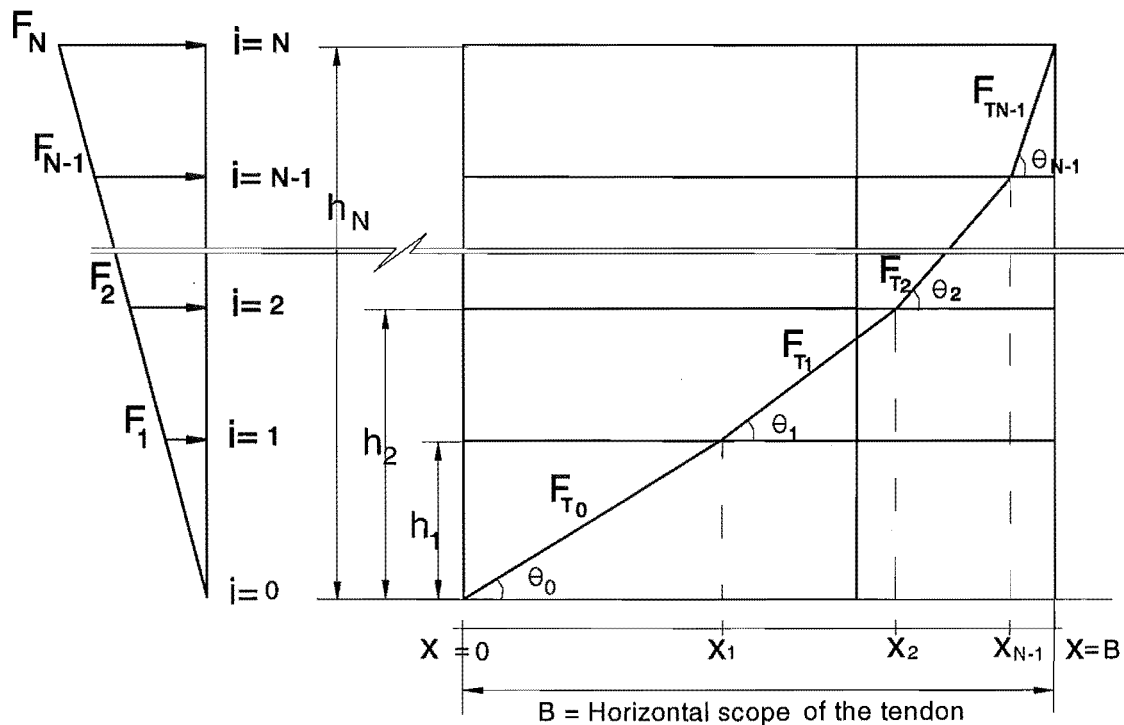


Fig (5-25) Determination of the tendon layout

As discussed in Chapter 3, the tendon layout can be determined by solving the tri-diagonal matrix equation defined by equation (5-3).

$$[R]\{x\} = \{D\} \quad 5-3$$

where  $[R]$  = coefficient matrix determined by:-

$$[R] = \begin{bmatrix} -(R_{0,1} + 1) & R_{0,1} & 0 & 0 & 0 & 0 & 0 \\ 1 & -(R_{1,2} + 1) & R_{1,2} & 0 & 0 & 0 & 0 \\ 0 & 1 & -(R_{2,3} + 1) & R_{2,3} & 0 & 0 & 0 \\ 0 & 0 & 1 & . & . & 0 & 0 \\ 0 & 0 & 0 & 1 & . & . & 0 \\ 0 & 0 & 0 & 0 & 1 & . & 0 \\ 0 & 0 & 0 & 0 & 0 & 1 & -(R_{n-3,n-2} + 1) \\ 0 & 0 & 0 & 0 & 0 & 0 & (R_{n-3,n-2}) \\ 0 & 0 & 0 & 0 & 0 & 1 & -(R_{n-2,n-1} + 1) \end{bmatrix}_{n-1,n-1} \quad 5-4$$

where the diagonal  $= -(R_{i-1,i} + 1)$   
 the above diagonal  $= (R_{i-1,i})$   
 the below diagonal  $= 1$   
 and  $i = 1, n - 1$

$$R_{i,i+1} = \sum_{j=i+1} F_j / \sum_{j=i+2} F_j \quad 5-5$$

in which  $h_{i+1}$  = storey height between level  $i$  and  $i+1$ , and

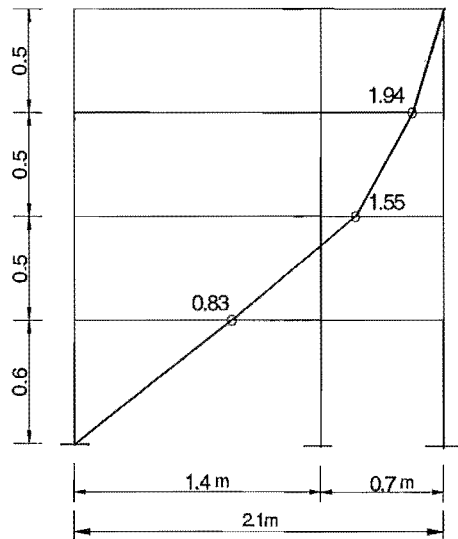
$\{x\}^T = \{x_1, x_2, \dots, x_{n-1}\}$  is the unknown column vector of tendon coordinates,

$$\{D\}^T = \{0, \dots, -R_{n-2,n-1} B\}$$

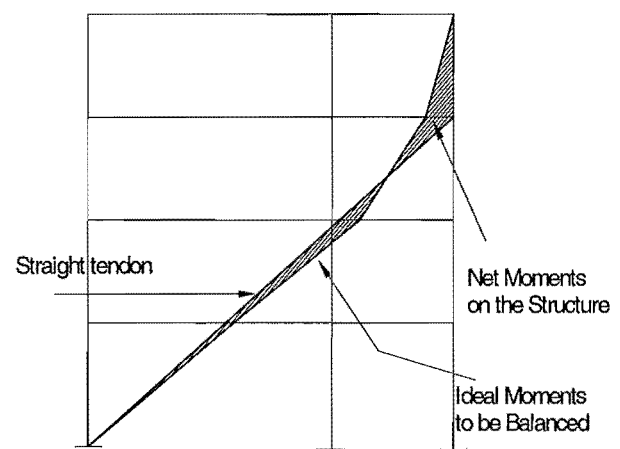
where  $B$  is the width of the tendon layout of the structure.

### 5.11.1 Tendon Profile

The profile of the tendon for the test structure using the above equations is shown below in Figure (5-26a).



a) Theoretical tendon profile



b) Straight tendon

Fig (5-26) Tendon profile

An approximate load balancing solution can be employed in which the draped tendon system is replaced with a straight tendon as shown in Figure (5-26b).

### 5.11.2 Layout of the System

The layout of the supplementary control system for the structure is shown in Figures (5-27) and (5-28). The diagonal damper-tendon members are located outside the structure with a clearance of 25 cm from each side and connected to the structure by

horizontal channel beams. The channel beams are fixed to the structure at the beam-column connections at the first three storeys. The horizontal members are connected to the diagonal tendon at the second and third floors to transfer the damping forces to the floors. Figure (5-29) shows view of the test structure with the supplemental control system on the shaking table.

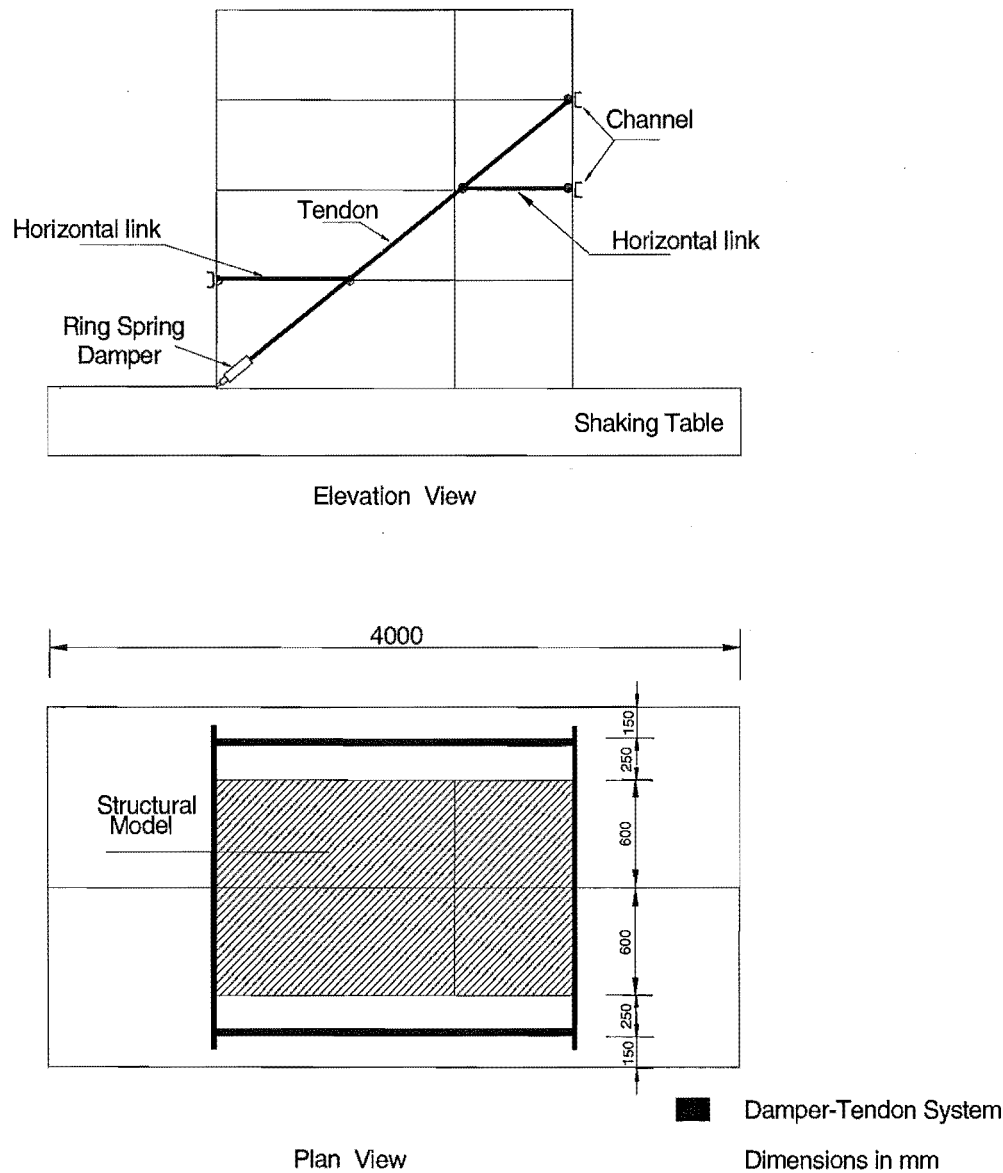
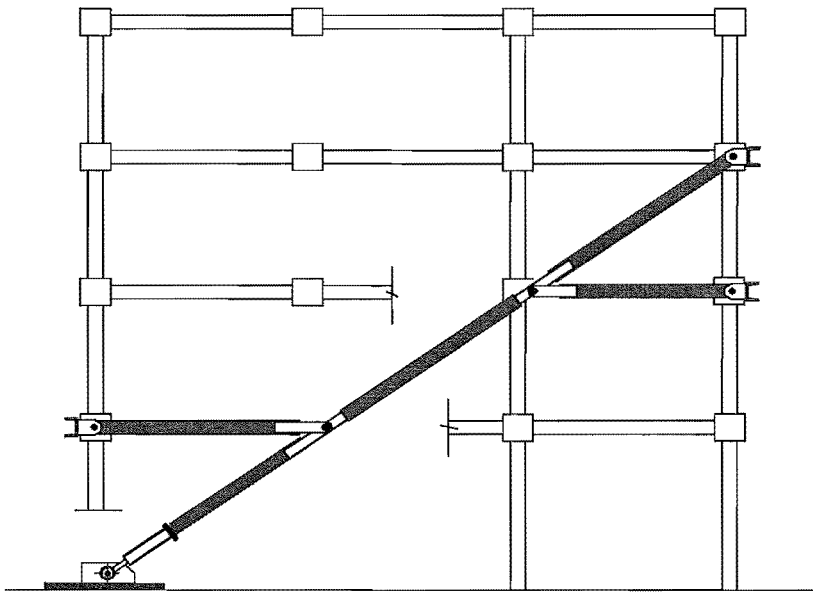
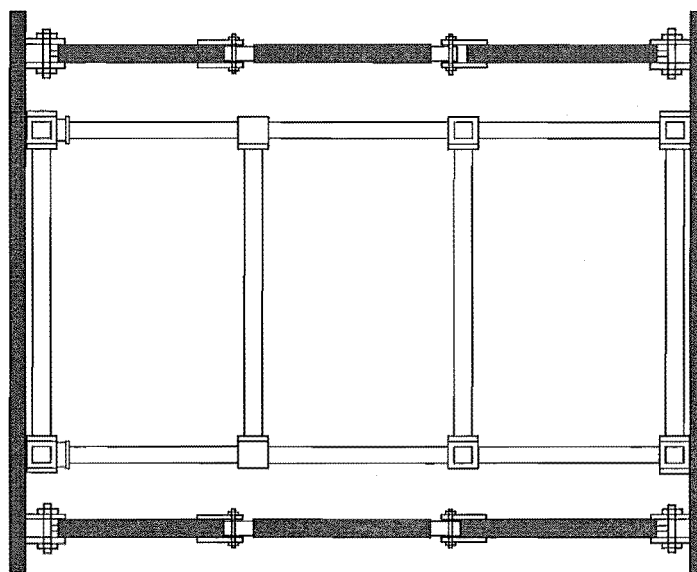


Figure (5-27) Layout of the supplemental control system with the structure.



ELEVATION VIEW



PLAN VIEW

■ Damper -Tendon System

Fig (5-28) Structural model with supplemental control system

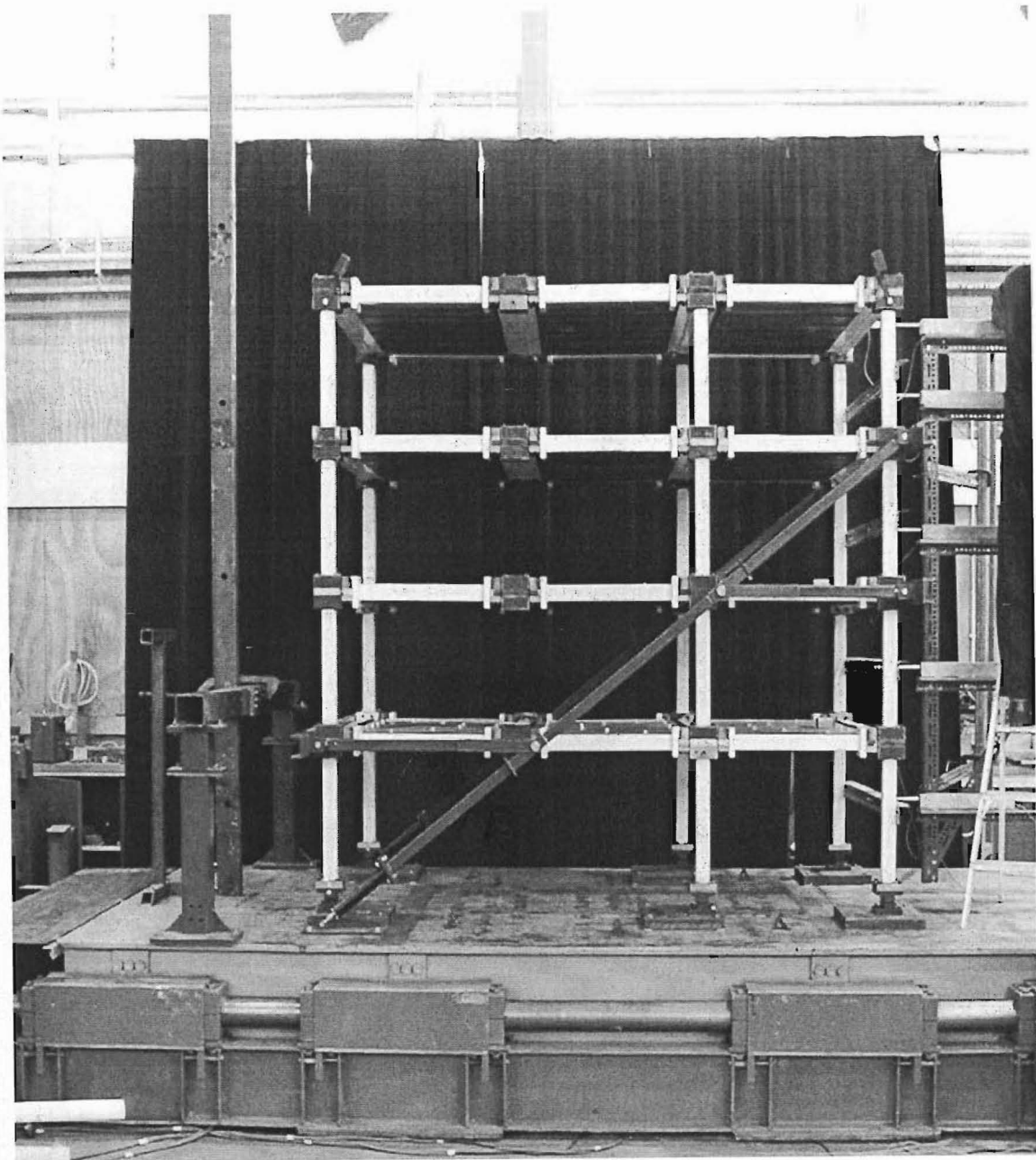


Fig (5-29) View of the test structure with the supplemental control system on the shaking table

## 5.12 Damper Connections

The characteristics of the ring springs dampers used in the experimental work were described in chapter 4. The damper is connected to the base plate by a bolt through the base plate brackets. The base plate with dimension (300x100x10) mm is fixed to the shaking table by two 12 mm bolts, as shown in Figure (5-30). The other end of the damper is connected to the diagonal tendon member by using a plate (100x100x10) mm welded to the tendon and connected to the damper by four bolts (Figure 5-31).

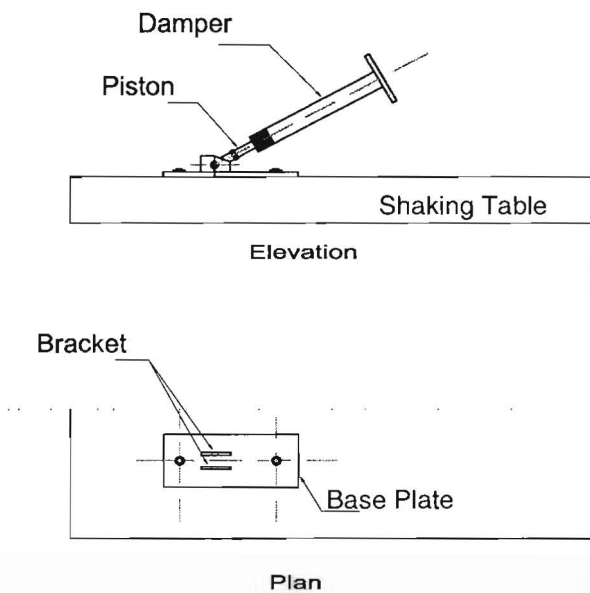


Fig (5-30a) Damper-Base connection

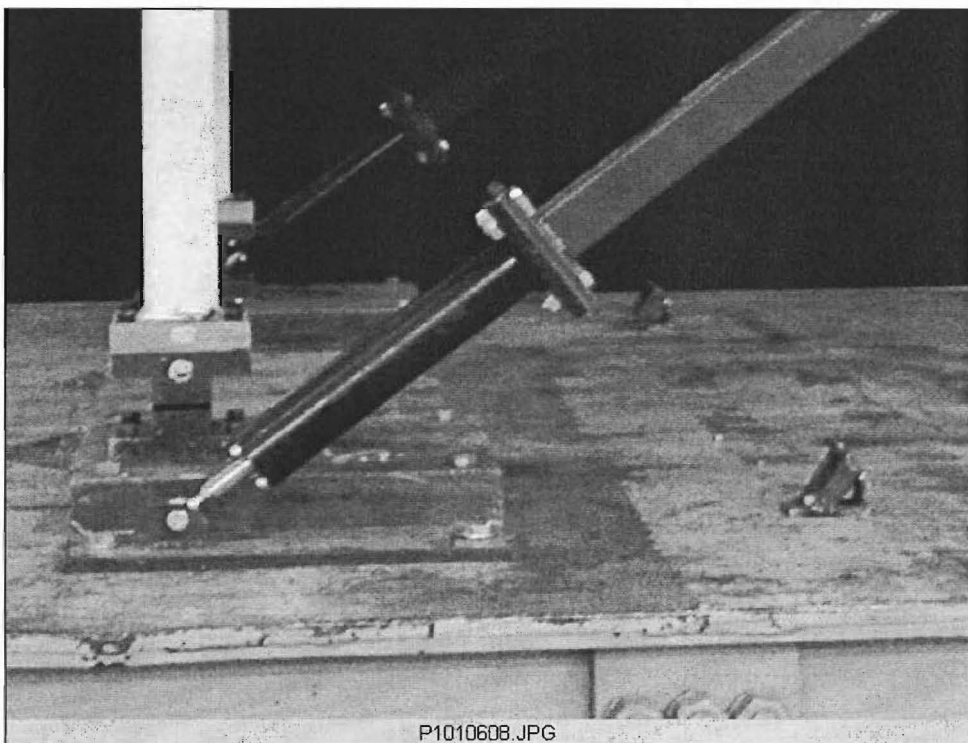


Fig (5-30b) Typical damper–base connection

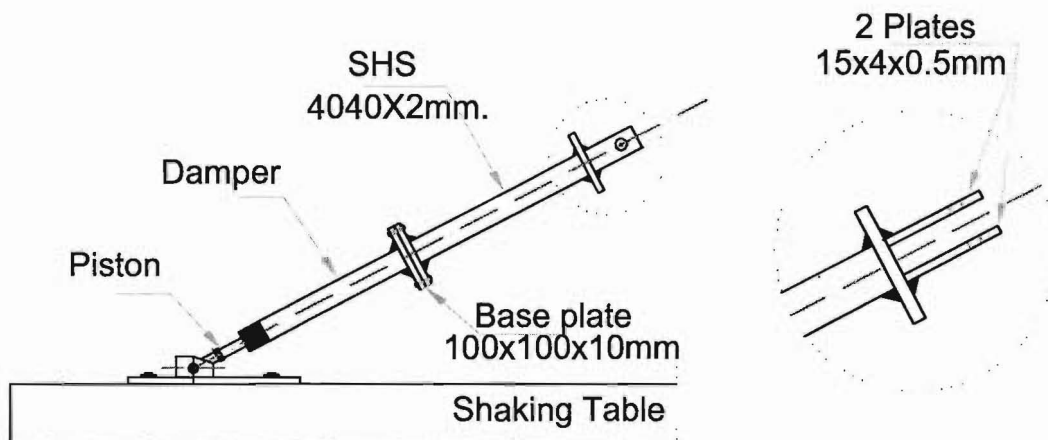


Fig (5-31a) Damper-tendon connection

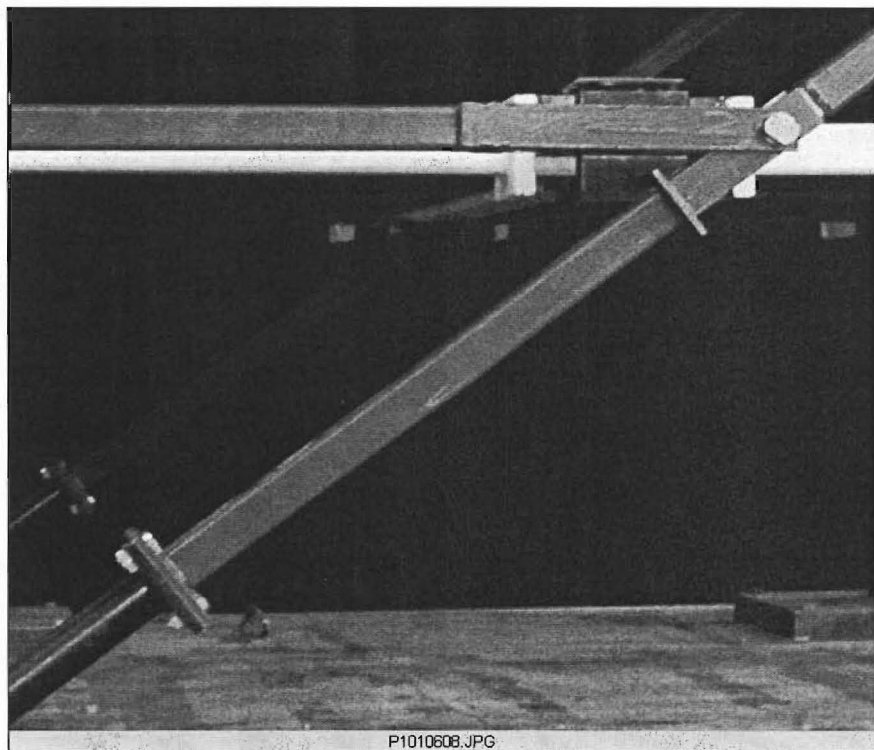


Fig (5-31b) Typical damper-tendon connection

### 5.13 Tendon Connections

The diagonal tendon and the horizontal members are made of hollow square  $40 \times 40 \times 2\text{mm}$  steel sections. The tendon has three segments; the lower, middle, and upper parts at the first, second, and third floors respectively. The horizontal members are placed parallel to the first and second floors. The tendon and horizontal members are linked by a pin mechanism. The connection between the horizontal members and the channel beams are also pin mechanisms, Figure (5-32).

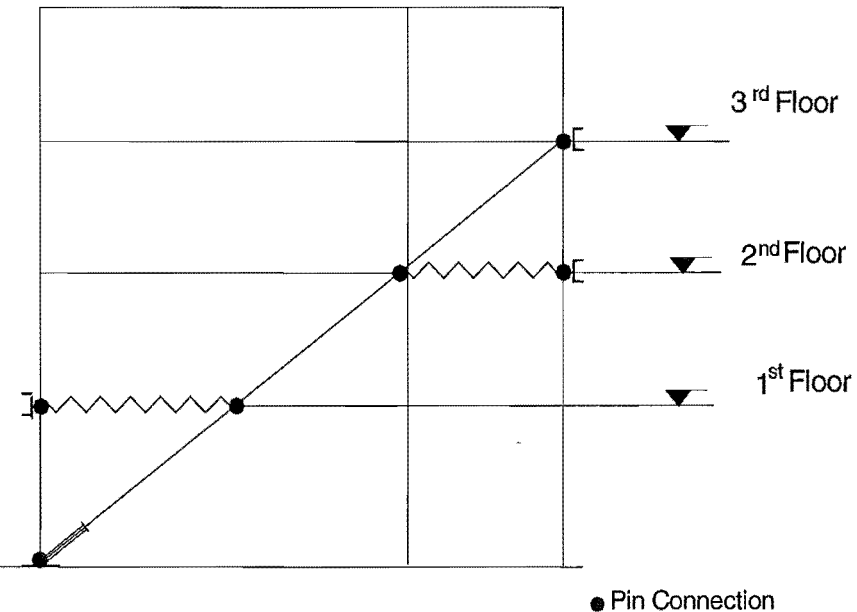


Fig (5-32a) Connection mechanism

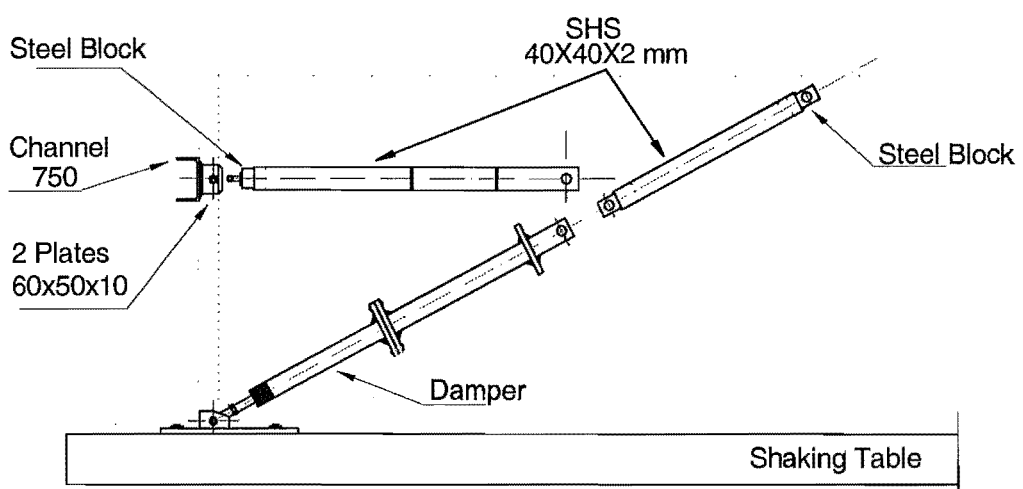


Fig (5-32b) Tendon-Horizontal member connection

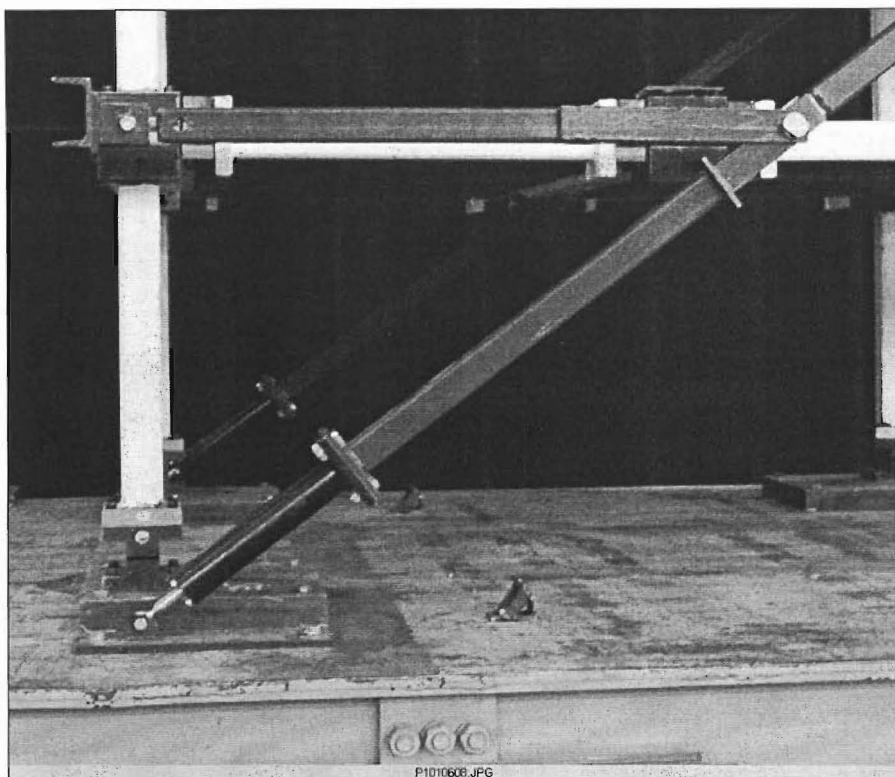


Fig (5-32c) View of the tendon connections

Figure (5-32) shows the details of the connections between the middle part of the tendon and the horizontal members. In the lower part of the tendon, two plates of 300x300x10 mm are welded on the sides of the hollow square section with a hole 20 mm in diameter to take the pin connection bolts. Two steel blocks of (30x30x100) mm are inserted and welded to the both ends of the middle segment of the tendon.

In the horizontal members, two plates are used as packing between the hollow square section of the beam and the outer plates to produce enough width to straddle the horizontal members with the other parts in a pin connection, Figure (5-33).

Three horizontal beams of 75x40 mm channel are fixed to the column-beam connections at the first, second, and third floors. The tendon is connected to the beams by fixing the same size of steel block into the end. Two brackets are welded to the beam and a pin connection is used to connect the tendon with the beams as shown in Figure (5-33).

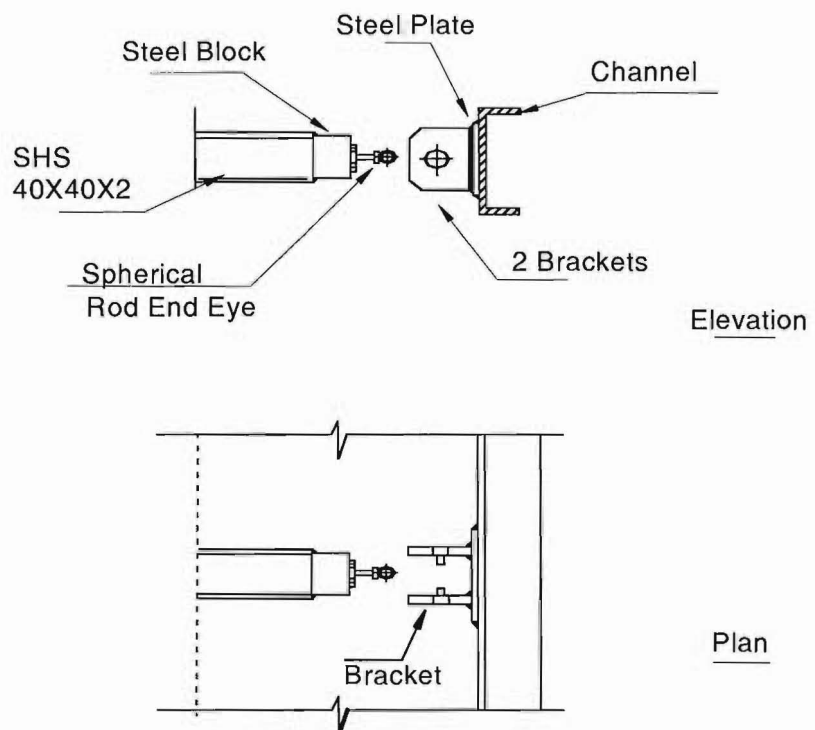


Fig (5-33a) Tendon-Beam connection at storey level

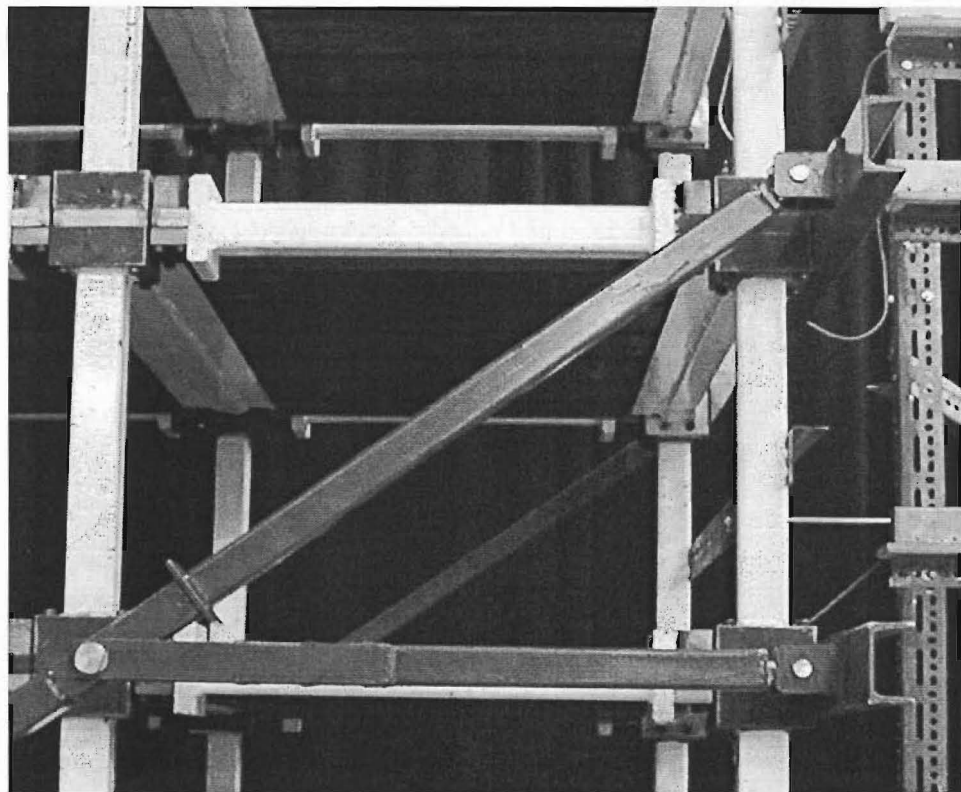


Fig (5-33b) Typical tendon-beam connections at storey level

## Chapter 6

### Experimental Investigation

#### **6.1 Introduction**

Dynamic testing of the test structure was performed on the shaking table in the Structures Laboratory. Linear potentiometers and accelerometers were used to measure the frame response. Several tests were carried out during the testing. The tests could be categorized into free vibration and different levels of earthquake shaking tests. The free vibration tests were conducted to obtain the fundamental period and the critical damping ratio of the structure with and without the supplemental control system. The different levels of the shaking tests were carried out to obtain the effect of the supplement control system (details are discussed in Chapter 7) to reduce the response of the structure. The results of these tests were then compared with those predicted analytically.

#### **6.2 Test Set-up**

##### **6.2.1 Shaking Table**

This facility is part of the Structures Laboratory of the Department of Civil Engineering at the University of Canterbury. The shaking table has a number of system-components that when combined result in a system capable of reproducing displacement-time histories. The detailed descriptions of the system and each component are presented. From the original set up of the shaking table, the control system has been upgraded. The Dartec M 1000/A was replaced by a MTS Test Star II, which allows the reproduction of earthquake like signals without the necessity of an external command, as it was necessary with the old controller. Figure (7-1), shows an updated scheme of the main components and of the system and how they interact with each other.

The shaking table has only one degree of freedom (East-West). The actuator transfers East-West forces to the table by pumping units. A feedback electric signal informs the controller the displacement of the table and then the controller sets the servo-valves up to produce a displacement equal to the target displacement. Velocity and acceleration are not tracked and therefore cannot control efficiently high frequency accelerations since they produce very small displacements. The main characteristics of the shaking table are given in Table 6-1.

Table (6-1) Characteristic of the shaking table.

Plan area	2.0 x 4.0 m
Height above ground	700 mm
Material	Steel
Weight	24 kN
Natural frequency (unloaded)	20 Hz (approx.)
Table top	12 mm steel plate
Maximum travel	$\pm 300$ mm
Maximum velocity attainable	1 m/sec
Static capacity	$\pm 250$ kN
Dynamic capacity	$\pm 200$ kN

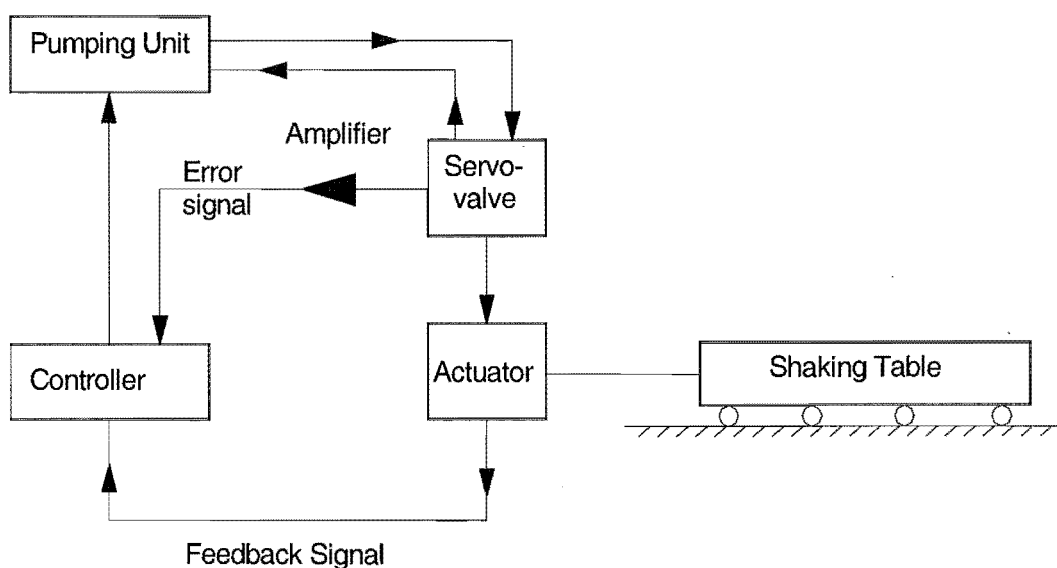


Fig (6-1) Schematic diagram of the shaking table and its main components.

## 6.2.2 Instrumentation

### 6.2.2.1 Displacements and Interstorey Drifts

Six linear potentiometers were used in the tests to measure the total displacements of each floor and the base, as well as the interstorey drift ratio at each floor. The potentiometers have spring loaded spindles and simply bear against a target plate. The method of calibrating is by taking an initial value, then lifting the spindle from the target plate and inserting a graduated steel scale rule of known dimension between the potentiometer spindle and the target plate and taking a second reading. This procedure is repeated with a range of scale rules to acquire a check on linearity and to determine a calibration factor for converting the output voltage to the known displacements. The potentiometers were mounted on a rigid frame away from the shaking table.

The measurements of the displacement were made at the mid-height of the columns and not at the floor levels because the end blocks will rotate due to the bending in the longitudinal beams. Thus, the measurements will not be correct. For more accurate measurements, the potentiometers were attached at the mid-height of the storeys and the displacements are calculated by taking the mean of the two potentiometer reading. This will be reasonably accurate as the column and beam members are relatively stiff and the rotations occur at the hinge locations (see Figure 6-2).

The results from the linear potentiometers were interpolated to obtain total floor displacements and interstorey drifts ratios. After obtaining the total displacements, the values were converted into relative displacements by subtracting the base displacements. Figure (6-3) presents a schematic of the location of the measuring devices and the method for obtaining total floor displacements.

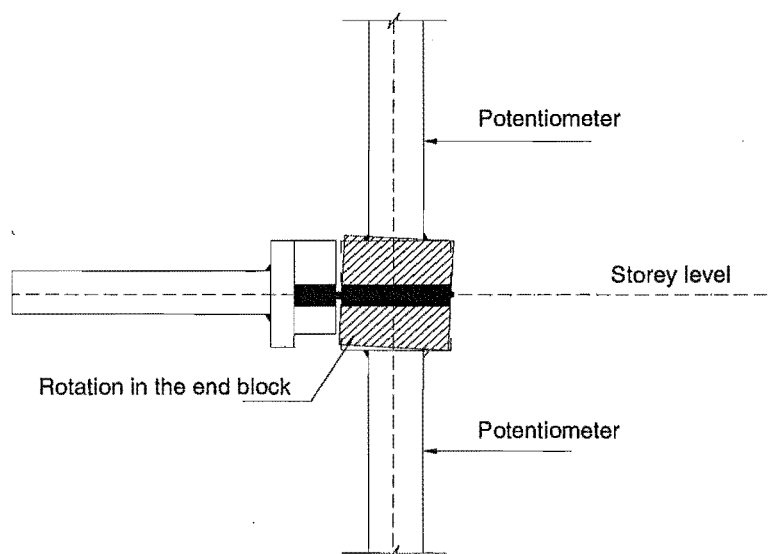


Fig (6-2) Rotation in the end block

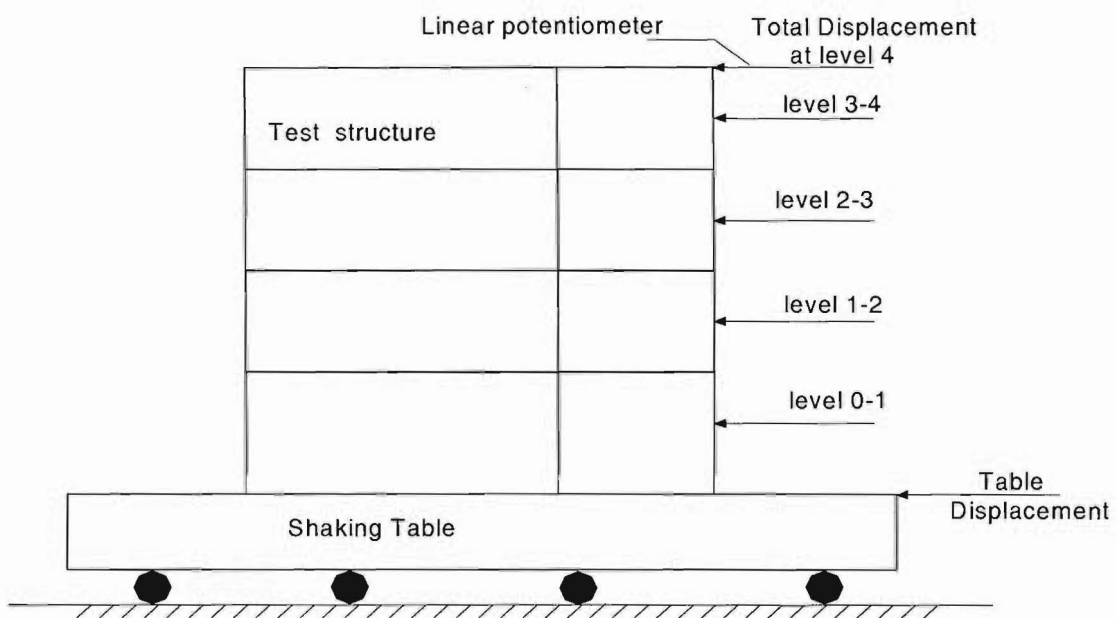


Fig (6-3a) Instrumentation set-up for obtaining floor displacement and interstorey-drift.

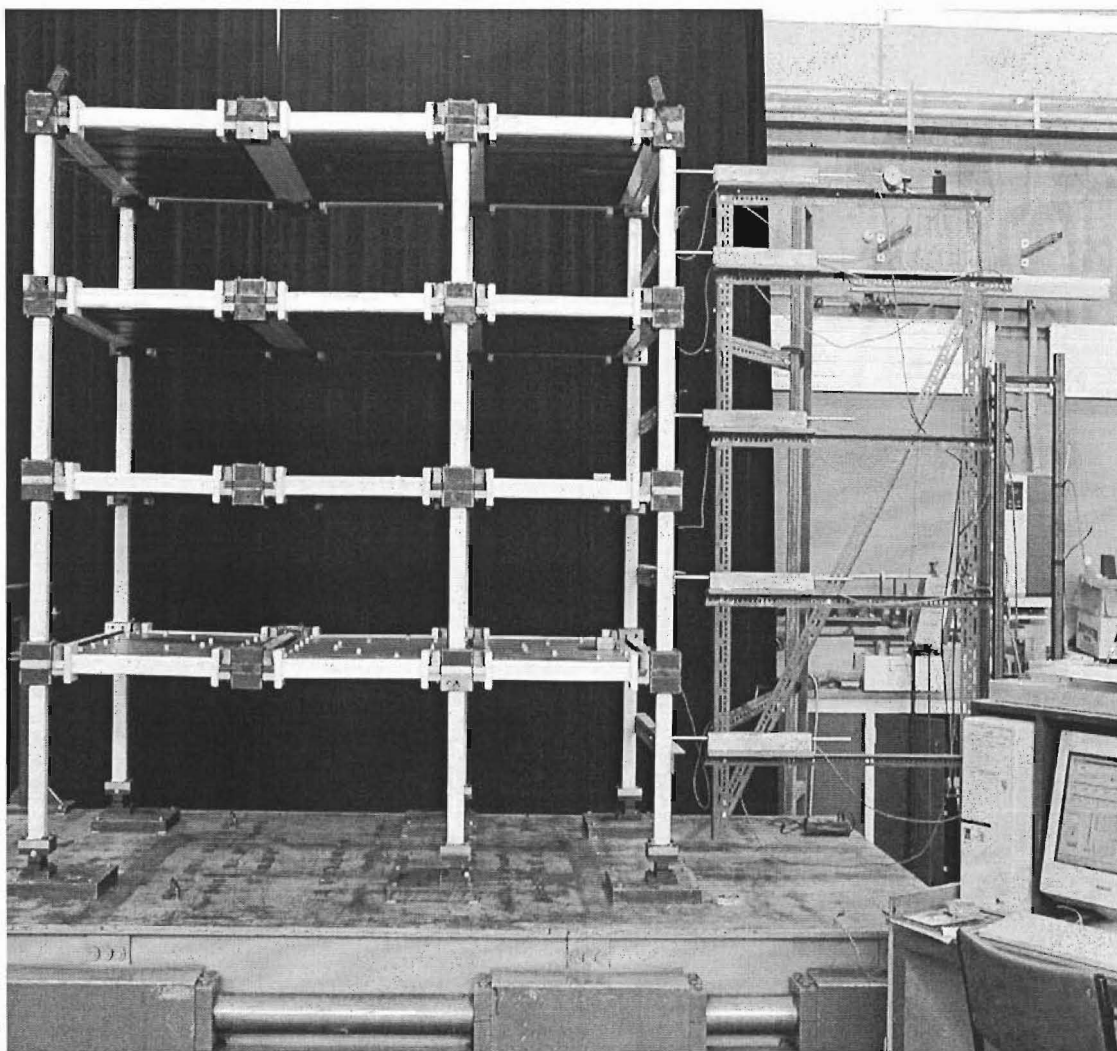


Fig (6-3b) Typical set-up of the potentiometers and structure.

Figure (6-3) and (6-4) show the set-up of the potentiometers to obtain the floor displacements and intersorey drifts. The relative displacements of the storeys are determined from the potentiometer records by using the following equations:

$$\Delta_1 = \frac{\delta_2 + \delta_1}{2} \quad 6-1$$

where

$\Delta_1$  = The total displacement of level 1.

$\delta_1$  = The potentiometer record at level 0-1.

$\delta_2$  = The potentiometer record at level 1-2 (see Figure 6-4).

and

$$\Delta_2 = \frac{\delta_3 + \delta_2}{2}$$

$$\Delta_3 = \frac{\delta_4 + \delta_3}{2} \quad 6-2$$

$$\Delta_4 = \delta_5$$

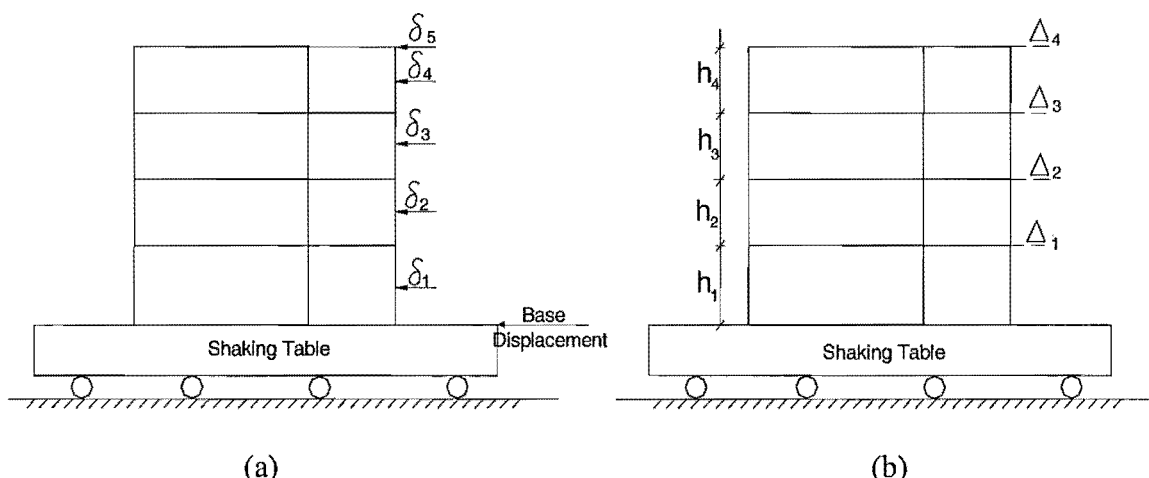


Fig (6-4)

After determination of the relative displacement of the floors as shown in Figure (6-4a), the interstorey drifts of the structure can be calculated as follows (Figure 6-4b):

$$I_4 = \frac{\Delta_4 - \Delta_3}{h_4} \quad 6-3$$

where

$I_4$  = The intersorey drift of level 4

$\Delta_4$  = The relative displacement of level 4

$\Delta_3$  = The relative displacement of level 3

$$I_3 = \frac{\Delta_3 - \Delta_2}{h_3} \quad 6-4$$

$$I_2 = \frac{\Delta_2 - \Delta_1}{h_2}$$

$$I_1 = \frac{\Delta_1 - \Delta_{table}}{h_1}$$

### 6.2.2.2 Floor Accelerations

Five unidirectional accelerometers were used in the tests to measure the total acceleration of the shaking table and each floor of the structure. The accelerometers were calibrated by rotating through 90° along its sensitive axis. This applies a change of gravitational force to the transducer equal to 1g. For measuring the total floor accelerations, the accelerometers were placed on the top plate at each level and on the shaking table, as shown in Figure (6-5)

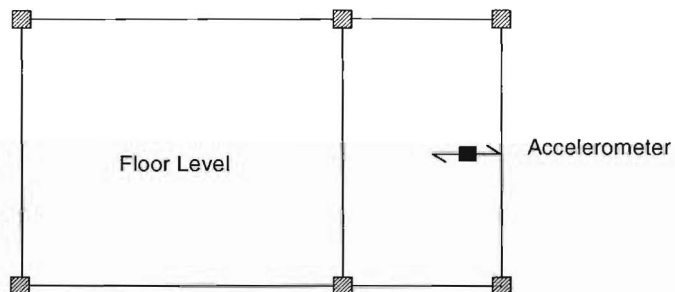


Fig (6-5a) Plan view of a floor showed the location of the accelerometers.

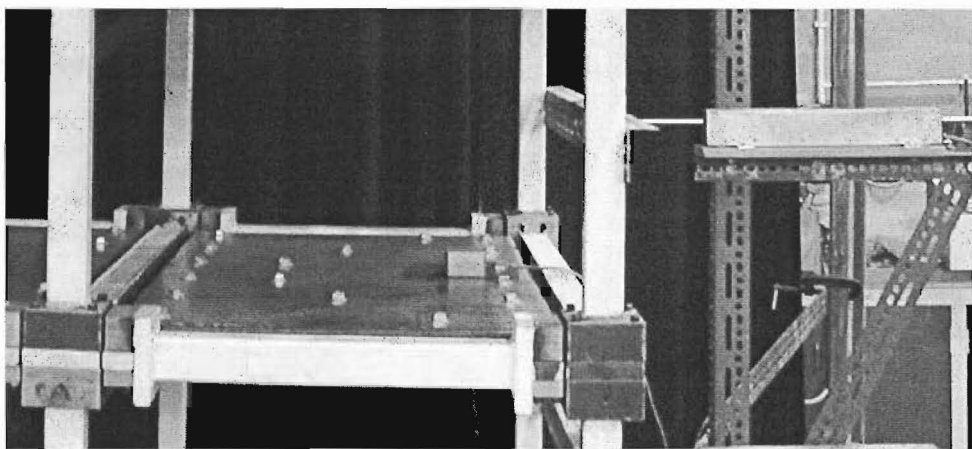


Fig (6-5b) typical view of a floor showed the location of the accelerometer

All the linear potentiometers and the accelerometers were wired to a high-speed data logger.

### 6.2.2.3 Data Logger

A data logger is a device with the capability of taking an analogue input signal, converting it to a string of digital data and storing it for retrieval at later time. Figure (6-6) shows a data logger.

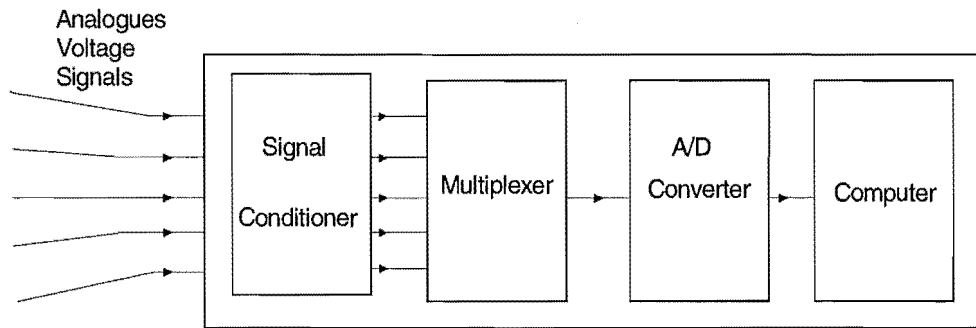


Fig (6-6) Data Logger

The analogue voltage signals from the transducers mounted on a test specimen are connected to the input connections of the data logger. The individual analogue signals are processed in the signal conditioner to adjust them to the optimum level for the A/D converter (An A/D converter is a device for converting an analogue signal into digital information).

Whenever a scan command is initiated from the computer, the Multiplexer Switches each channel, in sequence, to connect briefly with the A/D converter. While connected to the A/D converter, the analogue signal for the particular channel is converted to a representative string of digital data which is stored in computer memory. The Multiplexer then switches to the next channel to connect with the A/D converter. This process is repeated until all of the selected channels have been scanned. Eleven channels were used the tests. Six channels are used for recording the displacements from the linear potentiometers, and five channels are used for recording the accelerations from the accelerometers.

## 6.3 Free Vibration Tests

Free vibration tests were carried out by pulling the structure to one side by using a steel wire and then releasing it and allowing it to vibrate. The tests were used to obtain the fundamental period of the structure and its damping ratio with and without the supplemental control system. The amplitude of the acceleration applied to the structure was controlled by having a dial-gauge attached to the top linear potentiometer to observe the amount of displacement of the structure from his original position as shown in Figure (6-7). After achieving the target displacement, the steel wire was cut to allow the structure to vibrate freely.

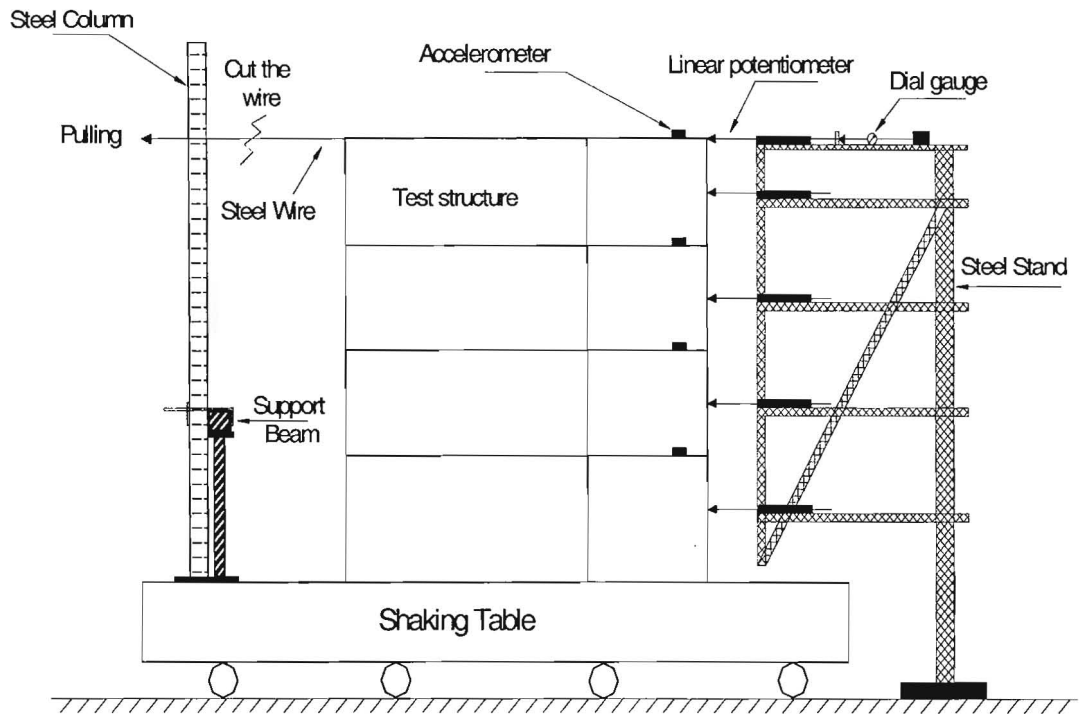


Fig (6-7a) Set-up of the free vibration test.

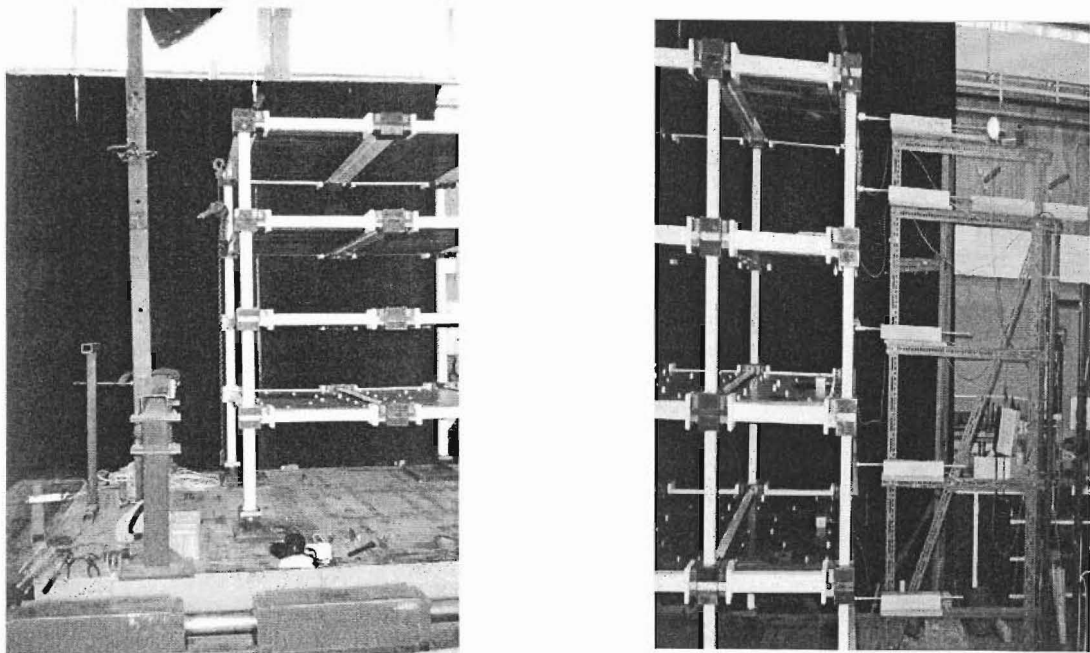


Fig (6-7b) typical set-up of the free vibration test

### 6.3.1 Free Vibration Tests without the Supplemental Control System

Before attaching the supplemental control system, two tests were carried out with 6.0 and 5.0 mm top floor displacements. 6 mm was chosen as the maximum displacement at the top of the frame in order to ensure that the frame behaviour remained elastic. The response with the 6.0mm of initial displacement is shown in Figure (6-8).

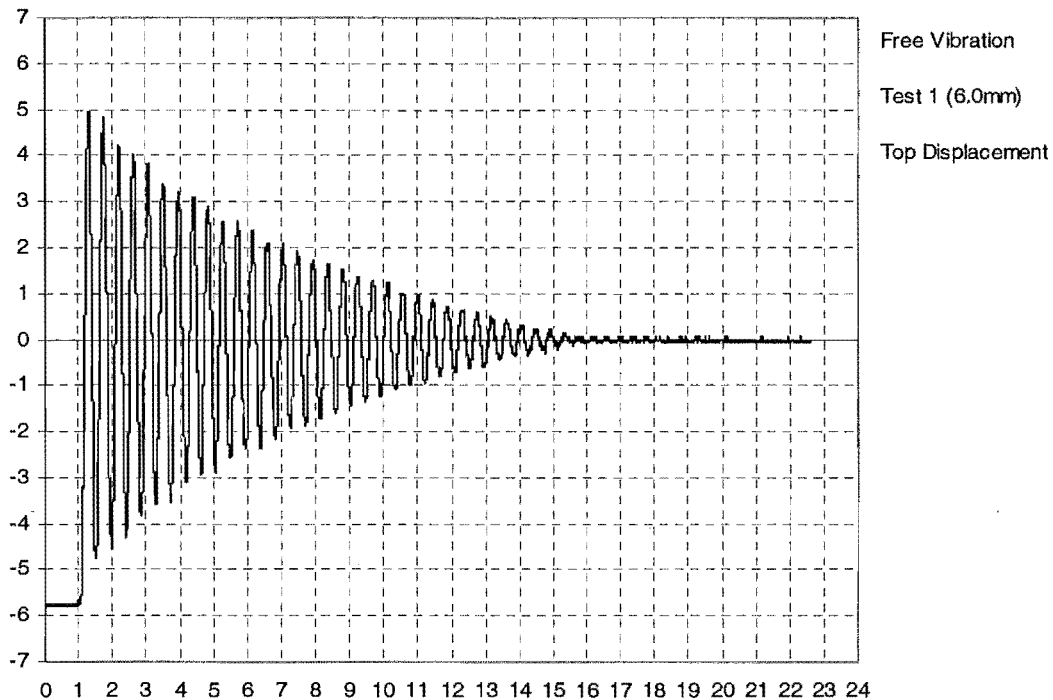


Fig (6-8) Displacement time-history at top level -test 1-(6mm)

The fundamental natural period and the damping ratio of the structure can be calculated from Figure (6-8) as follows:

No of cycles (for example) between 3 and 9 sec = 14 cycles

So, the natural period  $T_0 = 0.43$  sec

The total amplitude of the displacement at 3 seconds equals 6mm, and at 9 second equals 2.2 mm.

$$\text{So, } \delta_N = \ln \frac{y_1}{y_2} = 1.003 \quad 6-5$$

$$\text{Then, the damping ratio } \zeta_N = \frac{\delta_N}{2\pi N} = \frac{1.003}{2\pi(14)} = 1.14\% \quad 6-6$$

The same ratios can be obtained from the displacement time histories for other levels of the initial displacement of the structure as shown in Figure (6-9).

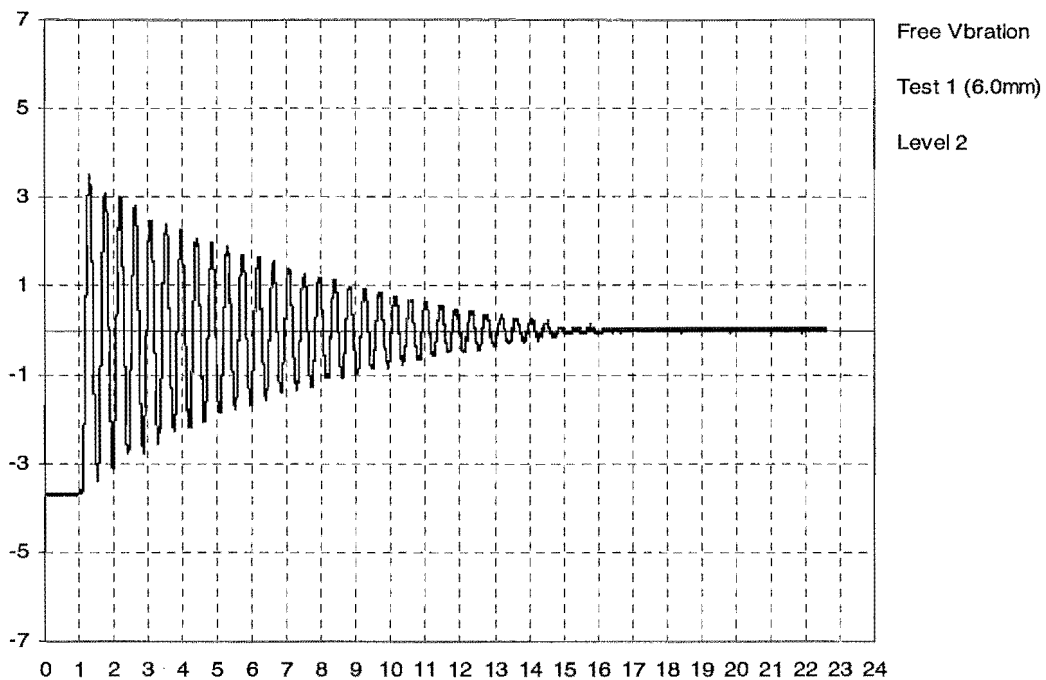


Fig (6-9) Displacement time-history at level 2-Test 1-(6mm)

Test 2 free vibration with maximum displacement of 5 mm at the top of the structure was carried out to confirm the results of test 1. The values of the natural period  $T$  and damping ratio  $\zeta$  are similar to those obtained from test 1. Figure (6-10) shows the plots of the time- history for test 2.

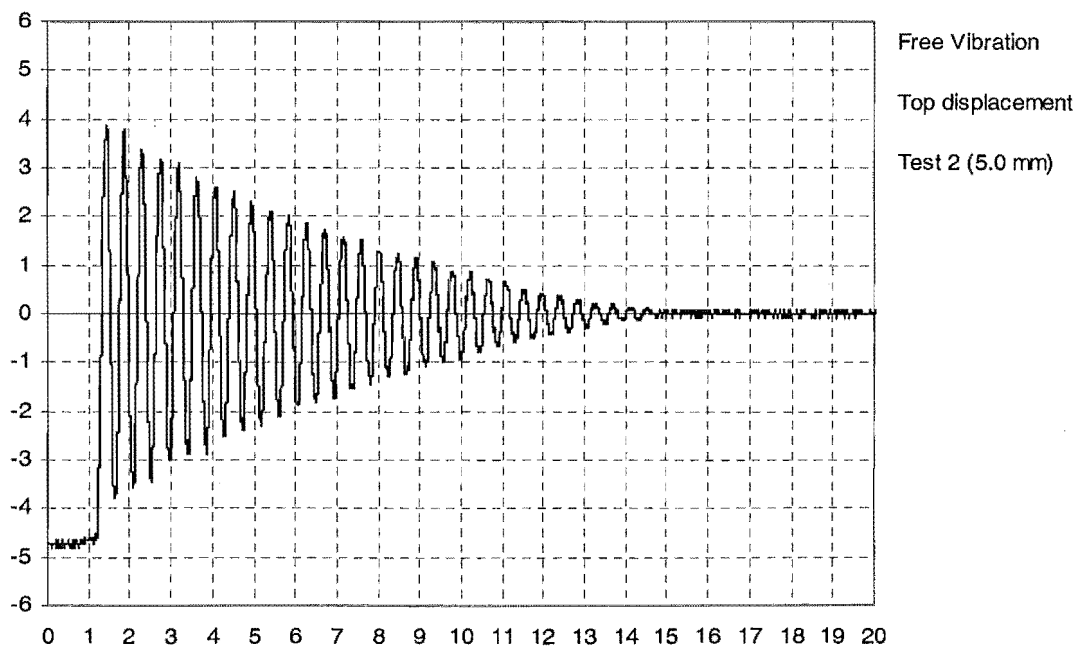


Fig (6-10a) Displacement time-history at top level -Test 2-(5mm)

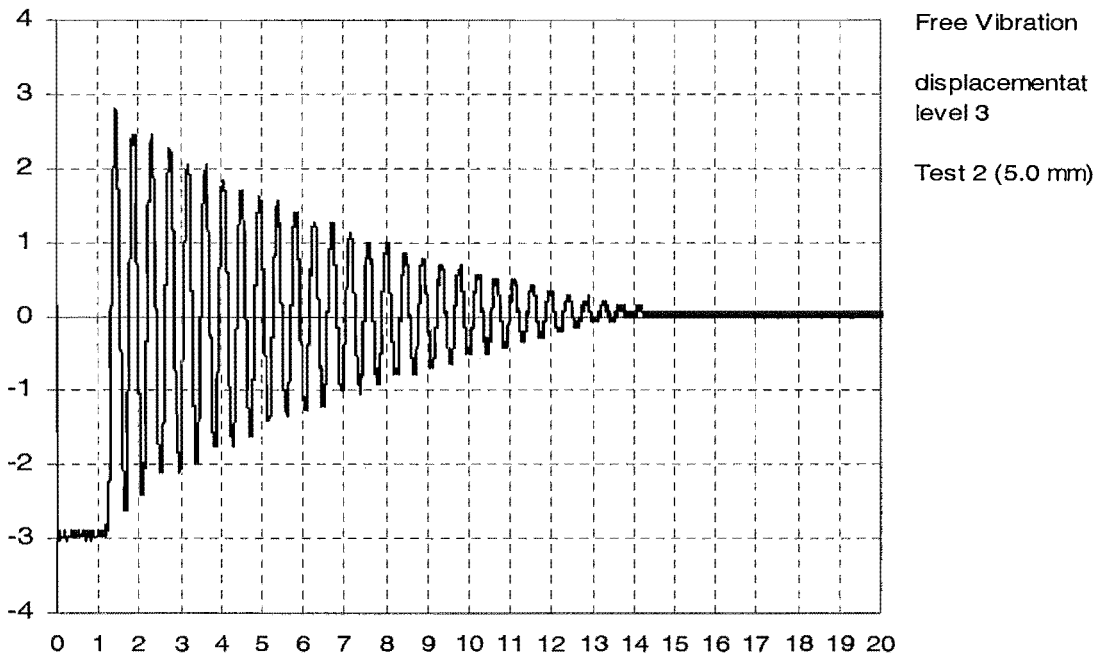


Fig (6-10b) Displacement time-history level 3 -Test 2-(5mm)

### 6.3.2 Free Vibration Tests with the Supplemental Control System

After adding the damping system to the test structure, the same procedure for the free vibration test was carried out to obtain the natural period and the damping ratio of the structure with the supplemental control system. It was found that the natural period was 0.25 sec, and the damping ratio was 7.68 % of critical damping. The results are compared with those for the original structure in Table (6-2).

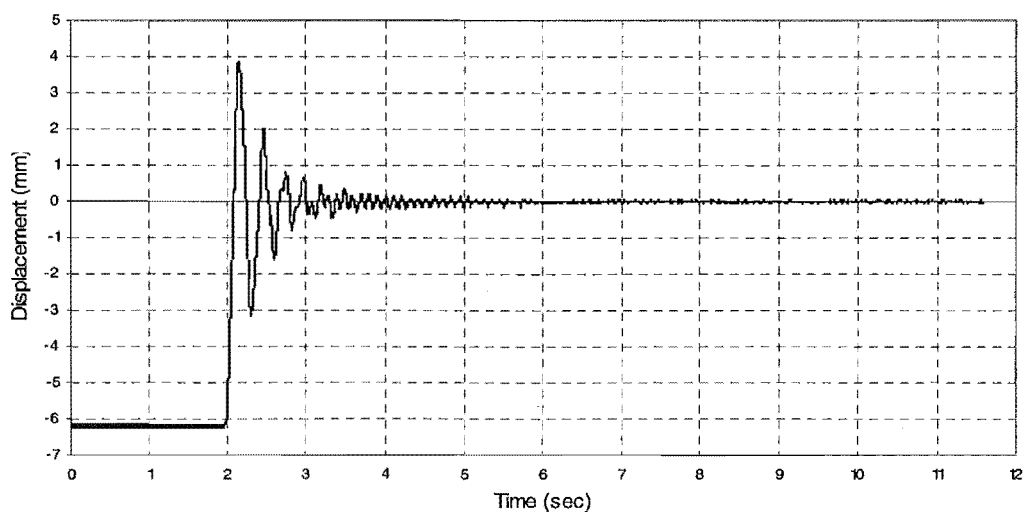


Fig (6-11) Displacement time history top level-Test 3- (6mm)

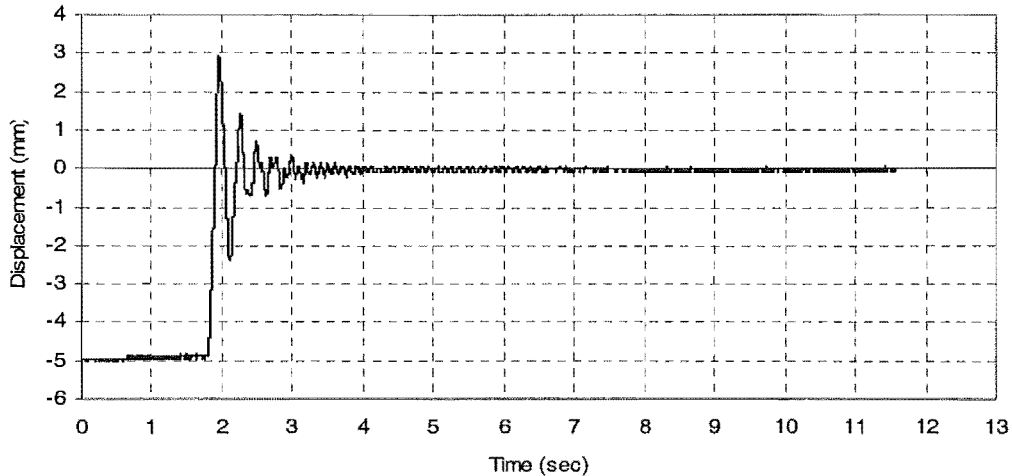


Fig (6-12) Displacement time history top level-Test 4- (5mm)

Table (6-2) Damping ratios of the structure.

	without the supplemental control system		with the supplemental control system	
	Test 1	Test 2	Test 3	Test 4
Damping ratio $\zeta$	1.14 %	1.15 %	7.68 %	6.83 %

These damping values are derived from the logarithm decrement from the free vibration testing of the frame.

#### 6.4 Computer Model

The structure was modelled for analysis using program, RUAUMOKO, developed by Carr [1] for two dimensional non-linear dynamic time-history analysis. The program is designed to produce a piece-wise time history non-linear response of a general two-dimensional framed structure to ground acceleration or time varying force excitation.

A two dimensional instead of a three-dimensional analysis was chosen because the response of the transverse frame and out-of-plane behaviour of the members were considered to be insignificant in this research project and a two-dimensional analysis would give sufficient information. This section describes the details of the inelastic dynamic analysis of the structural model.

##### 6.4.1 Elements

RUAUMOKO offers an option of defining a member with 4 nodal points. This type of member, the 4-node element, has an optional rigid link at both ends. The two outer nodes are the usual nodes where the member forces and stiffness act, and the two inner nodes define the lengths of the rigid links.

A 4-node member was used to model the joint block, the fuse and the beam-fuse to column-fuse connection, throughout the frame. One rigid link of the member models the joint block, while the other models the beam-fuse connection. The middle part of the member, in between the two inner nodes, is the flexible beam fuse.

For the column members, the 4 node members were selected with the rigid links modelling the joint blocks at the top and the bottom of the columns. 2-node members with no rigid links were used for the beam members.

#### **6.4.2 Nodes**

The model has 121 nodes and each node has 3 degrees of freedom. All the degrees of freedom of the base nodes are restrained for a fully fixed boundary condition. The inner nodes of the vertical four-node elements are slaved to the outer nodes to couple the degrees of freedom of the vertical displacements, while the nodes of the horizontal elements are slaved to the external nodes at each level to couple the degree of freedom of the horizontal displacements. This reduces the total number of degrees of freedom in the analysis, and hence speeds up the computation process.

#### **6.4.3 Member Elastic Properties**

The beam member type was adopted for all the elastic members, i.e. beams and columns, and the behaviour of the frame members followed the concept of the Giberson's one component model as described in the RUAUMOKO manual [1].

The spring member type was selected for all the fuses. A spring member can model a fuse more appropriately than a frame member since the fuse was designed to form a plastic hinge over its whole length, instead of just at two ends. The spring stiffness in the local X or longitudinal direction is assumed to be infinite while in the local Y or transverse shear direction is equal to  $GA/L$ , where G is the shear modulus, A is the area and L is the length of the section. The rotational stiffness of the section is equal to  $EI/L$ , where E is the elastic modulus and I is the moment of inertia of the section. The value of  $(EI)_{eff}$  was used for every beam fuse section to take into account the excess flexibility found in the quasi-static joint specimen tests. For the column base fuses, the flexural rigidity,  $EI$  was used instead of the effective flexural rigidity,  $(EI)_{eff}$  due to the rigidly of the column fuses.

#### **6.4.4 Earthquake Excitations**

Two different time-history records were used as an input to the shaking table controller to create the table excitation. The records were generated from the 'QUAKE' program developed by Carr [3]. The first record is El Centro 1940 N-S component, and the second record is Taft earthquake S69E component which was modified to be compatible with NZ4203:1992 [37].

Such excitation records were run on the shaking table to produce the shaking table record of the El Centro and Taft excitation as shown in Figure (6-13).

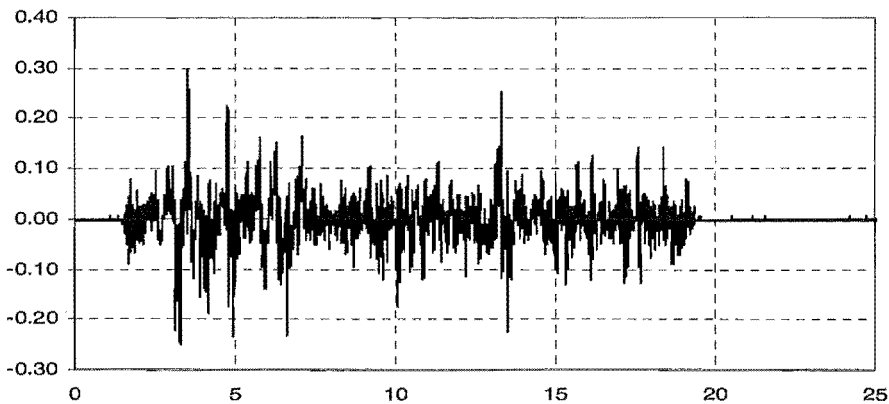


Fig (6-13a) 100% of El Centro shaking table acceleration

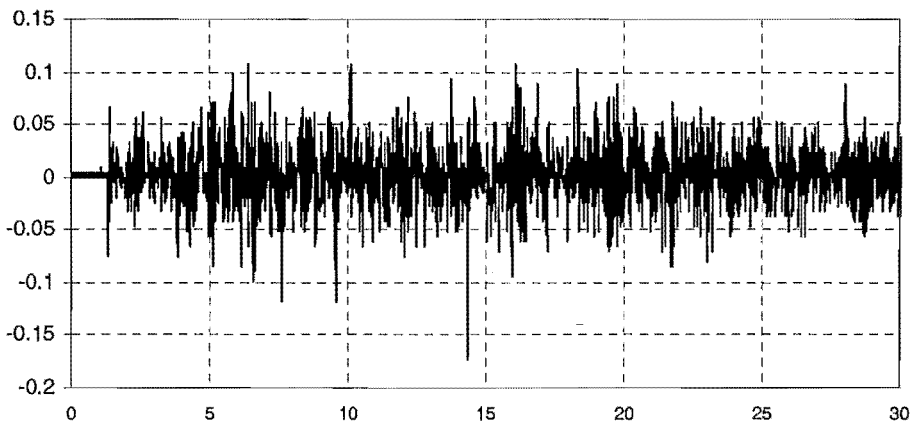


Fig (6-13b) 100% of 4203Taft shaking table acceleration

The El Centro record was chosen as it is a common well known benchmark earthquake record while the modified Taft record is modified to be compatible to the current design code NZS 4203:1992 [37] and scaled to match the capabilities of the shaking table.

## 6.5 Comparison between Experimental and Analytical Free Vibration

### 6.5.1 Free Vibration without the Supplemental Control System

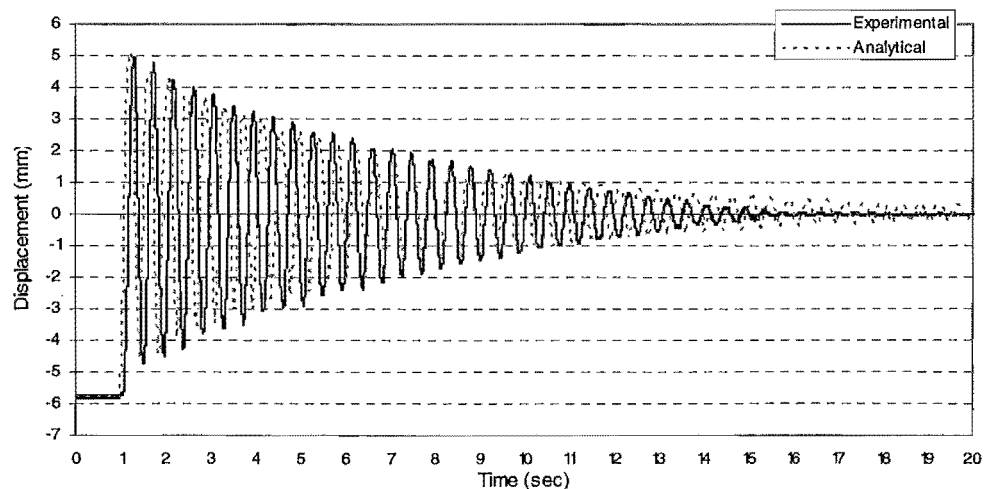


Fig (6-14) Experimental and analytical free vibration—Test 1—(6mm) at the top level.

In Figure (6-14), it can be seen that the analytical prediction of the displacement is similar to the experimental displacement but does indicate that the analytical model has less damping between 3 and 9 seconds and insufficient damping at more than 11 sec, i.e. the damping may be amplitude dependent.

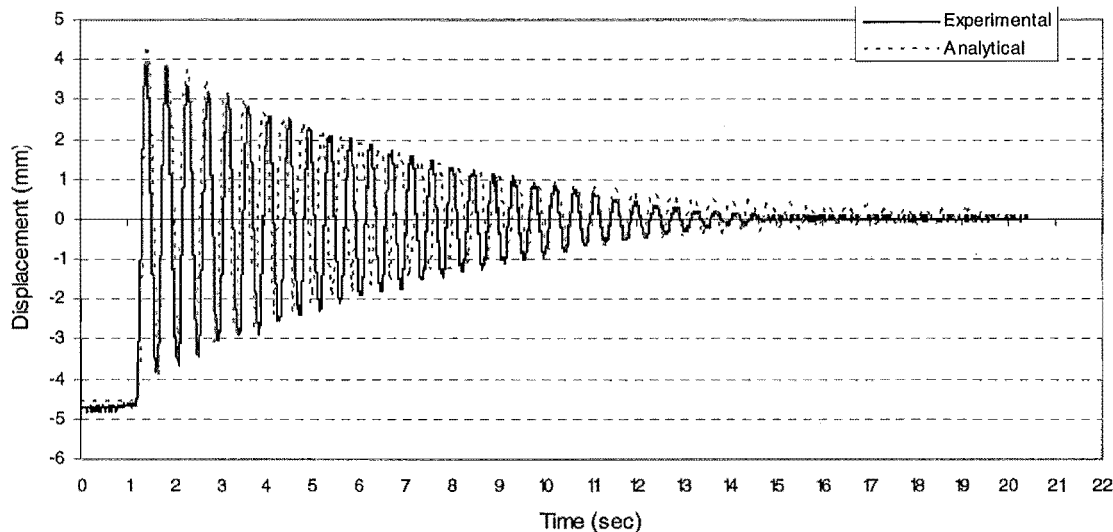


Fig (6-15) Experimental and analytical free vibration-Test 2-(5mm) at the top level.

### 6.5.2 Free Vibration with the Supplemental Control System

The free vibration test of the structure with the supplemental control system was carried out to compare the analytical prediction of the structure with the experimental results. Figure (6-16) shows the experimental and the analytical free vibration of the test structure. The results in the two cases are very close and after sec 3 there is not much response in the structure due to the damping of the supplemental control system acting as required.

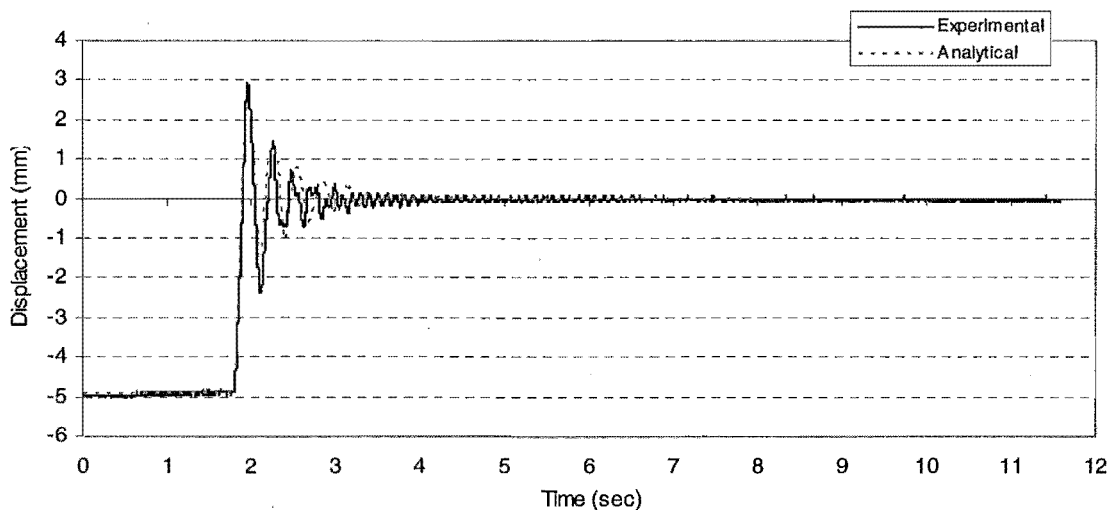


Fig (6-16) Experimental and analytical free vibration with the supplemental control system

### 6.5.3 Experimental and Analytical Time History Comparisons

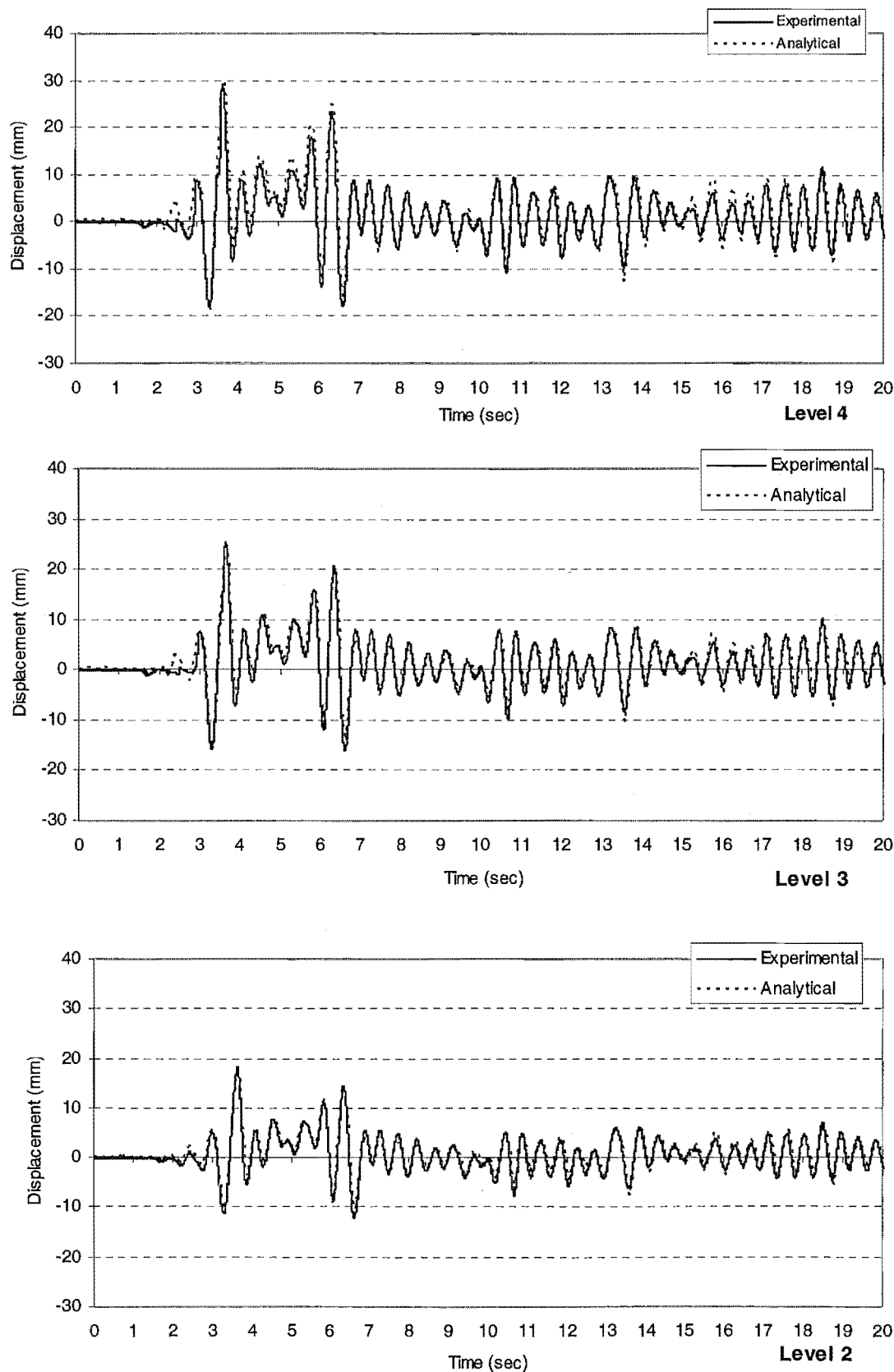


Fig (6-17) Experimental and analytical time history for the structure – El Centro 100% - shaking table acceleration

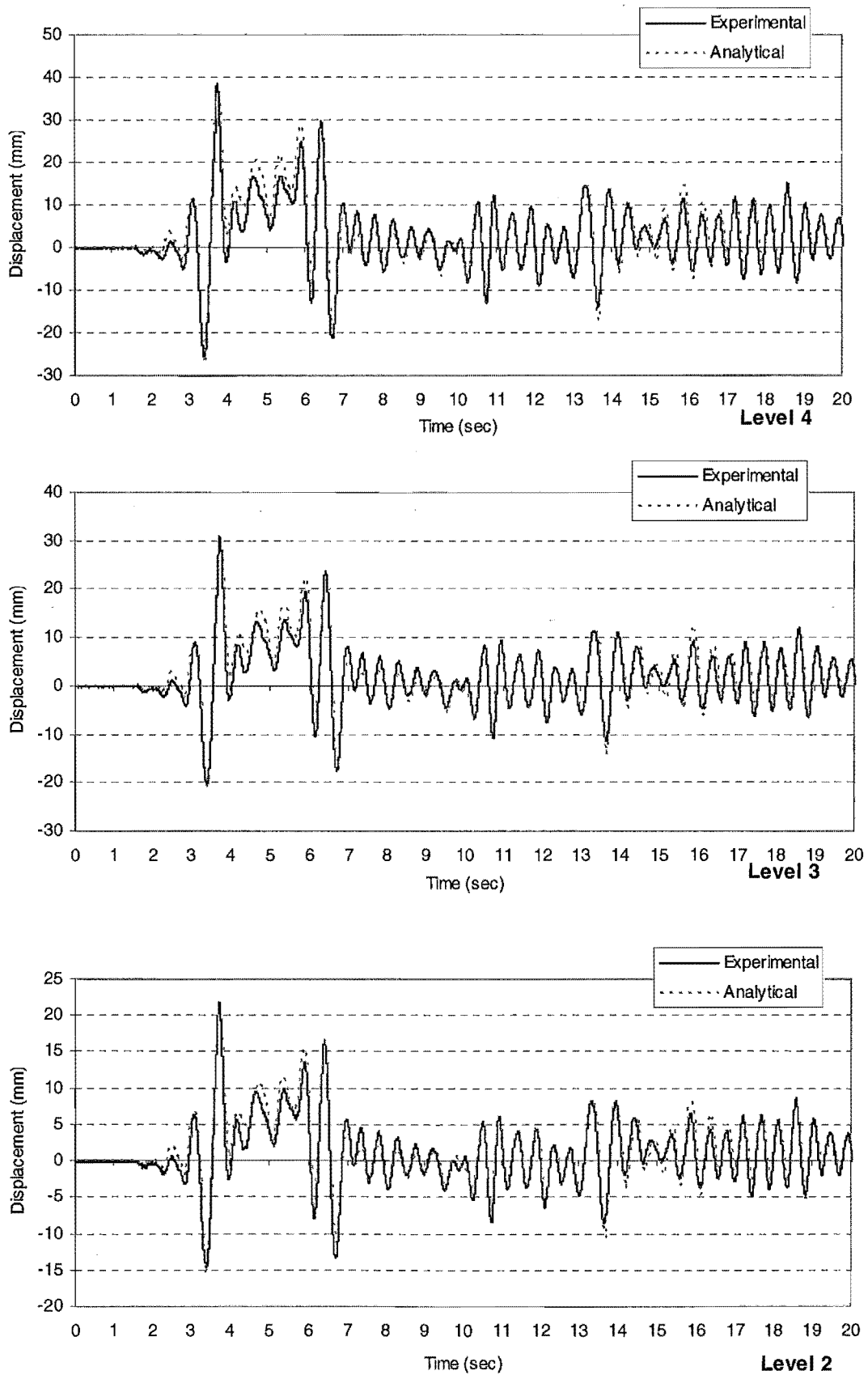


Fig (6-18) Experimental and analytical time history for the structure – El Centro 120% - shaking table acceleration.

The computational model was used to predict the response of the structure in different configurations. The free vibration tests with and without the supplemental damping system are shown in section 6.3.3. The values of the time histories responses, when compared in general, are similar.

Some selected displacement time history plots are shown in Figures (6-17) & (6-18). Experiments were conducted to validate the accuracy of the computational RUAUMOKO model. As can be seen from the figures, good agreement is evident between the experimental and the analytical predictions. The full time history analyses are described in Chapter 7 and shown in Appendix A.

## 6.6 Floor Acceleration

Experimental floor acceleration time histories of the top floor level of the test structure with 100, 80, and 50% El-Centro and 4203 Taft are provided in Figures (6-19) and (6-20), respectively. With 100% of the El Centro earthquake, there is no significant reduction with the high values of the accelerations during the first 19 seconds of the excitation. A reduction of up to 80% in the acceleration can be observed between the non-controlled and controlled structural response after the first 19 seconds. Similar acceleration responses of the top floor level were observed with 80% of the El-Centro excitation, while significant reductions of up to 65% of the maximum acceleration during the whole excitation period are shown for the 50% El-Centro case.

Reduction of up to 40% during the first 9 seconds can be observed with 100% of the 4203 Taft excitation as shown in Figure (6-20), while no significant reduction between the peak acceleration responses with 80% of the Taft excitation were observed.

Kelly [47] mentioned that friction devices possess slip-stick characteristics which may generate high frequency accelerations. However, it is more important that the maximum floor acceleration response of the structure does not get worse with the addition of the supplemental damping system but should be reduced over some periods of the earthquake excitations.

In investigating the displacement and interstorey response of the test structure in Chapter 7, the overall displacement response of the structure is found to be significantly reduced by the addition of the dampers by up to 50-80%. This means that there is some benefit if both displacements and interstorey drifts of the structure can be controlled to prevent structural damage by using ring spring dampers even though there is no significant reduction in the total floor accelerations which may cause damage to sensitive items of equipment that might be housed in the structure.

To determine the effect of the supplemental ring spring dampers in protecting the structure, the plastic rotation of the nodes at the top floor were also investigated. Figure (6-21) shows the plastic rotation of the node 45 at the top of the structure with and without the dampers. It can be seen that the damage to the structure is reduced by a factor of 3.4 compared with the rotation in the uncontrolled structure.

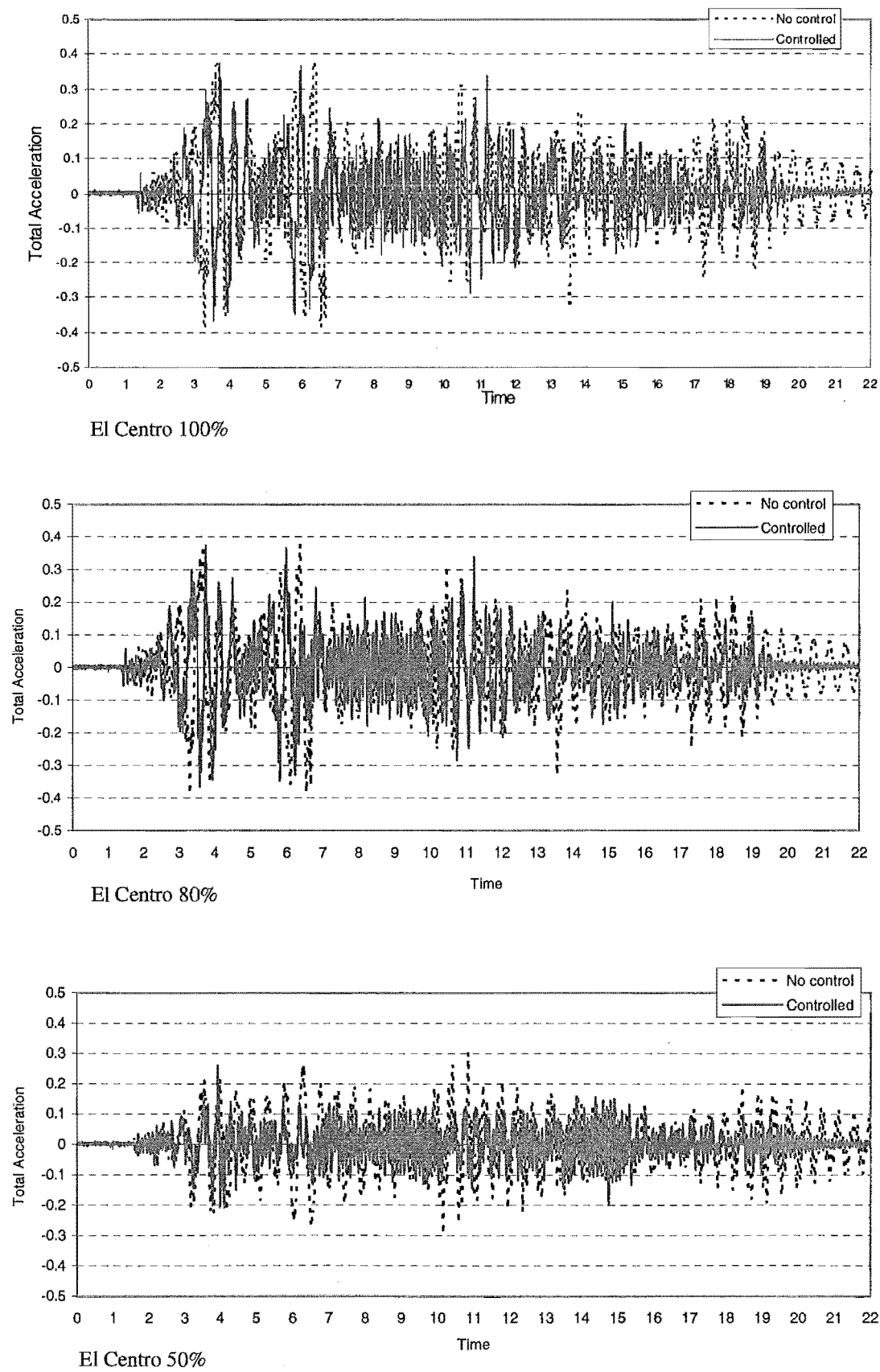


Fig (6-19) Experimental total acceleration of the top floor with 100, 80, and 50% El Centro, respectively.

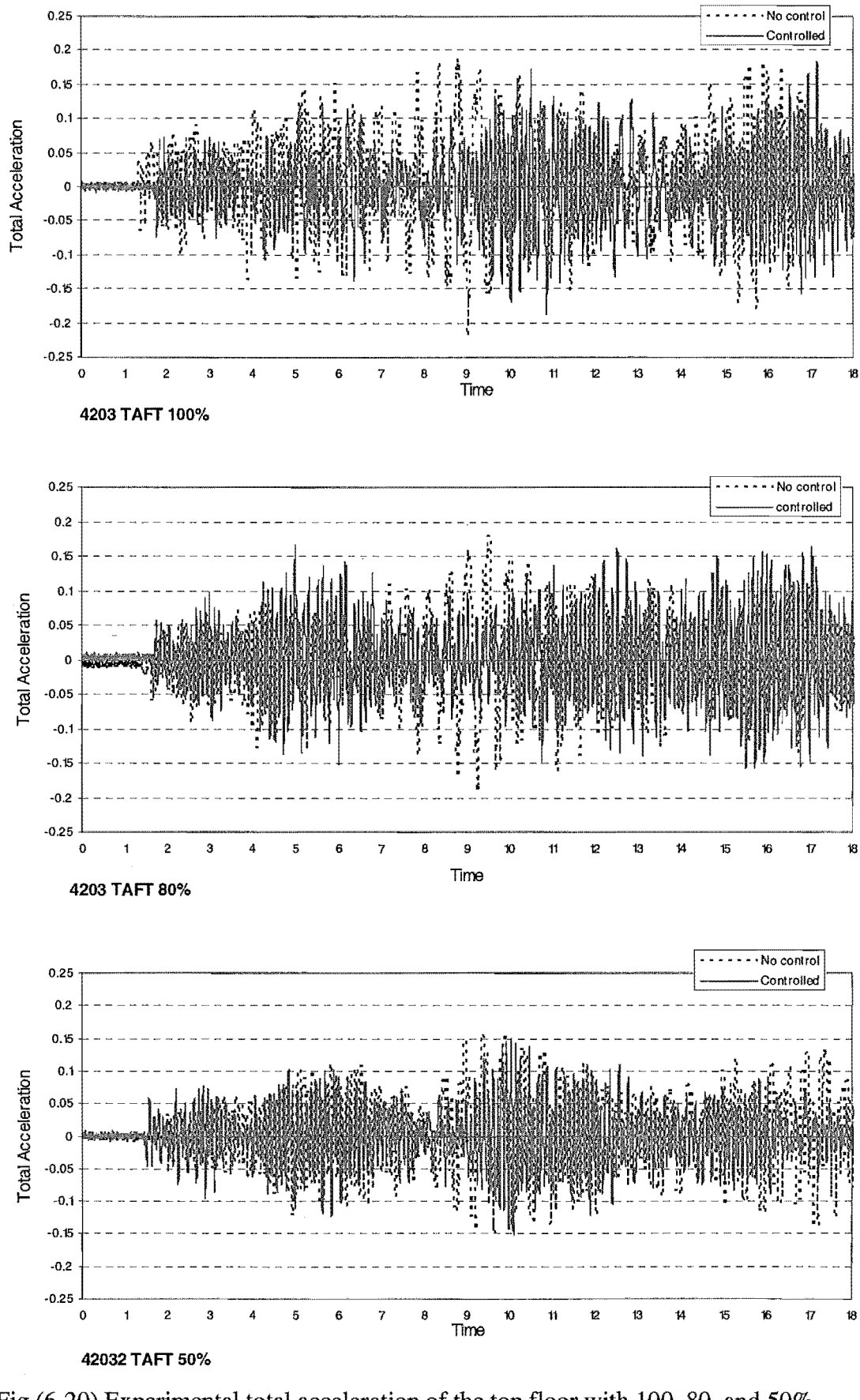


Fig (6-20) Experimental total acceleration of the top floor with 100, 80, and 50% 4203 TAFT, respectively.

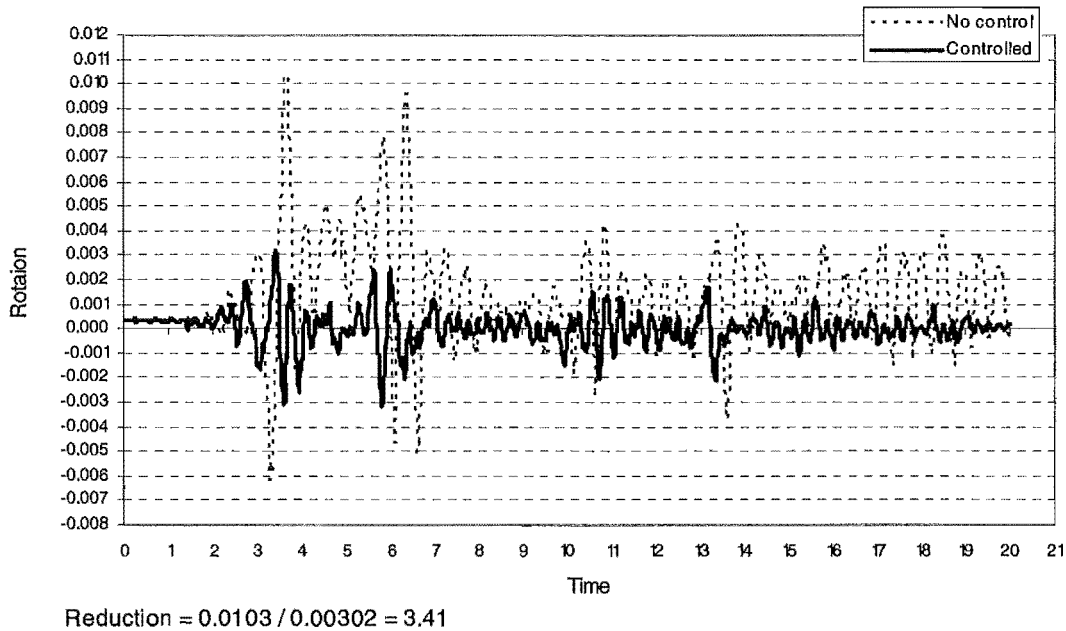
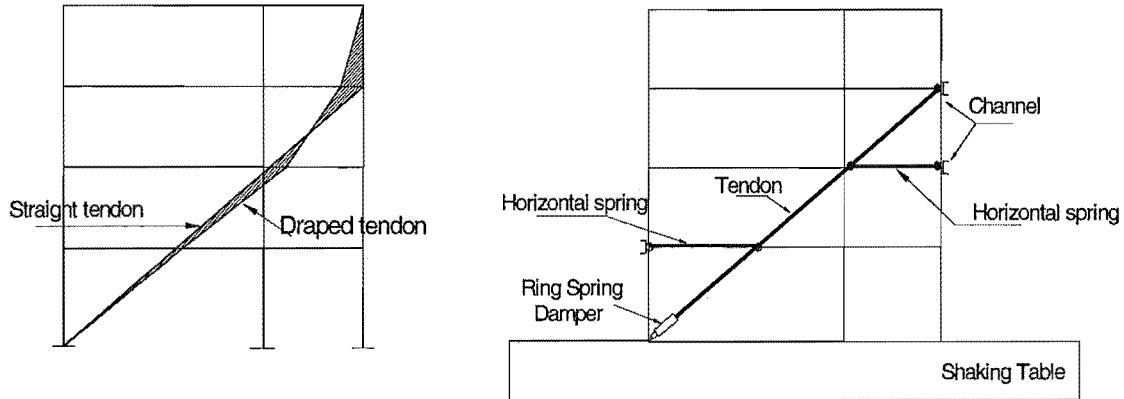


Fig (6-21) Rotation of the node 45 at level 4

## 6.7 Horizontal Members in the Supplemental Control System

As mentioned in Chapter 5, a draped tendon is replaced with the straight tendon in the experimental study to be easy to construct as shown in Figure (5-22a). The horizontal members are placed parallel and connected to the diagonal tendon at the second and third floors to transfer the damping forces to the floors (Figure 5-22b). The tendon and horizontal members are linked by a true pin mechanism. The connection between the horizontal members and the channel beams are also pin connections.



a) Straight and draped tendon

b) straight tendon with horizontal members

Fig (5-22) Tendon profile

To investigate the magnitude of the damper forces transferred by the horizontal members to the floor levels compared to the forces carried by the straight tendon, the time histories analysis with El Centro 100% are shown in Figure (6-23). It can be seen that the magnitude of the forces transferred by the horizontal members are very small when compared with the damper forces transferred by the straight tendon. It is an expected behaviour because with the straight tendon no forces should be transferred by the horizontal members according to the small deflection theory. With larger displacements the tendon is no longer actually straight and may able to transfer some damping forces to the storey levels of the structure.

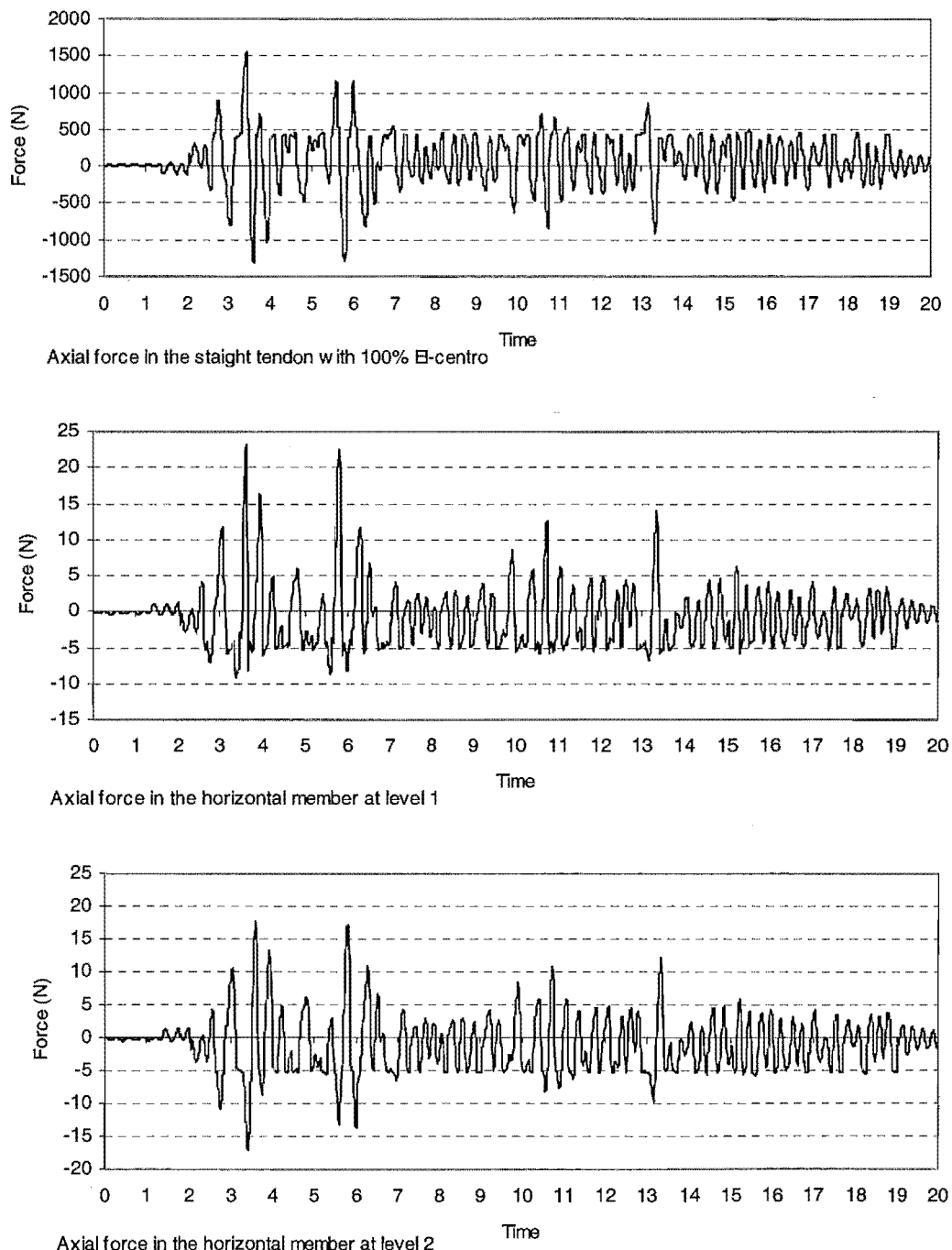


Figure (6-23) Time histories of the forces in the straight tendon and the horizontal members

## 6.8 Effect of Increasing the Stiffness of the Structure Due to Adding the Supplemental Control System

The stiffness of the structure increases by adding the supplemental control system to the structure. From the free vibration tests shown in section 6.5, it was found that the natural period of the original structure was 0.43 sec and the damping ratio was 1.1 % of critical damping. With the supplemental control system the natural period of the structure was 0.25 sec and the damping ratio 7.68% of the critical damping. This is because the dampers have a considerable stiffness.

To investigate the effect of increasing the stiffness of the structure due to adding the supplemental control system to the structure, the response spectra displacement is used with damping ratios, 1.1% and 7.68% of critical damping. As shown in Figure (6-24) the decrease in the spectral displacement of the structure with the supplemental control system is equal to 84% of the spectral displacement of the structure without the supplemental damping system as shown in Table (6-3). The horizontal members will also show forces generated by the horizontal inertia of the tendon system.

Table (6-3) Effect of increasing stiffness of the structure

Supplemental control System	Damping ratio %	Period of the structure	Spectral Displacement	% decrease in the displacement due increase in the stiffness
Without	1.1	0.43	0.032	
With	7.68	0.25	0.005	84%

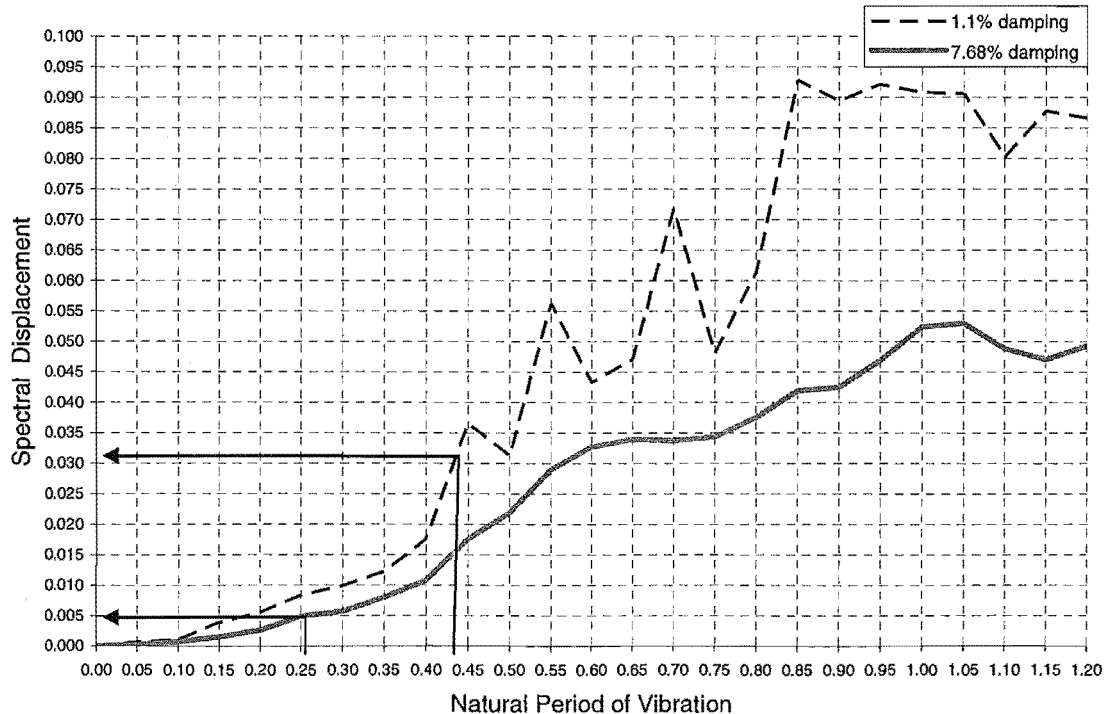


Fig (6-24) Spectral displacement of the structure with different ratio of the critical damping with and without the supplemental system.

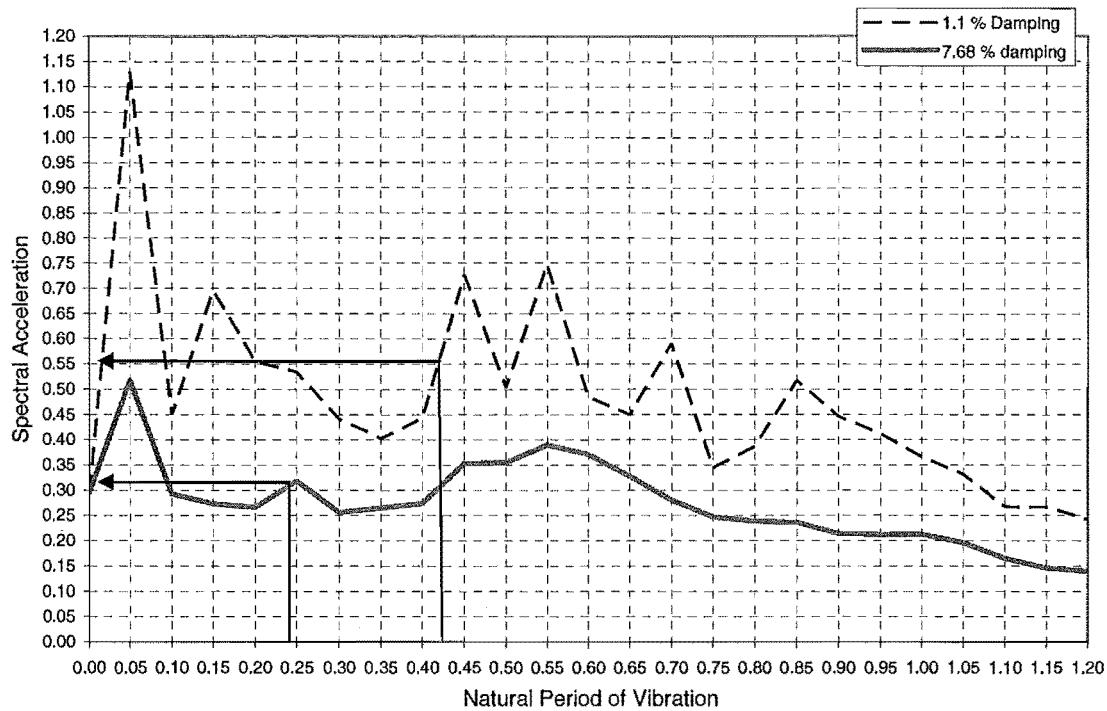


Fig (6-25) Spectral acceleration of the structure with different ratio of the critical damping with and without the supplemental system.

The supplemental control system reduced the overall response of the model structure. High initial stiffness is also considered beneficial under different levels of ground motions. Usually, stiffening of a frame structure leads to further reduction of deformations but at the expense of increased acceleration response. This is partly due to the higher lateral stiffness of the model structure with the supplemental control system.

The stiffness introduced by the dampers considerably reduces the displacement however the introduction of extra stiffness on its own would, in most case, imply an increase in the acceleration. The extra damping introduced by the ring springs controls this increase in acceleration. The extra damping has approximately halved the displacement that would have occurred due to the increase in stiffness above.

## Chapter 7

### Experimental Results

#### **7.1 Introduction**

An assessment of the effectiveness of ring spring dampers and the supplemental damping control system in reducing dynamic response can be made by comparison of the response of the same structure without and with dampers for the same earthquake input. The shaking table tests were conducted on the structural steel model described in Chapter 5 with and without the supplemental control system. One of the main objectives of performing this experimental study was to investigate the effectiveness of the supplemental control system discussed in chapter 4 and 5 in reducing the seismic response of the structure under recorded ground motion excitations.

#### **7.2 Experimental Procedure**

In this experimental study, thirty two shaking table tests were conducted using two different ground motions, namely 4203 TAFT and El Centro 1940 NS at various peak ground acceleration (PGA) levels from 0.17g to 0.3g, respectively. A sample of acceleration time histories for these ground motions are given in Figure 6-13. The record 4203 Taft was used first because it represents a low level of demand and in this case the structure does not go beyond the elastic limit. The first group of tests contains 16 runs and was carried out on the structure with the supplemental control system to ensure that the frame structure behaviour remained elastic. The second group of the tests with the same number of runs was carried out after the supplemental control system was taken off the structure. The summary of the tests are shown in Table (7-1).

Three floor displacement and interstorey drift time histories for the two ground excitation mentioned before were selected and are shown in the next sections to investigate the behaviour of the floor levels of the structure. The experimental results with and without the supplemental control system for 50, 100, and 120% El-Centro and 80, 100, and 120% 4203 TAFT are given in Figures (7-1) through Figures (7-18). For each test, the peak values of each floor are summarized in the tables. The overall experimental results may be found in Appendix A.

Table (7-1) Summary of the tests

Run Number	The structure with the supplemental control system		The supplemental control system was taken off the structure	Run Number	The structure without the supplemental control system	
	4023 Taft	El Centro			4203Taft	El Centro
Run 01	30%	—		Run 17	30%	—
Run 02	50%	—		Run 18	50%	—
Run 03	60%	—		Run 19	60%	—
Run 04	80%	—		Run 20	80%	—
Run 05	100%	—		Run 21	100%	—
Run 06	120%	—		Run 22	120%	—
Run 07	—	10%		Run 23	—	10%
Run 08	—	20%		Run 24	—	20%
Run 09	—	40%		Run 25	—	40%
Run 10	—	50%		Run 26	—	50%
Run 11	—	60%		Run 27	—	60%
Run 12	—	70%		Run 28	—	70%
Run 13	—	80%		Run 29	—	80%
Run 14	—	90%		Run 30	—	90%
Run 15	—	100%		Run 31	—	100%
Run 16	—	120%		Run 32	—	120%

### 7.3 El Centro Shaking Table Excitation

#### 7.3.1 Displacement of the Structure with El Centro 50%

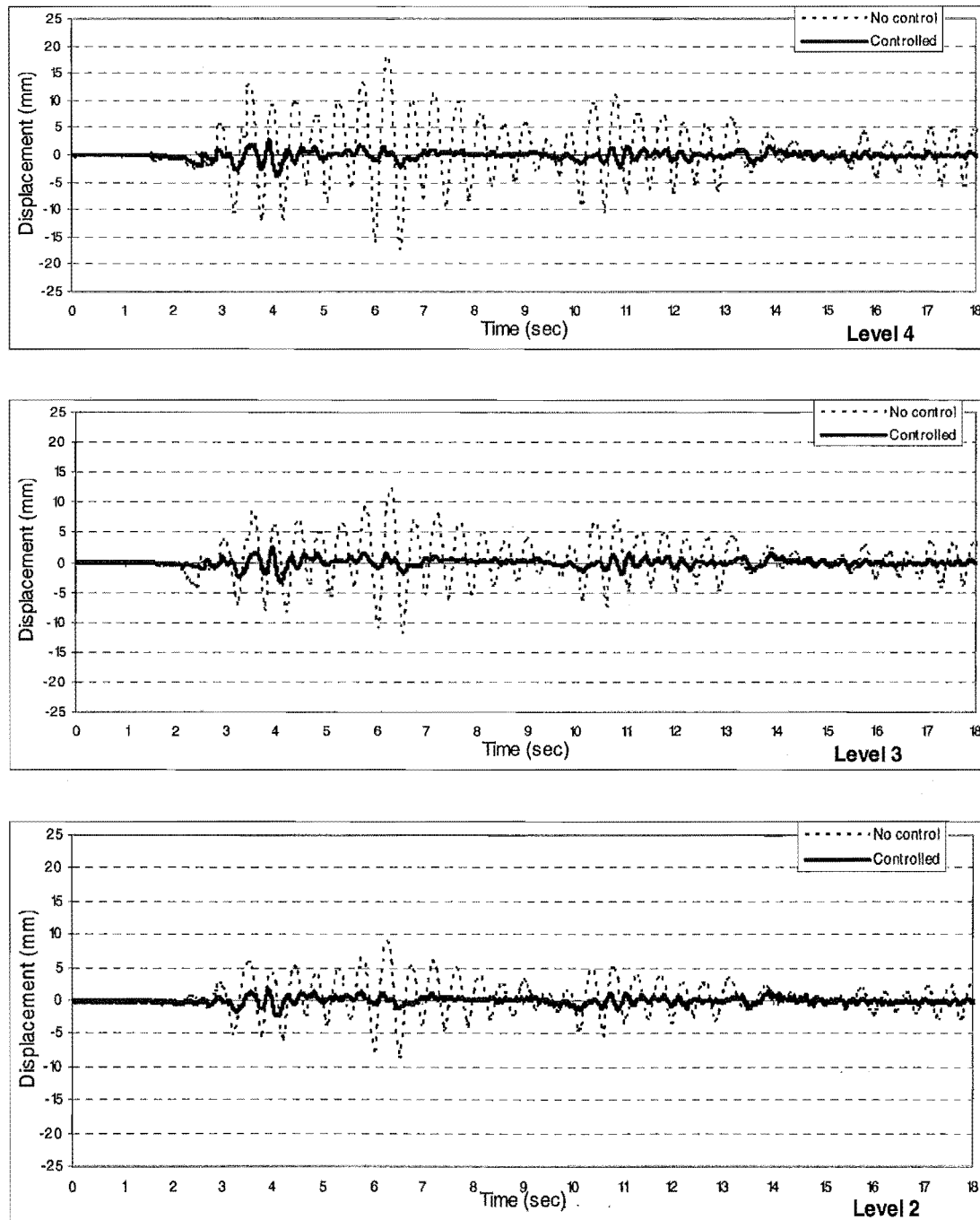


Fig (7-1) Displacement of the structure with and without the supplemental control system El Centro 50% - shaking table acceleration

### 7.3.2 Interstorey Drift with El Centro 50%

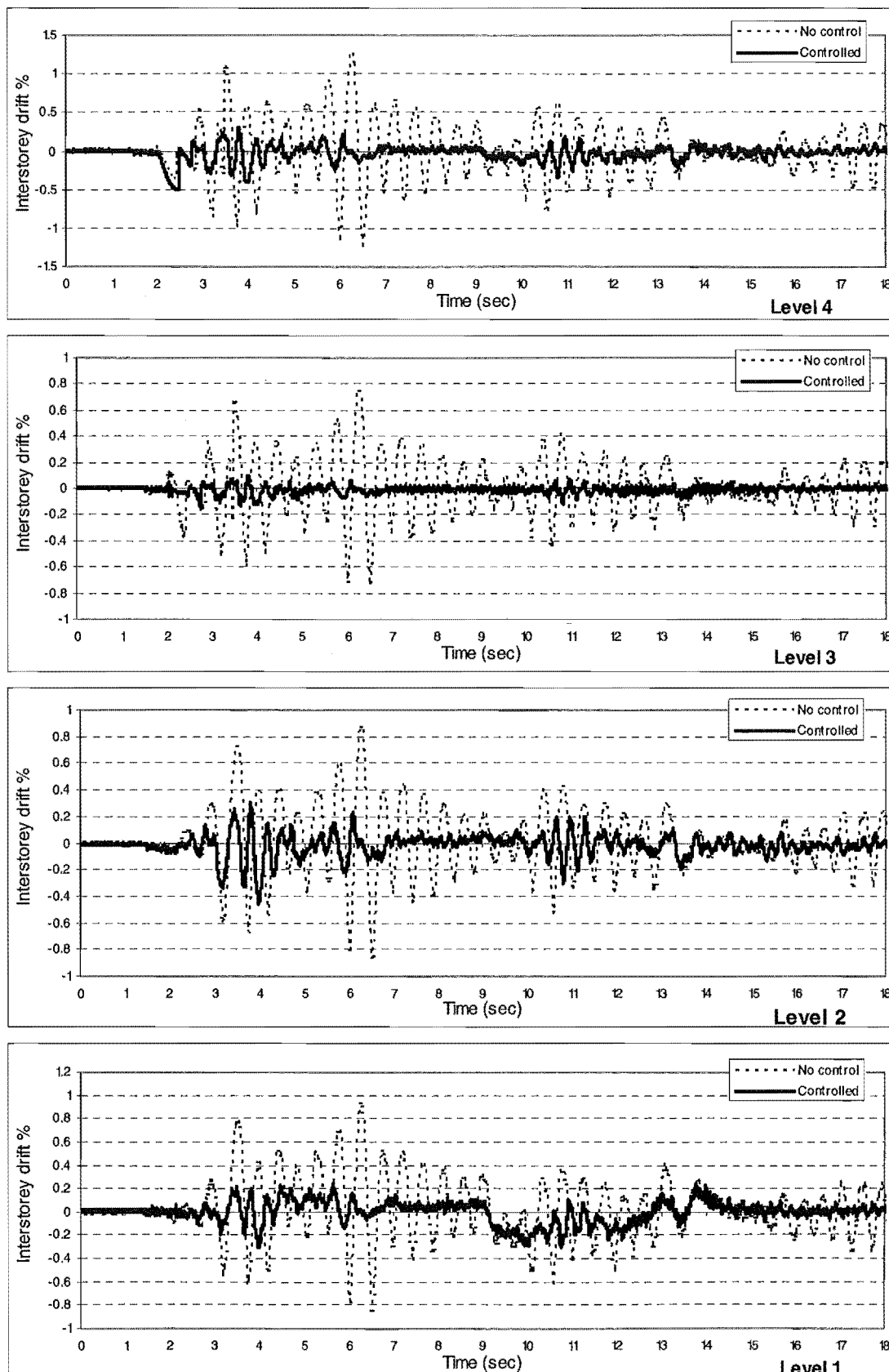


Fig (7-2) Interstorey drifts of the structure with and without the supplemental control system El Centro 50% -shaking table acceleration

### 7.3.3 Displacement and Interstorey Drift Ratios

Level	Displacement		Reduction	
	Without D-T*	With D-T	% of reduction	% average
4	17.5	3.3	81	80
3	10.6	2.13	80	
2	7.7	1.7	78	
1	3.5	0.7	80	

\* D-T is the supplemental damper-tendon system

Level	Interstorey drift %		Reduction	
	Without D-T	With D-T	% of reduction	% average
4	1	0.2	80	75
3	0.67	0.17	75	
2	0.77	0.2	74	
1	0.82	0.22	73	

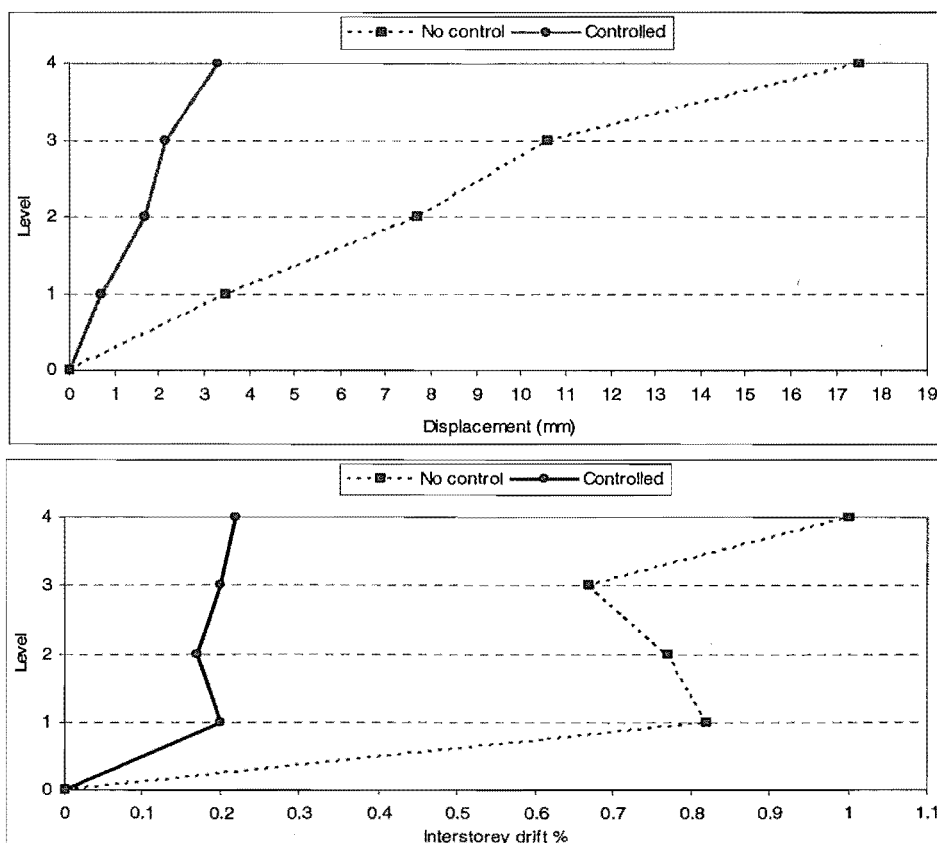


Fig (7-3) Displacement and interstorey drifts of the structure with and without the supplemental control system – El Centro 50%-shaking table acceleration

### 7.3.4 Displacement of the Structure with EL Centro 100%

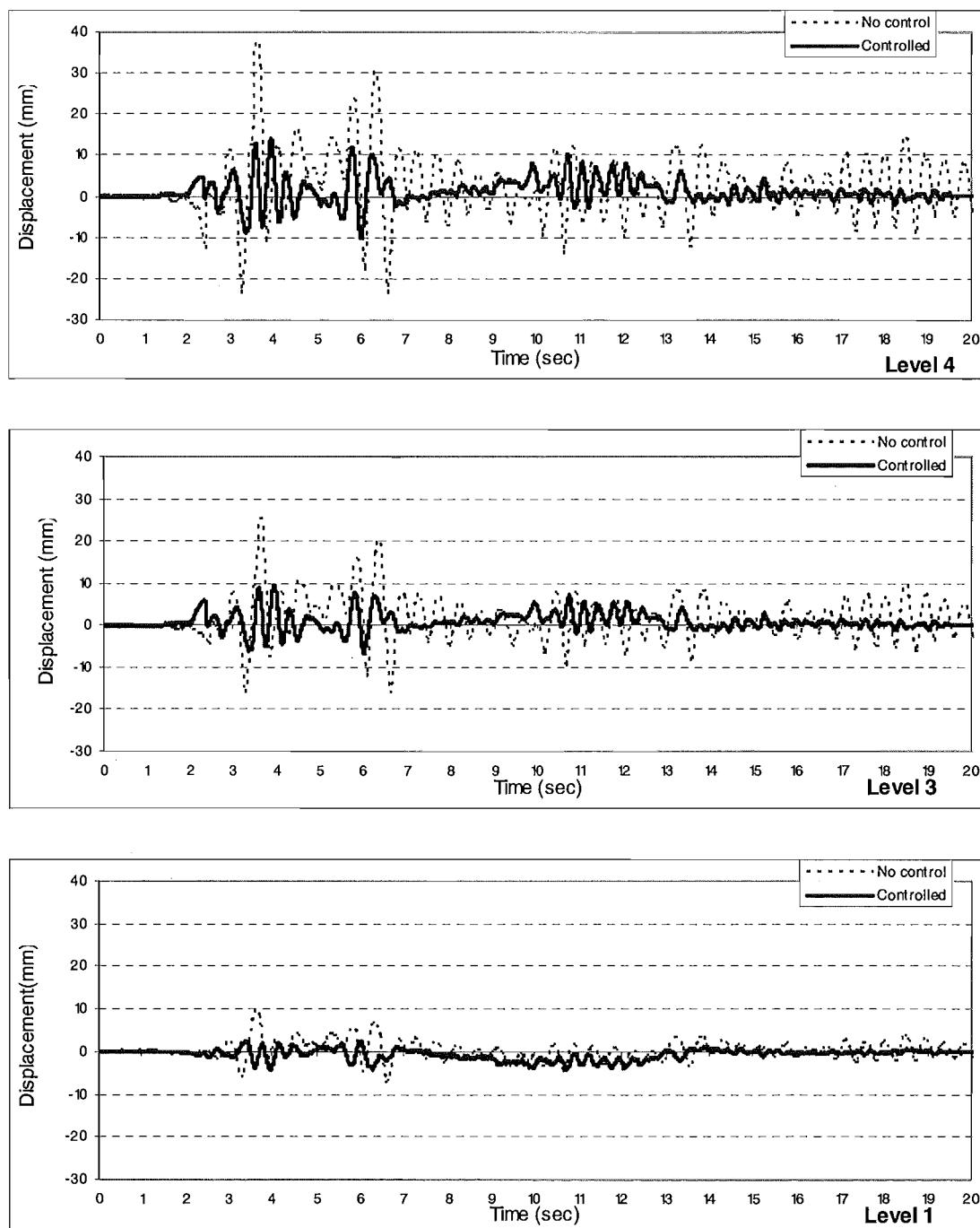


Fig (7-4) Displacement of the structure with and without the supplemental control system –El Centro 100% -shaking table acceleration

### 7.3.5 Interstorey Drift with El Centro 100%

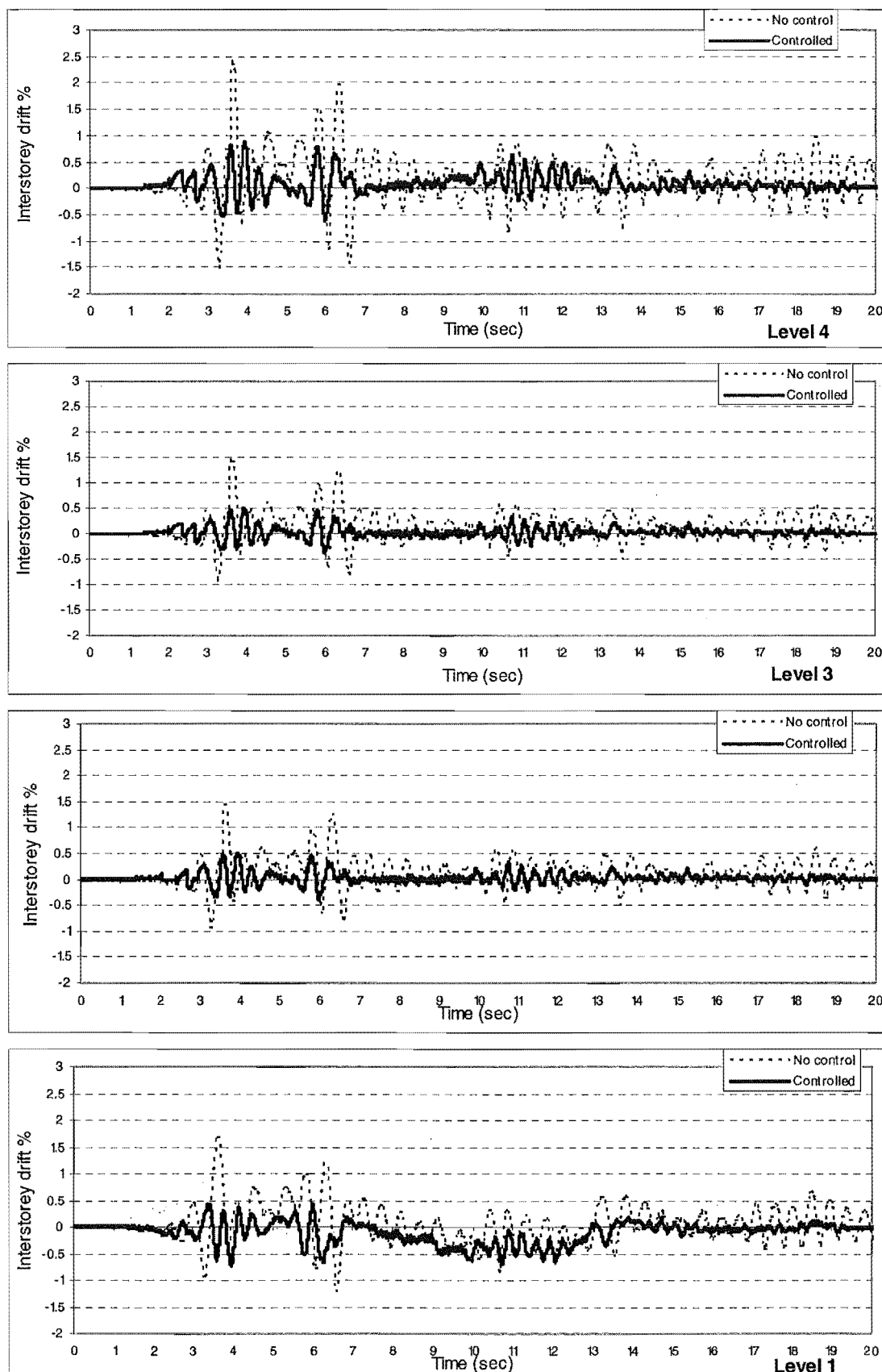


Fig (7-5) Interstorey drift of the structure with and without the supplemental control system- El Centro 100% - shaking table acceleration

### 7.3.6 Displacement and Interstorey Drift Ratios

Level	Displacement		Reduction	
	Without D-T	With D-T	% of reduction	% average
4	36	13	64	63
3	24	8.8	63	
2	17	6.3	63	
1	9.5	3.6	62	

Level	Interstorey drift %		Reduction	
	Without D-T	With D-T	% of reduction	% average
4	2.35	0.8	66	64
3	1.41	0.5	65	
2	1.4	0.47	66	
1	1.6	0.65	59	

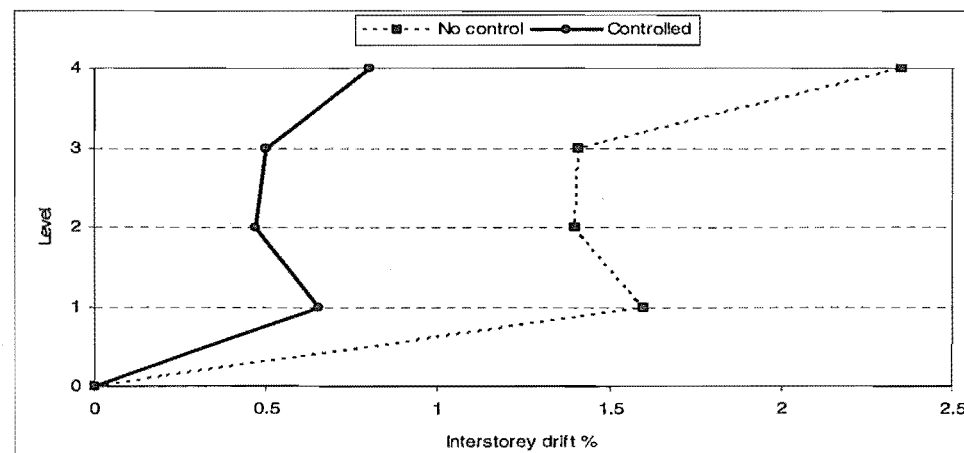
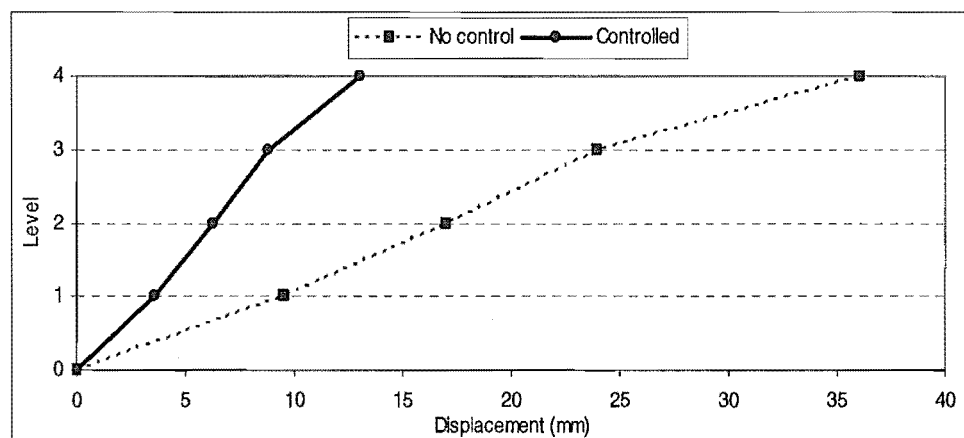


Fig (7-6) Displacement and interstorey drift of the structure with and without the supplemental control system-El Centro 100% - shaking table acceleration

### 7.3.7 Displacement of the Structure with El Centro 120%

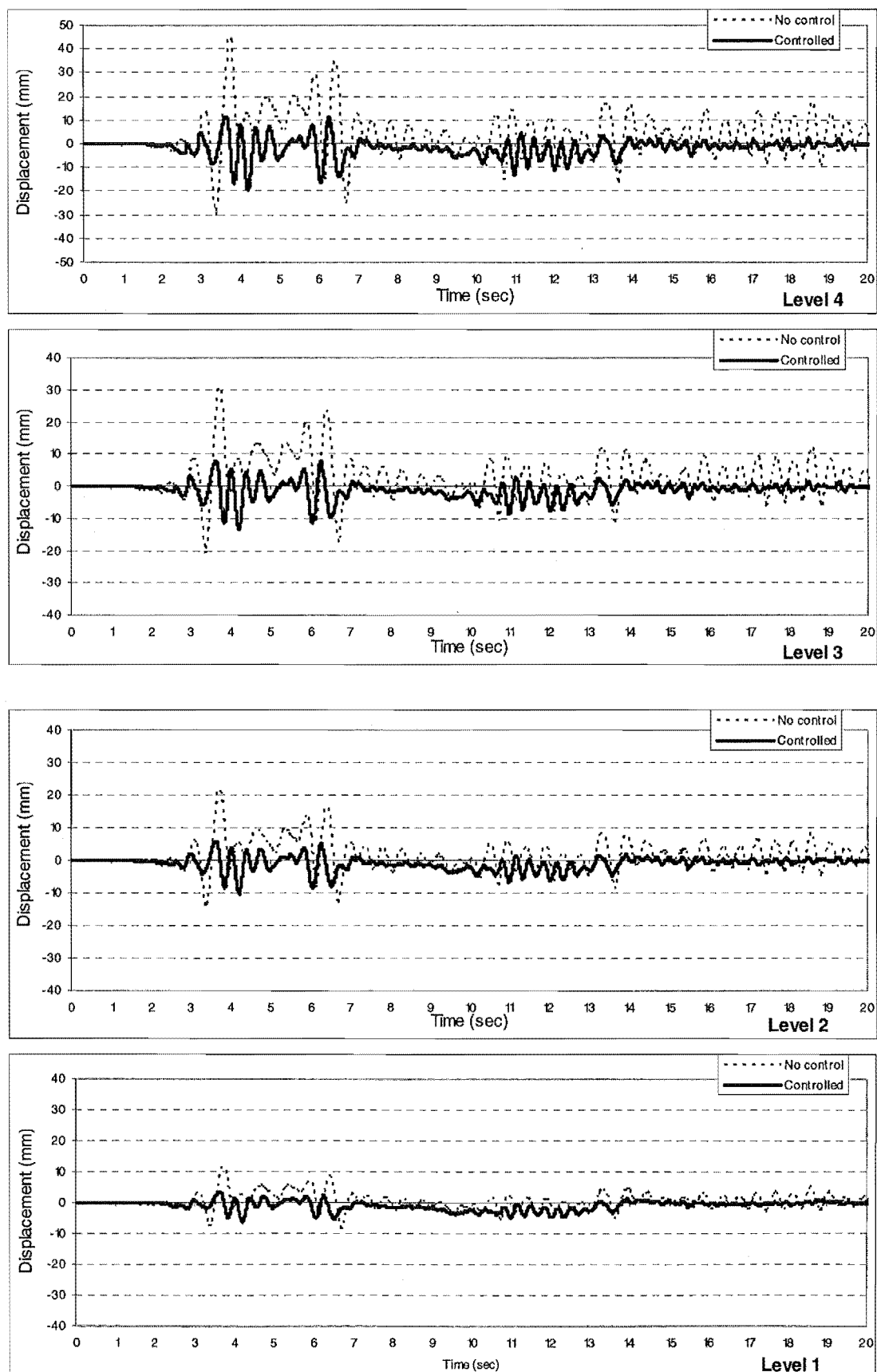


Fig (7-7) Displacement of the structure with and without the supplemental control system- El Centro 120% - shaking table acceleration

### 7.3.8 Interstorey Drift of the Structure with El Centro 120%

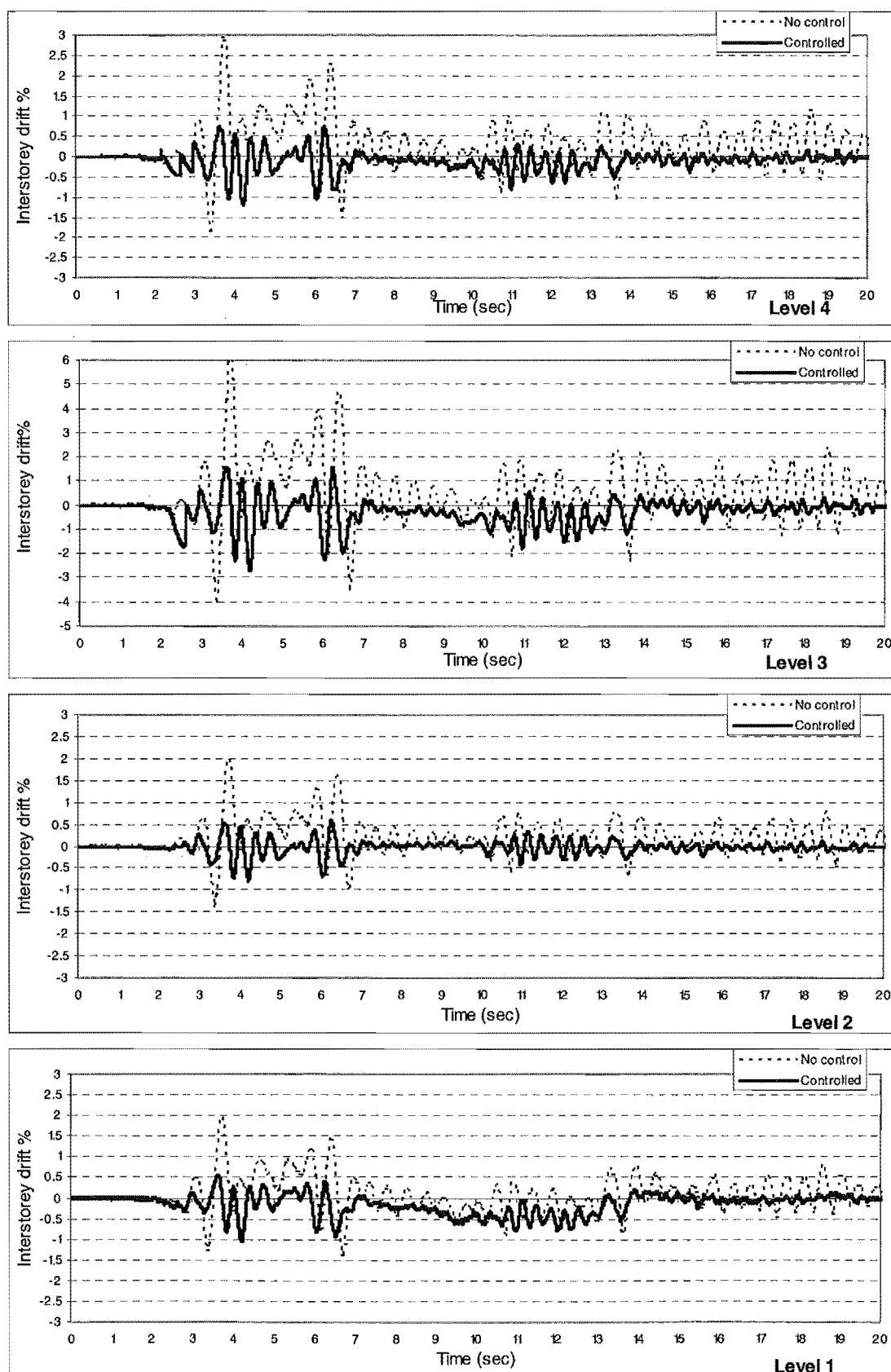


Fig (7-8) Interstorey drift of the structure with and without the supplemental control system- El Centro 120% - shaking table acceleration

### 7.3.9 Displacement and Interstorey Drift Ratios

Level	Displacement		Reduction	
	Without D-T	With D-T	% of reduction	% average
4	42.8	20	53	56
3	29	12.5	57	
2	20.5	8.8	57	
1	10.3	4.6	55	

Level	Interstorey drift %		Reduction	
	Without D-T	With D-T	% of reduction	% average
4	2.3	0.85	63	63
3	1.4	0.5	64	
2	1.4	0.5	64	
1	1.6	0.62	61	

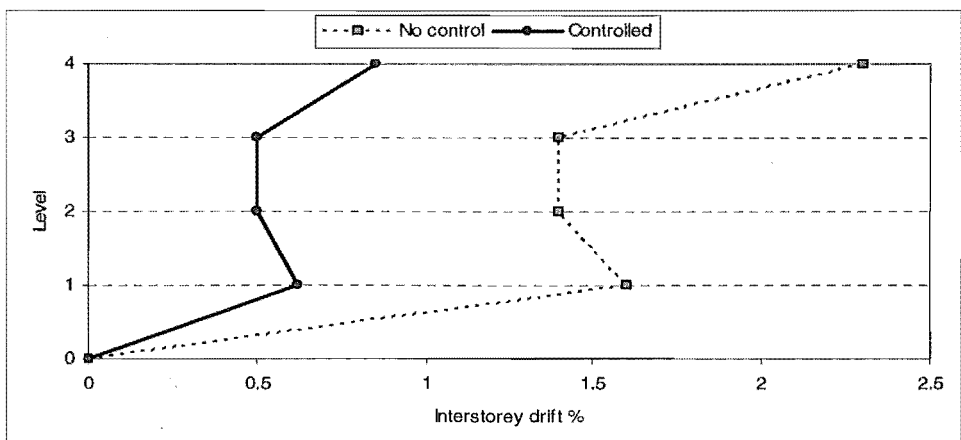
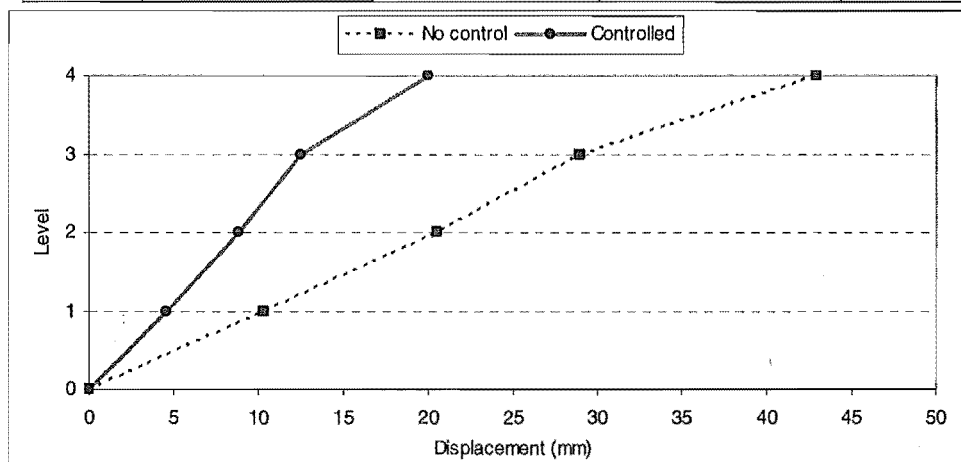


Fig (7-9) Displacement and interstorey drift of the structure with and without the supplemental control system- El Centro 120% -shaking table acceleration.

## 7.4 TAFT- Shaking Table Excitation

### 7.4.1 Displacement of the Structure with TAFT 80%

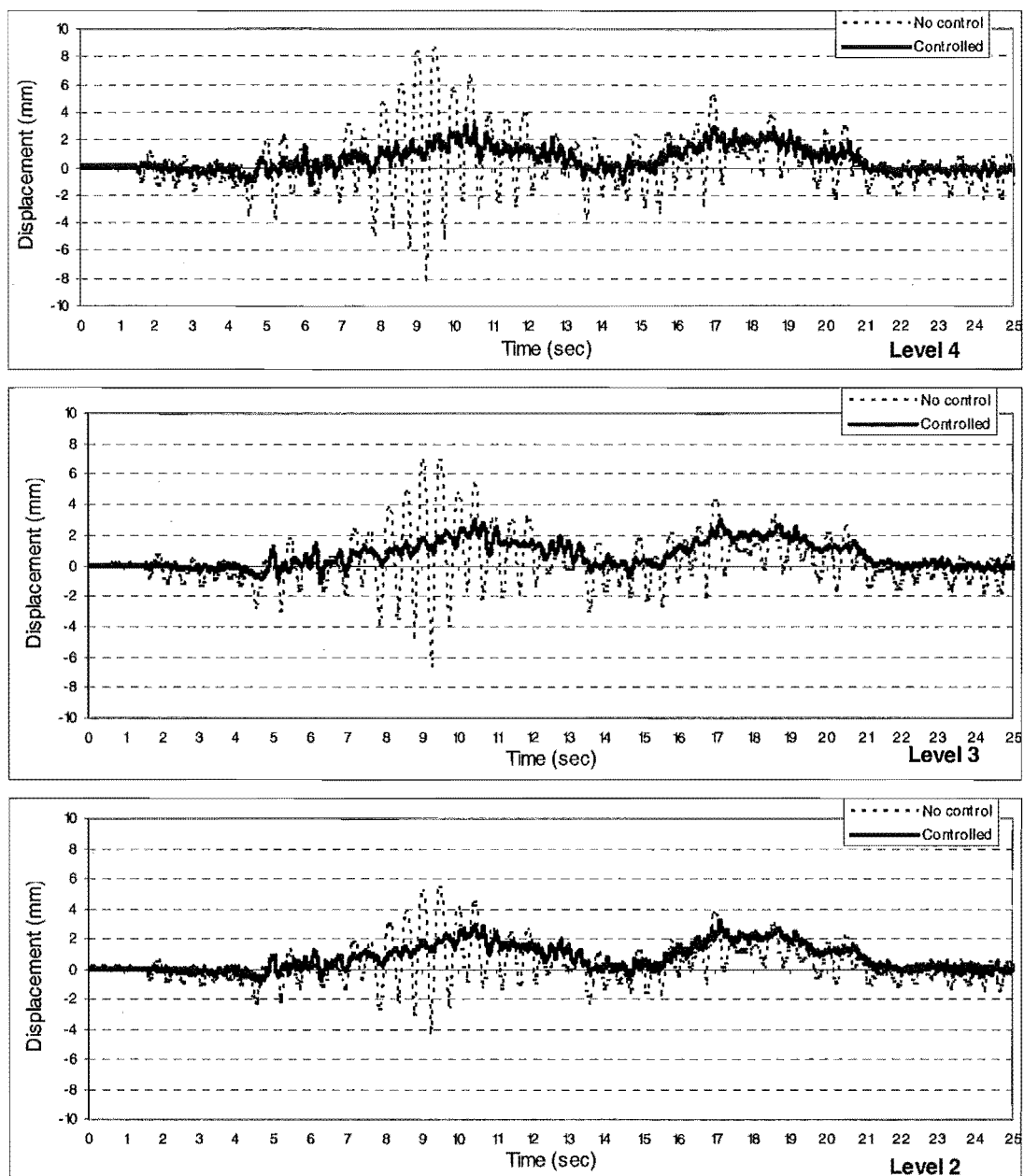


Fig (7-10) Displacement of the structure with and without the supplemental control system – TAFT 80%- shaking table acceleration.

#### 7.4.2 Interstorey Drift of the Structure with TAFT 80%

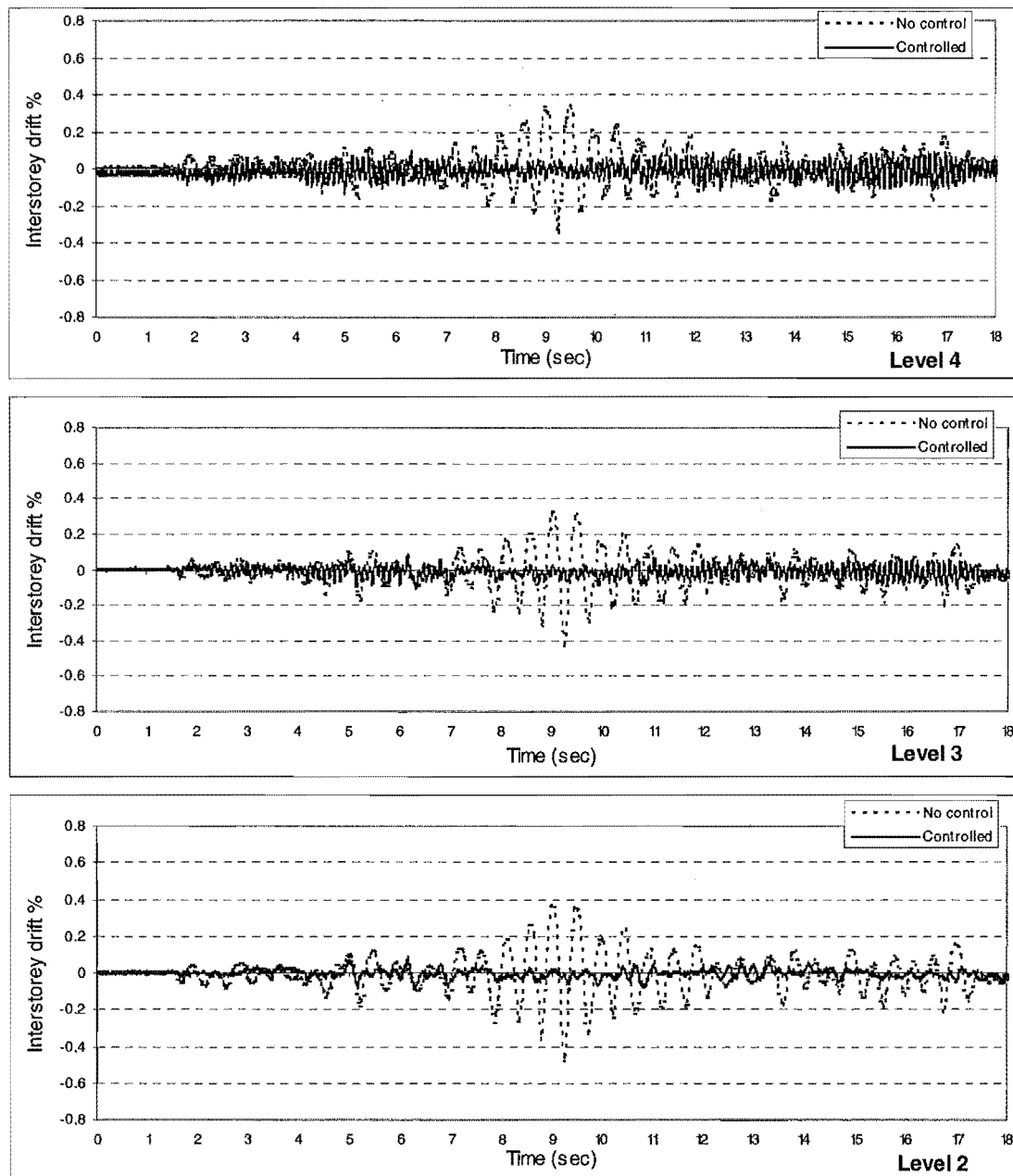


Fig (7-11) Interstorey drift of the structure with and without supplemental control system - TAFT 80%-shaking table acceleration

### 7.4.3 Displacement and Interstorey Ratios

Level	Displacement		Reduction	
	Without D-T	With D-T	% of reduction	% average
4	8.1	2.7	67	49
3	6.6	2.7	59	
2	5.1	2.7	47	
1	3.3	2.6	21	

Level	Interstorey drift %		Reduction	
	Without D-T	With D-T	% of reduction	% average
4	0.32	0.1	69	66
3	0.42	0.05	88	
2	0.47	0.05	89	
1	0.61	0.49	20	

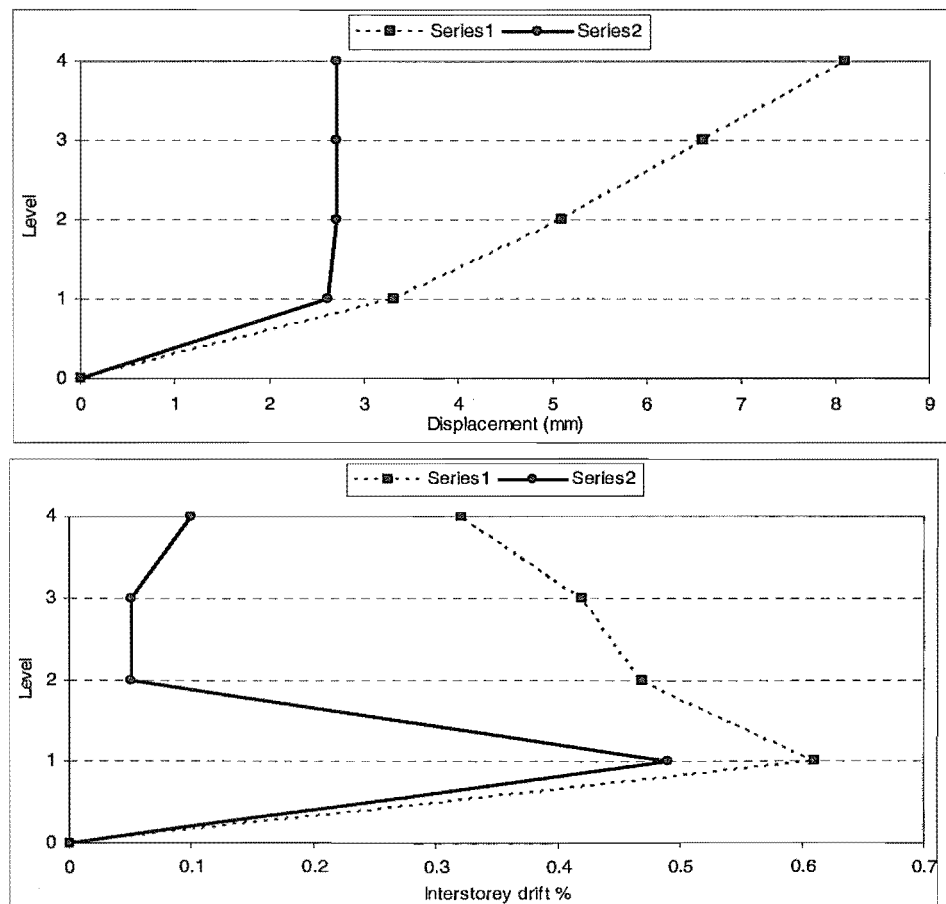


Fig (7-12) Displacement and interstorey drift of the structure with and without the supplemental control system- TAFT 80% -shaking table acceleration

#### 7.4.4 Displacement of the Structure with TAFT 100%

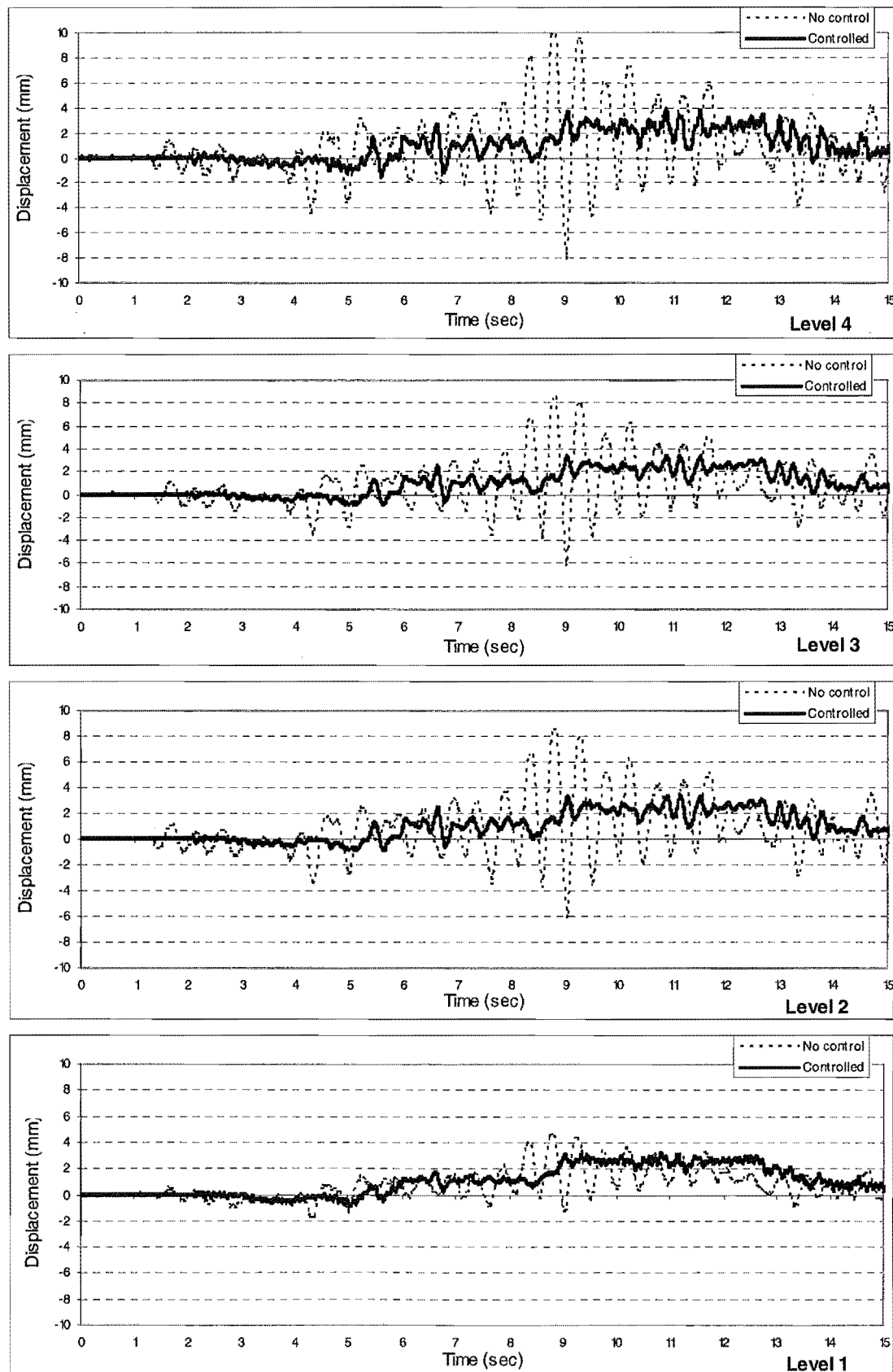


Fig (7-13) Displacement of the structure with and without the supplemental control system- TAFT 100% - shaking table acceleration

#### 7.4.5 Interstorey Drift of the Structure with TAFT 100%

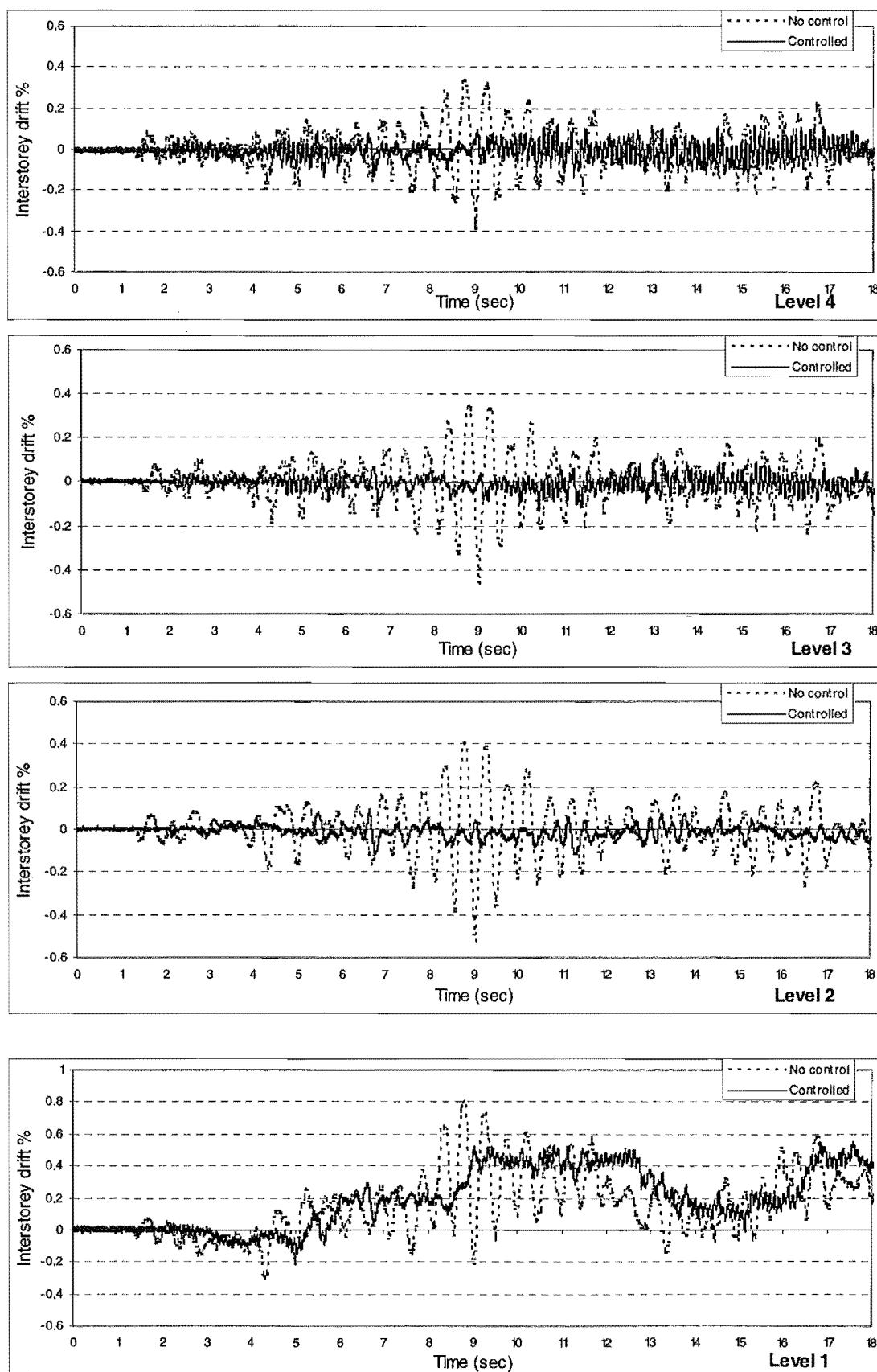


Fig (7-14) Interstorey drift of the structure with and without supplemental control system -4203TAFT 100%-shaking table acceleration.

#### 7.4.6 Displacement and Interstorey Drift Ratios

Level	Displacement		Reduction	
	Without D-T	With D-T	% of reduction	% average
4	10	3.9	61	56
3	8.3	3.2	61	
2	8.1	3.3	59	
1	4.6	2.7	41	

Level	Interstorey drift %		Reduction	
	Without D-T	With D-T	% of reduction	% average
4	0.38	0.11	71	71
3	0.45	0.07	84	
2	0.51	0.07	86	
1	0.8	0.47	41	

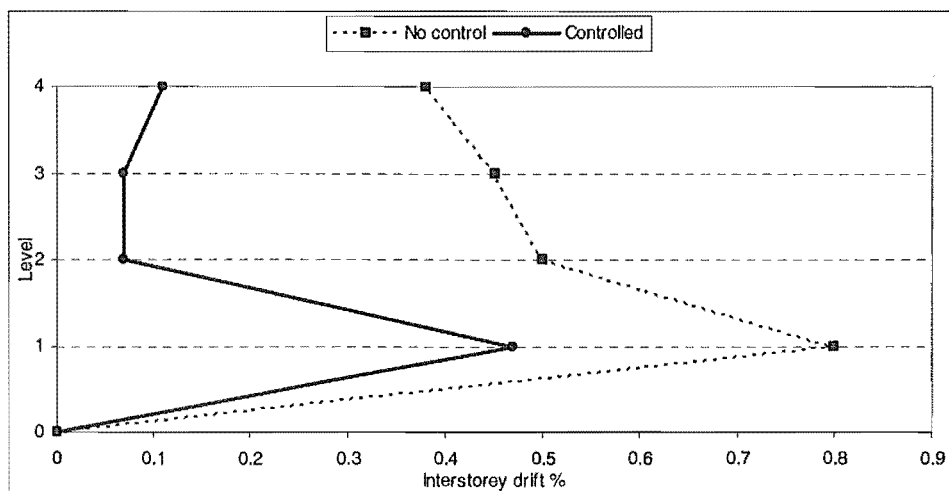
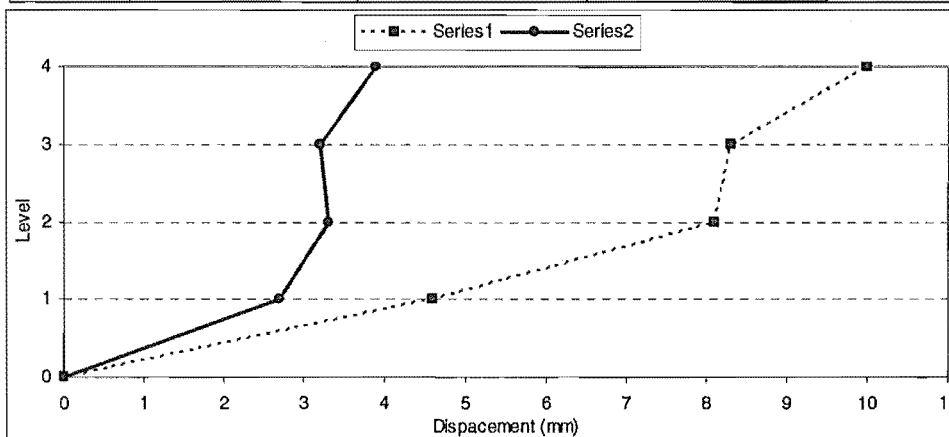


Fig (7-15) Displacement and interstorey drift ratios with and without the supplemental control system -TAFT 100%- shaking table acceleration

#### 7.4.7 Displacement of the Structure with TAFT 120%

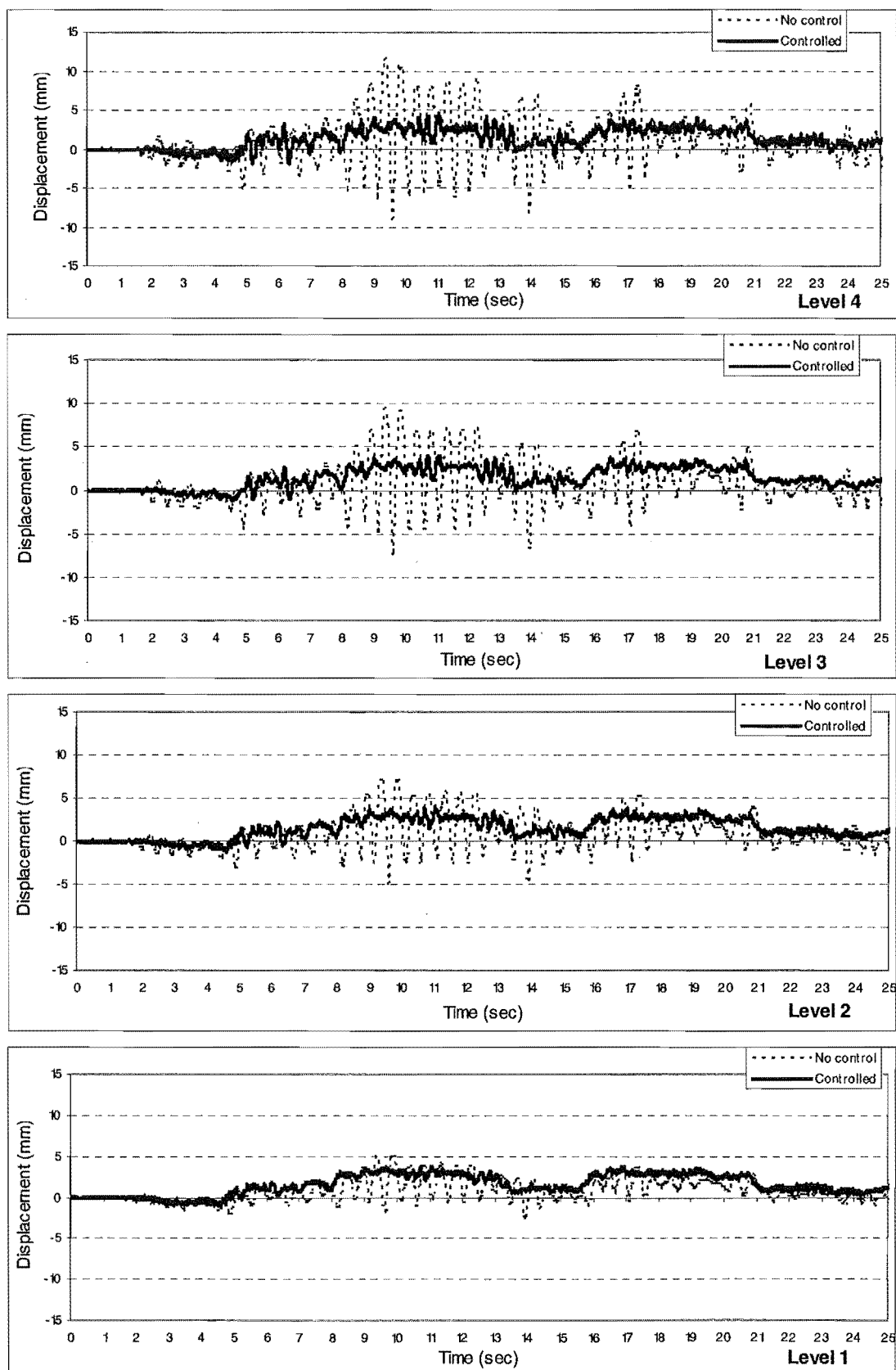


Fig (7-16) Displacement of the structure with and without the supplemental control system- TAFT 120%- shaking table acceleration

#### 7.4.8 Interstorey Drift of the Structure with TAFT 120%

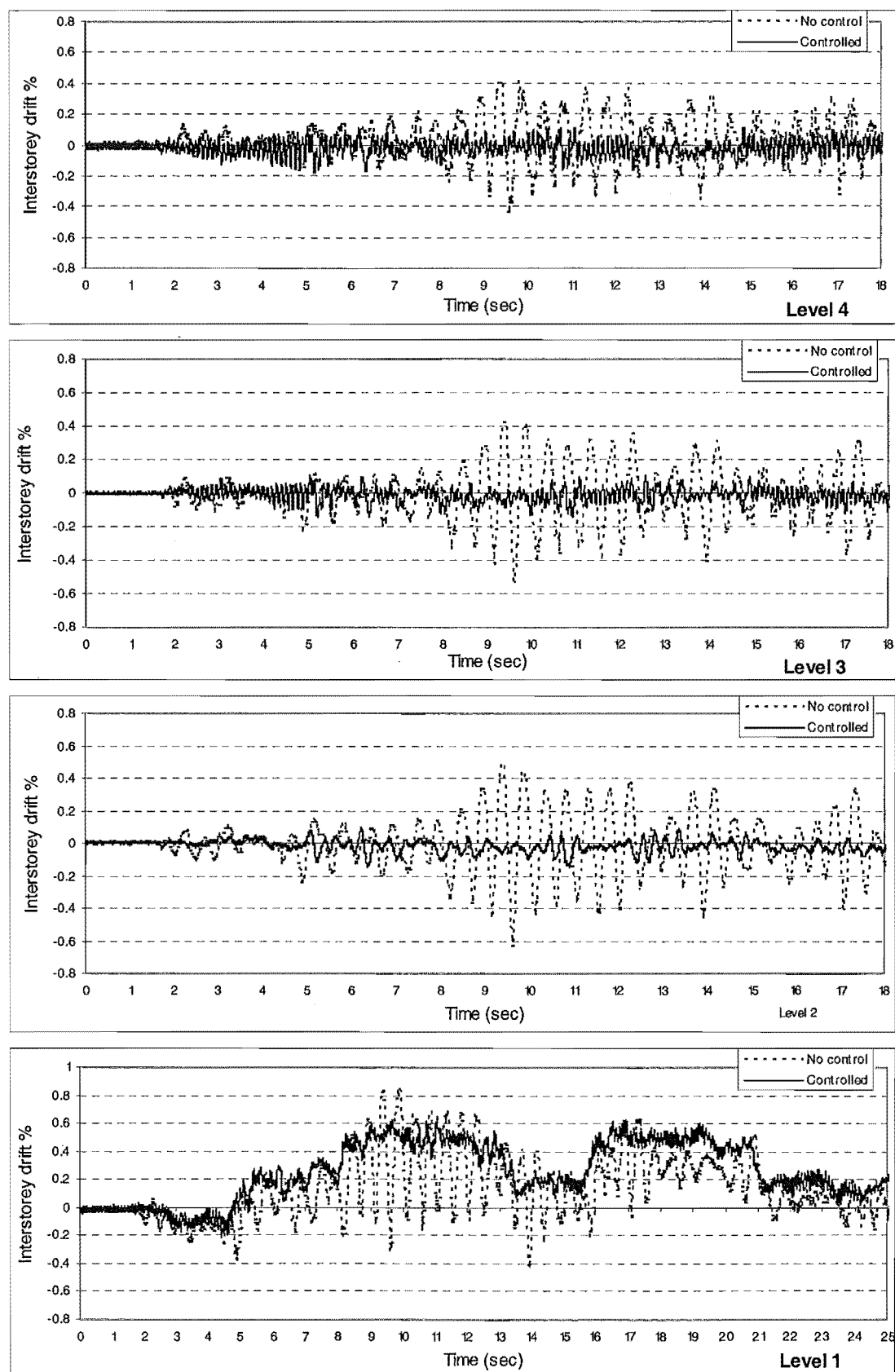


Fig (7-17) Interstorey drift of the structure with and without the supplemental control system- TAFT 120% - shaking table acceleration

#### 7.4.9 Displacement and Interstorey Drift Ratios

Level	Displacement		Reduction	
	Without D-T	With D-T	% of reduction	% average
4	10.9	4	63	55
3	9.1	3.4	63	
2	6.8	3.2	53	
1	4.6	2.8	39	

Level	Interstorey drift %		Reduction	
	Without D-T	With D-T	% of reduction	% average
4	0.37	0.08	78	71
3	0.45	0.07	84	
2	0.51	0.07	86	
1	0.77	0.5	35	

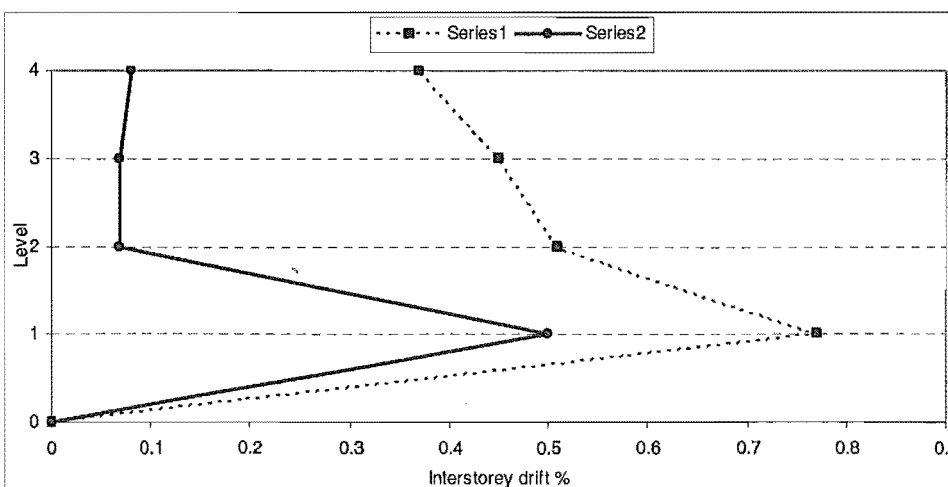
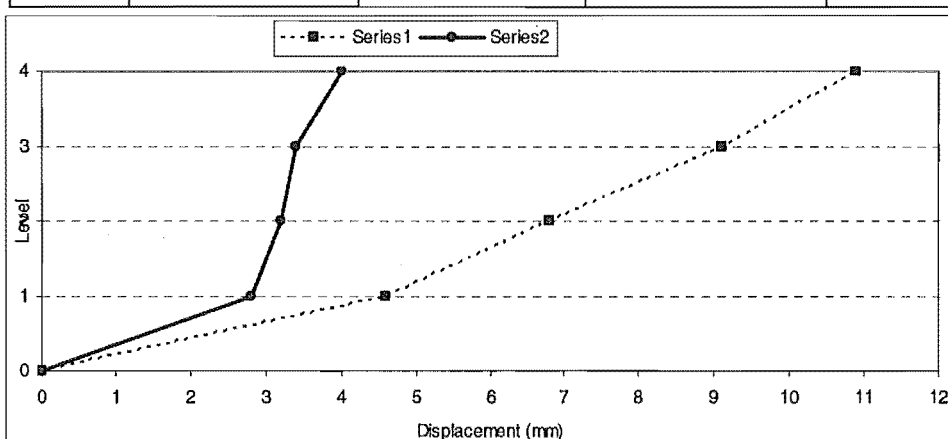


Fig (7-18) Displacement and interstorey drift ratios of the structure with and without the supplemental control system – TAFT 120%- shaking table acceleration.

## 7.5 Conclusion

The relative displacement and interstorey drift time histories for the structure with and without the supplemental damping system have been compared. The effectiveness of the ring spring dampers was obvious as they reduced the response up to 40-80% of the unrestrained response. The maximum response envelopes for the four storey test structure with and without the supplemental control system have been presented in the various figures and the tables. As can be seen, the overall response of the structure up to 40-80% is significantly reduced by the addition of the dampers. Adding damping and increase in the stiffness of the structure by using the ring spring dampers was sufficient to protect the structure from undergoing severe inelastic deformation in the test. It must be mentioned, that the contribution of the beam-column connections and column base fuses do not effect the response of the structure as they were designed to give the appropriate flexibility to the structure in the plastic hinge regions so that the combination of the hinge members and the stiff interconnecting beam members model the flexibility of a normal frame members.

Figures (7-1) through (7-18) show the displacement and the intersorey drifts time histories as well as the maximum response envelopes. With 50% El Centro, the maximum displacement at the top level of the structure was 17.5mm without the supplemental control system and was reduced to 3.3 mm with the supplemental system. The average of the reduction in displacement in the floors was about 80%. The same percentage of reduction can be seen at the first floor when the displacement peak value was decreased from 3.5mm to 0.7mm with an 80% reduction in the response, (section 7-3).

With 100% El Centro, the response at the top floor was 36mm reduced to 13mm in displacement with a reduction of about 64% by adding the supplemental control system. At the bottom of the structure the displacement was 9.5mm before adding the control system and reduced to 3.6mm after adding the supplemental control system. The reduction is about 62 % and the interstorey drifts reduced by the same magnitude as shown in section (7-4).

In section (7-6), the response of the top level of the structure with 80% 4203TAFT decreased from 8.1mm to 2.7mm which represents 67% reduction in the structural response. 61% percent of reduction in the response at the top floor level of the structure can be seen with 100% 4203TAFT, while 41% of the displacement reduction occurred at the first floor. It can be seen from the Figures (7-1) to (7-18) that the percentage of the reduction in the upper floors is larger than the lower floors. It might be due to the straight tendon profile which was used in this experimental study. Also the reduction with the El Centro excitation was larger than that with the 4203TAFT ground motion.

As discussed in section 6.6, there is no significant reduction in floor acceleration as shown in Figures (6-19) and (6-20), while significant reductions in displacement and interstorey response can be observed. This means that one can prevent structural damage but with the technique as applied there may be no significant reduction in the floor accelerations to prevent damage to sensitive items of equipment that might be housed in the structure. It is thus evident that significant ground shaking can be

withstood if supplemental control systems with ring springs dampers are used in the structure.

It should be mentioned that using the proposed supplemental damper-tendon system significantly reduces the displacement and intersorey drift of the structure by adding damping and stiffness to the structure. In the same time, no increases in the floor acceleration of the structure which is a real benefit of using ring spring dampers as opposed to adding conventional diagonal bracings to the frame structure.

Using bracing or spring elements alone through the total height of the frame structure i.e., only adding extra stiffness, may reduce the displacement of the structure but it would also increase, significantly, the floor acceleration of the structure which would cause damage to the sensitive items of equipment and other contents that might be housed in the structure.

## Chapter 8

### Design Considerations of Structures with Supplemental Damping Control Systems

#### 8.1 Introduction

The design of structures with supplemental damping control systems is, in general, an iterative process for which the design and analysis of the structure without the supplemental damping system should be carried out first. In this section, design algorithms are presented for the supplemental damping system configuration using a damper-tendon system. Two systems of tendons are presented. The first system comprises either a single draped tendon, an equivalent straight tendon, or a straight tendon to the top of the structure connected horizontally to the floor levels of the structure and attached to a damper. The second tendon system examined comprises two draped or two straight tendons attached with a damper on each side of the frame structure. Determination of the total effective damping of the structure with a supplemental damping system and the forces in the dampers at the ground floor of the structure are discussed. A twelve-storey two bay frame structure is used as the prototype building to determine the appropriate size of dampers which are to be used. Three different types of damping devices are examined.

#### 8.2 Total Damping

In the analytical design of structures with a supplemental control system, the total effective control represents all energy dissipation mechanisms of the structure including: the elastic inherent damping of the elastic structure, the possible plastic energy dissipation and the load balancing tendon contribution that will take the effect of the supplemental damping system into account (Figure 8-1).

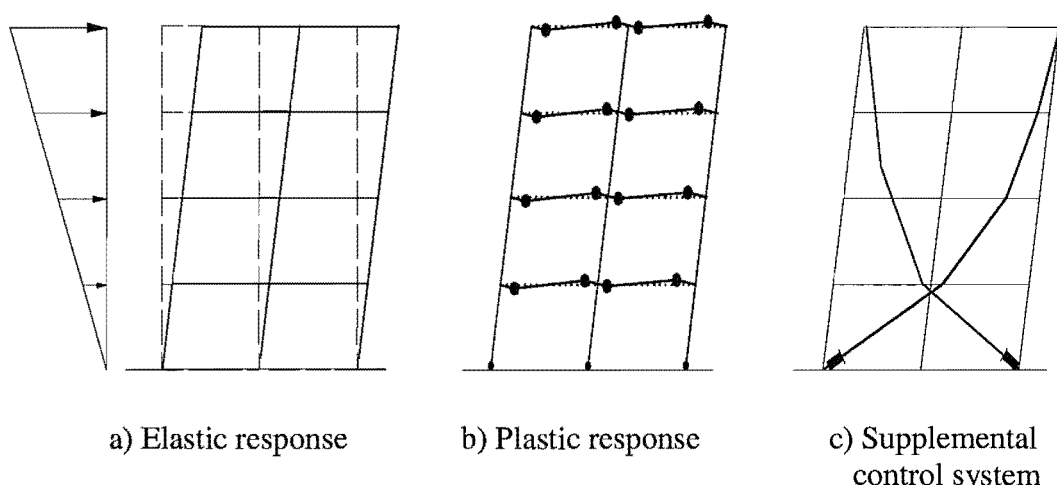


Fig (8-1) Damping mechanisms of the structure

The total effective damping represents all energy dissipation mechanisms of the structure, including:

- Inherent viscous damping  $\zeta_0$  (elastic damping).
- Damping associated with inelastic action  $\zeta_{hy}$  (hysteretic damping due to plastic work after yielding) of members in the structure.
- Damping due to the supplemental control system  $\zeta_{sup}$ .

Hence, the total damping  $\zeta_{Total}$  can be expressed as:

$$\zeta_{Total} = \zeta_0 + \zeta_{hy} + \zeta_{sup} \quad 8-1$$

### 8.2.1 Inherent Viscous Damping

The assumption in many building codes is that the elastic structure has 5% of critical viscous damping i.e.  $\zeta_0 = 0.05$ . This may need to be reconsidered if the building is likely to exhibit less than the generally assumed 5% of equivalent viscous damping.

### 8.2.2 Hysteretic Damping

The equivalent hysteretic damping due to yielding assuming a bi-linear hysteresis model can be calculated from [41]:

$$\zeta_{hy} = \frac{1 - \left[ \frac{1-r}{\sqrt{u_A}} - r\sqrt{u_A} \right]}{\pi} \quad 8-2$$

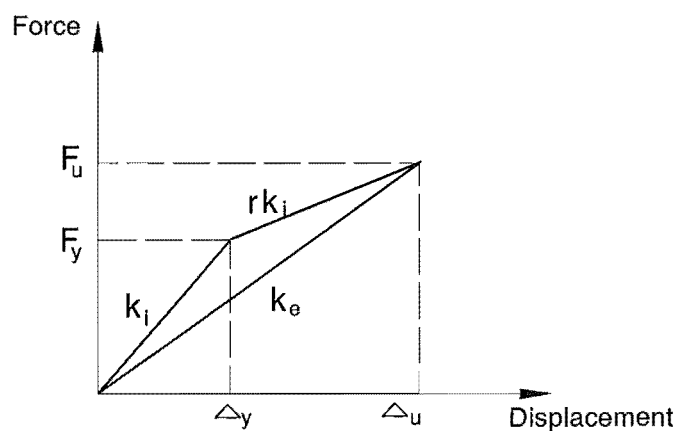


Fig (8-2) Force-displacement relationship

where

$$u_{\Delta} = \frac{\Delta_u}{\Delta_y}$$

$\Delta_u$  = maximum displacement.

$\Delta_y$  = yield displacement.

and

$r$  = the post-yield stiffness factor, see Figure (8-2).

In this research, the hysteretic damping in the structure due to yielding  $\zeta_{hy}$  is taken equal to zero as it is assumed that the structure remains elastic i.e.  $\zeta_{hy} = 0$  for the design level earthquakes and no yield is expected to occur in the structure. For the earthquake scaled of three times the design earthquakes the hysteretic damping is included and may be considered and calculated from equation (8-2)

### 8.2.3 Damping due the Supplemental Control System

The general behaviour of nonlinear devices is governed by the structural velocities. To successfully use spectral design methodologies such as capacity-demand spectrum, it is essential that actual structural velocities be used in the entire equivalent damping formulations. This is because if spectral velocities based on design displacement ( $s_v = \omega_0 s_d$ ) are used, errors are introduced, as the two velocities are not equivalent across the spectrum [64]. Therefore, it is desirable to use the actual maximum structural velocity in order to obtain consistent and more accurate estimations of damping system characteristics in terms of linearized quantities [63]. A Pseudo velocity spectrum is plotted in Figure (8-2-a) together with the spectra corresponding to the actual velocity. The difference between actual and pseudo velocity can be seen in this figure.

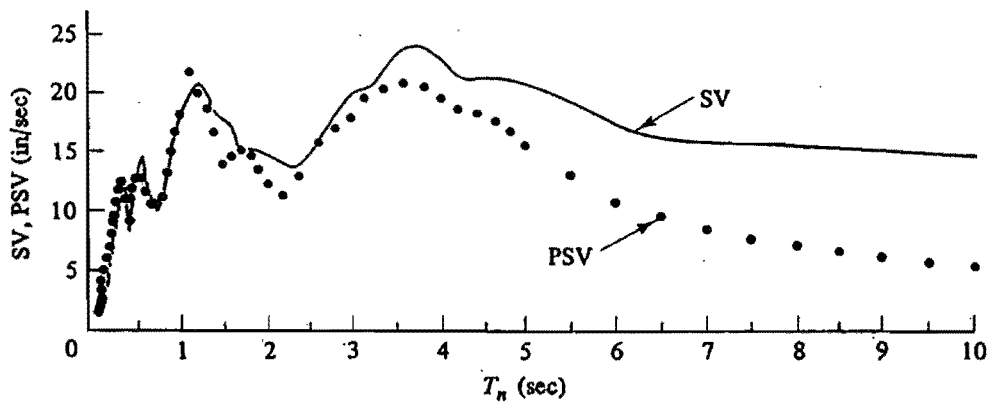


Fig (8-2-a) Response spectra and pseudo-response spectra for Eureka, Californian, earthquake of December 21, 1954 [64].

Response spectra have become a standard design tool to characterize the frequency content of an earthquake and the effective demands on a structure. Response spectra can be generated for various viscous damping ratios and presented by plotting the maximum value of the absolute displacement or  $S_d$ , relative velocity  $V$ , and

acceleration  $A$ , obtained by solving the equations of motion of the linear single-degree-of-freedom (SDOF) system for various natural periods,  $T_0$ , however, it has been a common practice to use the pseudo-relative velocity  $S_v (= \omega_0 S_d)$  and pseudo-acceleration  $S_a (= \omega_0^2 S_d = \omega_0 S_v)$  instead of their actual counterparts, as these quantities can be directly calculated from the corresponding spectral displacements for the range of natural frequencies ( $\omega_0$  in rad/sec).

Response spectra values are defined as follows:

$$\begin{aligned} S_d &= D = |x(t)|_{\max}, \quad V = |\dot{x}(t)|_{\max}, \quad A = |\ddot{x}(t)|_{\max} \\ S_v &= \omega_0 S_d \quad S_a = \omega_0 S_v = \omega_0^2 S_d \end{aligned}$$

in which

$x(t), \dot{x}(t), \ddot{x}(t)$  are the displacement, velocity and acceleration response time histories, respectively, and  $\omega_0 = 2\pi/T_0$  is the natural circular frequency of the SDOF system.

Response spectra can be divided into various period ranges, the characteristics of each of these regions become important when deriving the design response spectra. In general, in the short period (high frequency) range, pseudo acceleration approaches the maximum ground acceleration as the system deforms very little and the mass moves with the ground. Similarly, in the long period (low frequency) range, the maximum displacement response is practically equal to the maximum ground displacement.

The maximum displacement response  $S_d$  of a SDOF system subjected to ground acceleration  $p(t)$  may be expressed by the well-known Duhamal integral as [63]:

$$S_d = \left| \frac{1}{\omega_0} \int_0^t p(\tau) \sin \omega_d (t - \tau) \exp(-\zeta_0 \omega_0 (t - \tau)) d\tau \right|_{\max} \quad 8-2-a$$

When small amount of critical viscous damping is assumed ( $\omega_d = \omega_0 \sqrt{1 - \zeta^2}$ ) the displacement response can be differentiated with respect to time to obtain the corresponding velocity response from which the maximum velocity  $V$  can be calculated assuming that the damping  $\zeta_0 = 0$ , for simplicity, as:

$$V = \left| \int_0^t p(\tau) \cos \omega_0 (t - \tau) d\tau \right|_{\max} \quad 8-2-b$$

Moreover, using equation (8-2-a) with  $\zeta_0 = 0$ , the pseudo relative velocity can be written as:

$$S_v = \left| \int_0^t p(\tau) \sin \omega_0 (t - \tau) d\tau \right|_{\max} \quad 8-2-c$$

It is clear from equation (8-2-b) and (8-2-c) that the actual spectral velocity and pseudo velocity are different even for zero damping.

The following transformation is proposed for 5% damping by Pekcan [13, 15, and 63] as follows:

$$V = S_v \left( \frac{T}{0.75} \right)^{0.15} \quad 8-3-a$$

The approximate actual velocity spectra for higher damping values can be determined using the  $B_t$  factor as:

$$V_\zeta = \left( \frac{T}{0.75} \right)^{0.15} \left( \frac{S_v}{B_t} \right) \quad 8-3-b$$

where  $B_t$  is spectral amplification factor and is given by  $B_t = \left[ \frac{\zeta_{Total}}{0.05} \right]^{0.3}$

The non-dimensional damper capacity  $\varepsilon$  is defined as

$$\varepsilon = \frac{C_\alpha \dot{x}^\alpha}{W} \quad 8-3-c$$

where  $W$  is the total weight of the system,  $\dot{x}^\alpha$  is a standard velocity for dampers.

The normalised damper capacity  $\varepsilon$  defined in equation (8-3-c) and the proposed velocity transformation in equation (8-3-b) allows one to express the added damping due both linear ( $\alpha = 1.0$ ) and non-linear ( $\alpha < 1.0$ ) dampers in terms of spectral quantities, i.e., spectral displacement,  $S_d$  and demand  $C_d$  according to Pekcan [13,15, 63], is given by:

$$\zeta_{sup} = \frac{c_{sup}}{1 + \alpha} \left( \frac{2\pi}{0.75} \right)^{0.15(\alpha-1)} g^{0.5(0.85\alpha+0.15)} S_d^{0.5(1.15\alpha-0.15)} C_d^{0.5(0.85\alpha-1.85)} \quad 8-3$$

where

- $S_d$  = ( $x_{max}$ ) the target displacement (see section 8.2.3.1)
- $c_d$  = structural demand at  $S_d$  (see section 8.2.3.2)
- $c_{sup}$  = capacity of the supplemental damping system (Equation 8-5)
- $\alpha$  = damper power factor
- $g$  = ground acceleration

The shape of the loop used by Pekcan [13] is similar in form to that of the ring spring as shown in Figure (8-3). It seems appropriate to use the same  $\alpha = 0.2$  used in references [13, 59]. Then Equation (8-3) reduces to:

$$\zeta_{sup} = 0.93 c_{sup} (x_{max})^{0.04} (c_d)^{-0.84} \quad 8-4$$

and

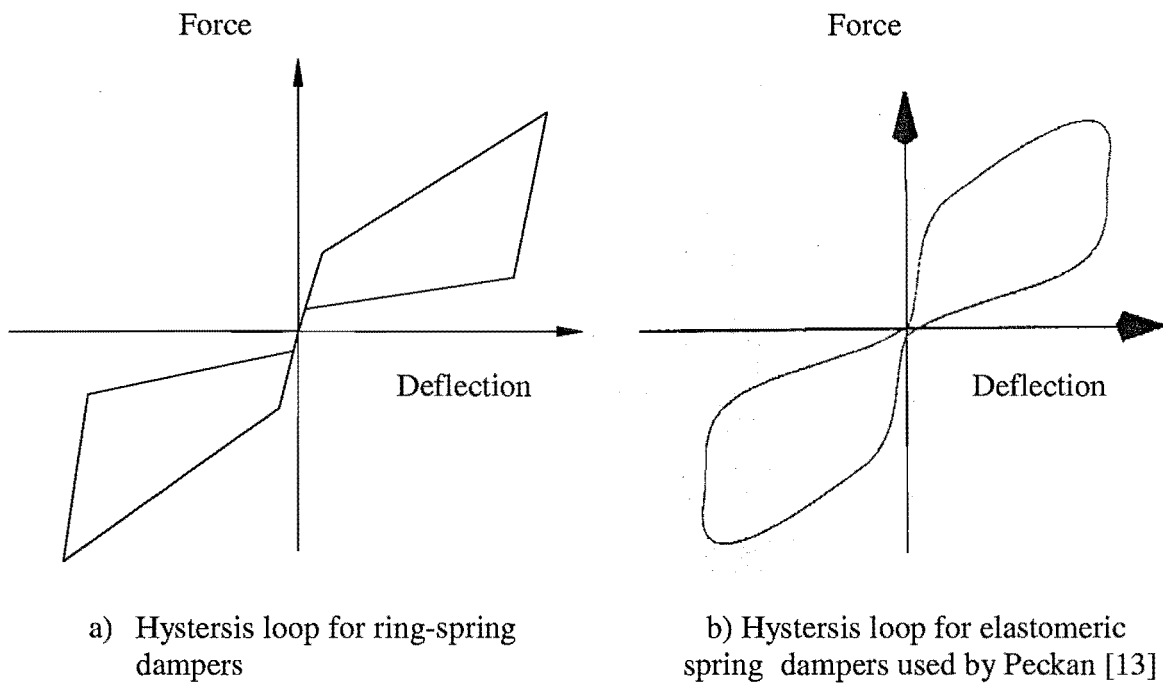
$$c_{\text{sup}} = c_d - c_{\text{str}}$$

8-5

where  $c_d$  = structural demand

$$c_{\text{str}} = \text{coefficient represents lateral force resisted by the structure} = \frac{V_b}{W_T}$$

where  $V_b$  = base shear and  $W_T$  = total weight of the structure.



a) Hysteresis loop for ring-spring dampers

b) Hysteresis loop for elastomeric spring dampers used by Peckan [13]

Fig (8-3) Hysteresis loops for ring-spring and elastomeric dampers

### 8.2.3.1 Target Displacement

The design objective is set by specifying the desired level of performance for a given ground motion. FEMA 273 [59] categorises the ground motion into main groups based on intensity of ground shaking. The first, Maximum Considered Earthquake (MCE) is defined as the level of ground shaking that has a 2% chance of being exceeded in a 50 year period (return period of 2500 years). The second, Maximum Assumed Earthquake (MAE) is the ground shaking that has a 10% chance of being exceeded in a 50 years period (return period of 500 years) but not less than 2/3 of the MCE [59].

The target displacement  $x_{\max}$  based on the performance criteria is selected as [59]:

$$x_{\max} = \theta_{\max} \cdot H_{\text{eff}} \quad 8-6$$

where  $\theta_{\max}$  is the design limit structural drift.

$$H_{\text{eff}} = 0.7H$$

where  $H$  is the total height of the structure.

### 8.2.3.2 Structural Demand

Lateral forces imposed on the structural system are quantified based on the design ground motion (MAE) and the target design response. A study by Pekcan [13] was carried out to develop the probability ranges for the ground motion demand in terms of amplification factors. The structural demand can be calculated from the following relationship [13 & 59]:

$$c_d = \left[ \frac{S_a}{2\pi B_l} \right]^2 \frac{g}{x_{\max}} \quad 8-7$$

where

$S_a$  = the spectral acceleration for a 1.0 second period [13].

$g$  = ground acceleration

$B_l$  = spectral amplification factor

where

$$B_l = \left[ \frac{\zeta_{Total}}{0.05} \right]^{0.3} \quad 8-8$$

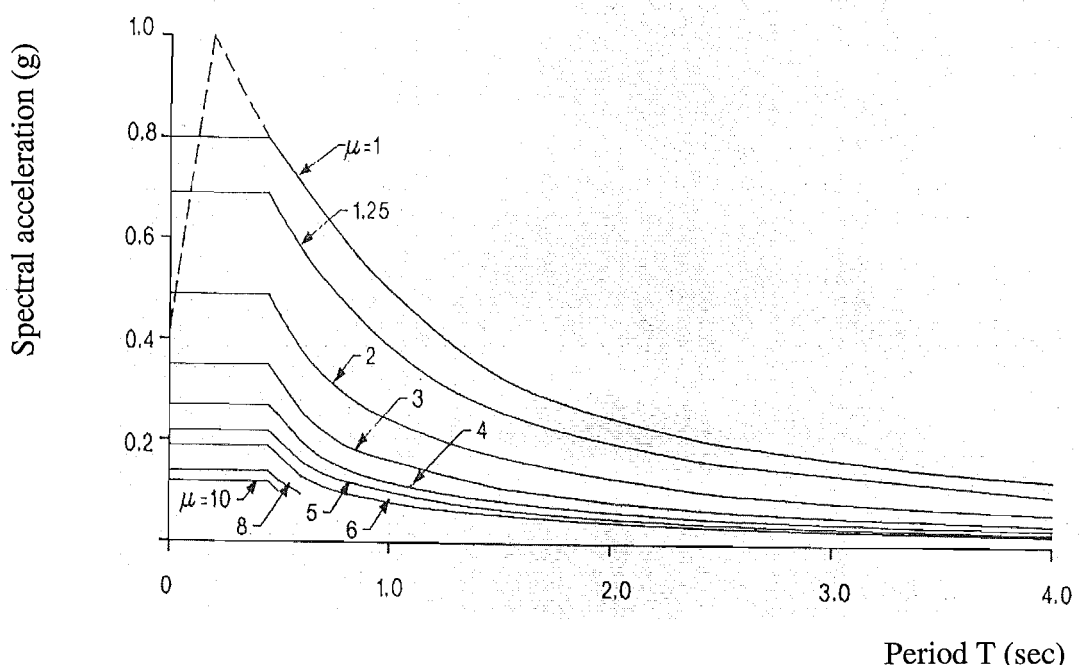


Fig (8-4) Basic seismic hazard acceleration coefficient (Intermediate soil sites)  
NZS 4203:1992 [37]

Figure (8-4) shows the basic seismic hazard acceleration coefficient in the New Zealand Code of Practice for General Structural and Design Loading for Building.

It should be noted here that the value of the total damping  $\zeta_{Total}$  is assumed and the demand is calculated using Equation (8-4) until the calculated value becomes close enough to the assumed value otherwise, several iterations may be required until  $\zeta_{assumed}$  is approximately equal to  $\zeta_{calculated}$ .

### 8.3 Design Verification

#### Step 1: Period of the Structure.

The period of the structure can be obtained from the computer program.

#### Step 2: Total Damping

The total damping is assumed initially. After several cycles of iteration in the analysis, the exact amount of the total damping  $\zeta_{Total}$  can be determined as described in section 8.2.

#### Step 3: Supplemental Damping System Layout

Determine the tendon layout based on the vertical distribution of the design base shear, shown in Figure (8-5), as discussed in Section 3.10.1

$$F_{Ti} \cos \theta_i = \sum_{j=i+1}^N F_j \quad i = 0, \dots, N-1 \quad 8-9$$

in which  $F_{Ti}$  are the Forces in the Tendon at the  $i^{th}$  level and  $\theta_i$  is the angle of inclination of the  $i^{th}$  floor Tendon and  $F_j$  is the horizontal lateral load at level  $j$ .

$$R_{i,i+1} = \sum_{j=i+1}^N F_j / \sum_{j=i+2}^N F_j \quad 8-10$$

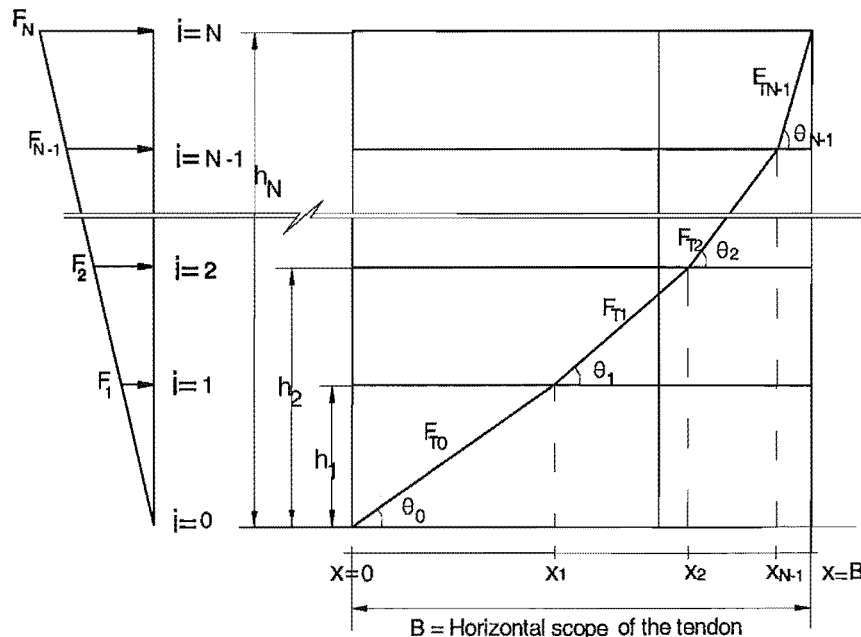


Fig (8-5) Determination of tendon layout

$$[R]\{x\} = \{D\}$$

8-11

where  $[R]$  = coefficient matrix determined by:-

$$[R] = \begin{bmatrix} -(R_{0,1} + 1) & R_{0,1} & 0 & 0 & 0 & 0 & 0 \\ 1 & -(R_{1,2} + 1) & R_{1,2} & 0 & 0 & 0 & 0 \\ 0 & 1 & -(R_{2,3} + 1) & R_{2,3} & 0 & 0 & 0 \\ 0 & 0 & 1 & . & . & 0 & 0 \\ 0 & 0 & 0 & 1 & . & . & 0 \\ 0 & 0 & 0 & 0 & 1 & . & . \\ 0 & 0 & 0 & 0 & 0 & 1 & -(R_{n-3,n-2} + 1) \\ 0 & 0 & 0 & 0 & 0 & 0 & (R_{n-3,n-2}) \\ 0 & 0 & 0 & 0 & 0 & 1 & -(R_{n-2,n-1} + 1) \end{bmatrix}_{n-1,n-1}$$

8-12

where the diagonal  $= -(R_{i-1,i} + 1)$

the above diagonal  $= (R_{i-1,i})$

the below diagonal  $= 1$

and  $i = 1, n - 1$

$\{x\}^T = \{x_1, x_2, \dots, x_{n-1}\}$  is the unknown column vector of tendon coordinates,

$\{D\}^T = \{0, \dots, -R_{n-2,n-1}B\}$

where  $B$  is the width of the tendon layout of the structure.

#### **Step 4: Damper Design (assuming ring-spring damping devices)**

1- Find the force in the damper from the following equation:

$$F_D = \frac{c_{\text{sup}} W_T}{\cos \theta_D} \quad 8-13$$

where  $F_D$  = force in damper.

$W_T$  = total weight of the structure.

$\theta_D$  = angle of damper.

2- Determine the number of ring spring elements.

To determine the number of ring spring elements, the target displacement of the structure should be calculated. The deformation of the supplemental system can then be calculated as:

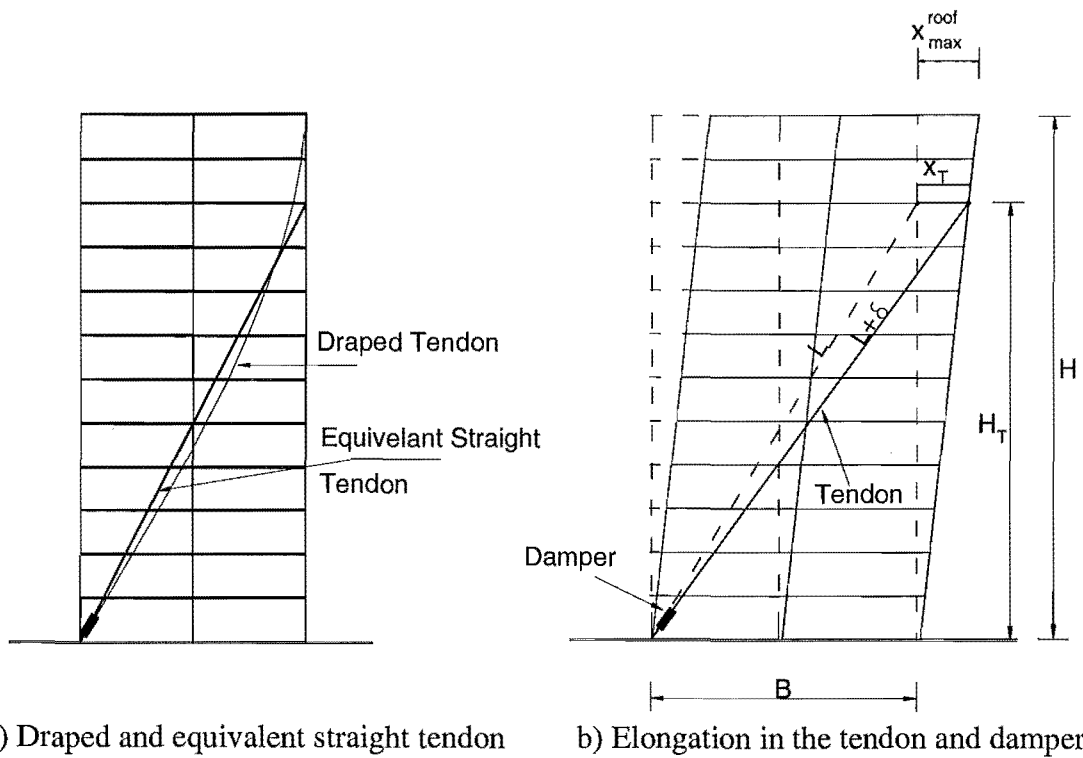


Fig (8-6)

The total elongation of the supplemental damping system is equal to the elongation of the damper plus the elongation of the tendon.

From Figures (8-6 and 8-7),

$$\tan \theta = \frac{H_T}{B}$$

$$\delta = x_T \cos \theta$$

$$x_T = x_{\text{roof}}^{\text{root}} \left( \frac{H_T}{H} \right)$$

where  $\delta$  is the total elongation of the system and equal to:

$$\delta = \delta_{\text{damper}} + \delta_{\text{tendon}}$$

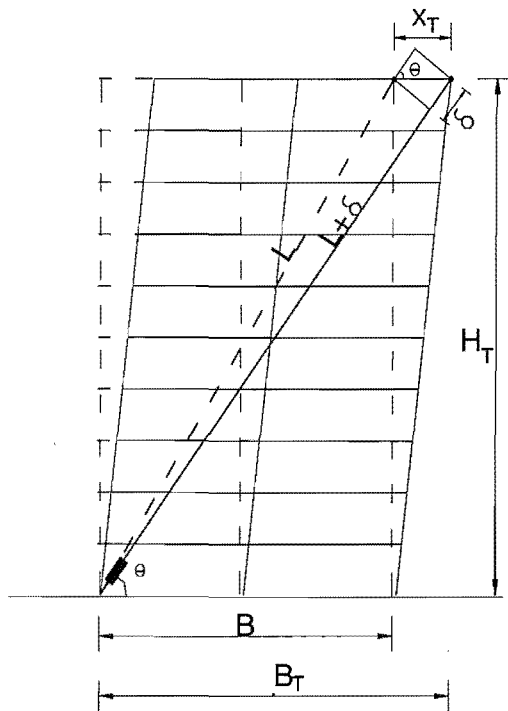


Fig (8-7) The elongation in the supplemental damping system

The elongation of the tendon is equal to:

$$\delta_{tendon} = \left( \frac{F}{K} \right)_{tendon} = F_{tendon} \cdot \left( \frac{L}{EA} \right)_{tendon} \quad 8-14$$

where  $A$  = cross sectional area of tendon  
 $E$  = Young's modulus of tendon  
 $L$  = total length of the tendon  
 $F$  = force in the tendon

For draped or segmental tendon,  $L = \sum L_i$  where  $L_i$  is the length of the tendon segment i.

The elongation of the damper is equal to:

$$\delta_{damper} = \delta - \delta_{tendon} \quad 8-15$$

The number of elements required is equal to:

$$n = \frac{\delta_{damper}}{S_e} \quad 8-16$$

where  $S_e$  is the spring displacement of one ring element (Table 4-1).

The total length of the elements in the damper is:

$$L_D = n \cdot h_e \quad 8-17$$

where  $L_D$  = length of the total numbers of elements.

$h_e$  = element height.

Part of the Table (4-1) Ring spring design data [33].

Diagram		Dimensions					Guide		Weight
F (kN)	$s_e$ (mm)	$W_e$ (j)	$h_e$ (mm)	$D_1$ (mm)	$d_1$ (mm)	$b/2$ (mm)	$D_2$ (mm)	$d_2$ (mm)	$G_e$ (kg)
600	4.4	1320.0	23.4	194.0	155.0	19.0	199.0	150.0	1.0615
720	4.4	1584.0	26.4	220.0	174.0	22.0	225.0	169.0	2.520
860	4.8	2064.0	25.8	262.0	208.0	21.0	268.0	202.0	3.315
1000	5.8	2900.0	35.8	300.0	250.0	30.0	306.0	245.0	5.410

## 8.4 Example

To investigate the amount of damping and the size of the ring spring damper which may be used in a real building, the reinforced concrete twelve storey two-bay frame (Modified Jury 1995) shown in Appendix D was used. The building dimensions and member sizes adopted as detailed in Appendix D. Figure (8-6a) shows the structure with draped and equivalent straight tendons.

### 8.4.1 Amount of Damping

The total damping of the structure  $\zeta_{Total}$  is calculated using Equation (8-1), where:

- the inherent damping of the structure  $\zeta_0 = 5\%$  (for a reinforced concrete structure).
- the hysteretic damping of the structure  $\zeta_{hy} = 0$  (as it is assumed that it will remain elastic).
- the damping due to supplement the damping system to the structure  $\zeta_{sup}$  can be calculated from Equation (8-4)

$$\zeta_{sup} = 0.93 \cdot c_{sup} (x_{max})^{0.04} (c_d)^{-0.84}$$

The target design drift  $\theta_{max}$  is chosen to be 1% for a 500 year event.

$$x_{max} = \theta_{max} \cdot H_{eff}$$

Hence,  $x_{max} = 0.01 (0.7 \times 43.5) = 0.304 \text{ m}$

Assume  $\zeta_{Total} = 17\%$

$$\text{Hence, } B_l = \left[ \frac{\zeta_{Total}}{0.05} \right]^{0.3} = \left[ \frac{0.17}{0.05} \right]^{0.3} = 1.44$$

From Figure (8-4), the spectral acceleration  $S_a = 0.5$

$$c_d = \left[ \frac{S_a}{2\pi B_l} \right]^2 \frac{g}{x_{max}} = \left[ \frac{0.5}{2\pi(1.44)} \right]^2 \frac{9.81}{0.304} = 0.098$$

$$\text{The capacity of the structure } c_{str} = \frac{V_b}{W_T}$$

From Table (8-1), the total weight of the structure  $W_T = 19,188 \text{ kN}$   
and the base shear  $V_b = 1530 \text{ kN}$

Hence, the capacity of the structure  $c_{str} = \frac{1530}{19,188} = 0.079$

From Equation (8-5), the capacity of the supplemental damping system  $c_{sup}$  is equal to:

$$\begin{aligned} c_{sup} &= c_d - c_{str} \\ &= 0.098 - 0.079 = 0.019 \end{aligned}$$

Using Equation (8-4), the supplemental damping  $\zeta_{sup}$  is equal to:

$$\zeta_{sup} = 0.93 (0.019) (0.0304)^{0.04} (0.098)^{-0.84} = 11.8 \%$$

The total damping is equal to:

$$\begin{aligned} \zeta_{Total} &= \zeta_0 + \zeta_{hy} + \zeta_d \\ \zeta_{Total} &= 5\% + 0\% + 11.8\% = 16.8\% \end{aligned}$$

#### 8.4.2 Force in the Damper

The force in the damper can be calculated using Equation (8-12), where the storey shear from Table (8-1) and Figure (8-8) is equal to 1530 kN. From the geometry,  $\cos \theta_D = 18.4 / 36.5 = 0.504$

$$F_D = \frac{c_{sup} W_T}{\cos \theta_D} = \frac{0.019(19,188)}{0.504} = 723 \text{ kN}$$

Table (8-1)

Level	W	h	W.h	Wh/ $\sum Wh$	$F_x$	Shear Forces
12	1535	43.8	67233	0.149	333	333
11	1571	40.15	63075	0.139	196	529
10	1571	36.5	57341	0.127	180	709
9	1571	32.85	51607	0.114	161	870
8	1595	29.2	46574	0.103	146	1016
7	1597	25.55	40803	0.09	127	1143
6	1623	21.9	35544	0.078	110	1253
5	1625	18.25	29656	0.065	92	1345
4	1625	14.6	23725	0.052	74	1419
3	1625	10.95	17794	0.039	55	1474
2	1625	7.3	11862	0.026	37	1511
1	1625	3.65	5931	0.013	19	1530

$$W_T = 19,188$$

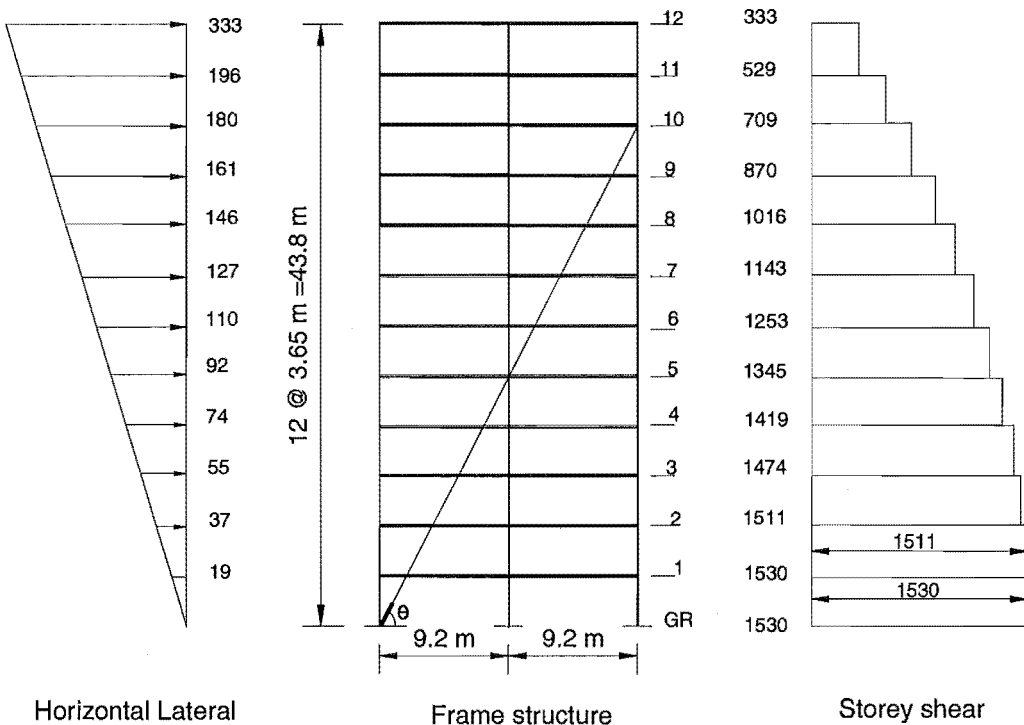


Fig (8-8) The horizontal lateral forces and the storey shear

The roof displacement  $x_{\max} = 0.304 \text{ m}$  (Section 8.4.1)

$$x_T = \frac{0.304(36.5)}{43.5} = 0.255 \text{ m}$$

$$\theta = \tan^{-1} \frac{H_T}{B} = \tan^{-1} \frac{36.5}{18.4} = 63.2^\circ$$

Hence, the total elongation in the system  $\delta$  is equal to:

$$\delta = x_T \cos \theta = 0.255 (\cos 63.2) = 0.115 \text{ m}$$

$$\text{The elongation in the tendon} = \frac{FL}{EA}$$

where  $F = 732 \text{ kN}$ ,  $L = 4.08 \text{ m}$ ,  $E = 200,000 \text{ MPa}$

$$\text{and } A = \frac{F}{f_s} = 33.40 \text{ cm}^2$$

$$\text{Hence, } \delta_{\text{tendon}} = \frac{720 \times 1000 \times (4.08 \times 1000)}{200,000 \times (3340)} = 4.4 \text{ mm}$$

The elongation in the damper  $\delta_{damper} = 115 - 4.4 = 110.6 \text{ mm}$

From Table (4-1), a damper with capacity  $F = 860 \text{ kN}$  can be used where the damper is placed in the ground floor of the structure. The spring travel of one element  $S_e = 4.8 \text{ mm}$  and the element height  $h_e = 25.8 \text{ mm}$ .

The number of ring spring elements required  $n = \frac{\delta_{damper}}{S_e} = \frac{110.6}{4.8} = 23 \text{ elements}$

The total length of the elements  $= n.h_e = 23 (0.0258) = 0.593 \text{ m} \cong 0.6 \text{ m}$

The total length of the damper with the elements, cartridge and piston is about 1.2 m

#### 8.4.3 Shape of the Tendon

The shape of the draped and equivalent straight tendons in the twelve storey frame are shown in Figure (8-9).

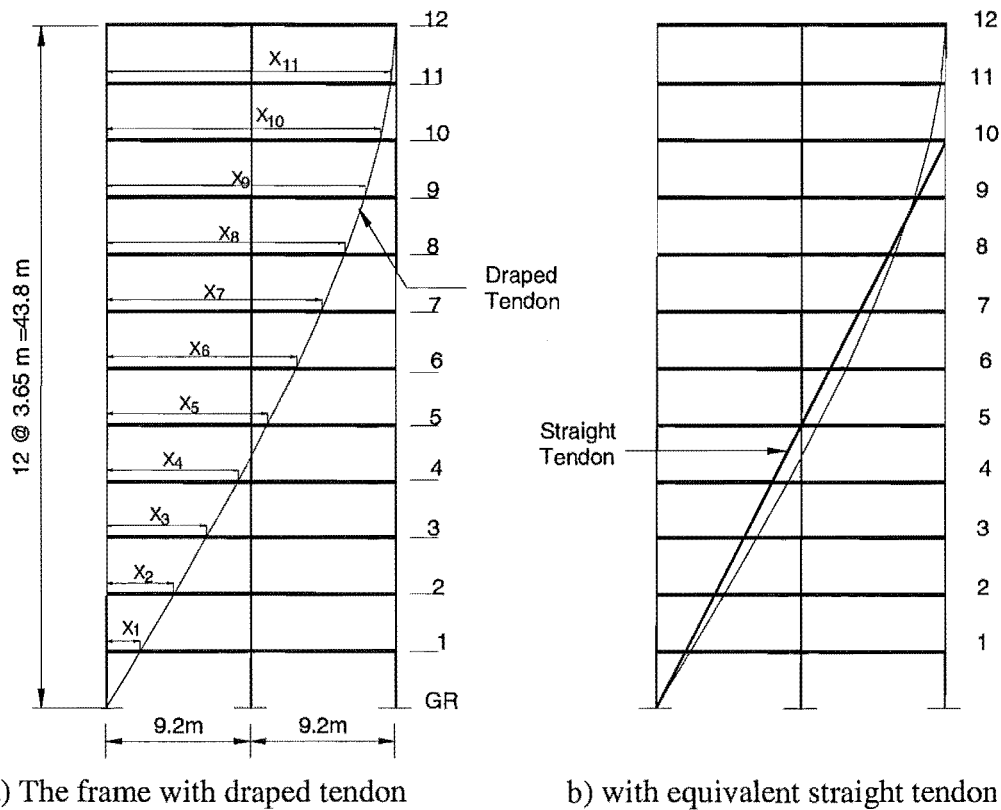


Fig (8-9) Twelve storey-two bay frame with draped and equivalent straight tendons.

From Equation (8-9), find the ratio of the storey shear at the  $i^{th}$  level to that at  $i+1^{th}$  level as:

$$R_{i,i+1} = \sum_{j=i+1} F_j / \sum_{j=i+2} F_j \quad 8-9$$

$$R_{0,1} = 1530 / 1511 = 1.012$$

$R_{0,1}$	$R_{1,2}$	$R_{2,3}$	$R_{3,4}$	$R_{4,5}$	$R_{5,6}$	$R_{6,7}$	$R_{7,8}$	$R_{8,9}$	$R_{9,10}$	$R_{10,11}$
1.021	1.024	1.038	1.053	1.017	1.093	1.119	1.159	1.285	1.336	1.588

Determine the shape of the draped tendon, using Equation (8-10). The matrix [R] is:

-2.012	1.012	0	0	0	0	0	0	0	0	0
1	-2.025	1.025	0	0	0	0	0	0	0	0
0	1	-2.038	1.038	0	0	0	0	0	0	0
0	0	1	-2.055	1.055	0	0	0	0	0	0
0	0	0	1	-2.073	1.073	0	0	0	0	0
0	0	0	0	1	-2.096	1.096	0	0	0	0
0	0	0	0	0	1	-2.125	1.125	0	0	0
0	0	0	0	0	0	1	-2.167	1.167	0	0
0	0	0	0	0	0	0	1	-2.285	1.285	0
0	0	0	0	0	0	0	0	1	-2.336	1.336
0	0	0	0	0	0	0	0	0	1	-2.588

And {D}

0
0
0
0
0
0
0
0
0
0
-29.23

Solving the Equation (8-10) gives the horizontal coordinates of the draped tendon which are:

$x_1$	2.14
$x_2$	4.25
$x_3$	6.32
$x_4$	8.31
$x_5$	10.19
$x_6$	11.96
$x_7$	13.57
$x_8$	15.01
$x_9$	16.26
$x_{10}$	17.23
$x_{11}$	17.95

It must be noted here that the  $x_{12}$  at the top of the structure is the width of the damping system in the structure which is equal to 18.40 m.

## 8.5 Time-History Analysis of the Structure Using Ring Spring Damper and a Single Tendon

With the twelve-storey frame, the three cases which were used with the ring spring damper and a tendon in one side of the frame structure were:

- Draped tendon (Figure 8-10a).
- Equivalent straight tendon (Figure 8-10b).
- Straight tendon to the top of the structure (Figure 8-10c).

It must be noted that with the equivalent straight tendon shown in Figure (8-9b), the tendon was supported at level ten. Hence for this case with an equivalent straight tendon, a support at level ten was also used (Figure 8-10b). Stiff horizontal links are used to transfer the damping forces provided by the dampers to the floors. The ring spring dampers are used to provide the damping forces and transfer them to the rest of the structure by using the tendon system.

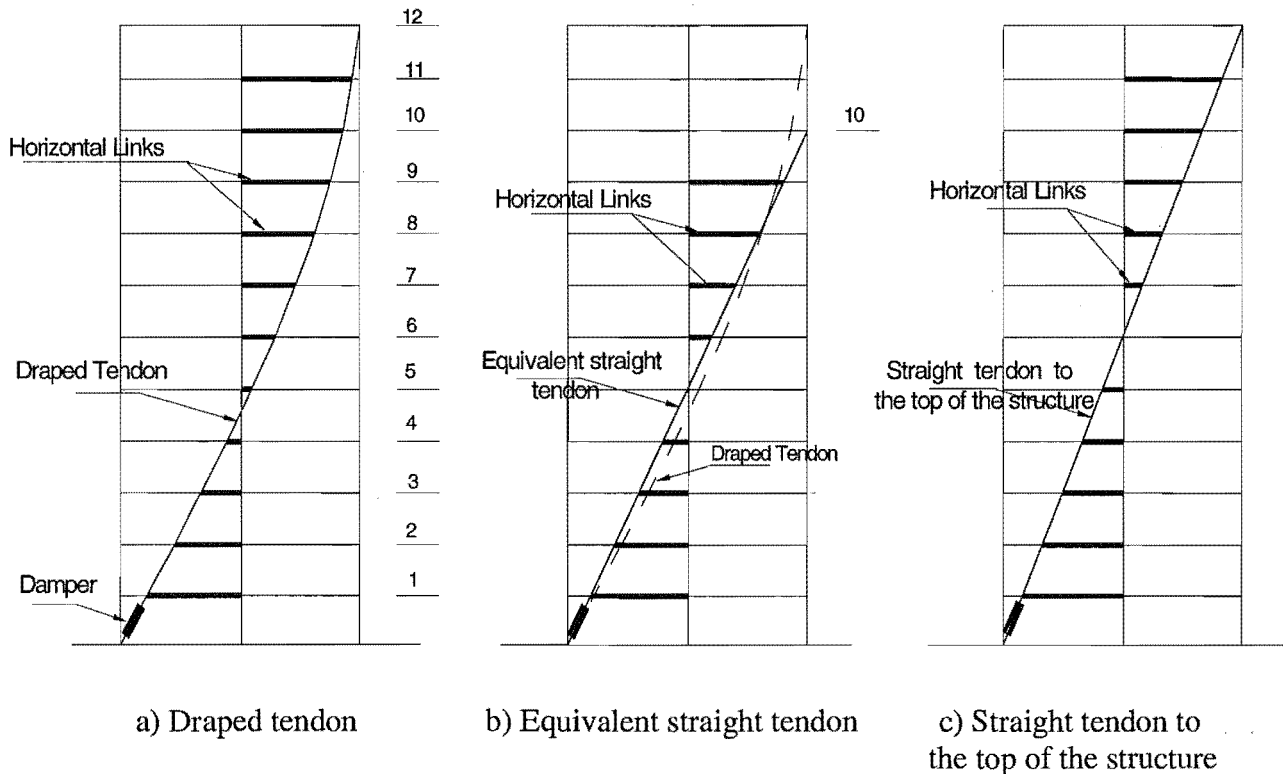


Fig (8-10) Tendon profile.

### 8.5.1 Tendon Properties

The tendon is supported at each floor level as shown in Figure (8-10). The force in the tendon is equal to:

$$F_{Tendon} = 723 \text{ kN} \quad \text{and area of the cross section } A_{tendon} = \frac{F}{f_s} = 33.6 \text{ cm}^2$$

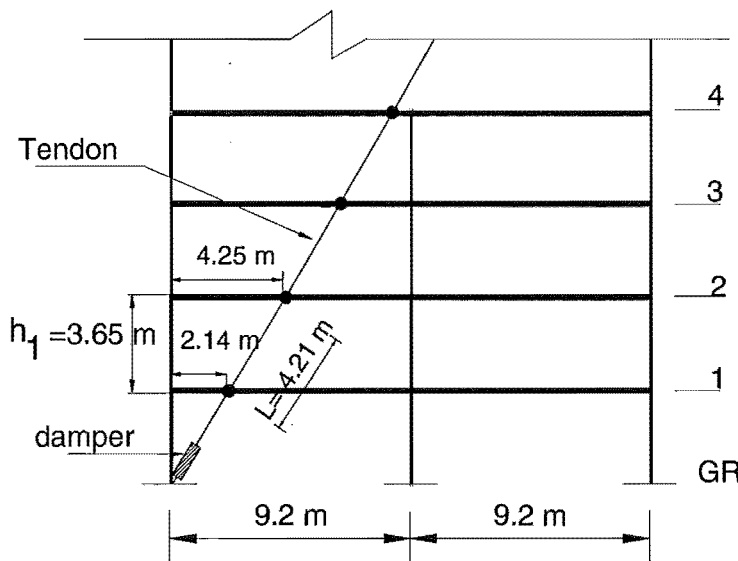


Fig (8-11) The tendon supported at each floor

For the tendon, choose a circular steel tube with  $R = 101.6 \text{ mm}$ ,  $A = 34.99 \times 10^2 \text{ mm}^2$  and  $I = 350 \times 10^4 \text{ mm}^4$ . The dimensions and the properties of the tube steel section are shown in Table (8-2).

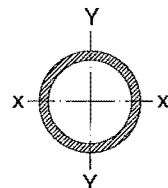


Table (8-2) Dimensions and Properties - Tube Sections

Outside Diameter mm	Thickness mm	Mass Kg/m	Area of Section $\times (10^2) \text{ mm}^2$	Moment of Inertia $\times (10^4) \text{ mm}^4$	Elastic Section Modulus $\times (10^3) \text{ mm}^3$
101.6	12.5	27.48	34.99	350.0	69.69
127.0	12.5	35.3	44.96	746	117.0

The stiffness of the tendon is equal to:

$$k_x = \frac{EA}{L} = \frac{200,000(3499)}{4210} = 1.66E5 \text{ kN/m}$$

where  $L$  is the supported length of the tendon (see Figure 8-11).

$$\text{The critical load } P_{cr} = \frac{\pi^2 EI}{L^2} = \frac{\pi^2 (200,000)(350,000)}{(4210)^2} = 389.4 \text{ kN}$$

$P_{tendon} > P_{cr}$  not safe. Choose circular tube steel with outside diameter equal to 127.0 mm (Table 8-2).

$$\text{Then, } P_{cr} = \frac{\pi^2 (200,000)(746,000)}{(4210)^2} = 830 \text{ kN} > P_{tendon} = 723 \text{ kN o.k.}$$

$$\text{and the stiffness of the tendon } k_x = \frac{(200,000)(4496)}{(4210)} = 2.13E5 \text{ kN/m.}$$

### 8.5.2 Draped Tendon

To get the target displacement as calculated in Section 8.4.1 where  $x_{max} = 0.304 \text{ m}$ , the El Centro excitation record is scaled to 300% with ground acceleration equal to 1.05g. The structure without and with the damping control system is used using RUAUMOKO [1]. The draped tendon shown in Figure (8-10a) is analysed to show the effect of the damping system on the response of the structure. Figure (8-12) shows the roof displacement in both cases without and with the damping system. The peak displacement of the top floor level is decreased from 0.62 m without using the damping system to 0.3 m (the target displacement) with the damping system. The percentage decrease is about 52 %.

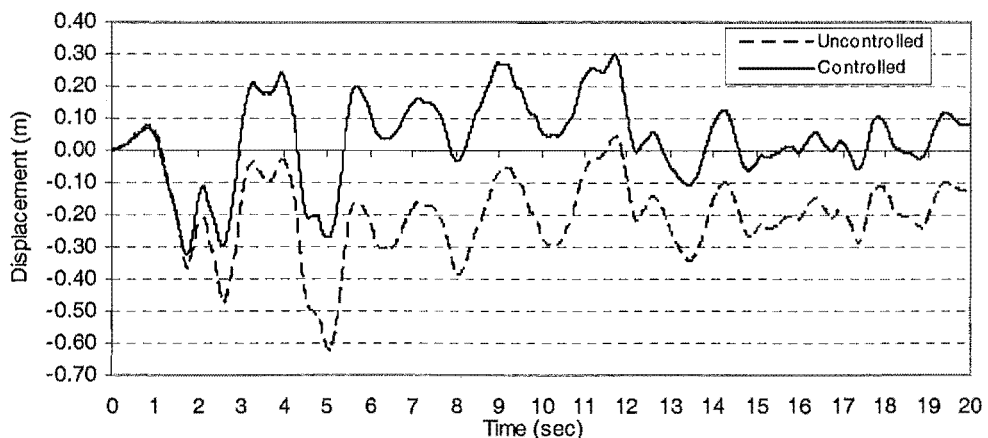


Fig (8-12) Roof displacement with and without the supplemental control system-draped tendon with 300% El Centro excitation.

The hysteresis loop of the ring spring damper is shown in Figure (8-13a). The shape of the hysteresis loop of the damper in the loading and unloading cycles is very similar to the theoretical shape of the hysteresis loops shown in chapter 4. The maximum force in the damper is equal to 730 kN and the deformation in the ring elements is equal to 0.12 m. The values of the forces and the deformation in the damper are very close to the analytical values in section 8.4.2 where  $F = 730$  kN and the deformation in the damper  $\delta_{\text{damper}} = 0.11$  m. Figure (8-13b) shows the force-deformation relationship in the tendon where the force in the tendon equals to 680 kN and the deformation is equal to 0.0035 m. The values of the forces and the deformation for the tendon from the analytical results are 735 kN and 0.004 m respectively.

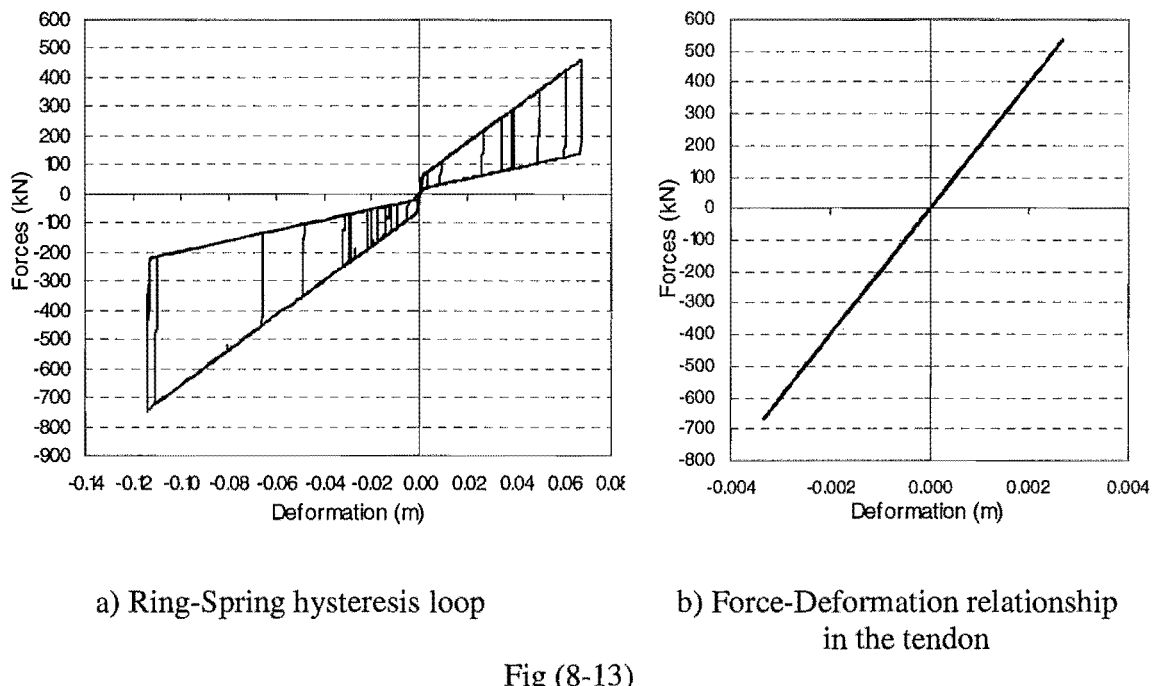


Fig (8-13)

Figure (8-14) shows the force-deformation relationships for the horizontal links in different floor levels of the structure. The maximum values of the forces in the links at the first floor is 65 kN and increased to about 250 kN at level 10. The elongation in the links can be seen to be very small due to the stiffness of the link members which is essential to transfer the damping forces created by the damper to the floor levels of the structure.

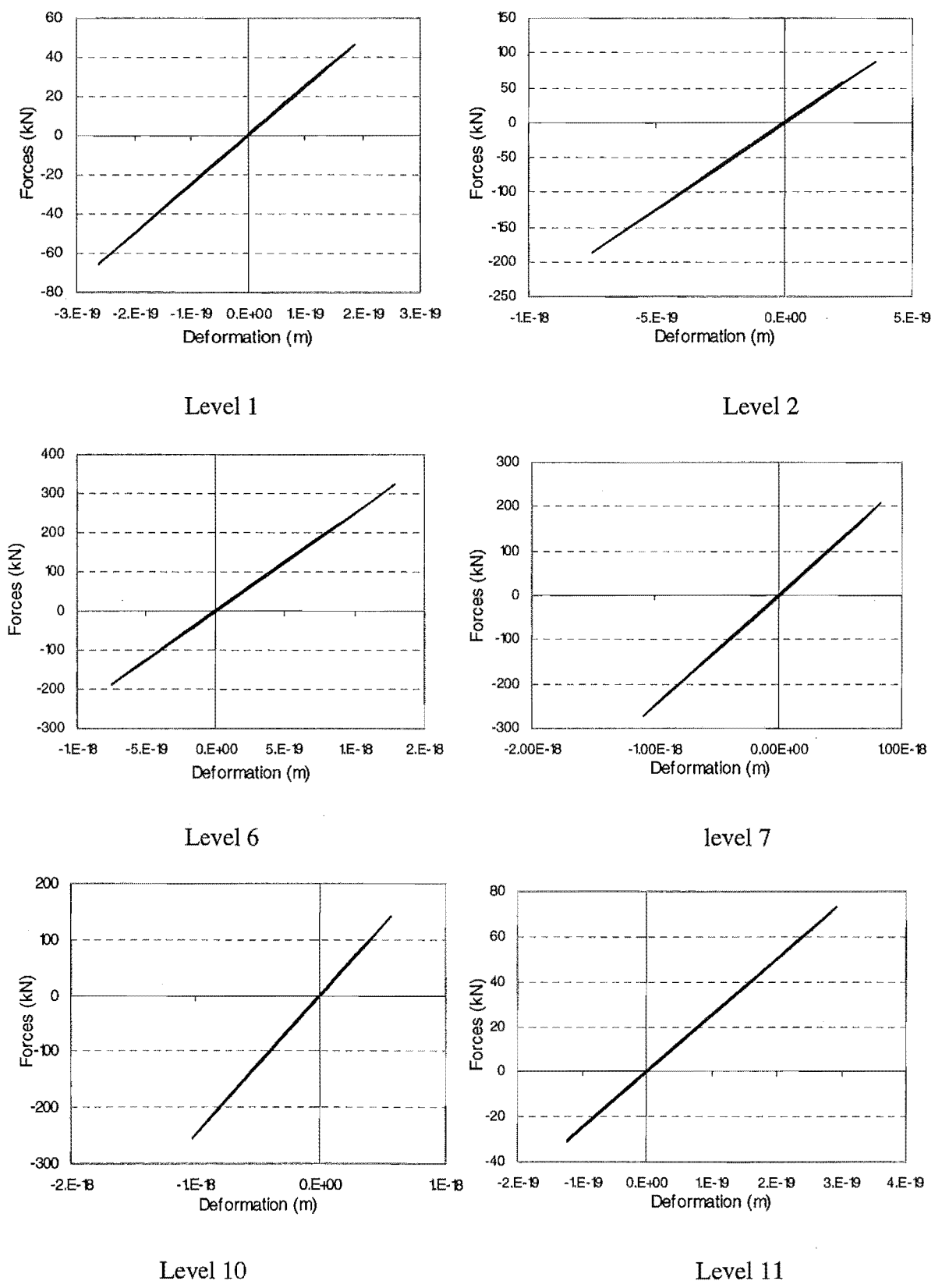


Fig (8-14) Force-Deformation relationships in the horizontal links at different floor levels of the structure.

### 8.5.3 Equivalent Straight Tendon

The time-history analyses are repeated with an equivalent straight tendon with 300% El Centro earthquake excitation to investigate the effect of changing the shape of the tendon on the response of the structure and the hysteresis loop of the ring spring dampers. In Figure (8-15), the peak displacement of the top floor level is equal to 0.42 m which is larger than the peak displacement of 0.3 m with the draped tendon. Figure (8-16) shows a comparison between the roof displacement of the structure with draped and equivalent straight tendons. It can be seen that with a draped tendon the response of the structure under earthquake excitation is smaller than the response with equivalent draped tendon. As shown in Figure (8-17) the force in the damper is equal to 1000 kN with elongation 0.16 m. It means a big size of the damper with large displacement may be needed. Hence, the draped tendon gives a smaller response of the structure and smaller size of the damper which is an advantage over an equivalent straight tendon.

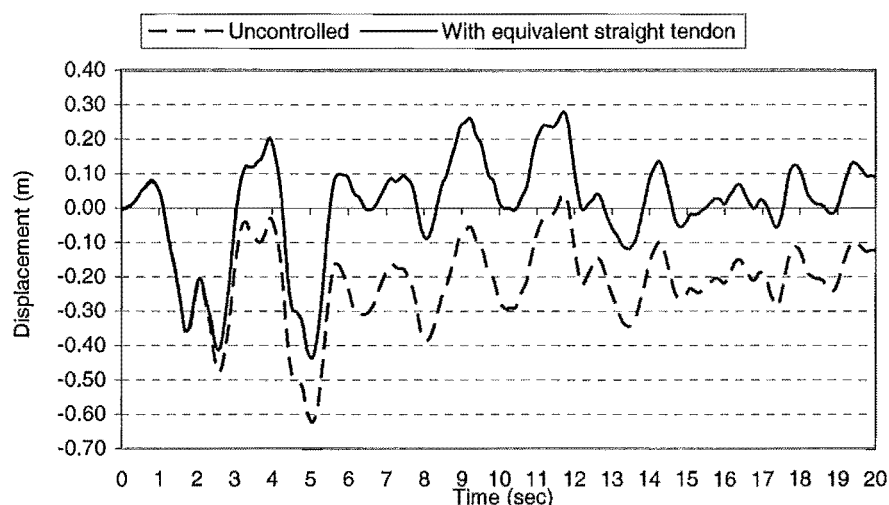


Fig (8-15) Roof displacement with and without the supplemental control system-equivalent straight tendon- 300% El Centro excitation.

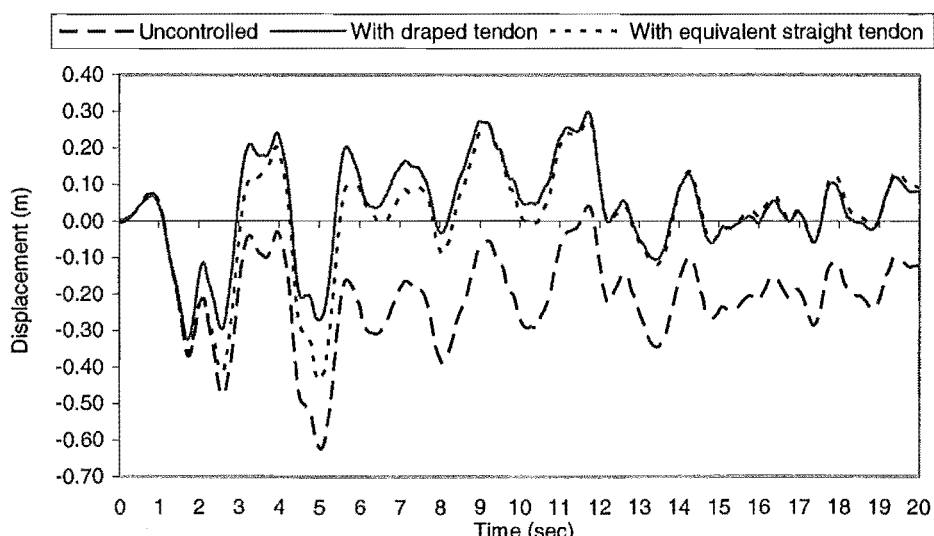


Fig (8-16) Roof displacement with draped and equivalent straight tendon – 300% El Centro excitation.

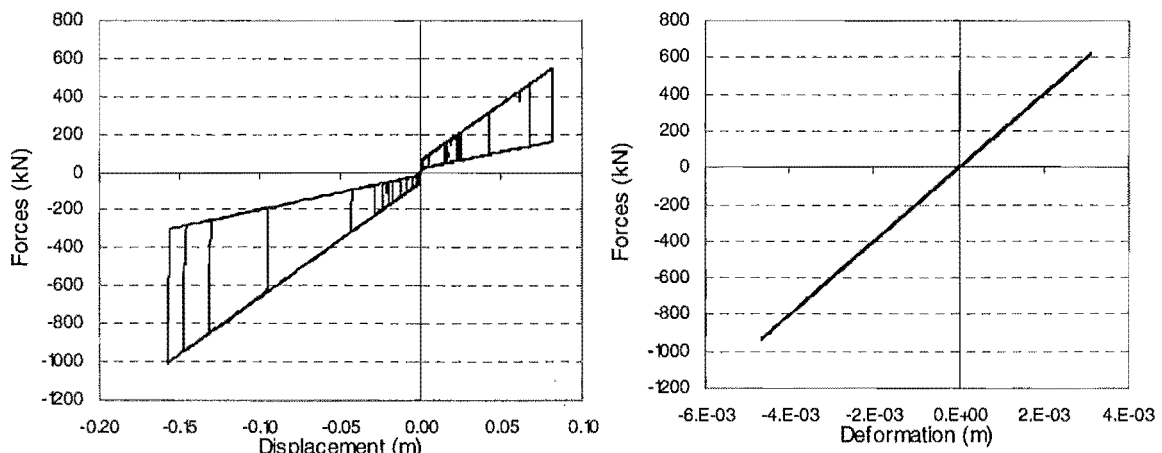


Fig (8-17)

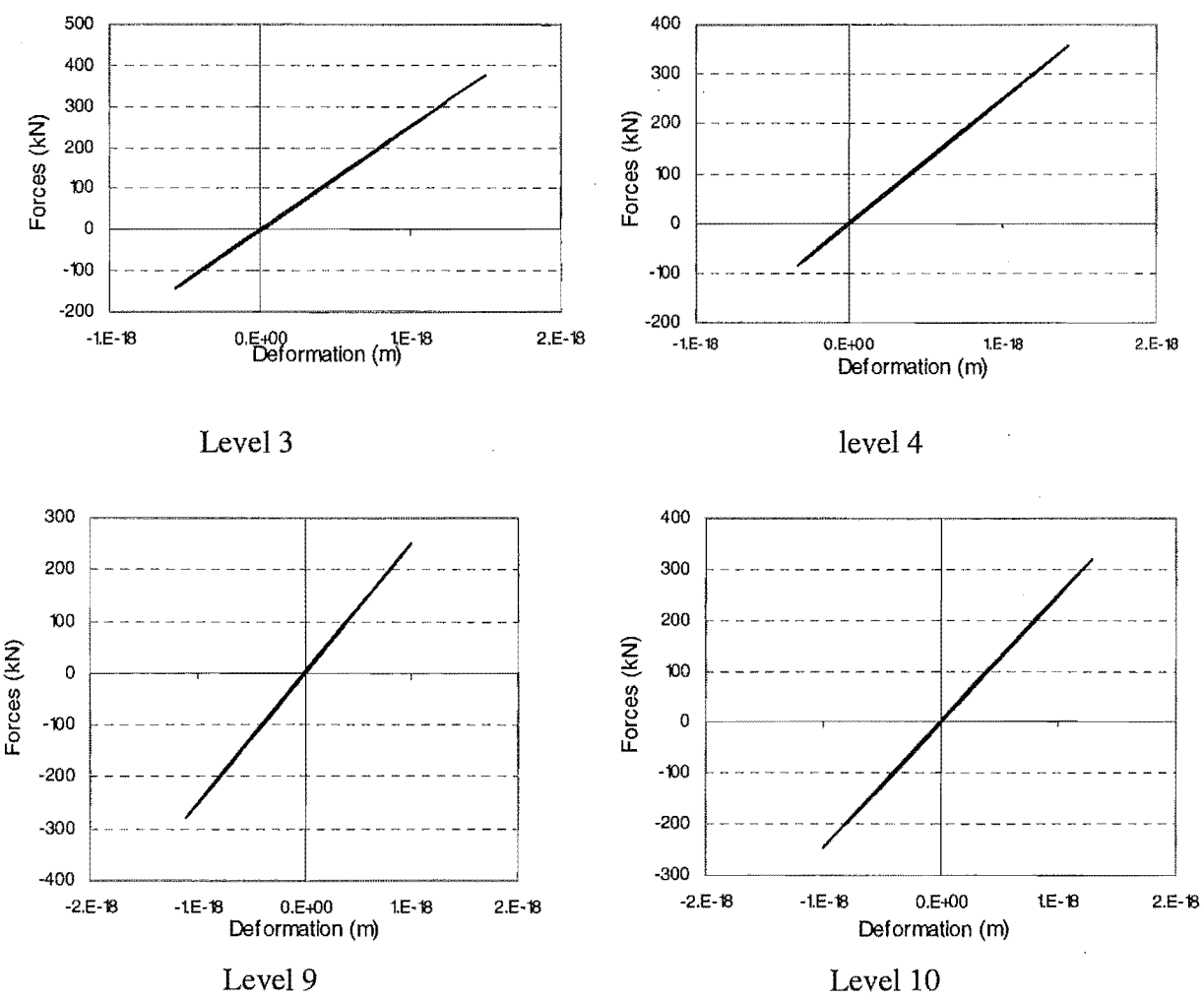


Fig (8-18) Force-Deformation relationship in the horizontal links in different floor levels of the structure.

### 8.5.4 Straight Tendon to the Top of the Structure

In this case, a straight tendon to the top of the structure as shown in Figure (8-10c) is used. The time-history analyses are repeated with 300% El Centro earthquake excitation. Figure (8-19) shows the roof displacement of the structure with and without the supplemental damping system. Using the straight tendon gives the same target displacement of the roof level equal to 0.3m which is similar to the peak displacement with draped tendon. Figure (8-20) provides a comparison between structural response with draped, equivalent and straight tendon to the top of the structure. It can be seen that the response of the structure with the draped and the straight tendon to the top are very close. The force in the damper is equal to 620 kN with deformation equal to 0.1 m (Figure 8-21). The force-deformation relationships in the horizontal links at different levels of the structure are shown in Figure (8-22).

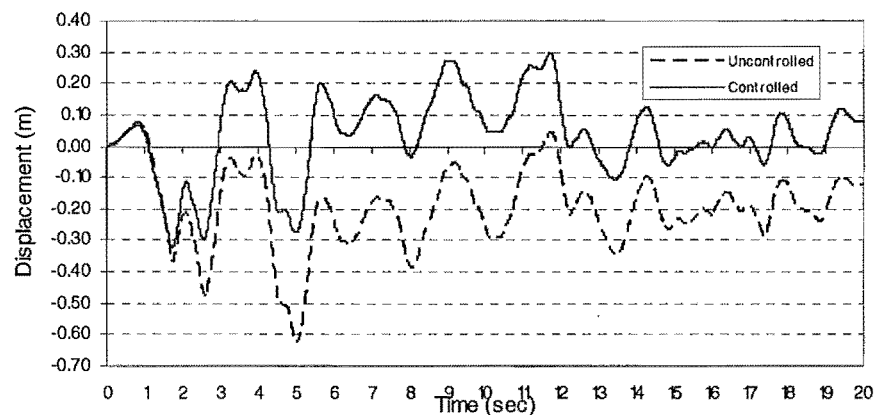


Fig (8-19) Roof displacement of the structure with the straight tendon to the top- 300% El Centro excitation

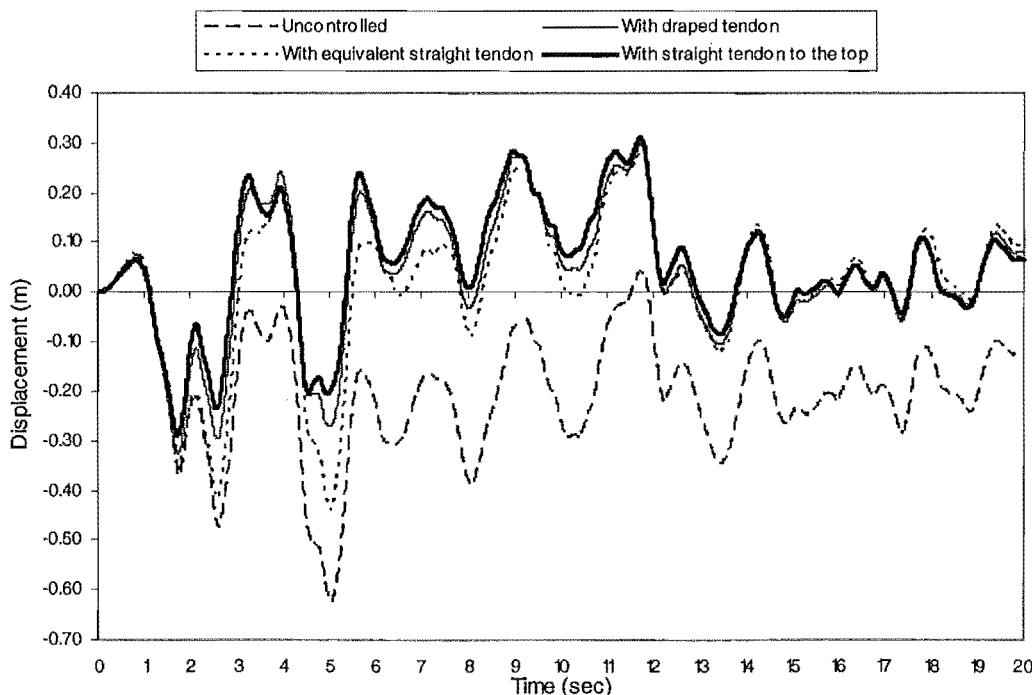


Fig (8-20) Roof displacement with draped tendon, equivalent straight tendon and straight tendon to the top- 300% El Centro excitation.

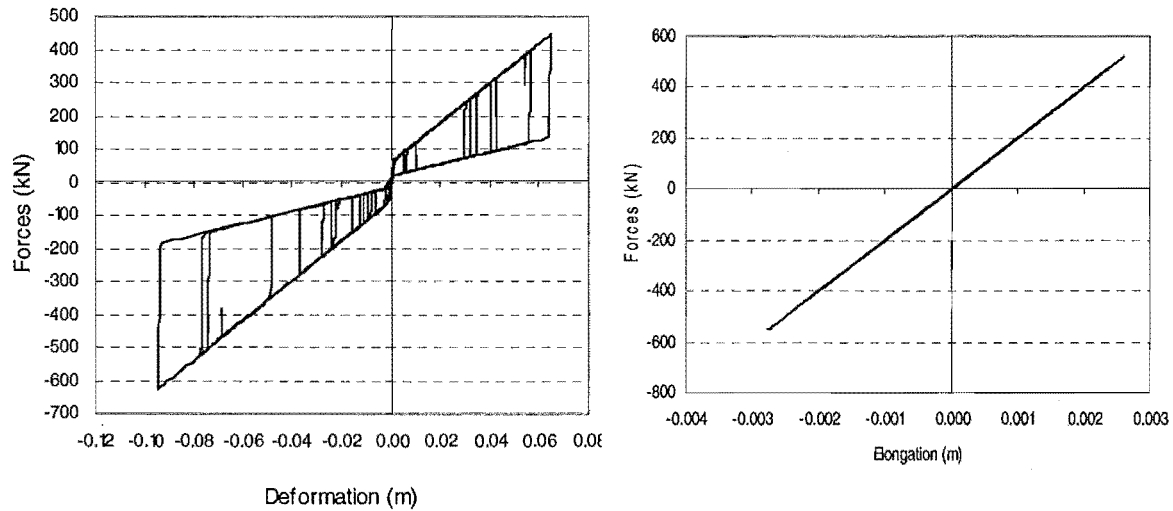


Fig (8-21)

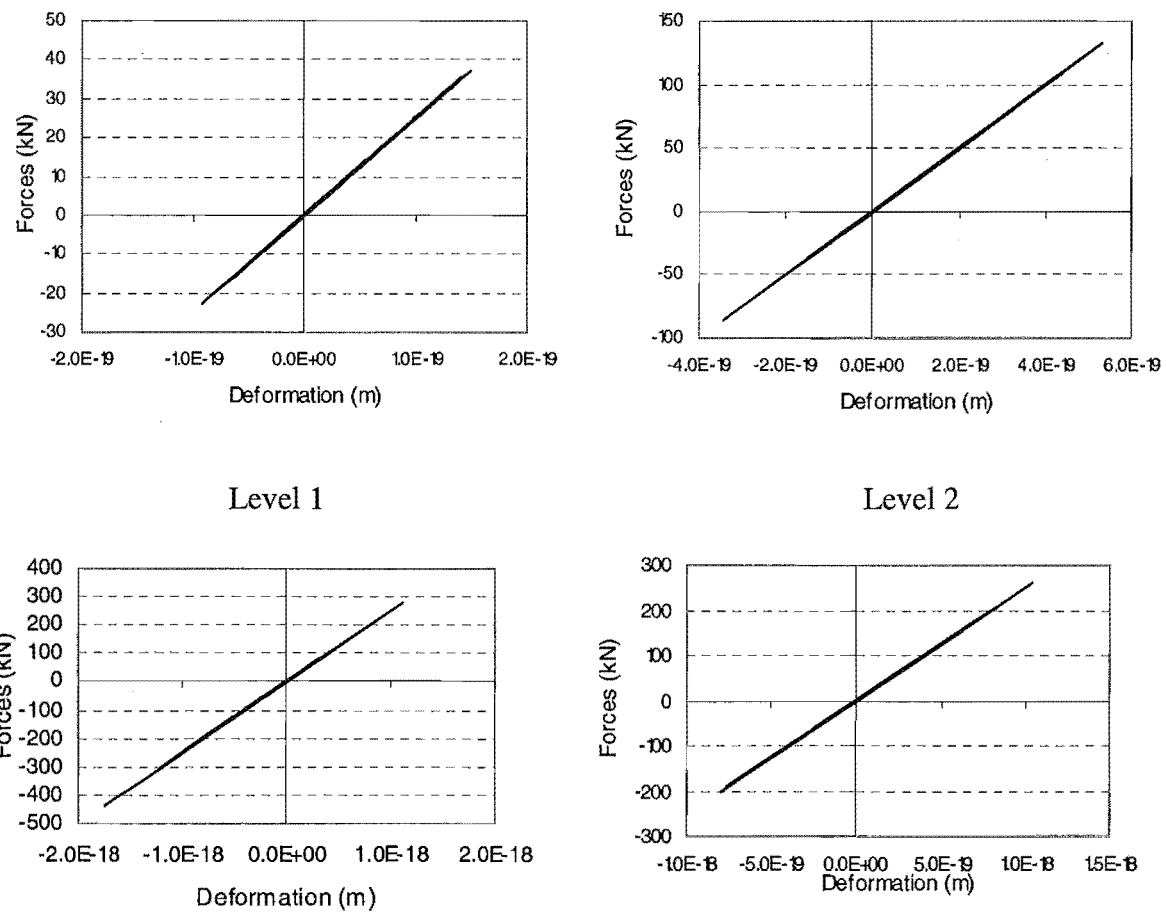


Fig (8-22) Force-Deformation relationship in the horizontal link at level 6,7,10 and 11.

## 8.6 Double Tendons

In this case, as shown in Figure (8-23), two tendons are used one on each side of the structure. Horizontal links are connected to each tendon and supported to the floor of the structure. A ring-spring damper is placed at the bottom of the tendon in each side.

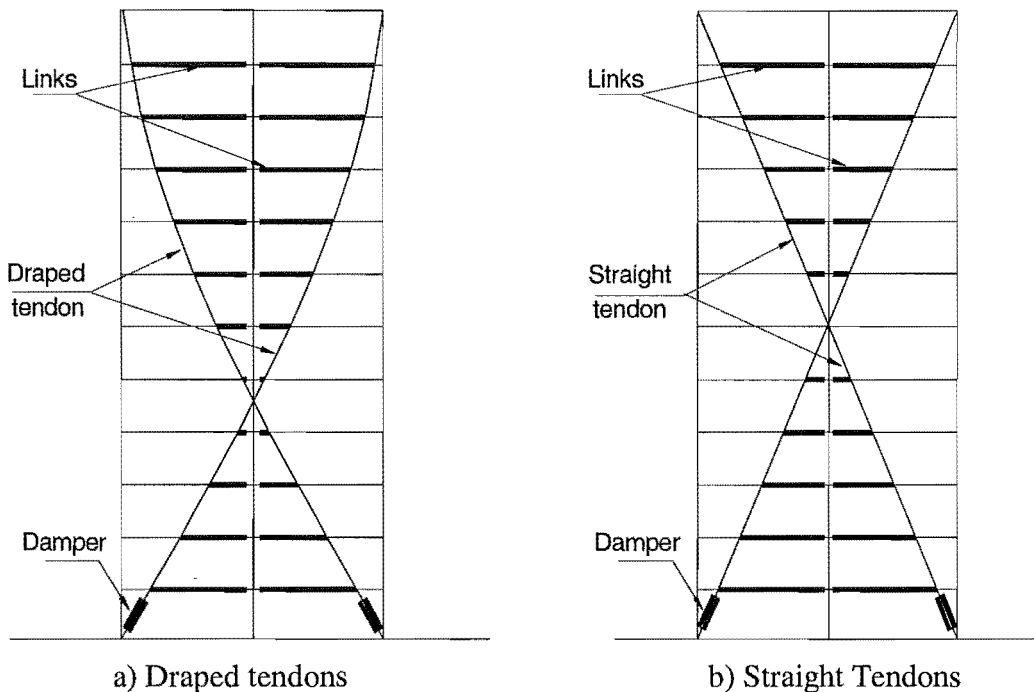
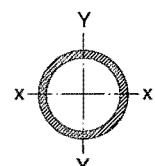


Fig (8-23) Double Tendon Profiles

Half of the tendon stiffness of one tendon in previous cases ( $2.1E5$  kN/m) is used for each tendon with  $k_x$  is equal to  $1.11E5$  kNm. Table (8-3) shows the dimensions and properties of the tendon.

Table (8-3) Dimensions and Properties - Tube Sections



Outside Diameter mm	Thickness mm	Mass Kg/m	Area of Section $\times(10^2)mm^2$	Moment of Inertia $\times(10^4)mm^4$	Elastic Section Modulus $\times(10^3)mm^3$
101.6	8.0	18.50	23.52	260.0	51.08

$$k_x = \frac{EA}{L} = \frac{200,000(2352)}{4210} = 1.11E5 \text{ kN/m}$$

where  $k_x$  is the stiffness of one tendon

$E$  is the modulus of elasticity

$A$  is the cross section area

and  $L$  is the supported length of the tendon (see Figure 8-12)

### 8.6.1 Double Draped Tendons

The roof displacement of the structure with the double draped tendon and two ring spring dampers is shown in Figure (8-24). The peak value is about 0.28m which is slightly less than peak values with one tendon and damper in one side of the structure.

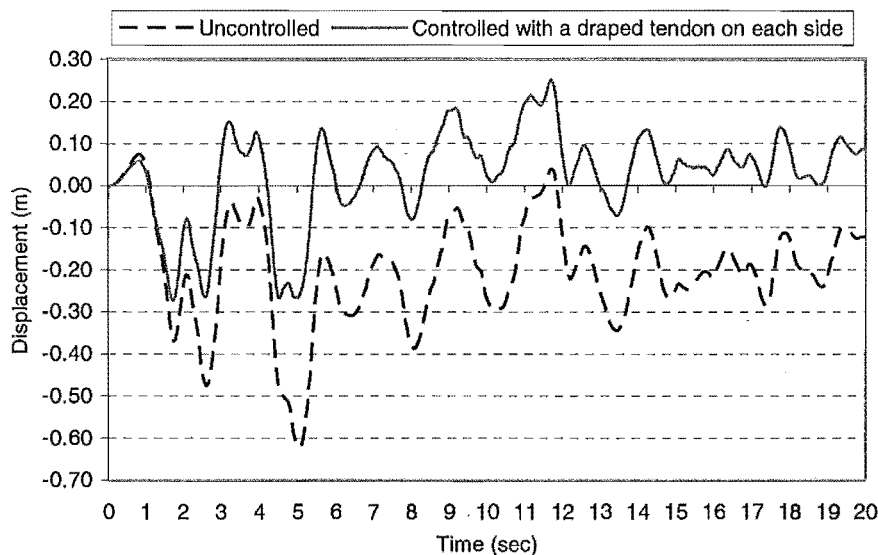


Fig (8-24) Roof displacement of the structure with double draped tendons-300% El Centro excitation.

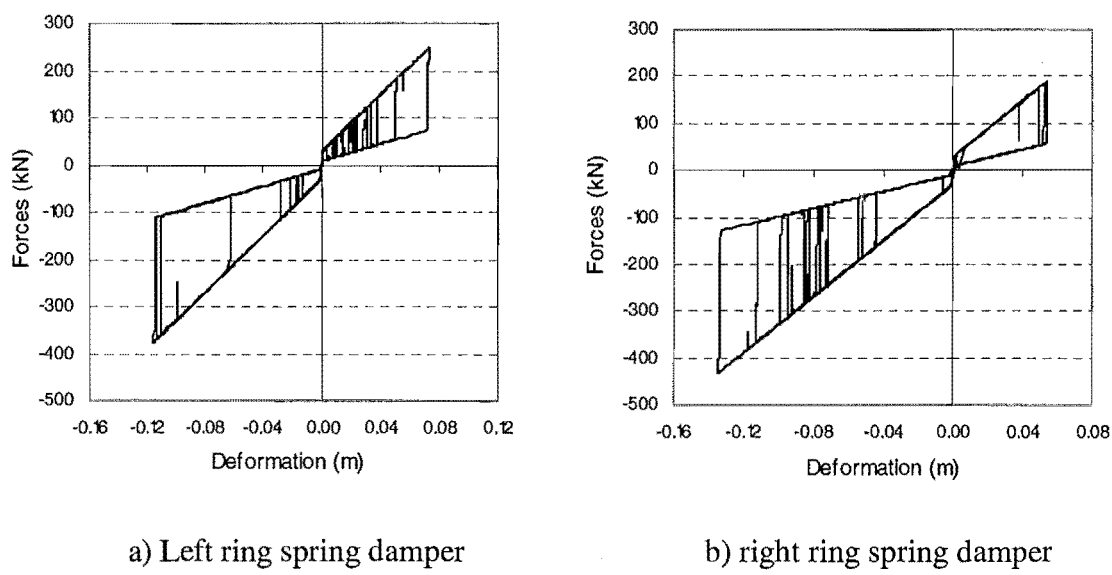


Fig (8-25) Hysteresis loops for the left and the right ring spring dampers with double draped tendon – 300% El Centro excitation

From Figure (8-25) the force in the left damper is equal to 390 kN and equal to 420 kN in the right damper. The deformations are equal to 0.12 m and 0.135 for left and right damper respectively. From Table (4-1) a ring spring damper with capacity equal

to 510 kN can be used. The spring travel of one element  $S_e = 3.9$  mm and the element height  $h_e = 22.4$  mm.

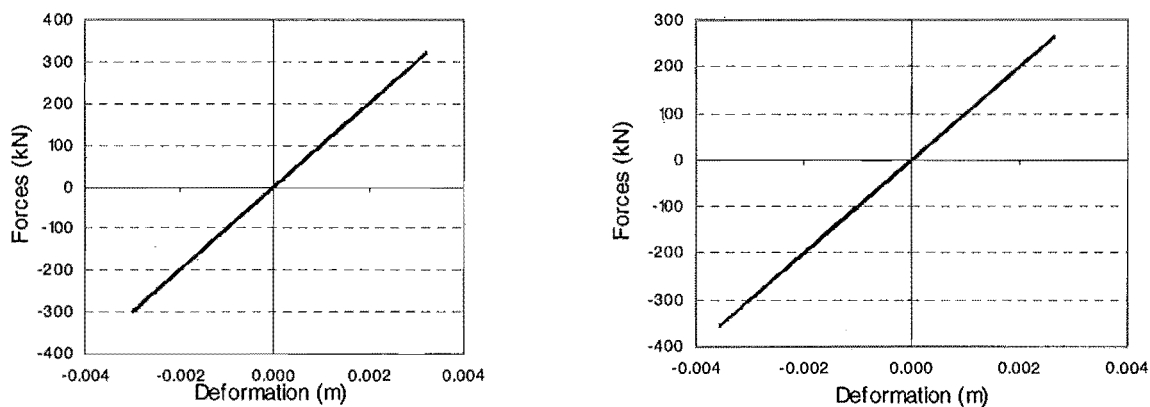
Part of the Table (4-1) Ring spring design data [33].

Diagram		Dimensions					Guide		Weight
F (kN)	$s_e$ (mm)	$W_e$ (j)	$h_e$ (mm)	$D_1$ (mm)	$d_1$ (mm)	$b/2$ (mm)	$D_2$ (mm)	$d_2$ (mm)	$G_e$ (kg)
350	3.7	648.0	20.0	166.0	134.0	16.0	170.0	130.0	0.822
510	3.9	995.0	22.4	198.0	162.0	18.5	203.0	157.0	1.515

$$\text{The number of ring spring elements required } n = \frac{\delta_{\text{damper}}}{S_e} = \frac{135}{3.9} = 35 \text{ elements}$$

The total length of the elements =  $n.h_e = 35 (0.0224) = 0.78$  m

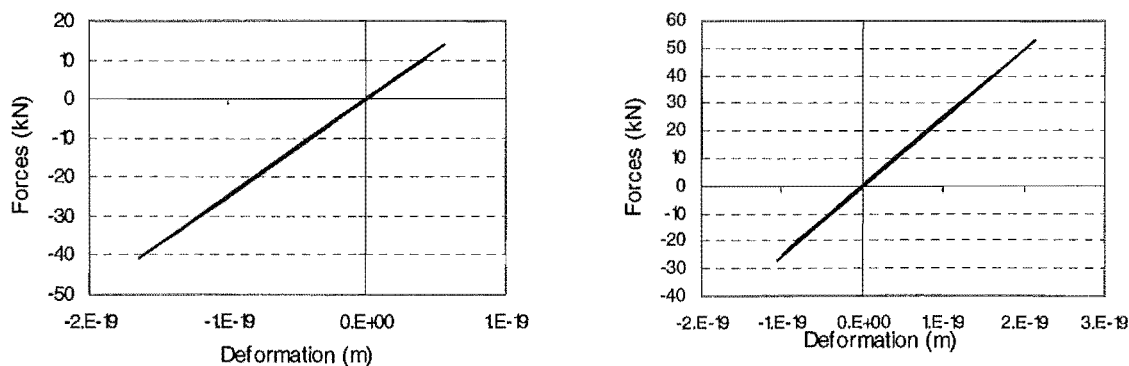
The total length of the damper with the elements, cartridge and piston is about 1.5 m



a) left tendon

b) Right tendon

Fig (8-26) Force- Deformation relationship in the left and right tendon



Left link at level 1

Right link level 1

Fig (8-27) Force-Deformation relationship in the links at level 1

Using double draped tendon gives a smaller peak roof displacement for the structure but at the same time using a single tendon in one side with one damper leads to saving in both cost and ease of construction. The numbers of elements (tendon, damper and horizontal links) required for the supplemental system using one tendon and damper is half the number of the elements and connections when using double tendon.

### 8.6.2 Double Straight Tendons

The analyses of the structure are repeated using the double straight tendon shown in Figure (8-23b) which may be simpler to construct throughout the structure. Figure (8-28) shows a comparison between the roof displacement using double draped and double straight tendons. No significant difference in the roof response between the two cases can be observed.

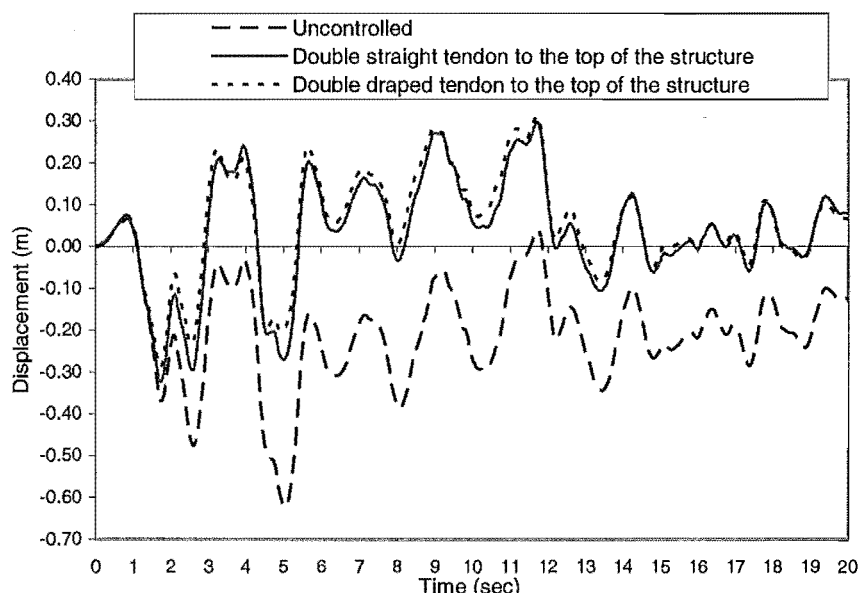
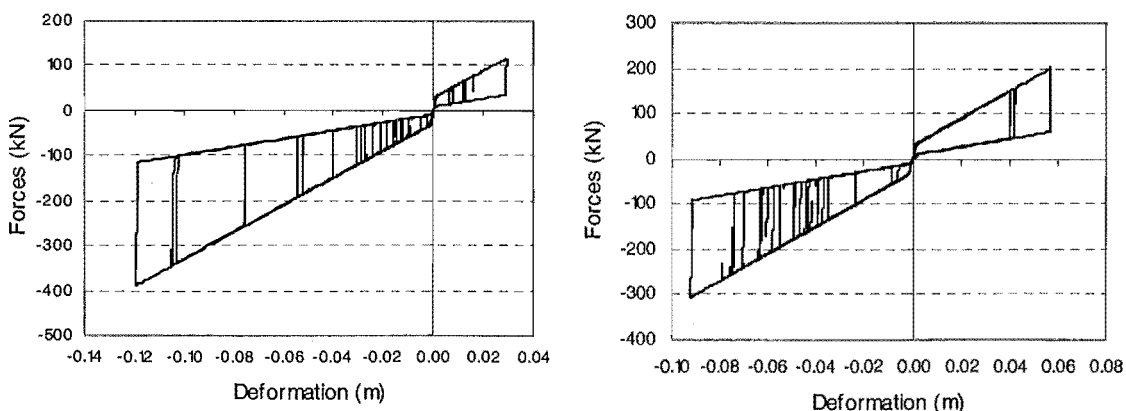


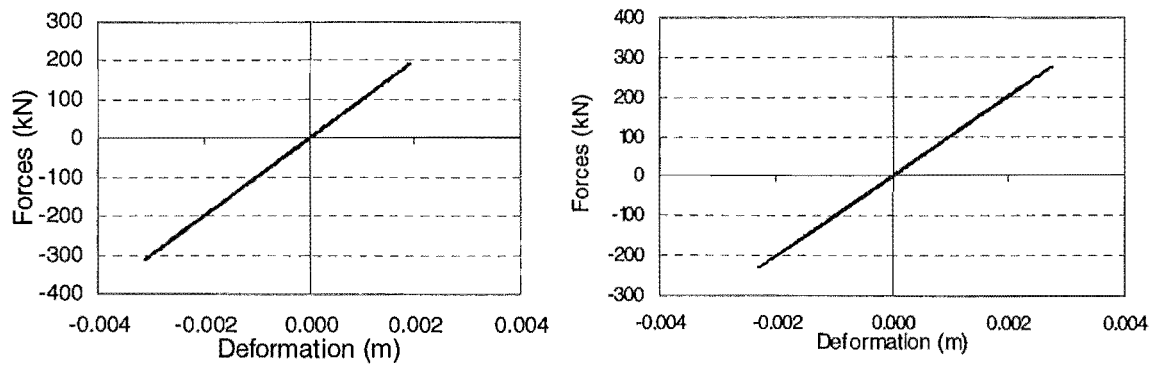
Figure (8-28) Roof displacement with double draped and double straight tendons-300% El Centro excitation.



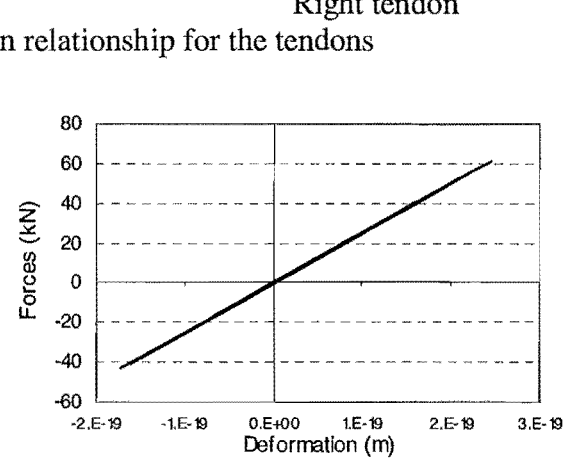
a) Left damper

b) Right damper

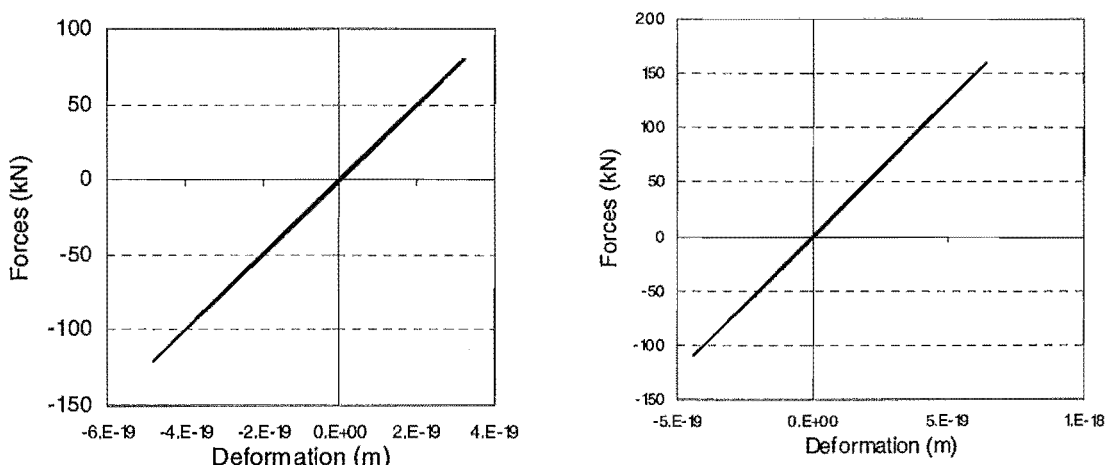
Fig (8-29) Hysteresis loops for the ring spring dampers



Left tendon  
Fig (8-30) Force-Deformation relationship for the tendons



Left link  
Fig (8-31a) Force-Deformation relationship in the links at level 1



Left link  
Fig (8-31b) Force-Deformation relationship in the links at level 11

By comparing the response of the structure with the double draped tendons and the double straight tendons as shown in Figure (8-28), it can be seen that the roof displacement is very similar in the two cases which means using the double straight tendons in the control system gives good results and is very similar to the case when the single draped tendon is used.

The force in the dampers varies between 300 kN and 400kN for the right and the left damper respectively as shown in Figure (8-29). The deformation in the left is equal to 0.12 m with 420 kN which is very close to the force and the deformation in the draped tendon case. It means that the same properties and dimensions for the ring spring dampers used with the double draped tendons can be used with the double straight tendons and which give same response of the structure under the earthquake excitation.

## 8.7 Discussion

In sections 8.5 and 8.6, two systems of structural control have been investigated. In the first system, three different shapes of a single draped tendon, an equivalent straight tendon, and a straight tendon to the top of the structure are used as shown in Figure (8-10). In a second system, a double draped tendon and a straight tendon to the top of the structure with a damper in each side of the frame structure are used as shown in Figure (8-23). In the first system, the draped and the straight tendon to the top of the structure give a very similar roof displacements and hysteresis loop shapes for the ring spring dampers. The forces in the dampers and the elongation in the elements of the dampers are very close in both cases of the draped and straight tendon to the top of the structure. The forces in the horizontal links vary from the bottom to the top of the structure due to the damping forces being transferred from the damper through the tendon and to the horizontal links at the floor levels of the structure. The elongations in the horizontal links are very small due to the stiffness of the link members which is essential to transfer the damping forces to the floor levels. An equivalent straight tendon to level ten of the structure gives a larger peak displacement of the roof level compared with the draped and the straight tendon profile to the roof which is a disadvantage of this tendon profile.

The alternative solution is to use two tendons, one on each side of the frame structure. In this case, draped and straight tendons to the top of the structure are used as shown in Figure (8-23). The stiffness and the cross section of the tendon are half of the stiffness and the cross section in the first system. The force in each damper is about half of the force in the damper with one tendon. The same roof displacement with draped and straight tendons in both systems is reached with about 50% decrease in the roof displacement from the case without using the supplemental damping system.

Using one straight tendon to the top of the structure on one side of the frame structure may be the appropriate shape of the tendon which gives the target displacement of the roof level of the structure and leads to savings in both cost and ease of construction. The numbers of elements (tendon, damper and horizontal links) required for the supplemental system using with one tendon and damper is half of the elements and connections when using double tendon.

## 8.8 Tendon Flexibility

To investigate the effect of the tendon flexibility with the damping control system on the seismic response of the structure, analyses were carried out on the twelve storey frame structure with a bigger value of the tendon cross section area. The cross section of the tendon used in the previous analyses ( $2.1E5$  kN/m) with a single straight tendon and the tendon increased to ten times ( $2.1E6$  kN/m) and the analyses are repeated to compare the structural displacement and acceleration in the both cases.

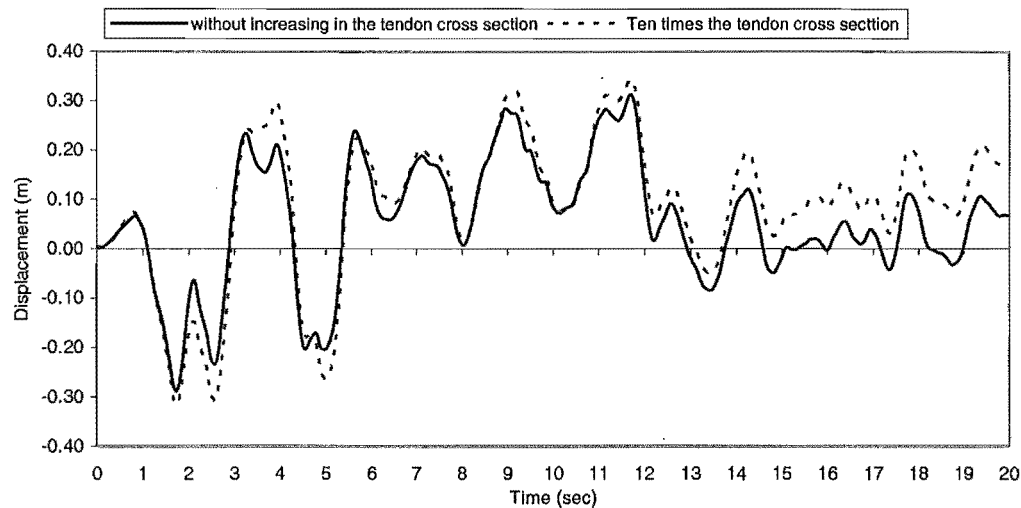


Fig (8-32a) Roof displacement of the structure

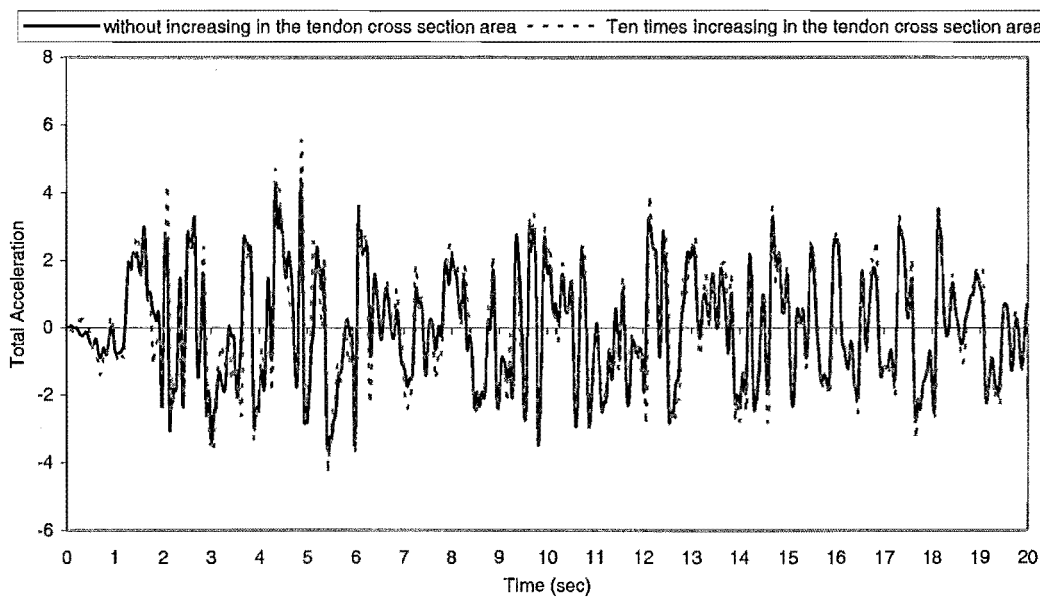


Fig (8-32b) Roof acceleration of the structure with ten times values of the tendon cross sections area – El Centro excitation.

Figure (8-32a) shows that the displacement of the structure was slightly reduced due increasing the tendon cross section but the acceleration increased at 2 seconds and between 4 and 6 seconds as shown in Figure (8-32b). The peak value of the

acceleration increased from  $4 \text{ m/sec}^2$  to  $5.5 \text{ m/sec}^2$  (27%) by increasing the tendon cross section area. This means that using a larger cross section area for the tendon which will provide more damping due to the increase of the stiffness of the system but at the expense of increased acceleration response.

Stiffness as well as deformations may increase or decrease in the structure, depending on the effect of the devices and the cross sections of the tendon elements. The important fact is that lateral resisting forces increase cumulatively going from the top level to the lower levels and finally to the foundations. Therefore, it implies that the supplemental damping system that resists and transfers the lateral seismic forces to the ground level should have capacity in proportion to the storey shear. Using a larger cross section area for the tendon elements than necessary increases the stiffness of the damping system but it may cause high levels of accelerations of the floor structure which may cause damage to sensitive items of equipment that might be housed in the structure.

## 8.9 Viscous Fluid Dampers

A comparison between ring spring dampers and other types of dampers, for example, viscous fluid or lead dampers should be made to help a designer to choose the most suitable type of damper which can be used in the structural control design. In the next sections the comparison between the response of the structure with ring springs, viscous fluid and lead dampers is discussed.

In section 2.4.4, a viscous fluid damper was described and as shown the damper is a device containing compressible silicon oil which is forced to flow via the action of a stainless steel piston rod with a bronze head. The head includes a state-of-the-art fluidic control orifice design with a passive bimetallic thermostat to compensate for temperature changes. In addition, an accumulator is provided to compensate for the change in volume due to rod positioning (see Figure 2-12). The main characteristic of the damper is that it has a “viscous” behaviour where the force is proportional to the velocity.

### 8.9.1 Operation of Viscous Dampers

The force in a damper is a result of flow through orifices leading to a pressure differential across the piston head. Most practical devices are built using differently shaped orifices in which the pressure differential is dependant on a fractional power of the velocity [54]:

$$F = C_D |\dot{u}|^\alpha \operatorname{sgn} \dot{u} \quad 8-19$$

For dampers with cylindrical orifices the force is [54]:

$$F = b\Delta p = \frac{b\rho}{2n^2 C_0^2} \left( \frac{A_p}{A_0} \right)^2 \dot{u}^2 \sin \dot{u} \quad 8-20$$

where  $b$  = constant.

$\Delta p$  = the pressure differential which depends on the area of the piston.

$A_p$  = area of piston.

$A_0$  = area of orifices.

$n$  = number of orifices.

$\rho$  = density of fluid.

$C_0$  = the discharge constant.

$\dot{u}$  = velocity

Where  $\sin \dot{u}$  indicates the sign of velocity  $\dot{u}$  and  $\alpha$  is a power between 0.5 to 2.0. A lower power is used for high velocity. For seismic protection applications, linear dampers with  $\alpha = 1$  would be more appropriate [54].

### 8.9.2 Size of Fluid Dampers

The size of fluid dampers depends on the stroke and maximum capacity of the damper. Two groups of dampers of low and high capacity can be classified as follows [54]:

#### 8.9.2.1 Low Capacity Viscous Fluid Dampers (10 Kip to 30 Kip output)

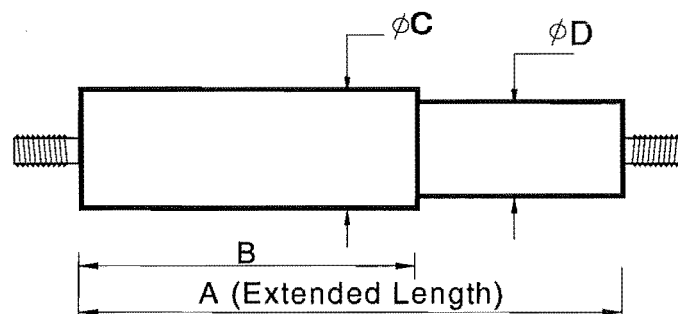


Fig (8-33) Low capacity viscous fluid damper

Table (8-4) Dimensions of low capacity viscous fluid dampers

Capacity		A		B		C		D	
Kip	kN	inch	mm	inch	mm	inch	mm	inch	mm
10	44.6	17.5	444	11.9	302	3.0	76	2.5	63
20	89.2	20.5	521	12.7	323	4.0	102	3.4	86
30	133.8	22.5	571	14.1	358	5.0	127	4.4	112

### 8.9.2.2 High Capacity Viscous Fluid Dampers (100 Kip to 2000 Kip output)

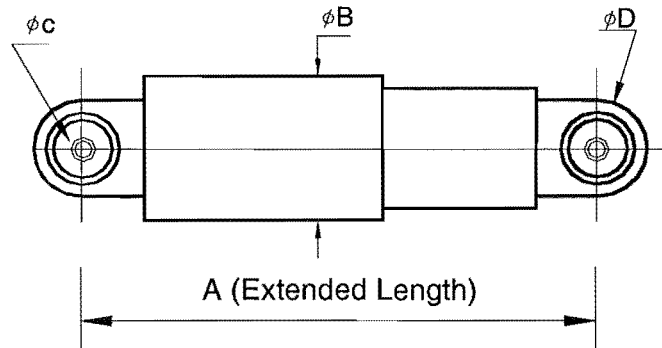


Fig (8-34) High capacity viscous fluid damper

Table (8-5) Dimensions of high capacity viscous fluid dampers

Capacity		A		B		C		D	
Kip	kN	inch	mm	inch	mm	inch	mm	inch	mm
100	446	131	3327	7.5	190	2.5	63	3.2	81
200	892	132	3353	9	228	2.75	70	3.9	99
300	1338	138	3505	11.5	292	3	76	4.25	108
600	2676	155	3937	16	406	6	152	7.5	190
1000	4460	166	4216	23	584	6	152	9	229
2000	8920	180	4572	26	660	8	203	11	279

The feature of a pure viscous damper that the damping force is out-of-phase with the displacement which can be a particularly desirable attribute for passive damping applications for buildings [55]. Non-linear viscous behaviour can be achieved through specially shaped orifices to alter the flow characteristics with fluid velocity.

The values of damping coefficient, C, of viscous fluid dampers equals:

$$C = \text{Force} / \text{Velocity}$$

A structure with a high damping coefficient fluid damper provides a better performance for seismic resistance [56]. Time history analyses of the twelve storey building described previously with and without viscous fluid dampers was carried out to obtain the damping coefficient for the fluid damper which gives a similar response to that of the structure with ring spring dampers.

### 8.9.3 Structural Response with Viscous Fluid dampers (Dashpots)

Comparison between the effect of using ring spring dampers and viscous fluid dampers (dashpots) on the response of structures can be made as shown in Figure (8-35).

The size of the dashpots which are required to get the same response for the roof displacement of the structure using the ring spring dampers can be determined by changing the damping coefficient of the dashpots ( $C$ ) until the roof displacement of the structure with ring spring dampers and dashpots are similar. The forces in the dashpots can be found from the force-velocity relationships of the dashpots. From Tables (8-4 and 8-5), the size of the viscous fluid dampers (dashpots) can be selected as is discussed in the next section.

A time-history analyses were carried out with dashpots dampers to get the same response of the structure as with ring spring dampers. The roof displacement of the structure with and without the dashpot dampers with El Centro is shown in Figure (8-35). It can be seen that the natural periods of the structural response have not changed with using dashpots dampers to control the seismic response of the structure which means that the viscous fluid dampers (dashpots) do not increase the stiffness of the structure.

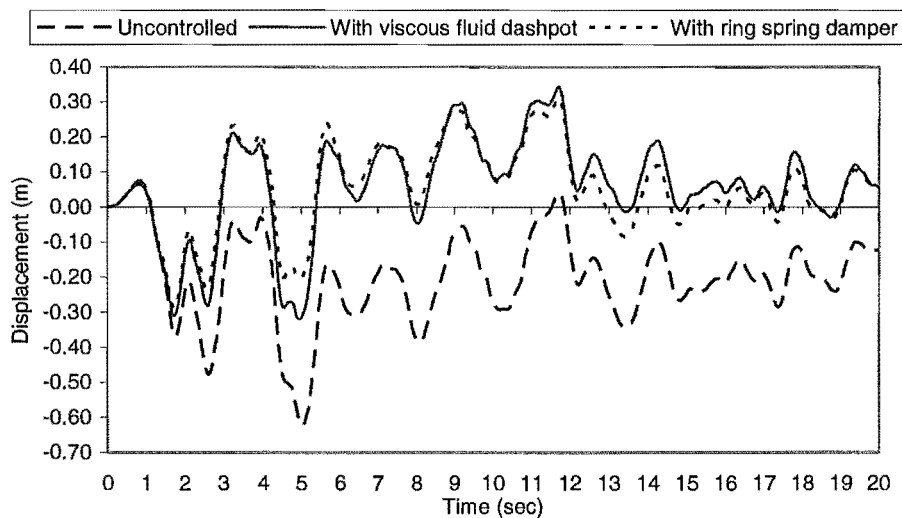


Fig (8-35) Roof displacement of the twelve-storey frame without and with dashpots attached to the straight tendon – 300%El Centro excitation.

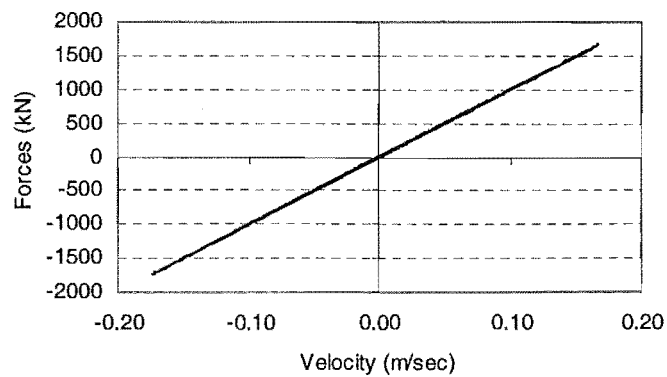


Fig (8-36a) Force-Velocity relationship of the dashpot.

From Figure (8-36a) the maximum force in the dashpot is equal to 1700 kN and the maximum velocity equal to 0.17 m/sec where  $C = 10,000 \text{ kN/m/sec}$ . From Table (8-6), a dashpot with capacity 600 kip can be used where:

$$\begin{aligned} \text{The capacity of the dashpot} &= 600 \text{ Kip} &= 2676 \text{ kN} \\ \text{The length of the dashpot} &= 155 \text{ inch} &= 3.93 \text{ m} \\ \text{The diameter} &= 16 \text{ inch} &= 0.4 \text{ m} \end{aligned}$$

A dashpot with length 3.93 m can be used to get the same response in the structure as for the case with ring spring dampers. It should be noted here that the length of the double acting ring spring dampers used to give the same response of the structure is about 1.2 m which means that the length of the ring spring damper is about 1/3 of the length of the viscous fluid damper which is considered one of the advantages of ring spring dampers when compared to viscous fluid dampers. This is considered one of the advantages of ring spring dampers when compared to viscous fluid dampers.

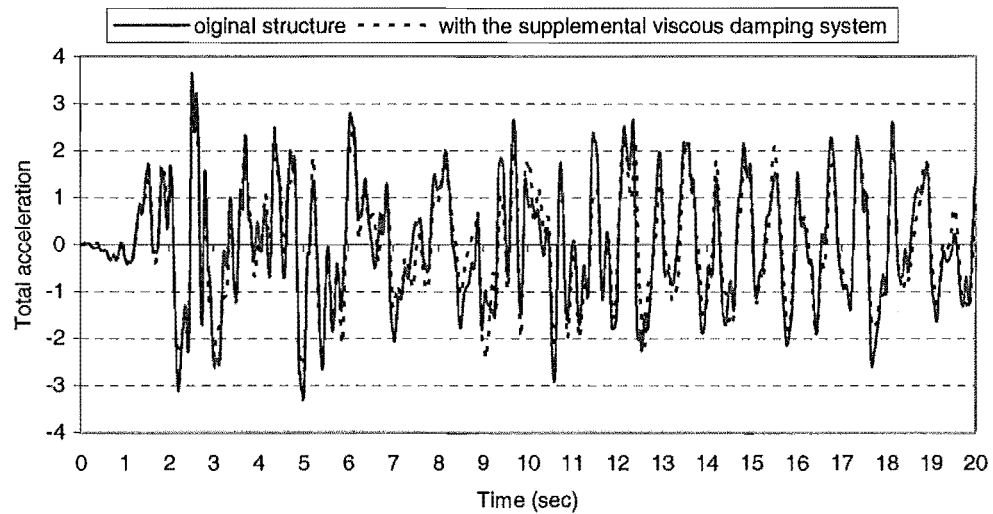


Fig (8-36b) Roof acceleration of the structure without and with the supplemental viscous damping system.

Figure (8-36b) compares the roof total accelerations of the structure with added viscous damping and the original structure without the supplemental damping. In the original structure the accelerations were reduced by the significant amount of plastic work, and hence damage in the structure. The occurrence of inelastic deformation will also lead to elongation of the periods of free-vibration further reducing the effective accelerations experienced in the building. If there were no supplemental damping or alternatively inelastic behaviour in the structure the roof acceleration would have been much larger. With the supplemental damping system the acceleration have been lowered without the implied damage to the structure caused by inelastic action. The actual accelerations are similar to those of the highly ductile original frame. If one accepts the principle of equal displacement, as accepted in many of seismic design standards the accelerations are those of the equivalent elastic structure divided by the structure ductility factor.

## 8.10 Lead Shear Dampers

A compact lead-shear damper such as the PENGUIN VIBRATION DAMPER (PVD) has been developed by PENGUIN ENGINEERING Ltd, New Zealand. This is a compact damping device which can be used to provide supplemental damping for structures. The damping of this device is achieved through the plastic deformation of a lead core. The use of lead enables the PVD to undergo many cycles of plastic work, dissipating large amounts of energy, while maintaining its mechanical properties. This is achieved through the dynamic recrystallization of lead [58].

Because the PVD uses the plastic deformation of lead to provide damping and lead will virtually not fail under cyclic loading, it is unlikely that the PVD will fail by fatigue within the design life of a structure. Many other types of energy dissipation have only a limited number of loading cycles before fatigue failure occurs [58].

### 8.10.1 Lead Damper Hysteresis

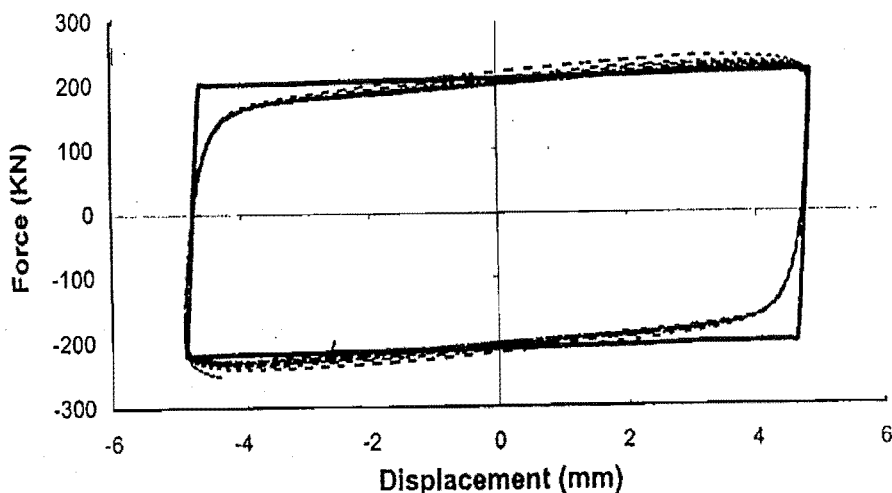


Fig (8-37) Elasto-Plastic hysteresis model for the 200 kN lead shear damper [21].

The maximum capacity of one type of the lead-shear damper developed by Penguin Engineering is 200kN. The hysteresis model which represents the force-displacement relationship of the lead dampers is the Elasto-Plastic model as shown in Figure (8-37). This model of the lead damper is used in the analytical non-linear time history analysis to compare the results obtained from using dashpots, lead dampers and ring spring dampers. The first step is to determine the force-displacement relationship using a yield force,  $F_y = 211$  kN [21], in the analysis and compare the results with the response of the structure with dashpots and ring spring dampers. As the values of the damper stiffness were not available, the stiffness used was taken to be the same that of the ring spring dampers. The second step is to determine what size of lead shear damper is required to give a similar response to that obtained using the ring spring dampers.

### 8.10.2 Time History Analysis with the Lead-Shear Dampers

To determine the capacity of the lead shear damper which gives a controlled response of the structure close to the response of the structure with ring spring damper, the analyses repeated with different capacities of the lead shear damper starting with 200kN capacity and iterating until a value of 435 kN capacity as shown in Figure (8-38) was reached.

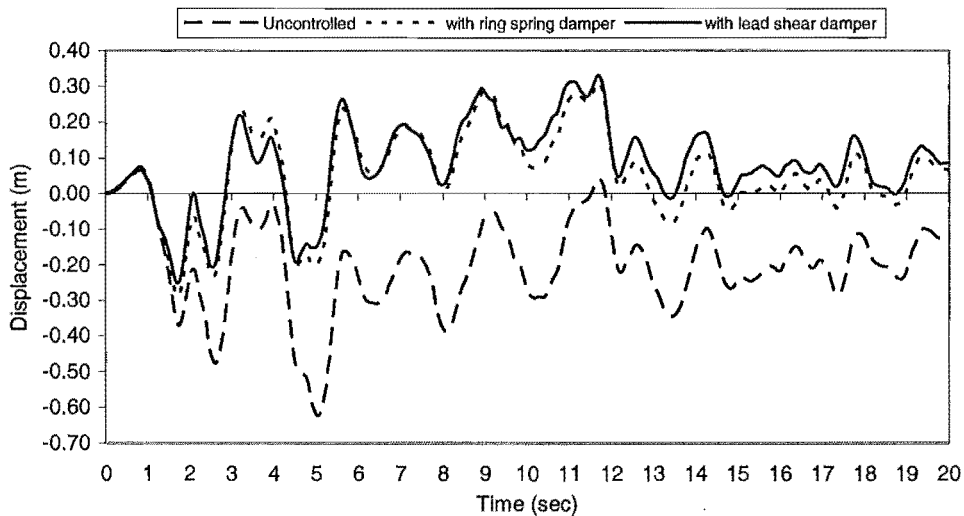


Fig (8-38) Roof displacement of the structure with ring spring dampers and lead dampers with capacity 435 kN- 300% El Centro excitation

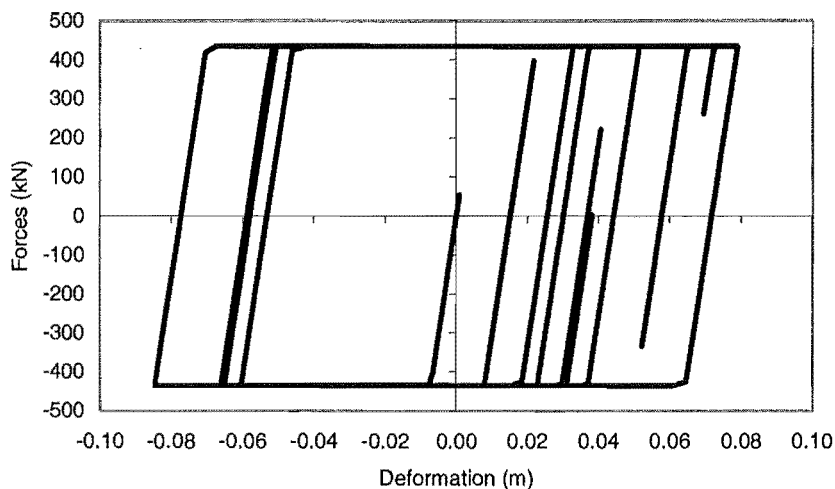


Fig (8-39) Hysteresis loop of the lead shear damper with capacity 435 kN

The shape of the hysteresis loop of the lead damper shown in Figure (8-39) with capacity 435 kN is very close to the theoretical shape shown in Figure (8-37). It must be noted here that the maximum force in the hysteresis loop with the lead shear damper (435 kN) is less than the maximum force in the hysteresis loop with the ring spring damper (730 kN) because the energy dissipated area in the loading and unloading cycles for lead shear damper are larger than the energy dissipated area in the loading and unloading cycles for ring spring damper.

### 8.11 General Comparison between Ring Spring, Viscous Fluid and Lead Shear Dampers

A general comparison between ring spring dampers, viscous fluid dampers and lead shear dampers is shown in Table (8-6). Ring spring dampers have some features and characteristics that make them very useful as seismic control devices. Ring spring dampers are constructed of steel materials in which no possible leakage of liquid and no refilling or maintenance of any of the parts is needed which are potential problem in the viscous fluid dampers. Ring spring dampers absorb large amount of the input energy with low weight and small size which is in contrast to viscous fluid dampers. However, viscous fluid dampers do not increase the stiffness of the structure and consequently the accelerations of the structure and its contents. Most of the characteristics and the properties of the ring-spring dampers and the lead shear dampers are similar as are indicated in Table (8-6).

Table (8-6) General comparison between ring spring dampers, viscous fluid dampers and lead shear dampers

Ring Spring Dampers	Viscous Fluid Dampers	Lead Shear Dampers
Displacement dependence	Velocity dependence	Displacement dependence
Hysteretic-displacement relationship	Linear force-velocity relationship	Hysteretic-displacement relationship
Totally passive (no dependence on outside energy sources)	Totally passive (no dependence on outside energy sources)	Totally passive (no dependence on outside energy sources)
Solid state	Contains liquid	Contains lead (solid state)
Can installed at any mounting angle	May be affected by mounting angle	Not effected by mounting angle
No liquid leakage and no refilling any of parts are needed	Liquid leakage possible and refilling parts may be needed	No liquid leakage but refilling parts may be needed
No maintenance required	Maintenance may be required	Maintenance may be required
Not effected by temperature	Affected by temperature	Affected by temperature
Increase stiffness of structure	Should not increase stiffness of structure	Increase stiffness of structure
Double and single acting devices	Double acting devices	Double acting devices
Small stroke absorber	Large stroke absorber	Small stroke absorber
Small length and diameter	Large length and diameter	No published tables of dimensions

## 8.12 Summary

Guidelines have been presented for determining the appropriateness of including a supplemental damping system in a structure. A straightforward preliminary design methodology was introduced. The overall capacity of the structure with the supplemental damping system can be determined by a series of analyses in two stages, a) elastic modal analysis and b) inelastic analysis. Based on the preliminary design, the desired amount of damping is chosen and the damper-tendon system is calculated. The design of the supplemental system is iteratively determined using the above described procedure. The second part of the design verification process is to conduct a series of inelastic history analyses for a variety of ground motions. An iterative solution technique was employed here.

Analyses were carried out to show the comparison between using two arrangements of tendons with three different types of damper. The draped or the straight tendon profile to the top of the structure on one side of the frame structure can be used to give the same controlled response of the roof level of the structure. An equivalent straight tendon (connected to the structure at level 10) gives less control in the roof displacement which may due to the tendon elements and the horizontal links not being connected to the top of the structure. The double tendon arrangement with a draped or a straight tendon give a structural response as that is close to the response in the first system but it may be more expensive and not easy to construct in a real building. The viscous fluid dampers attached to the tendon in the supplemental damping system can give similar control response of the structure as with the ring spring dampers but with the size of the dashpots being three times that of the ring spring damper size.

Finally, as mentioned before, supplementary ring spring dampers at the ground floor of structure transfers the control forces provided by the devices through the rest of the structure using straight tendons that significantly reduce and control the response of the structure when excited by earthquake ground motions. Ring-spring dampers are passive devices with no dependence on outside energy sources. With ring-spring dampers, no maintenance is required nor can leakage occur because they are constructed of steel. Ring-spring dampers have a small length and diameter when compared with other types of dampers such as viscous fluid dampers.

The main feature of the concept which is adopted in this research is using only one damper on one side or two dampers, one on each side of the structure, to produce the control forces needed, and transfer them to the rest of the building by using the tendon. With the Damper-Tendon system, it is not necessary to distribute dampers throughout the height of the structure.

## Chapter 9

### Conclusions and Recommendations

#### **9.1 Summary**

Structural control using a supplemental damping system provides a cost-effective way of controlling structural deformation and damage under earthquake excitations. Such a system can be easily incorporated into a structure, either during its initial design or as a retrofit strategy. The supplemental system can be readily replaced, if necessary, after a major earthquake without interfering with the primary structural system. The displacements and deformations of the structure can be greatly reduced without the need for increasing the stiffness (member sizes) of the primary structure. This type of structural control is suitable for retrofitting a non-ductile structure and also provides a good alternative solution for designing new building structures to resist earthquake excitations.

Several types of active, semi-active and passive structural control systems are outlined in the thesis and the way in which they work is described to show the advantages and disadvantages of each system. An active control system is one in which an external power source controls actuators that apply forces to the structure in a prescribed manner. The disadvantage is that the required power supply may not be available during a major earthquake due to damage to the electrical power supply system. Semi-active control systems are a class of active control systems for which the external energy requirements are orders of magnitude smaller than typical active control systems as the power is used only to control the behaviour of the passive devices. Passive control systems prevail in engineering practice due to their simplicity, reliability and the low cost of installing and maintaining them. Passive structural control is, in general, grouped into two approaches: seismic base isolation and supplemental damping. Seismic isolation is achieved by isolating the structure from the ground excitation earthquake by moving the period of the structure away from the predominant period of the ground motion and by increasing the equivalent damping level of the structure by hysteretic behaviour of the isolation devices. Providing additional damping constitutes the basic concept of the supplemental damping method, which involves controlling structural response by increasing the system damping. The mechanical dissipaters employed in supplemental damping schemes, can be simple, inexpensive, and exhibit reliable and repeatable characteristics. Adding damping in structures is the approach considered in this research.

This research has focused on added damping in structures by using a passive control system. One type of a passive control damper is called a ring spring damper and the behaviour of these devices has been investigated and examined. Ring spring dampers do not depend on external power sources to effect the control action. They are constructed of only steel materials in which no liquid leakage is possible and no refilling or other maintenance is needed. Several tests covering the complete loading-unloading cycle in the compression and tension region were carried out on the two ring spring dampers on a universal testing machine to determine the hysteretic

characteristics of these ring spring devices. Experimental testing of ring spring dampers showed their hysteresis characteristics depend on their stiffness. Details of the characteristics, the dynamic behaviour and the advantages in the behaviour of ring spring dampers have been shown. The details of the damper devices used in the experimental tests are presented.

A combined experimental and analytical study of an energy dissipation system for structures has been presented in this thesis. The control system consists of ring spring dampers installed at the ground floor of the structure acting via a tendon connected to the structure with horizontal links. The control forces are generated by the dampers and transferred by the supplemental system to the structure by the tendon and the horizontal links so as to oppose the inertia forces in the structure. The tendon layout is preferably designed to counteract the inertial forces in a way to reduce the overturning moments, giving a draped tendon profile as a result. However, a straight tendon profile may be used as a simplification of this lateral load balancing concept. A dynamic time history analysis program "Ruamoko" was used to analytically predict the responses and these were then compared with the experimental results for the prototype test structure.

The seismic response of a four storey, two bay steel frame structure with and without the supplemental damping system has been investigated. This frame was used to verify the usefulness of using the supplemental system in reducing the seismic response of the structure under earthquake loading. Dynamic tests of the structure were carried out on the shaking table. The tests could be categorized into free vibration and different levels of earthquake shaking tests. The free vibration tests were conducted to obtain the fundamental period and the critical damping ratio of the structure with and without the supplemental control system. The different levels of the shaking tests were carried out to obtain the effect of the supplement damping system in reducing the earthquake response of the structure. The results of these tests were then compared with those computed analytically. The effectiveness of the ring springs dampers was obvious in reducing the response of the structure under earthquake excitations.

A reinforced concrete twelve storey, two bay frame structure was analysed to investigate the size of the dampers required and the shape of the tendon system which may be used in real buildings. A comparison was made between two damper-tendon systems. The first system comprises either a single draped tendon, an equivalent straight tendon, or a straight tendon to the top of the structure connected horizontally to the floor levels of the structure and attached to a damper. The second tendon system examined comprises two draped or two straight tendons attached with a damper on each side of the frame structure. The analyses show that using one straight tendon to the top of the structure on one side of the frame structure may be the appropriate shape of the tendon which gives the target displacement of the roof level of the structure and leads to saving in both cost and ease of construction.

Comparisons between ring spring dampers, viscous fluid dampers and lead shear dampers show that ring spring dampers have a smaller length and diameter than the equivalent viscous dampers which are required for the same reduction of the structural response. Most of the dynamic characteristics and the properties of the ring-spring dampers and the lead shear dampers are the same. Guidelines for determining the

amount of damping, the shape of the tendon and the size of the dampers which may be used in a real building have been investigated. It should be noted that the decrease in response amplitude with increasing damping is highly dependent on the nature of the applied excitations.

The proposed supplemental damper-tendon system significantly reduces the displacement and intersorey drift of the structure by adding damping and stiffness to the structure. In the same time, no increases in the floor acceleration of the structure which is a real benefit of using ring spring dampers as opposed to adding conventional diagonal bracings to the frame structure.

Using bracing or spring elements alone through the total height of the frame structure i.e., only adding extra stiffness, may reduce the displacement of the structure but it would also increase, significantly, the floor acceleration of the structure which would cause damage to the sensitive items of equipment and other contents that might be housed in the structure.

## 9.2 Conclusions

The objectives of this study were to investigate the effectiveness of an innovative supplemental control system in reducing the seismic response of structures under earthquake ground motion excitations.

- The theoretical behaviour of ring spring dampers was verified by experimental tests. These tests results showed that the ring spring hysteresis characteristics behaved in accordance with the theoretical behaviour. The force-displacement hysteresis loops of the double acting ring spring dampers are stable and identical in both tension and compression. The energy dissipation characteristics of the dampers were clearly demonstrated. There are suitable sizes of ring-spring dampers for use in real buildings.
- The supplemental damping system dissipated a significant amount of the input earthquake energy in the structure. This study provided experimental tests that were used to validate the computational modelling strategies.
- Experimental results have shown that the response of the structure is significantly improved by using the supplemental damping system. Stiffening of the test structure from the damping control system leads to further reduction of the structure's deformation.
- The analytical study consisted of calculation of the time-history response of the structure and comparisons with the experimental results. The analytical response of the structure with the supplemental damping system produced results in good agreement with the results of the experiments.
- A damper-tendon system requires only one or two dampers attached to the system in the ground floor to produce the damping forces and then transfer them to the rest of the building by using a tendon system. This is in contrast to

many earlier studies where dampers were required to be placed at many parts in the structure. Hence there is no need to determinate the optimal placement or the optimal numbers of the dampers to be used. Using draped or straight tendon profiles gives similar reductions of the response for the structure.

- The load balancing technique in the seismic design/retrofit of buildings proved to be promising as the seismic response was reduced considerably even when using an equivalent straight tendon. Either straight or draped tendon profiles may be used. However, a draped tendon profile having the shape of overturning moment diagram balances the implied inertia forces associated with the earthquake ground accelerations.

### **9.3 Main Contributions of This Research**

- Structural control by adding damping is an alternative seismic energy dissipation approach for avoiding structural damage due to lateral loading. The properties and characteristics of different types of added damping systems have been shown. Passive systems are extremely reliable in contrast to active and semi-active systems. With passive control systems, there is no dependence on external power sources which may not be available during and after major earthquakes. Hence, a passive control system was adopted in this research to show its characteristics and effectiveness in reducing the response of structures under earthquake excitations. Strategies for adding damping to reduce seismic response of structures by using supplemental damping systems have been investigated. This study has shown that the adopted supplemental damping system is effective in controlling the structural response and how a valuable option as adding damping could protect the structure from damage under earthquake excitations. This work has enabled designers to confidently use such systems to protect their structures.
- Controlling structural response by incorporating suitable damping devices within a structure to provide the additional damping to augment the damping inherent in the structure has been proposed. A suggested passive damper such as ring-spring has been used. Evaluation of the characteristics of ring spring dampers have been carried out to show the effectiveness of ring spring dampers in reducing the response of structure. This research has shown how different types of dampers can be used to control the structural deformation and damage under earthquake excitations and how to select the suitable damper size and how to design the tendon layout.
- One of the problems indicated in the earlier use of added damping are related to the number and location of the damping devices. This research has focused on using a tendon system in a concept called a “damper-tendon system”. Only one or two dampers per frame are installed at the ground floor to produce the damping forces and these forces are then transferred to the rest of the building by using the tendon system. The damper-tendon system provides an alternative and more economical solution to the added damping approach

when compared with the earlier methods which had dampers located in many floors in the structure

- Different tendons profiles have been proposed including draped and straight tendons with two types of steel and concrete structures to determine a layout of the tendons to transfer the damping forces from the dampers to the structure.
- Experimental and analytical tests with and without the supplemental damping systems have been performed to investigate the effectiveness of the supplemental damping system in reducing the seismic response of the structure. This research has shown that the experimental tests and the analytical studies show very good agreement with each other.
- Guidelines for determining an appropriate supplemental damping system, the amount of damping, the layout of the tendon systems and the size of the dampers which may be used in real buildings have been suggested.

#### **9.4 Recommendations for Further Research**

In this research work, various aspects have indicated that some areas of the use of adding damping systems require further work. Further research of the following issues is needed:

- The effectiveness of supplemental damping control systems for structures having a wider range of different natural periods of free-vibration and geometries need to be investigated to ensure that the results found in this study are applicable over wider ranges of structures having different stiffness and mass distributions.
- For a structure designed with supplemental damping control systems, the effectiveness of the dampers under different intensities of earthquake excitation needs to be investigated in more detail, especially the effect of the near-source type ground motions which are generally accompanied by large velocity and displacement pulses. The investigation should show what changes are required for different types of ground motions.
- Practical design of the links and the supporting bearings at each floor slab of the structures and how they connected in real buildings should be undertaken to further the application of the added damping approach. This includes investigating the effect of various configuration details on the seismic response of the structures.
- The connections between the damper and the tendon at the ground floor and between the tendon and the floor at the top of the tendon need to be designed and detailed for real buildings to ensure that practical installation is possible.

- Other types of damper devices may lead to an improved seismic response of the structure when compared with the effectiveness of the ring spring dampers. The seismic control of such structures needs to be investigated both experimentally and analytically to show the advantages and disadvantages of using ring-spring dampers in reducing the seismic response of the structures.
- The effect of using a pre-stressed tendon system on the response of structures needs to be investigated. The investigation may be helpful in reducing the buckling load in the tendon under compressive damper forces by ensuring that the tendon system is always under tensile forces. This will stabilize the tendon so as to give a more efficient structural layout. The effect of different pre-stress levels on the response of the structure needs to be carried out experimentally and analytically.
- Further research is required in considering a three-dimensional modelling of the structures with the supplemental damping system under both single and concurrent orthogonal seismic excitations to investigate the effects of the damping system. This must also include the investigation of the torsional effects of the damping system with various types of damping devices.

## REFERENCES

- [1] Carr, A.J., (2000), "RUAUMOKO- Inelastic dynamic analysis program", Computer Program Library, Department of Civil Engineering, University of Canterbury.
- [2] Carr, A.J., (2000), "DYNAPLOT- post-processor for RUAUMOKO", Computer Program Library, Department of Civil Engineering, University of Canterbury.
- [3] Carr, A.J., (2000), "QUAKE", Computer Program Library, Department of Civil Engineering, University of Canterbury.
- [4] Carr, A.J., (2000), "HYSTERES", Computer Program Library, Department of Civil Engineering, University of Canterbury.
- [5] Hill, K.E., (1994), "Dynamic Properties of Ring Springs for use as seismic energy dissipations", Proc. N.Z. Nat. Soc. Earthq. Eng. Annual Conf., Wairakei, Mar. 1994, pp 96-101.
- [6] Hill, K.E., (1994), "Fundamental Dynamic Characteristics of Ring Springs", Vibrations Assoc. of N.Z. Annual Conf., Christchurch, May, pp 182-90.
- [7] Hill, K.E., (1995), "The Utility of Ring Springs in Seismic Isolation Systems", Ph.D Thesis, Department of Mechanical Engineering, University of Canterbury.
- [8] Hill, K.E., (1995), "A Prototype Ring Spring Cartridge for Mitigating Transient and Seismic Inputs", Proc. IPENZ Annual Conf., Palmerston North, Feb., Vol2, pp 145-150.
- [9] Hill, K.E., (1995), "Application of Ring Springs to Seismic Isolation Systems", Proc. N.Z., Nat. Soc. Earthq. Annual Conf., Rotorua, Mar. pp 21-27.
- [10] Hill, K.E., (1995), "Seismic Isolation of Columnar Structures Utilising Ring Springs", Pacific Conf. on Earthq. Eng., Melbourne, Australia, Nov. Vol. 1, pp 101-110.
- [11] Kao, G.C. (1998), "Design of Shaking Table Tests of a Four-Storey Miniature Structure Built with Replaceable Plastic Hinges", ME Thesis, Department of Civil Engineering, University of Canterbury.
- [12] Pekcan, G., Mander, J.B., Chen, S.S., (1995), "Experimental Performance Analytical Study of a Non-Ductile Reinforced Concrete Frame Structure Retrofitted with Elastometric Spring Damper", Technical Report NCEER-95-0010, July, National Center for Earthquake Engineering Research, SUNY at Buffalo.

- [13] Pekcan, G., (1998), "Design of Seismic Energy Dissipation Systems for Reinforced Concrete and Steel Structures, Ph.D Thesis, State University of New York at Buffalo, Buffalo.
- [14] Pekcan, G., Mander, J.B., Chen, S.S., (1999), "Experimental Investigation and Computational Modelling of Seismic Response of a 1: 4 Scale Model Steel Structure with a Load Balancing Supplemental Damping System", Technical Report NCEER-99-0006, April, National Center for Earthquake Engineering Research, SUNY at Buffalo.
- [15] Pekcan, G., Mander, J.B., Chen, S.S., (1999)," Design and Retrofit Methodology for Building Structures with Supplemental Energy Dissipating Systems", Technical Report NCEER-99-0021, December, National Center for Earthquake Engineering Research, SUNY at Buffalo.
- [16] Pekcan, G., Mander, J.B., Chen, S.S., (2000), "Seismic Retrofit of End-Sway Frames of Steel Deck-Truss Bridges with a Supplemental Tendon System: Experimental and Analytical Investigation", Technical Report NCEER-00-0004, July, National Center for Earthquake Engineering Research, SUNY at Buffalo.
- [17] Pekcan, G., Mander, J.B., Chen, S.S., (2000), "Experiments on Steel MRF Building with Supplemental Tendon System", Journal of Structural Engineering, ASCE, Vol. 126, No.4, pp 437-444.
- [18] Pekcan, G., Mander, J.B., Chen, S.S., (2000), "Balancing Lateral Loads Using Tendon-Based Supplemental Damping System", Journal of Structural Engineering, ASCE, Vol. 126, No. 8, pp896-905.
- [19] Filiatrault, A., Trembley, R., Kar, R., (2000), "Performance of Friction Spring Seismic Damper", Journal of Structural Engineering, ASCE, Vol. 126, No.4, April.
- [20] Jury, R.D., (1978), "Seismic Load Demands on Columns of Reinforced Concrete Multi-Storey Frames", ME Thesis, Department of Civil Engineering, University of Canterbury
- [21] Lin, X., (1999), "Analysis and Design of Building Structures with Supplemental Lead Dampers under Earthquake and Wind Loads", Ph.D Thesis, Department of Civil Engineering, University of Canterbury.
- [22] Soong, T.T., (1990), Active Structural Control: Theory and Practice, Longman, London, and Wiley, New York.
- [23] Soong, T.T., and Constantinou, M.C. (1994), Passive and Active Structural Vibration Control in Civil Engineering, Springer-Verlag, Wien-New York.
- [24] Soong, T.T., and Dargush, G.F., (1997), Passive Energy Dissipation Systems in Structural Engineering, John Wiley& Sons.

- [25] Constantinou, M.C., Soong, T.T., Dargush, G.F., (1998), "Passive Energy Dissipation Systems for Structural Design and Retrofit", Multidisciplinary Center for Earthquake Engineering Research (MCEER).
- [26] Zhang, R. and Soong, T.T., (1992), "Seismic Design of Viscoelastic Dampers for Structural Applications", Journal of Structural Engineering, ASCE, Vol. 118, No. 5, pp1375-1392.
- [27] Hahn, G.D. and Sathiavag, K.R., (1992), "Effect of added-Damper Distribution on the Seismic Response of Buildings", Commuters& Structures, Vol. 43, No. 5, pp 941-950.
- [28] Singh, M.P., and Moreschi, L.M. (2002), "Optimal Placement of Dampers for Passive Response Control", Earthquake Engineering and Structural Dynamics 31, pp955-976.
- [29] Hanson, R.D., and Soong, T.T., (2001), Seismic Design with Supplemental Energy Dissipation Devices, EERI Monograph No.8, Oakland (CA): Earthquake Engineering Research Institute.
- [30] Spencer, B.F., and Sain, M.k., (1997), "Controlling Building: A New Frontier in Feedback", IEEE Control Systems Magazine, Special Issue Emerging Technologies, Vol. 17, No. 6, pp 19-35.
- [31] Soong, T.T., and Spenser, B.F., (2002), "Supplemental Energy Dissipation: state-of-the-art and state-of-the-practice", Engineering Structures, Vol. 24, pp 243-259.
- [32] Yang, J.N., Kim, J., Agrawal, A.K., (2000), "Resetting Semi-active Stiffness Dampers for Seismic Response Control", Journal of Structural Engineering, ASCE, Vol. 126, No.12, pp 1427-1433, December.
- [33] RINGFEDER GmbH, (1995), Friction Springs, Ringfeder in Mech. Eng., Report R60E, RINGFEDER CORPORATION, Krefeld, Germany, 40 pp, (<http://www.ringfeder.de>).
- [34] Thelning, K., (1975)," Steel and its Heat Treatment", Butterworths, London and Boston.
- [35] FEMA 273, (1997), "NEHRP Guidelines for the Seismic Rehabilitation of Buildings", Federal Emergency Management Agency, Building Seismic Safety Council, Washington, D.C.
- [36] FEMA 274, (1997), "NEHRP Commentary on the Guidelines for the seismic Rehabilitation of Building", Federal Emergency Management Agency Building Seismic Safety Council, Washington, D.C.

- [37] NZS4203 (1992), Code of Practice for General Structural and Design Loading for Building, NZS4203:1992 and Commentary, Standards New Zealand, Wellington.
- [38] Dodd, L.L. and Restrepo-Posada, J.I., (1995), "Model for Predicting Cyclic Behaviour of Reinforcing Steel", Journal of Structural Engineering, ASCE, Vol. 121, No. 3, March, pp1375-1392.
- [39] Scholl,R. and EERI, M., (1993), "Fundamental Design Issues for Supplemental Damping Application", Earthquake Spectra, Vol.9, No.3, August, pp 627-636.
- [40] Paulay, T. and Priestley, M.J.N., (1992), "Seismic Design of Concrete and Masonry Building", John Wiley & Sons Inc. New York.
- [41] Priestley, M.J.N. and Kowalsky, M.J., (2000), "Direct Displacement-Based Seismic Design of Concrete Building", Bulletin of New Zealand Society for Earthquake Engineering, Vol. 33, No.4, December, pp 421- 444.
- [42] NEHRP- National Earthquake Hazard Reduction Program (1994), "NEHRP Recommended Provisions for Seismic Regulations for New Building and Other Structures", Federal Emergency Management Agency, Report No. FEMA 222A, Washington, D.C.
- [43] NEHRP- National Earthquake Hazard Reduction Program (1997), "NEHRP Recommended Provisions for Seismic Regulations for New Building and Other Structures", Federal Emergency Management Agency, Report No. FEMA 302, Washington, D.C.
- [44] Hirasawa, M., Mikame, A., Takasawa, Y., (1988), "Aseismic Design of a Base Isolated Building and Verification Tests of an Isolator", Ninth World Conference on Earthquake Engineering, Japan, Vol.5, pp723-728.
- [45] Kawamura, S., Kitazawa, K, Hisano, M., (1988), "Study on a Sliding-Type Base Isolation and Element Properties", Ninth World Conference on Earthquake Engineering, Japan, Vol.5, pp735-740.
- [46] Robinson, W. H., (1982), "Lead-Rubber Hysteretic Bearings Suitable for Protecting Structures During Earthquakes", Earthquake Engineering and Structural Dynamics, Vol. 10, pp 593-604.
- [47] Symans, M.D. and Constantinou, M.C., (1999), "Semi-Active Control Systems for Seismic Protection of Structures: a state-of-the art Review", Journal of Engineering Structures 21, pp 469-487.
- [48] Skinner, R.I., Robinson, W.H. and McVerry, G.H. (1993), An Introduction to Seismic Isolation, John Wiley & Sons Ltd, West Sussex, England.
- [49] Kelly, M.K., (1986), "Aseismic Base Isolation: Review and Bibliography" Soil Dynamics and Earthquake Engineering, Vol.5, No3, pp202-216.

- [50] Pall, A.S., and Pall, R., (1993), "Friction-Dampers Used for Seismic Control of New and Existing Building in Canada" In: Proc. ATC 17-1 Seminar on Isolation, Energy Dissipation and Active Control. San Francisco, Vol. 2, pp 675-686.
- [51] Housner, G.W., Bergman, L.A., and others (1997), "Structural Control; Past, Present, and Future", Journal of Structural Engineering, ASCE, Vol. 123, No. 9, September, Special Issue.
- [52] Hunt, S.J, (2002) "Semi-Active Smart-Dampers and Resetable Actuator for Multi-Level Seismic Hazard Mitigation of Steel Moment Resisting Frame", M.E. Thesis, Department of Mechanical Engineering, University of Canterbury.
- [53] Shepherd, R. and Erasmus, L.A. (1988), "Ring Spring Energy Dissipators in Seismic Resistant Structures", Ninth World Conference on Earthquake Engineering, Japan, Vol.5, pp 767-772.
- [54] Reinhorn, A.M., Li, C., and Constantinou, M.C. (1995), "Experimental and Analytical Investigation of Seismic Retrofit of Structures with Supplemental Damping: Part 1- Fluid Viscous Devices", Technical Report NCEER-95-0001, January, National Center for Earthquake Engineering Research, SUNY at Buffalo.
- [55] Reinhorn, A.M., and Li, C. (1995), "Experimental and Analytical Investigation of Seismic Retrofit of Structures with Supplemental Damping: Part III – Viscous Damping Walls", Technical Report NCEER-95-00013, October, National Center for Earthquake Engineering Research, SUNY at Buffalo.
- [56] Pong, W.S., Tsai, C.S., and Lee, G.C. (1994), "Seismic Study of Building Frames With Added Energy-Absorbing Devices", Technical Report NCEER-94-00016, June, National Center for Earthquake Engineering Research, SUNY at Buffalo.
- [57] Constantinou, M.C., and Symans, M.D. (1992), "Experimental and Analytical Investigation of Seismic Response of Structures with Supplemental Fluid Viscous Dampers", Technical Report NCEER-92-00032, December, National Center for Earthquake Engineering Research, SUNY at Buffalo.
- [58] Monti, M.D., Zhao, J.X., Gannon, C.R., and Robinson, W.H. (1998), "Experimental Results and Dynamic Parameters for the Penguin Vibration Damper (PVD) for Wing and Earthquake Loading", Bulletin of the New Zealand Society for Earthquake Engineering, September, Vol. 31, No.3. pp 177 - 193.

- [59] Ajrab, J.J., (2000), "Rocking Wall-Frame Structures with Supplemental Damping Devices", ME Thesis, Department of Civil Engineering, Structural and Environmental Engineering, State University of New York at Buffalo.
- [60] Constantinou, M.C., Tsopelas, P., Hammel, W. and Sigaher, A.N. (2001), "Toggle-Brace-Damper Seismic Energy Dissipation Systems", Journal of Structural Engineering, Vol.127, No.2, February, pp 105-112.
- [61] Sigaher, A.N., Erri, M. and Constantinou, M.C. (2003), "Scissor-Jack-Damper Energy System", Earthquake Spectra, Vol. 19, No.1, February, pp133-158.
- [62] Garcia, D.L., (2001), "A Simple Method for the Design of Optimal Damper Configurations in MDOF Structures", Earthquake Spectra, Vol. 17, No. 3, August, pp 387-398.
- [63] Pekcan, G., Mander, J.B., Chen, S.S., (1999), "Fundamental Considerations for the Design of Nonlinear Viscous Dampers", Earthquake Engineering and Structural Dynamics 28, pp 1405-1425.
- [64] Berg, G.V., (1989), "Elements of Structural Dynamics", Prentice Hall, Inc. Englewood Cliffs, New Jersey.

**Appendix A**  
**Shaking Table Results with El Centro Excitation**

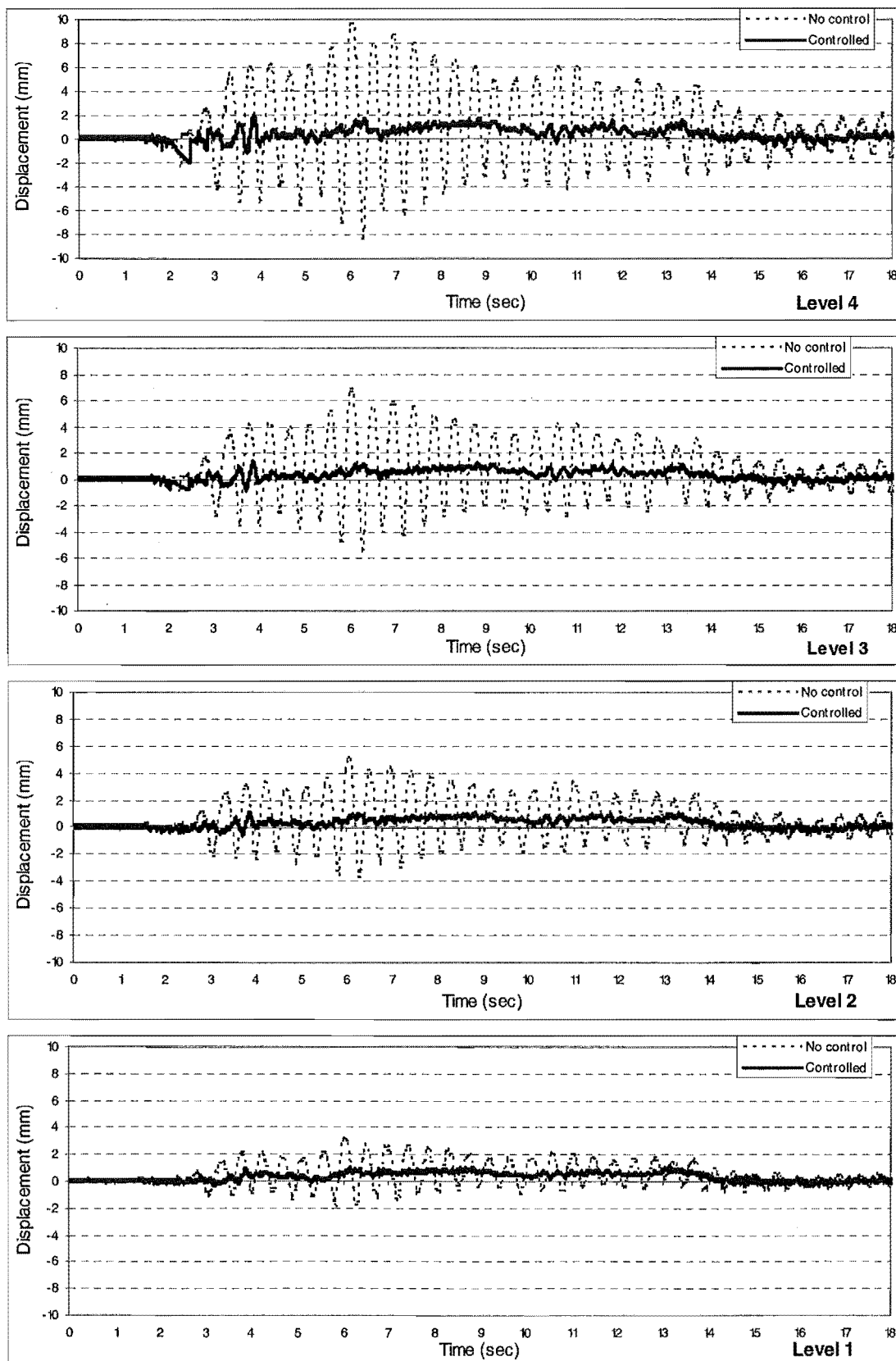


Fig (A-1) Displacement of the structure with and without the supplemental control system- **El Centro 20%**-shaking table acceleration.

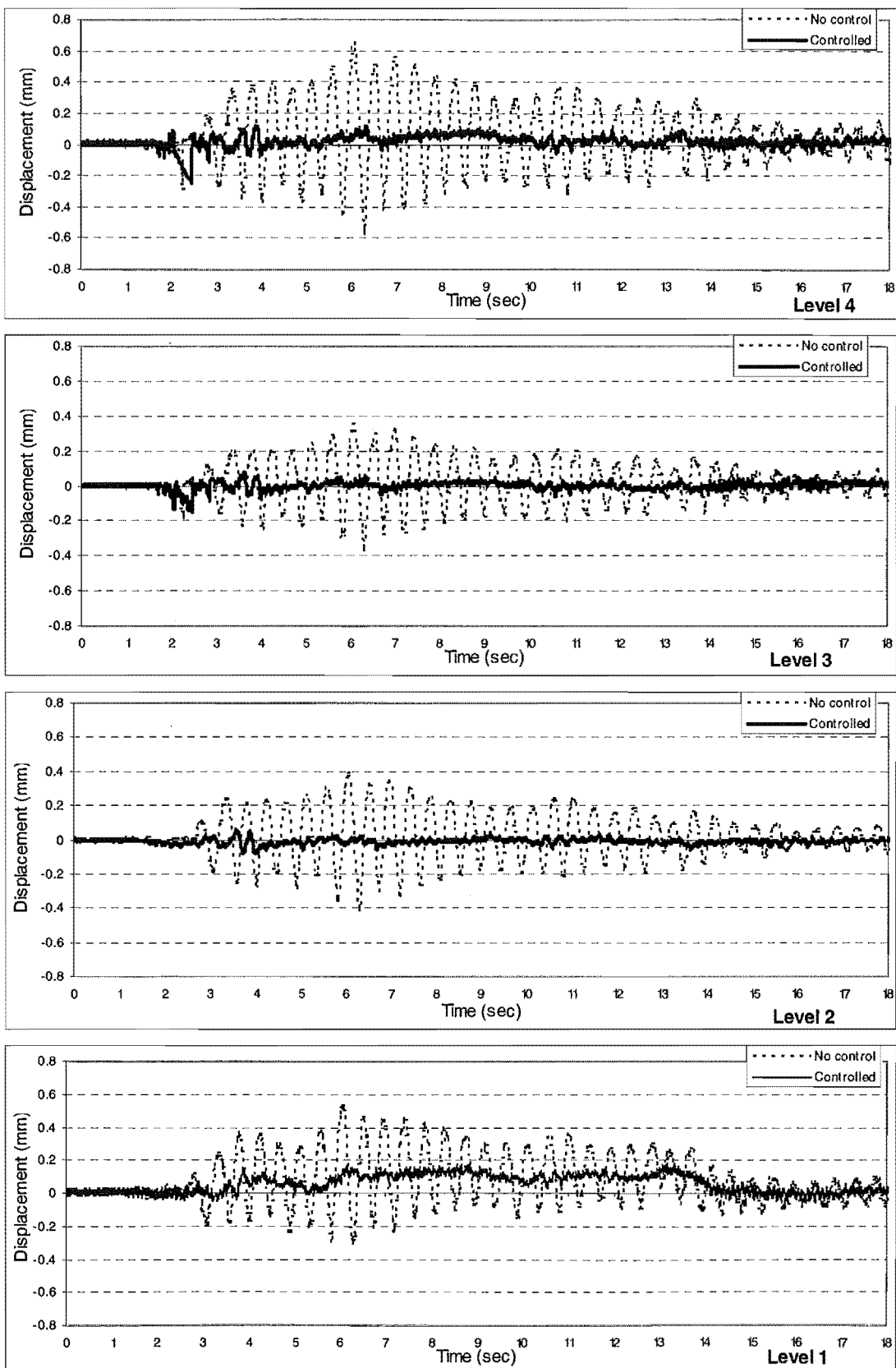


Fig (A-2) Intersorey drift of the structure with and without the supplemental control system-**El Centro 20%**-shaking table acceleration.

Level	Displacement		Reduction	
	Without D-T*	With D-T	% of reduction	% average
4	9.5	2	79	79
3	6.5	1.2	82	
2	4.7	0.82	83	
1	2.9	0.84	71	

\* D-T is the supplemental damper-tendon system

Level	Interstorey drift %		Reduction	
	Without D-T	With D-T	% of reduction	% average
4	0.63	0.25	60	69
3	0.34	0.14	59	
2	0.4	0.05	88	
1	0.51	0.16	69	

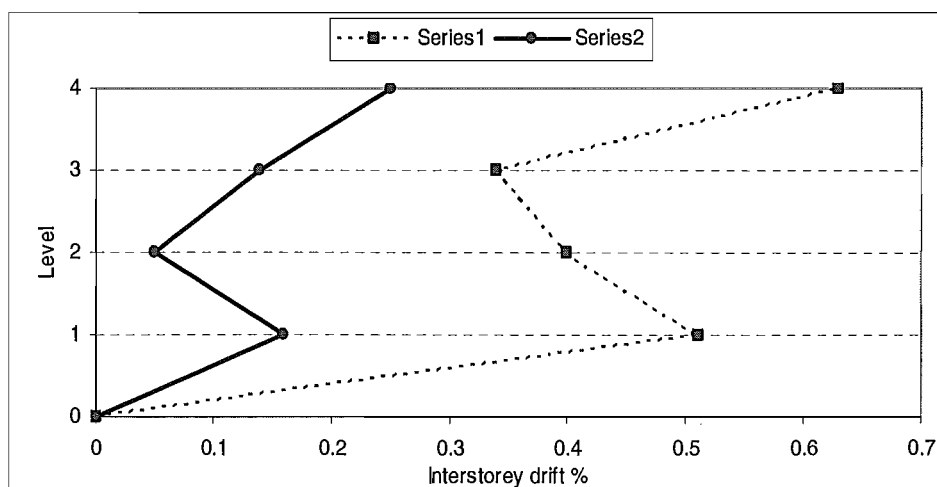
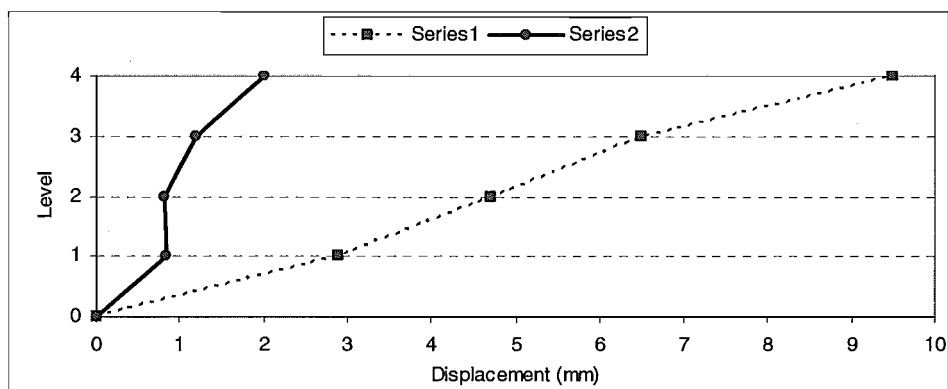


Fig (A-3) Displacement and intersorey drift ratios of the structure with and without the supplemental control system- **El Centro 20%** - shaking table acceleration.

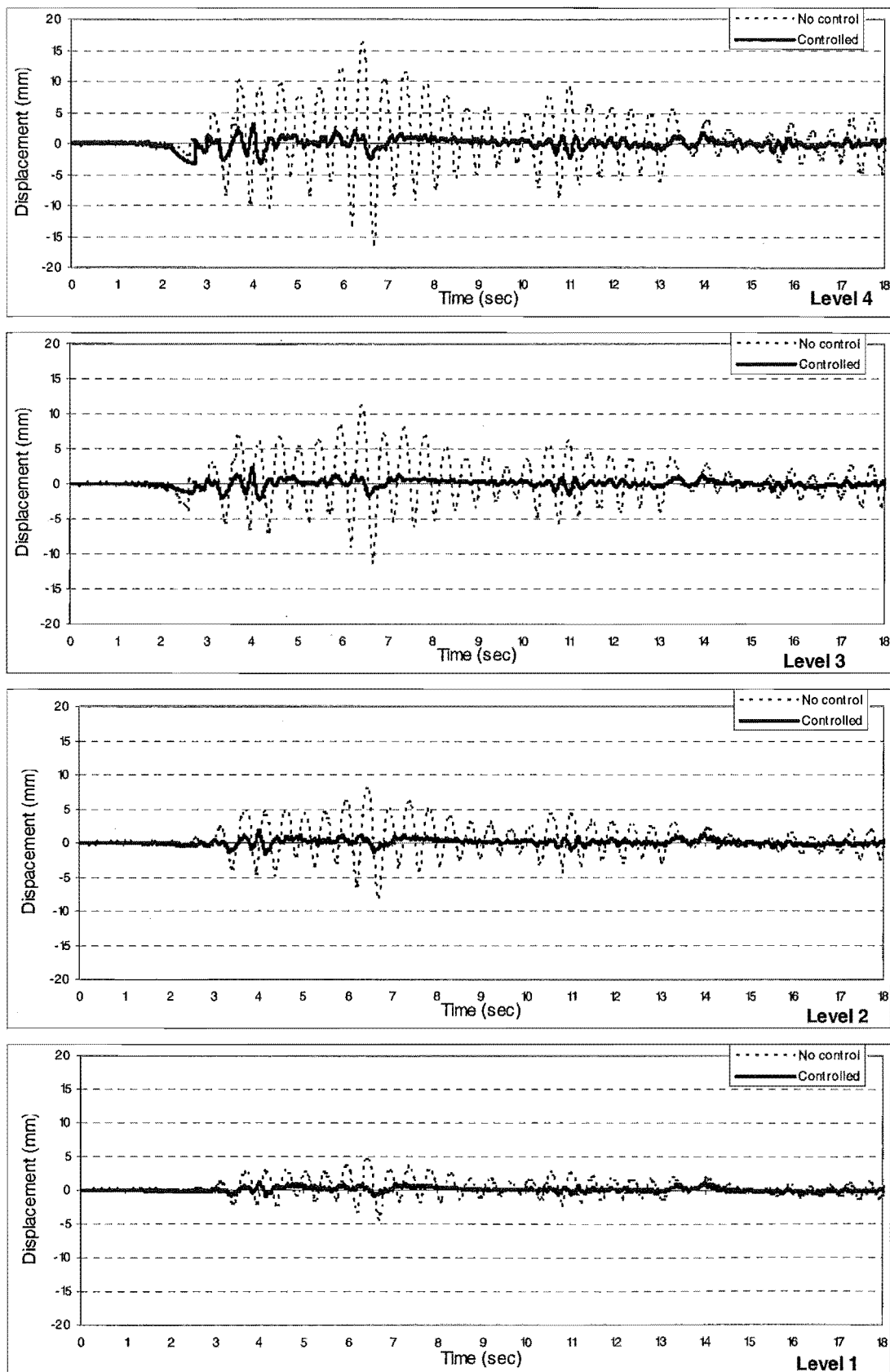


Fig (A-4) Displacement of the structure with and without the supplemental control system- **El Centro 40%**-shaking table acceleration.

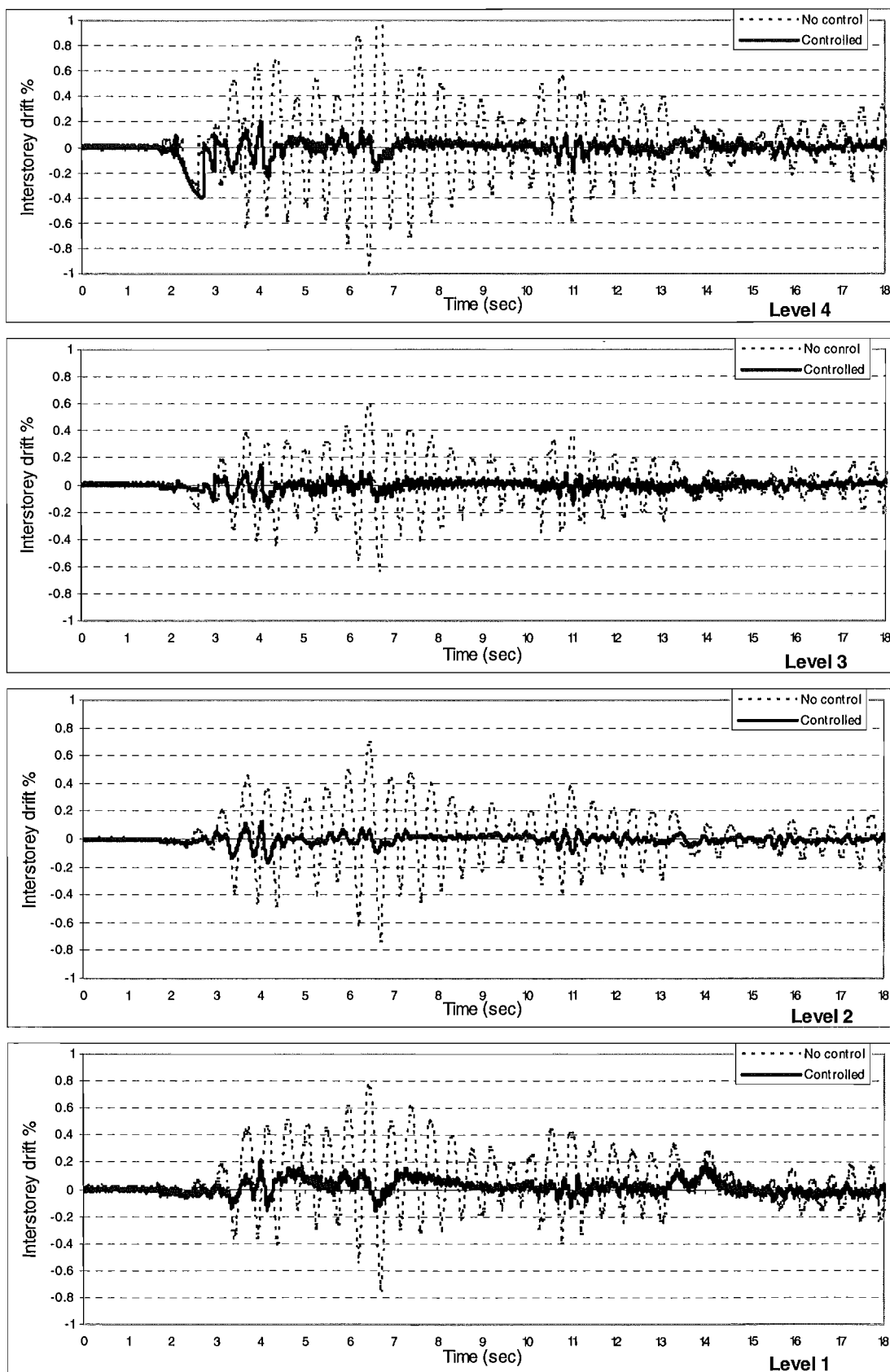


Fig (A-5) Intersorey drift of the structure with and without the supplemental control system –**El Centro 40%**- shaking table acceleration.

Level	Displacement		Reduction	
	Without D-T	With D-T	% of reduction	% average
4	15.7	3.1	80	84
3	10.6	1.5	86	
2	7.4	1.04	86	
1	3.74	0.6	84	

Level	Interstorey drift %		Reduction	
	Without D-T	With D-T	% of reduction	% average
4	1	0.38	62	75
3	0.61	0.11	82	
2	0.71	0.14	80	
1	0.72	0.18	75	

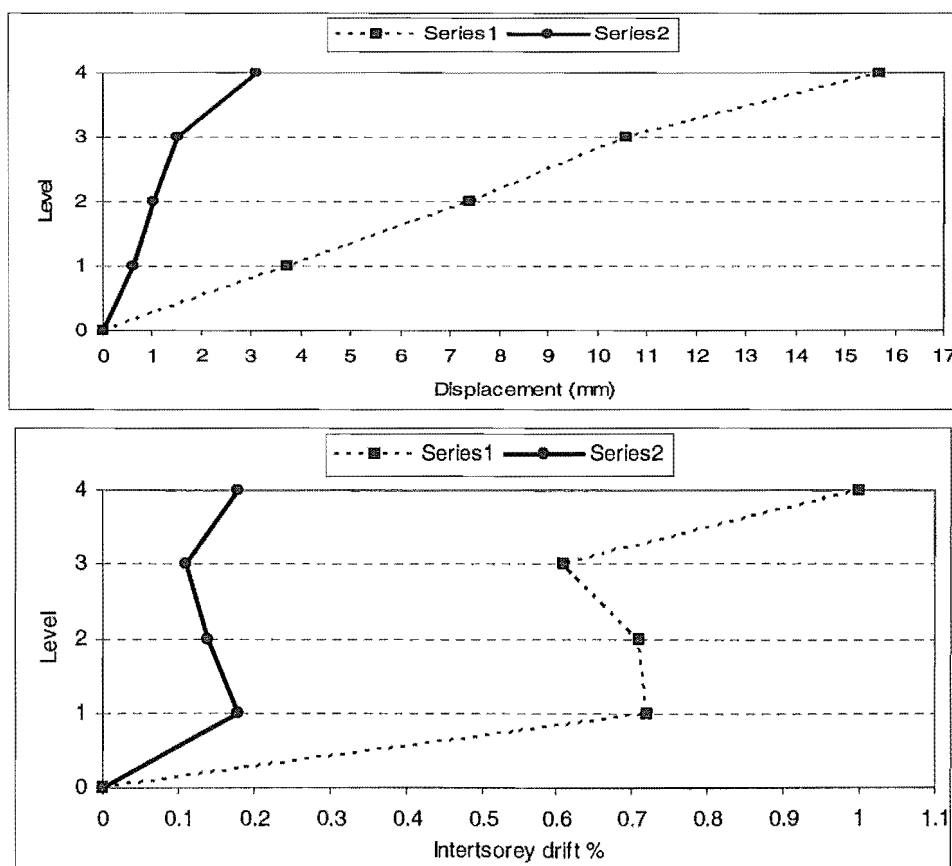


Fig (A-6) Displacement and intersorey drift ratios of the structure with and without the supplemental control system- **El Centro 40%** - shaking table acceleration.

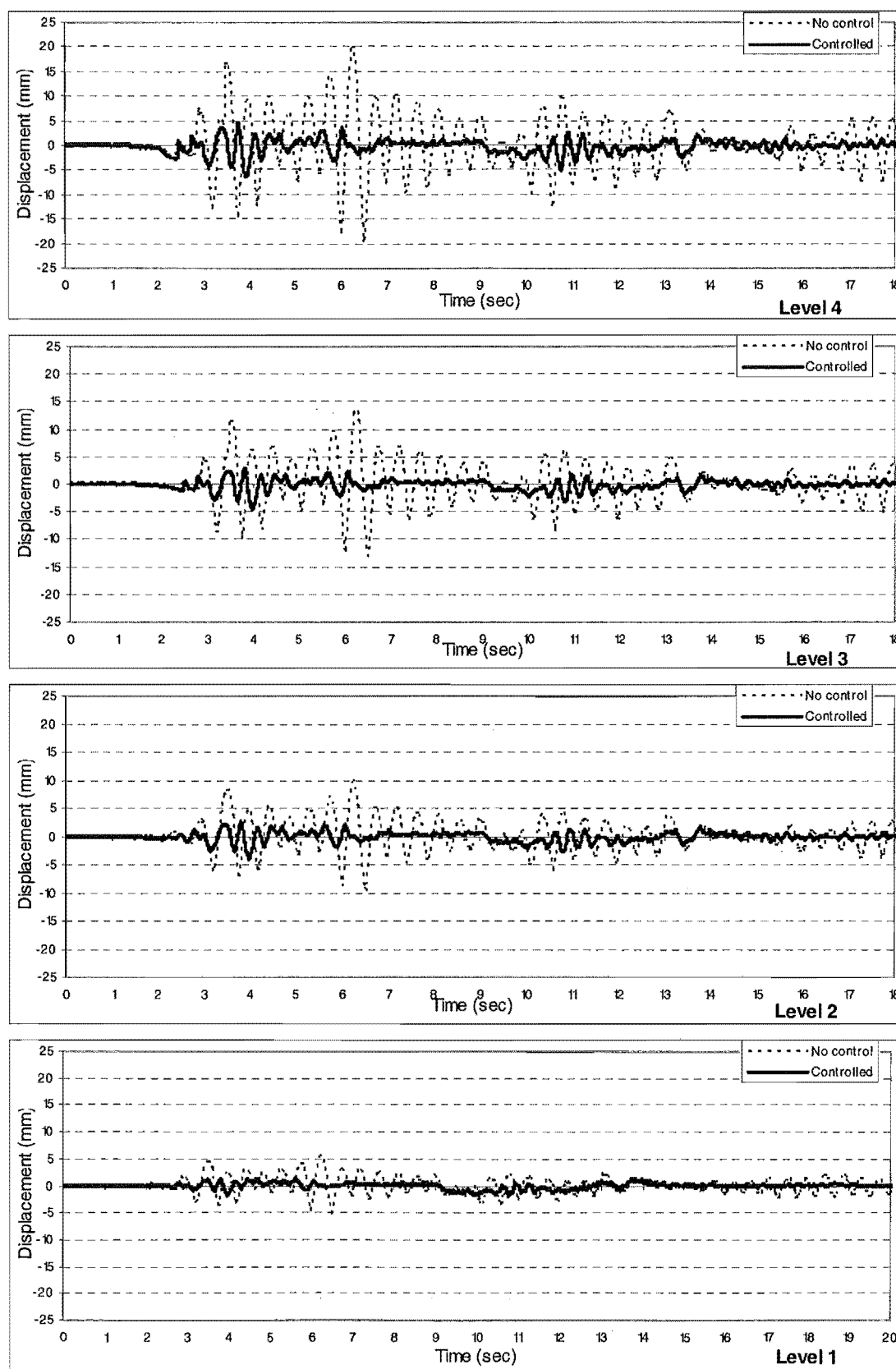


Fig (A-7) Displacement of the structure with and without the supplemental control system- **El Centro 60%**-shaking table acceleration

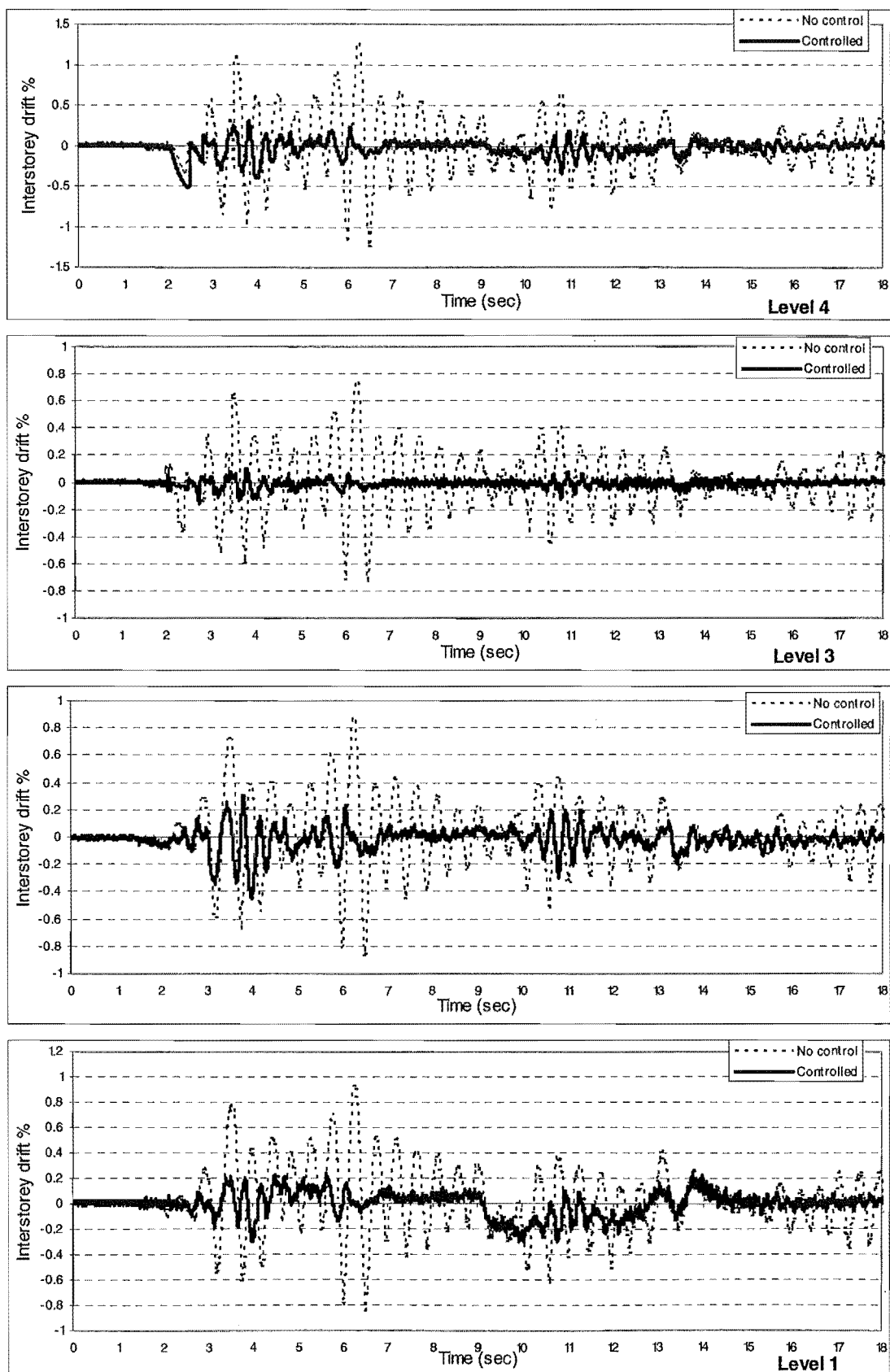


Fig (A-8) Intersorey drift of the structure with and without the supplemental control system –El Centro 60%– shaking table acceleration.

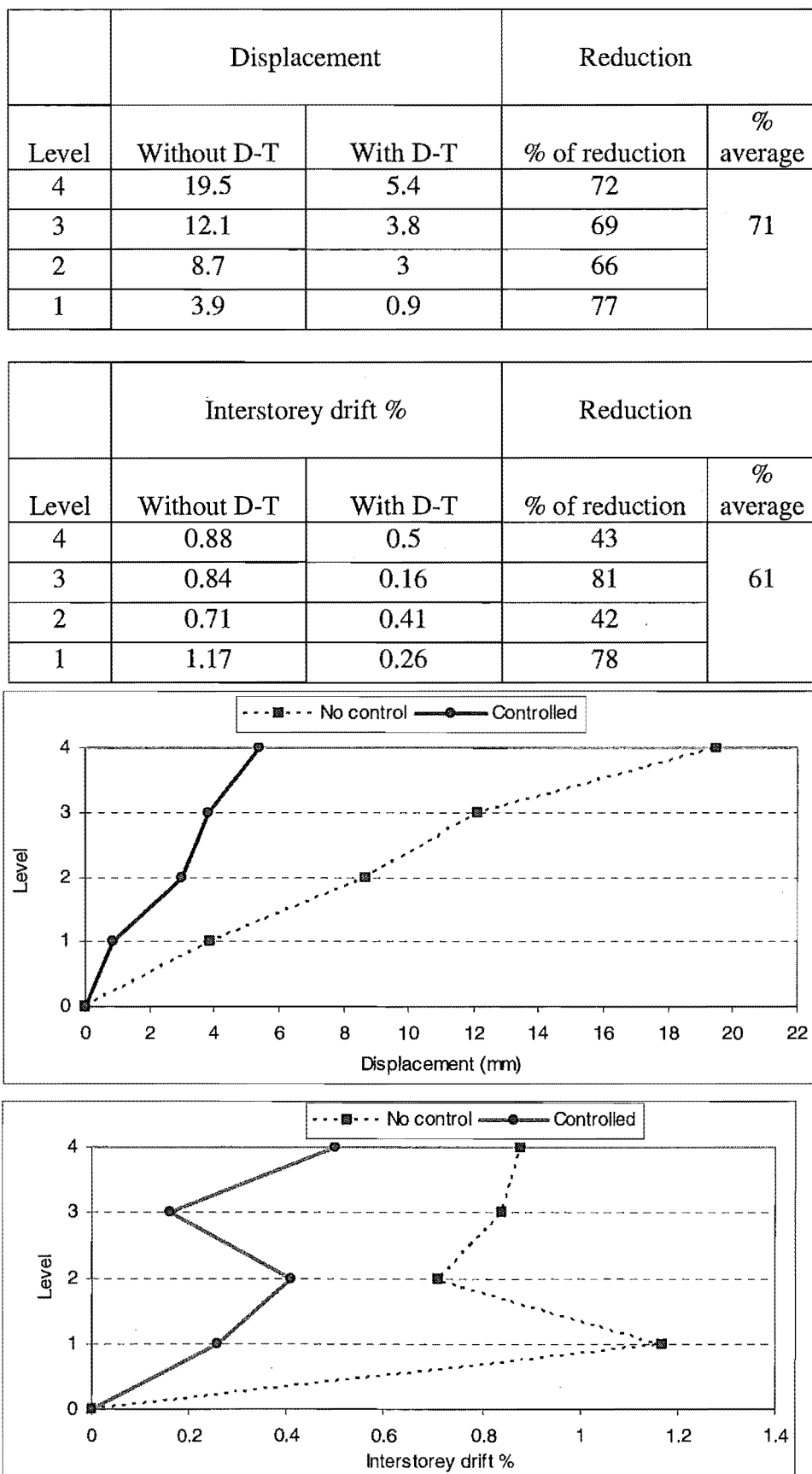


Fig (A-9) Displacement and intersorey drift ratios of the structure with and without the supplemental control system- **El Centro 60%** - shaking table acceleration

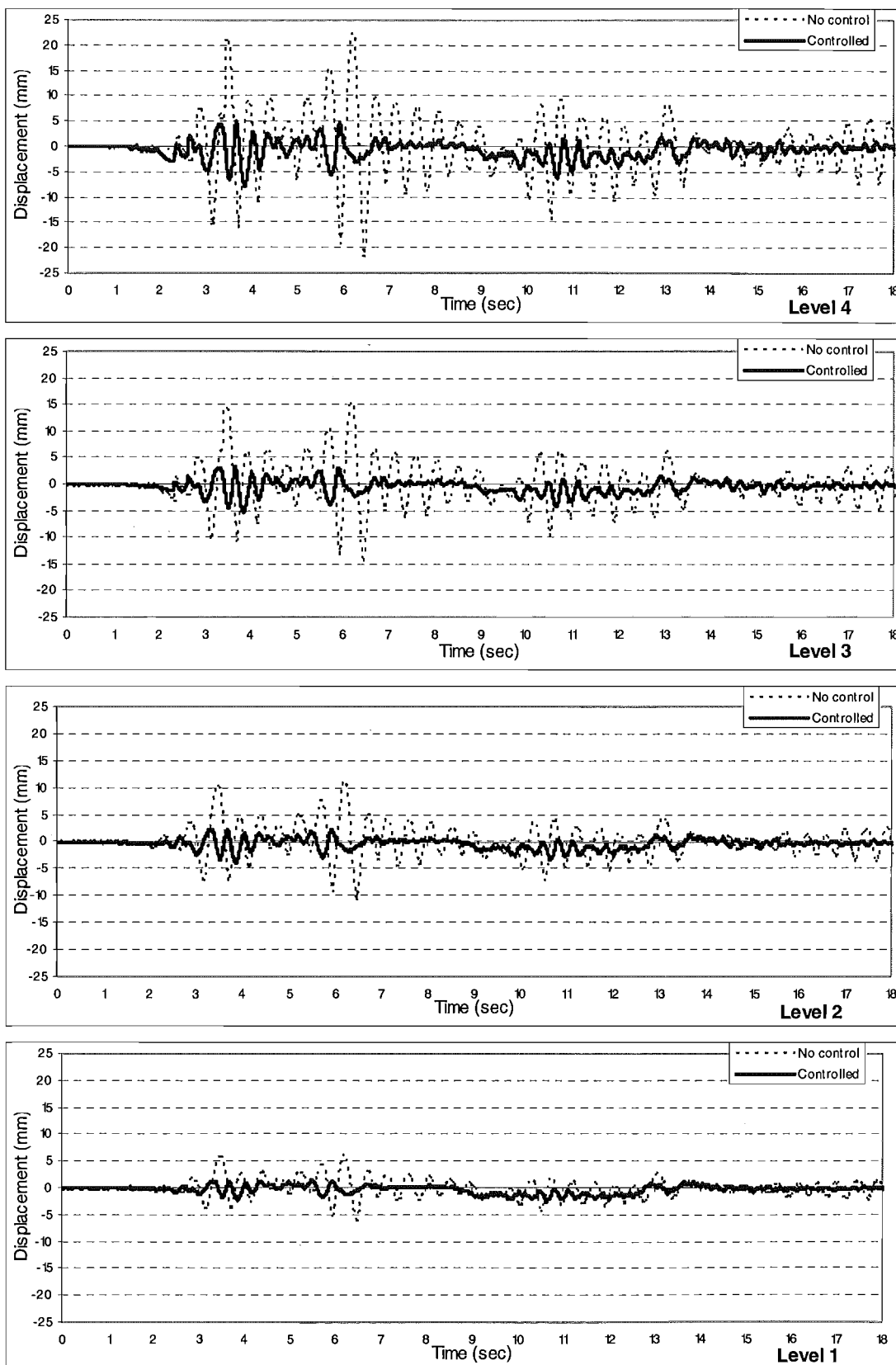


Fig (A-10) Displacement of the structure with and without the supplemental control system- El Centro 70%-shaking table acceleration

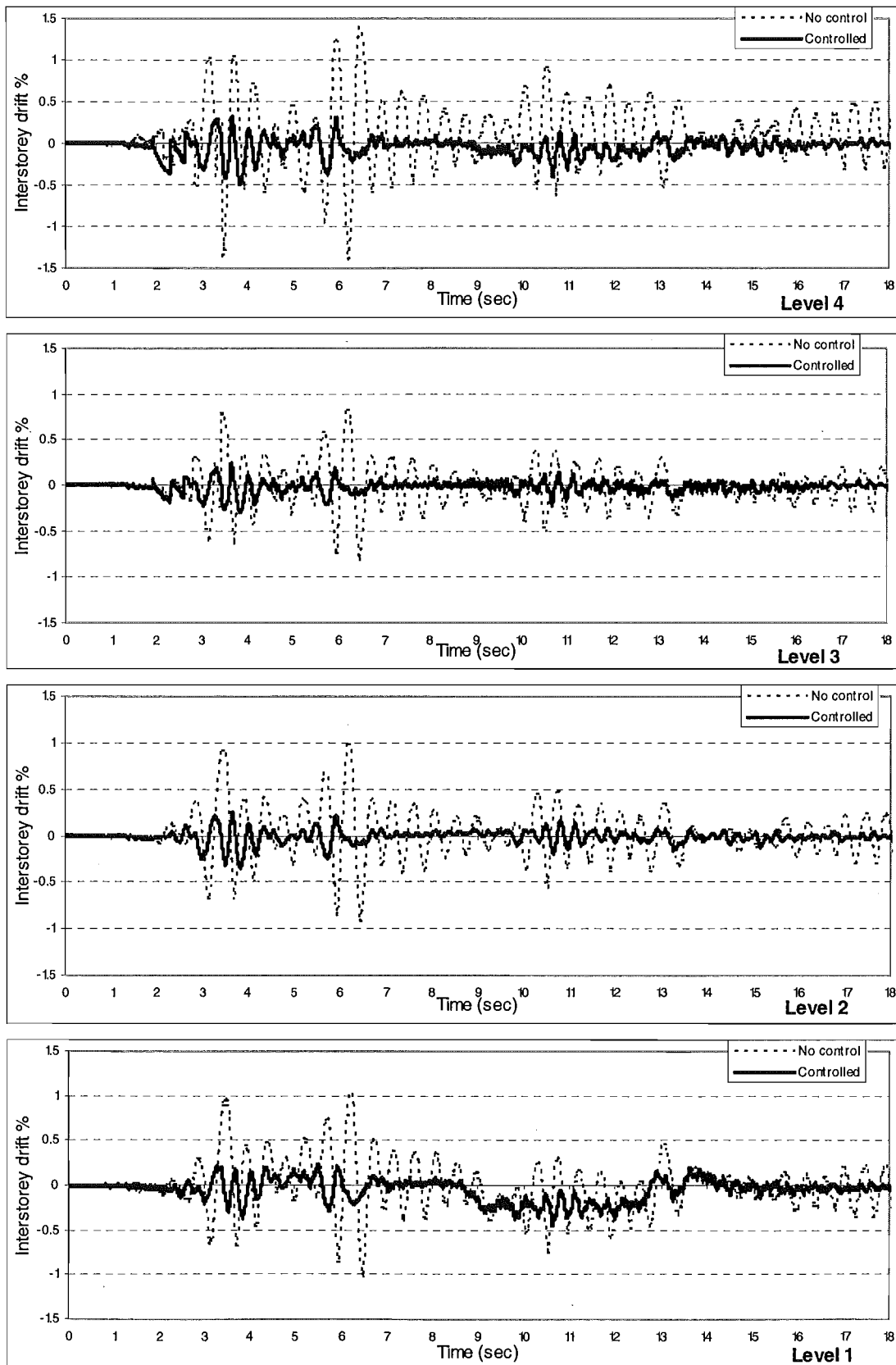


Fig (A-11) Intersorey drift of the structure with and without the supplemental control system –**El Centro 70%**- shaking table acceleration.

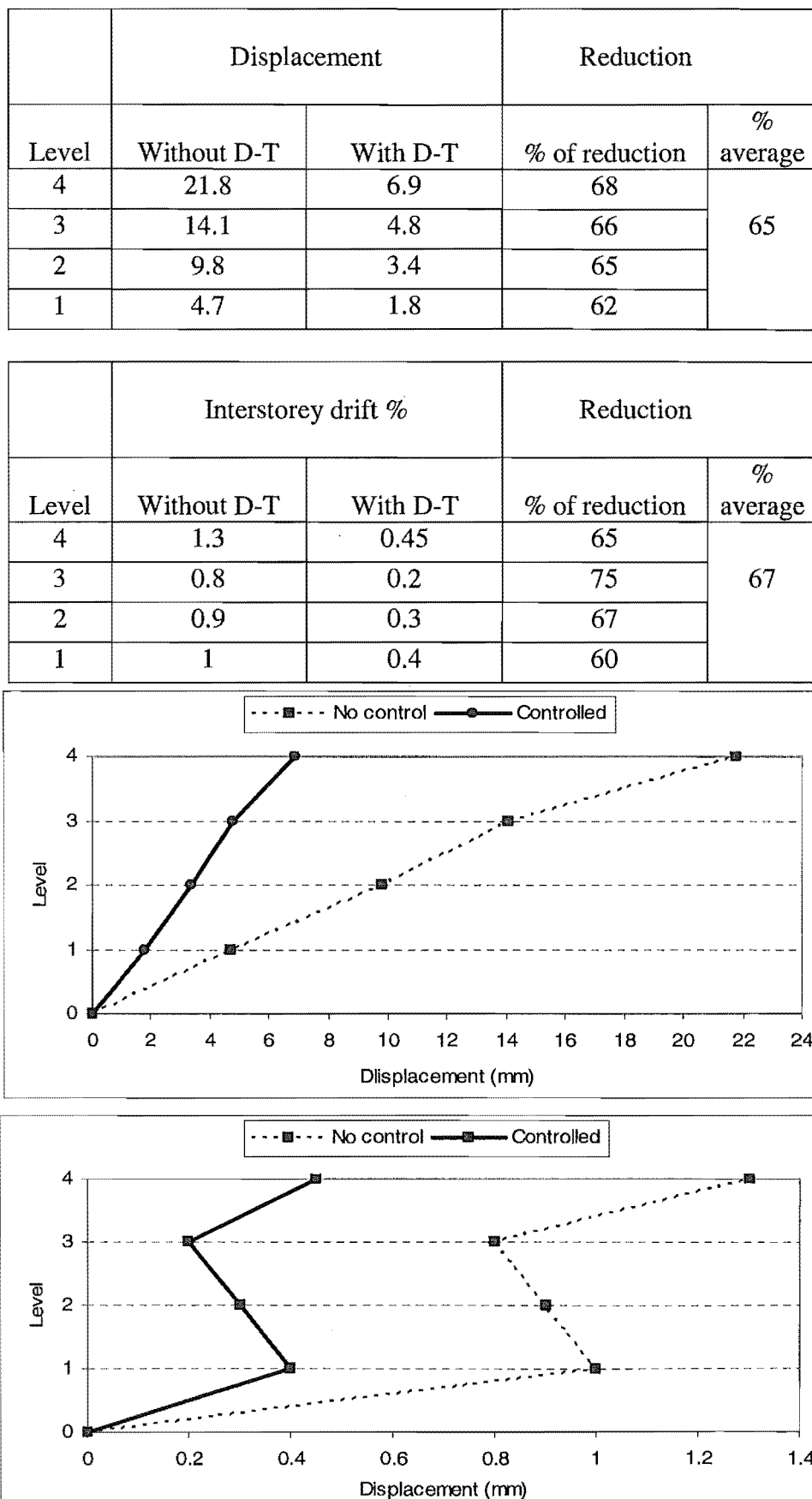


Fig (A-12) Displacement and intersorey drift ratios of the structure with and without the supplemental control system- **El Centro 70%** - shaking table acceleration

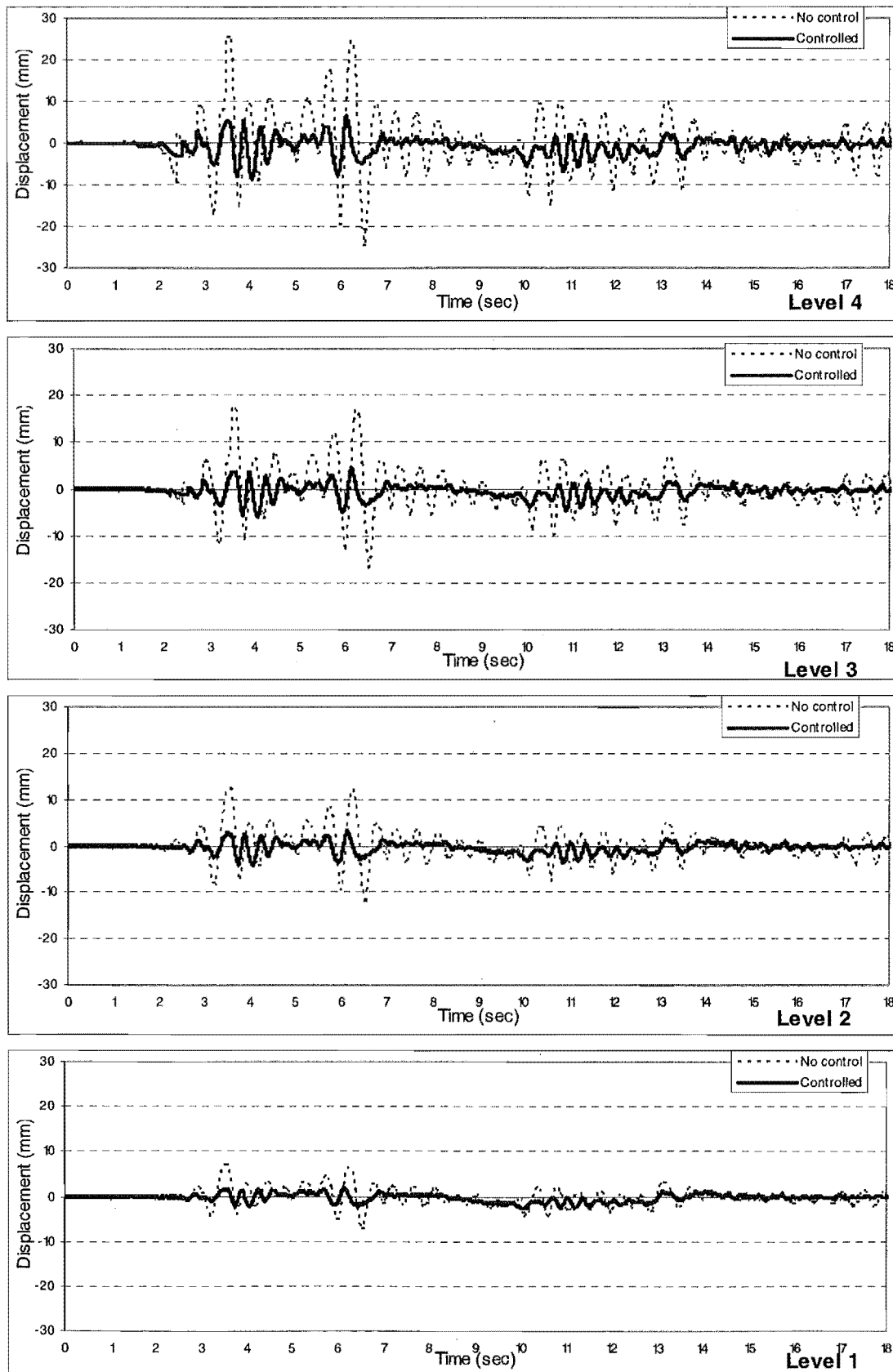


Fig (A-13) Displacement of the structure with and without the supplemental control system- **El Centro 80%**-shaking table acceleration

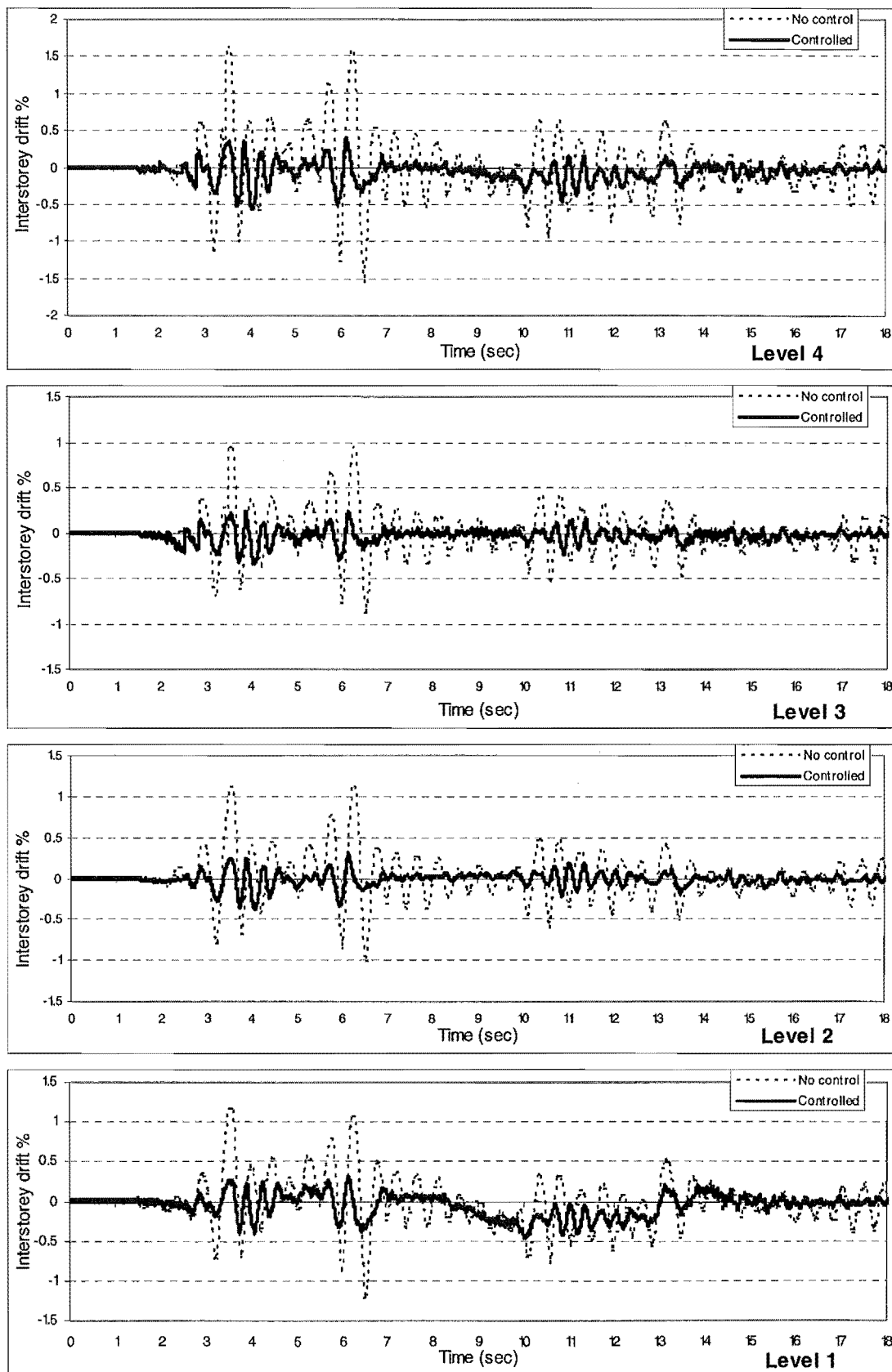


Fig (A-14) Intersorey drift of the structure with and without the supplemental control system –**El Centro 80%**- shaking table acceleration.

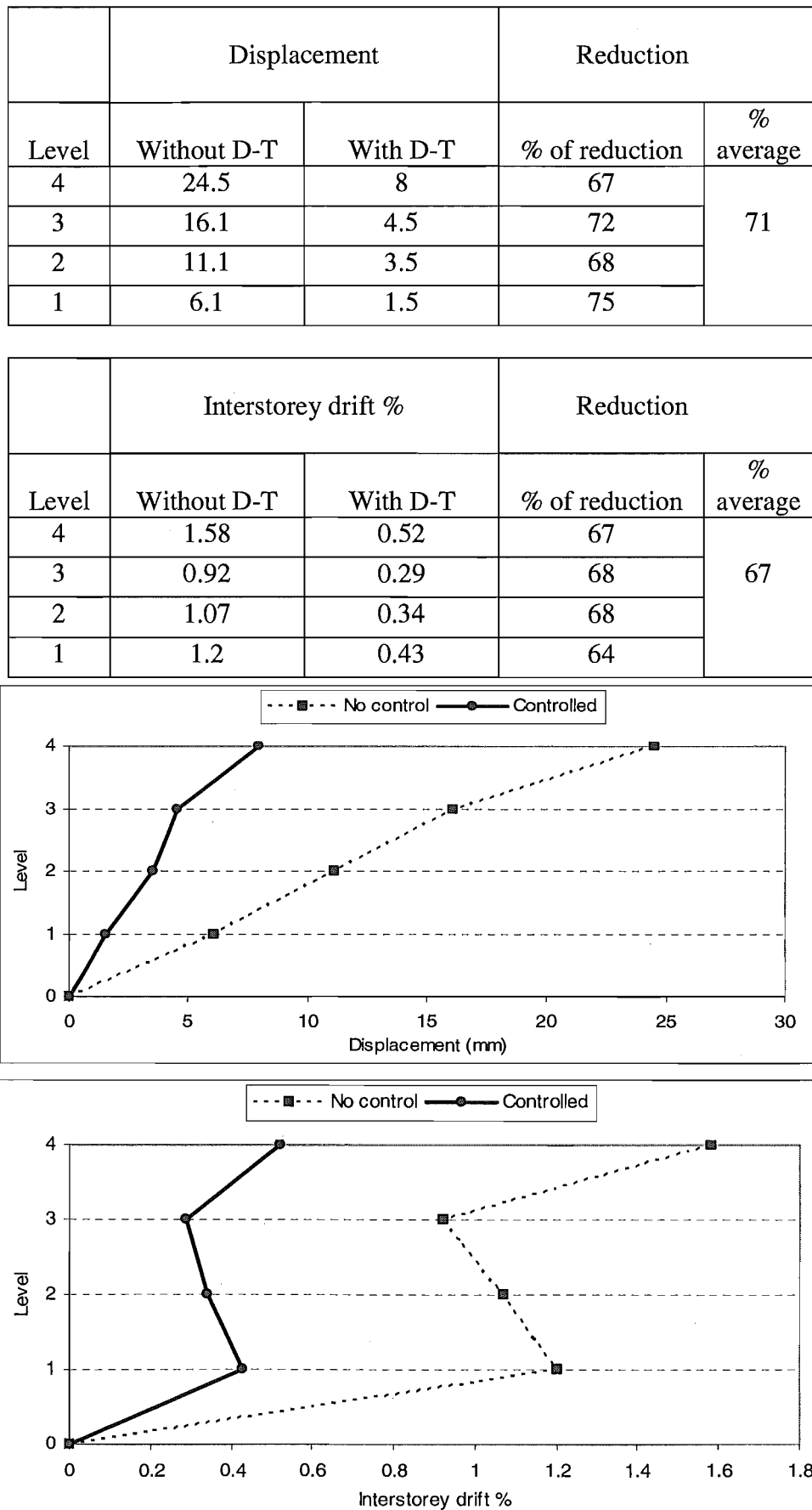


Fig (A-15) Displacement and intersorey drift ratios of the structure with and without the supplemental control system- **El Centro 80%** - shaking table acceleration

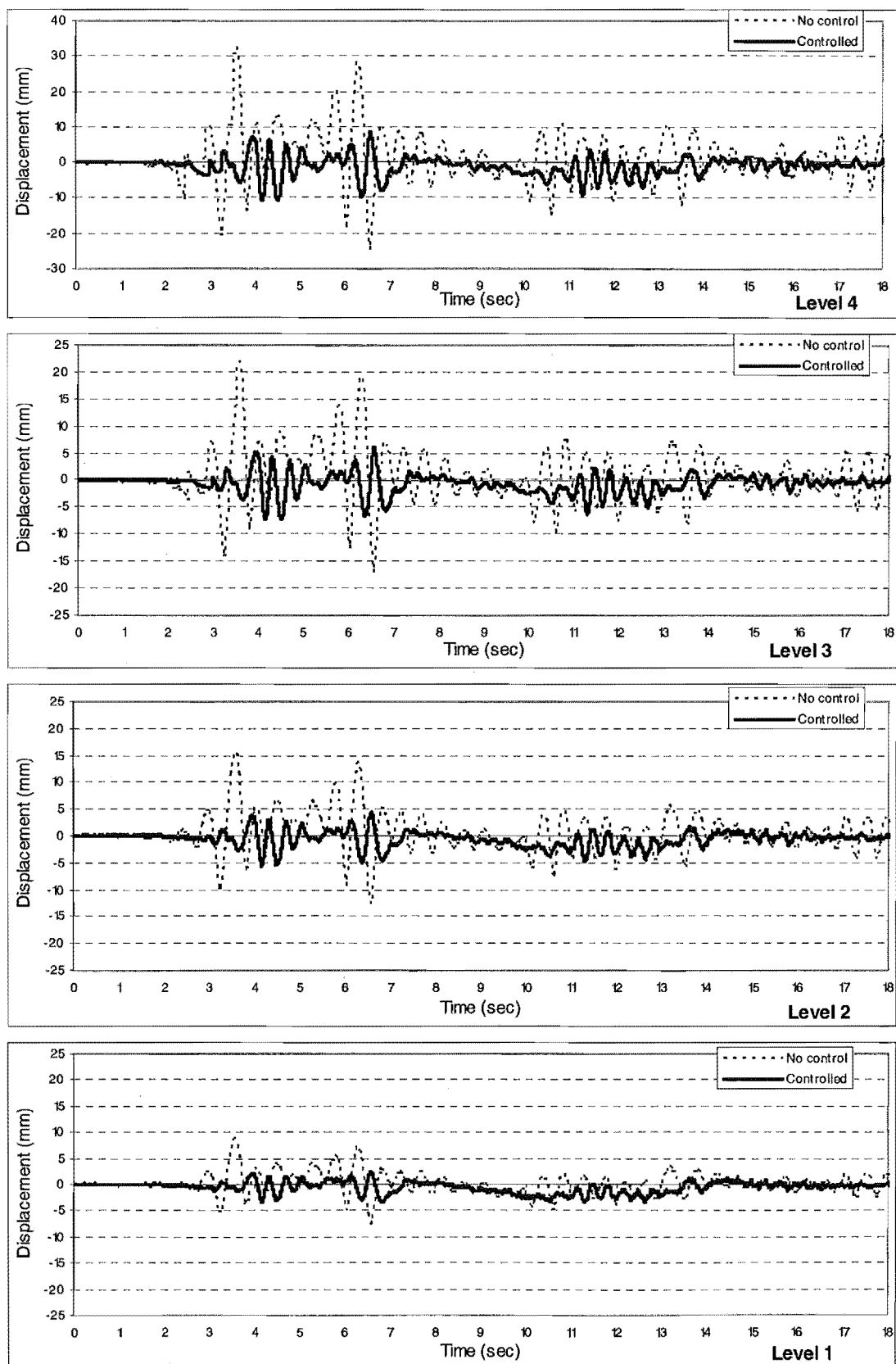


Fig (A-16) Displacement of the structure with and without the supplemental control system- El Centro 90%-shaking table acceleration

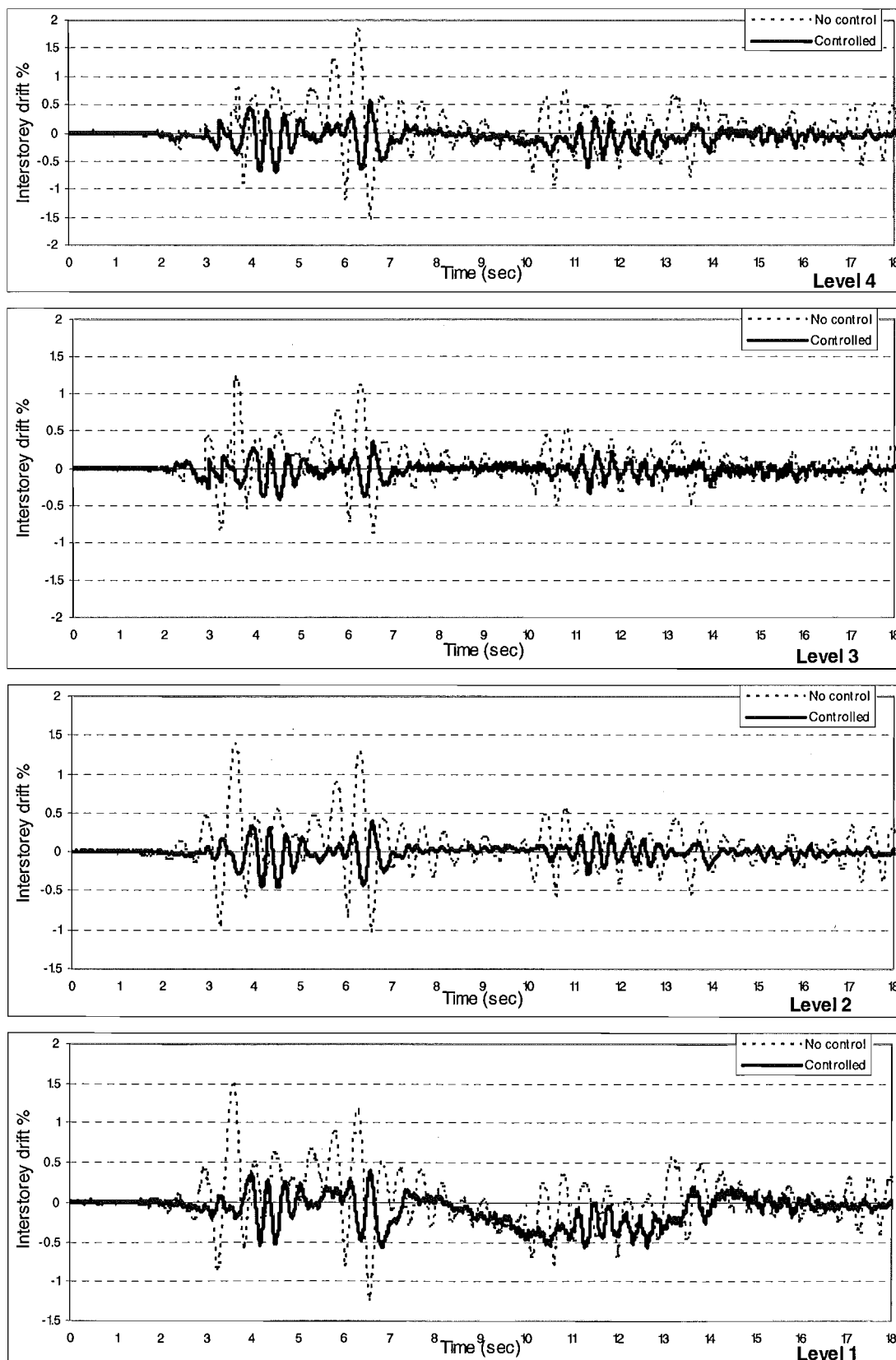


Fig (A-17) Intersorey drift of the structure with and without the supplemental control system –**El Centro 90%** - shaking table acceleration.

Level	Displacement		Reduction	
	Without D-T	With D-T	% of reduction	% average
4	30.8	10	68	62
3	20.8	6.3	70	
2	11.5	5	57	
1	6.6	3	55	

Level	Interstorey drift %		Reduction	
	Without D-T	With D-T	% of reduction	% average
4	1.74	0.61	65	67
3	1.15	0.37	68	
2	1.31	0.39	70	
1	1.38	0.51	63	

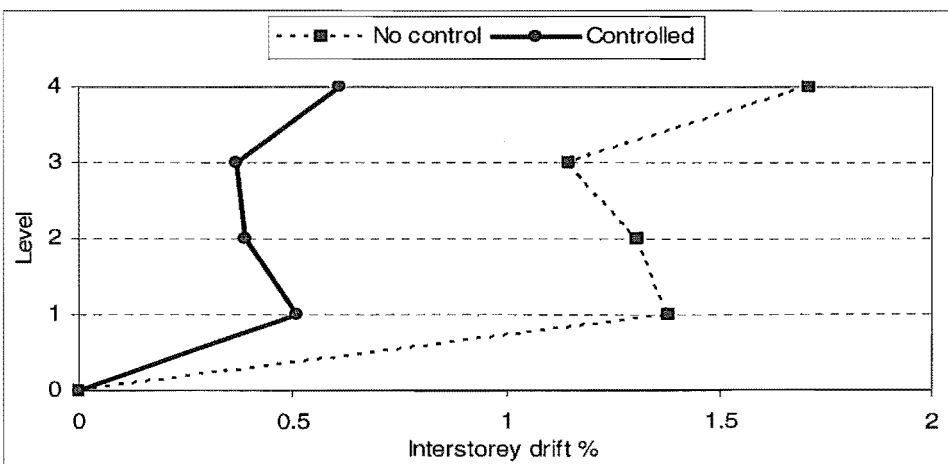
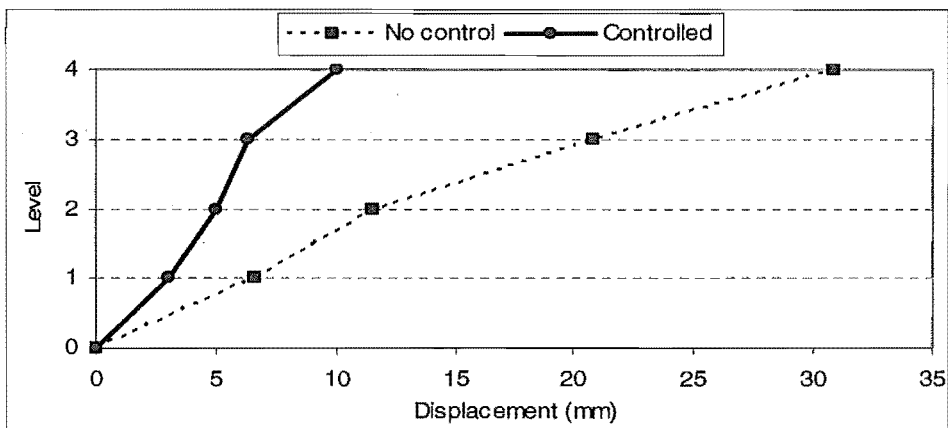


Fig (A-18) Displacement and intersorey drift ratios of the structure with and without the supplemental control system- El Centro 90% - shaking table acceleration

## Appendix B

### Shaking Table Results with Taft Excitation

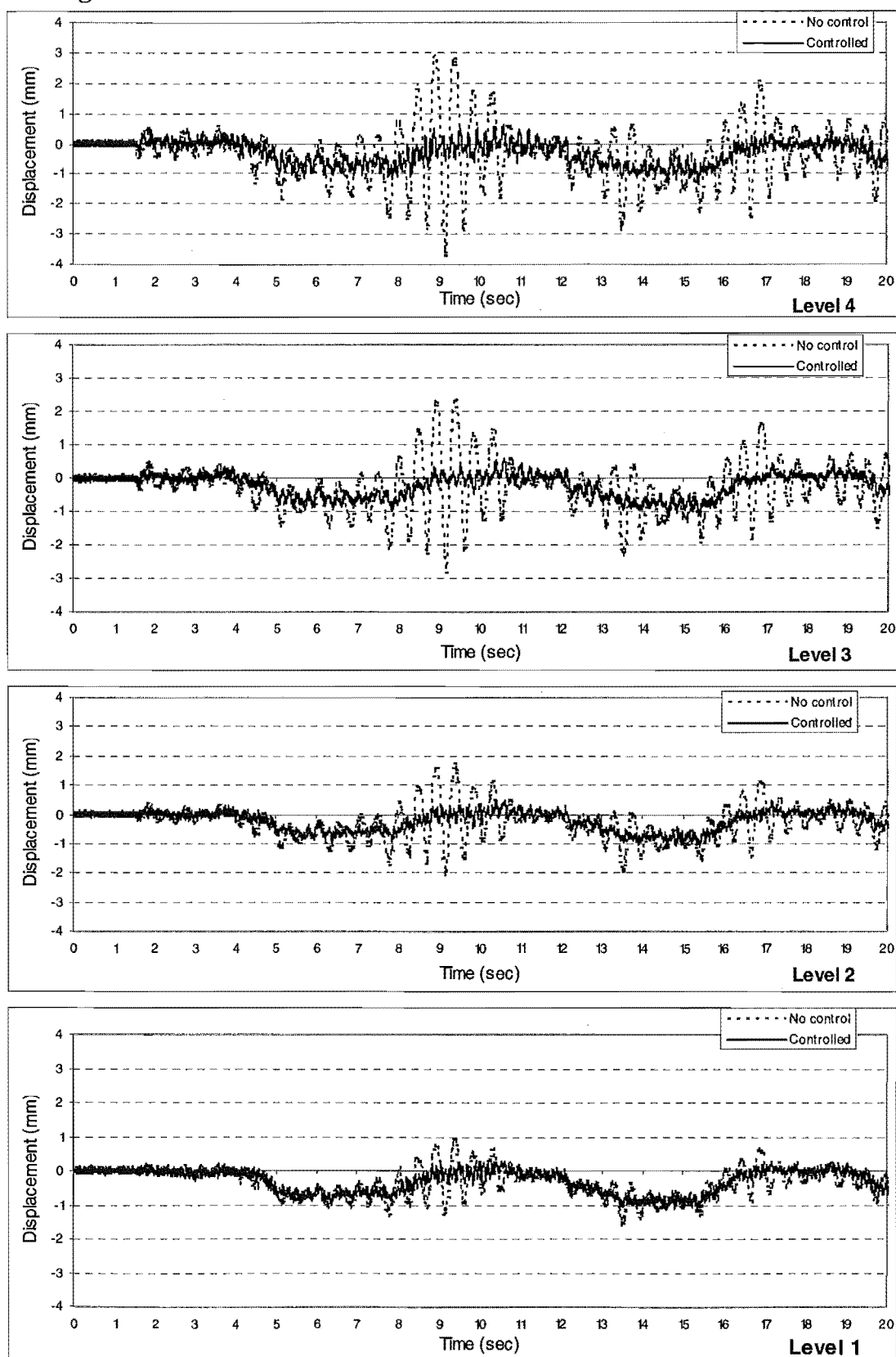


Fig (B-1) Displacement of the structure with and without the supplemental control system- 4203 TAFT 30%-shaking table acceleration

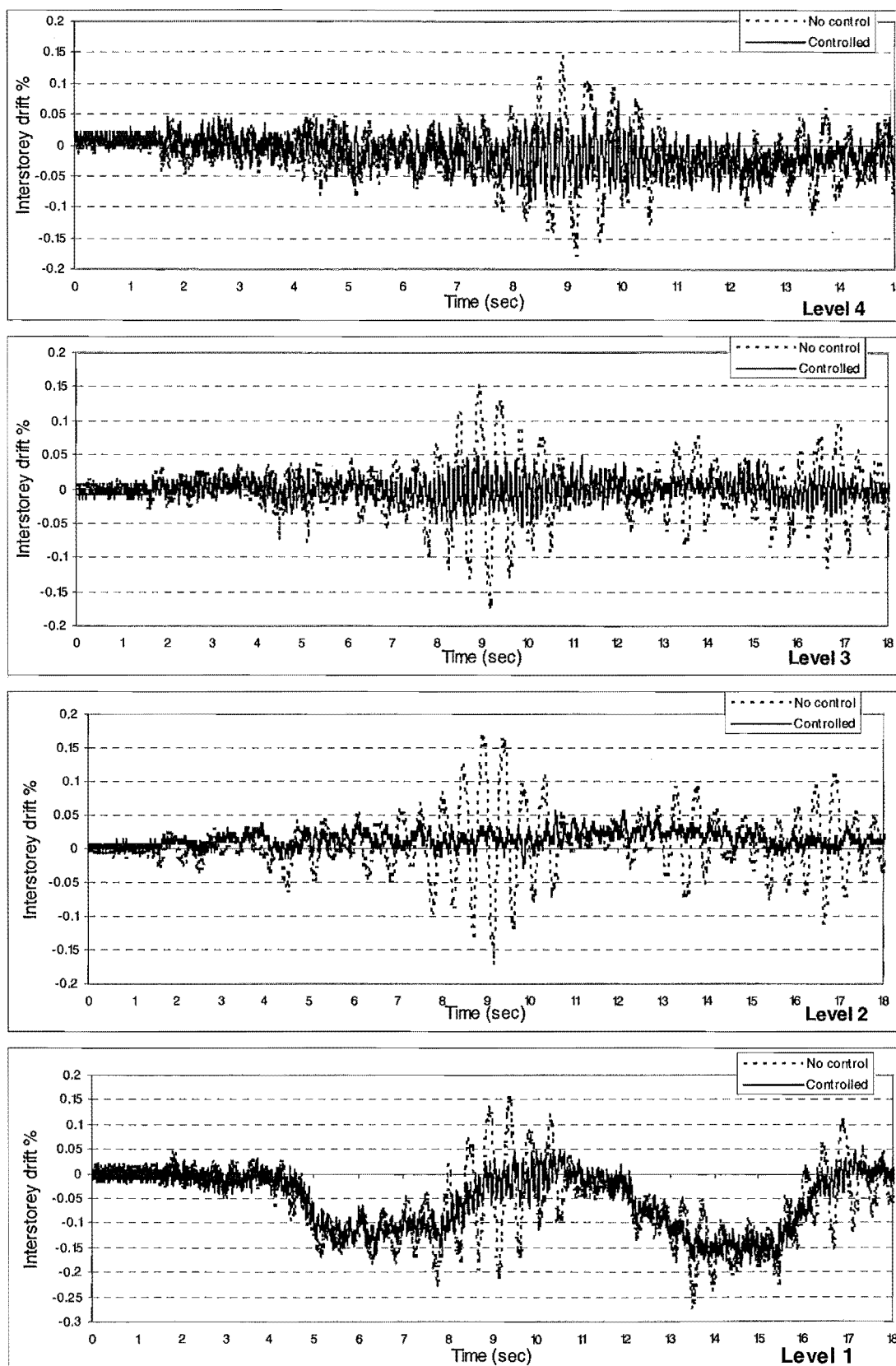


Fig (B-2) Intersorey drift of the structure with and without the supplemental control system –4203 TAFT 30% - shaking table acceleration.

Level	Displacement		Reduction	
	Without D-T	With D-T	% of reduction	% average
4	3.6	1	72	58
3	2.7	0.9	67	
2	2	0.9	55	
1	1.46	0.9	38	

Level	Interstorey drift %		Reduction	
	Without D-T	With D-T	% of reduction	% average
4	0.17	0.7	59	60
3	0.17	0.04	76	
2	0.17	0.05	71	
1	0.26	0.17	35	

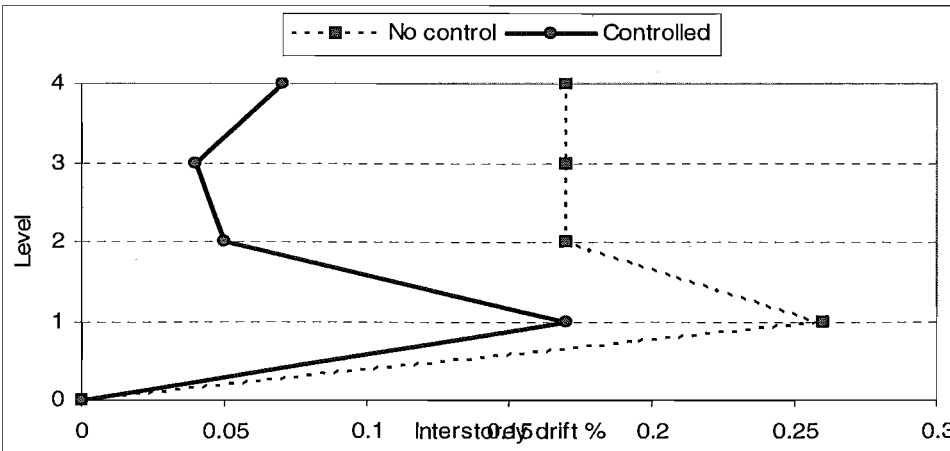
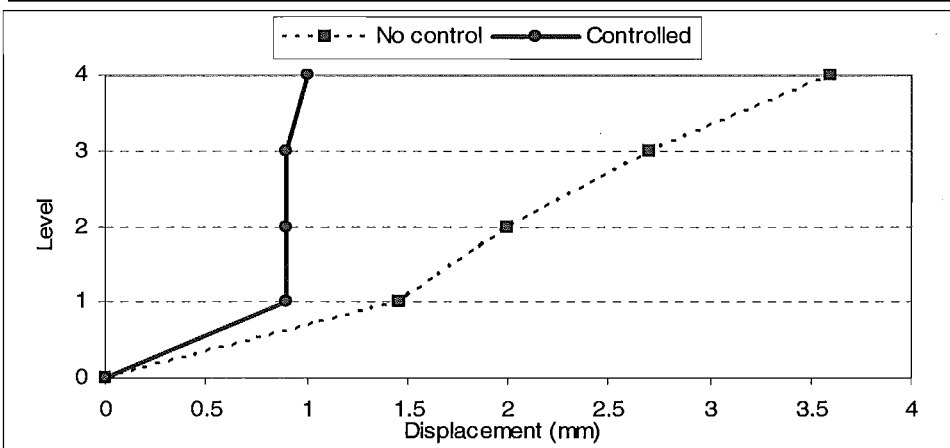


Fig (B-3) Displacement and intersorey drift ratios of the structure with and without the supplemental control system- 4203 TAFT 30% - shaking table acceleration.

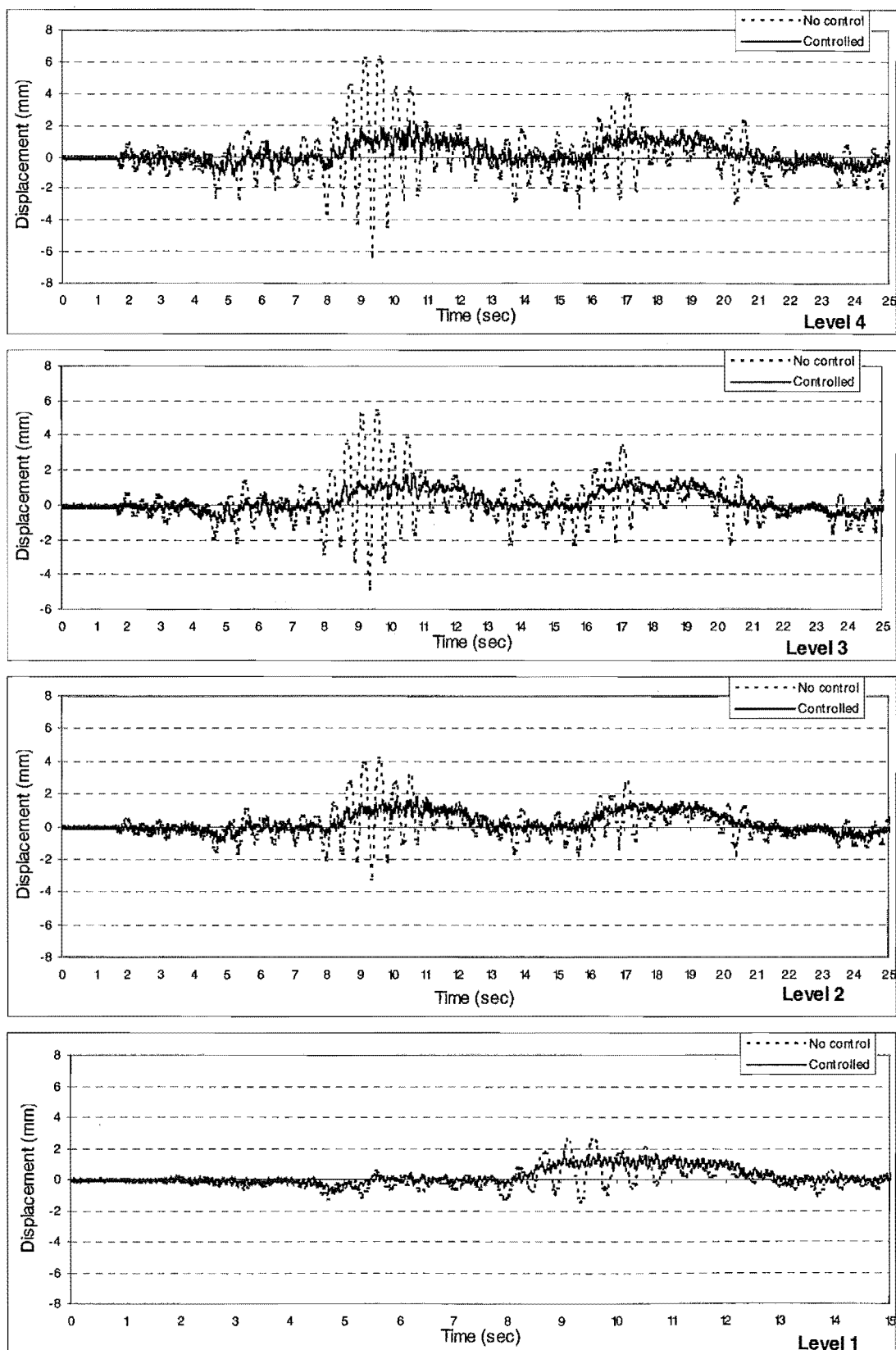


Fig (B-4) Displacement of the structure with and without the supplemental control system –4203 TAFT 60%– shaking table acceleration.

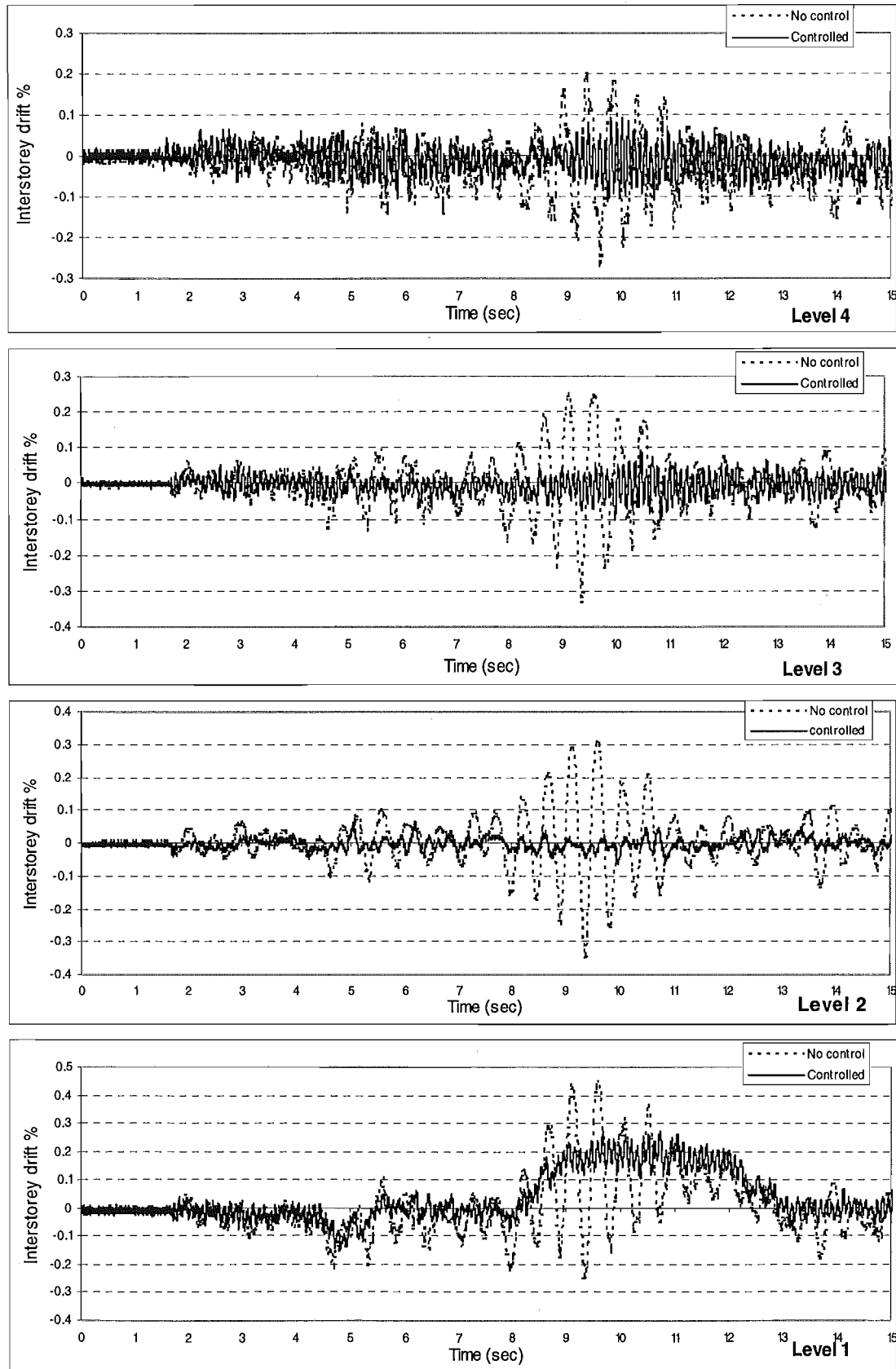


Fig (B-5) Intersorey drift of the structure with and without the supplemental control system -4203 TAFT 60% - shaking table acceleration.

Level	Displacement		Reduction	
	Without D-T	With D-T	% of reduction	% average
4	6.01	1.68	72	64
3	5.22	1.56	70	
2	4.11	1.63	60	
1	2.26	1.08	52	

Level	Interstorey drift %		Reduction	
	Without D-T	With D-T	% of reduction	% average
4	0.26	0.09	65	67
3	0.32	0.07	78	
2	0.34	0.06	82	
1	0.044	0.26	41	

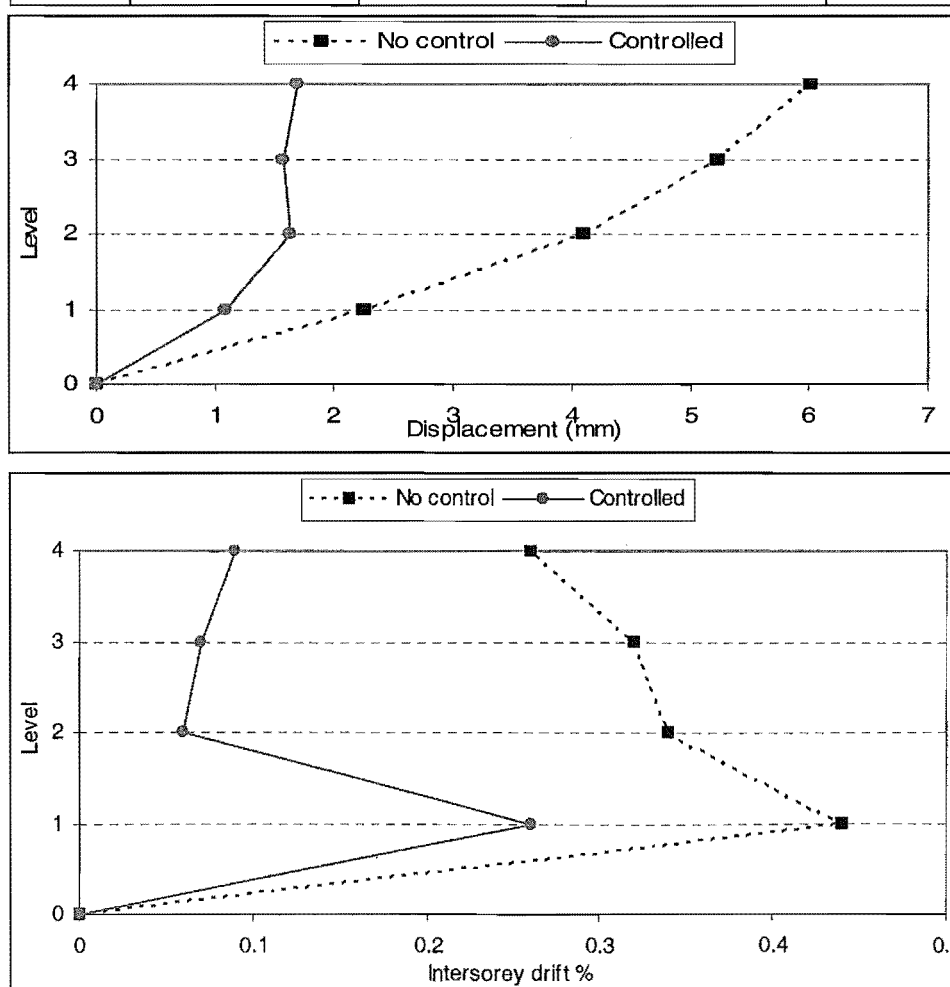


Fig (B-6) Displacement and intersorey drift ratios of the structure with and without the supplemental control system- 4203 TAFT 60% - shaking table acceleration.

## Appendix C

The four storey-two bay steel frame adopted in this research discussed in chapter 4, shown in Figure (C-1). The important information concerning this frame for time-history analysis is summarized as follows:

**Structure:** Four storey steel frame – inelastic time history.

**Analysis Details:**

Number of space dimensions	= 2
Number of equations per node	= 3
Number of nodes	= 121
Number of degrees of freedom	= 363
Number of members	= 51
Number of member types	= 16

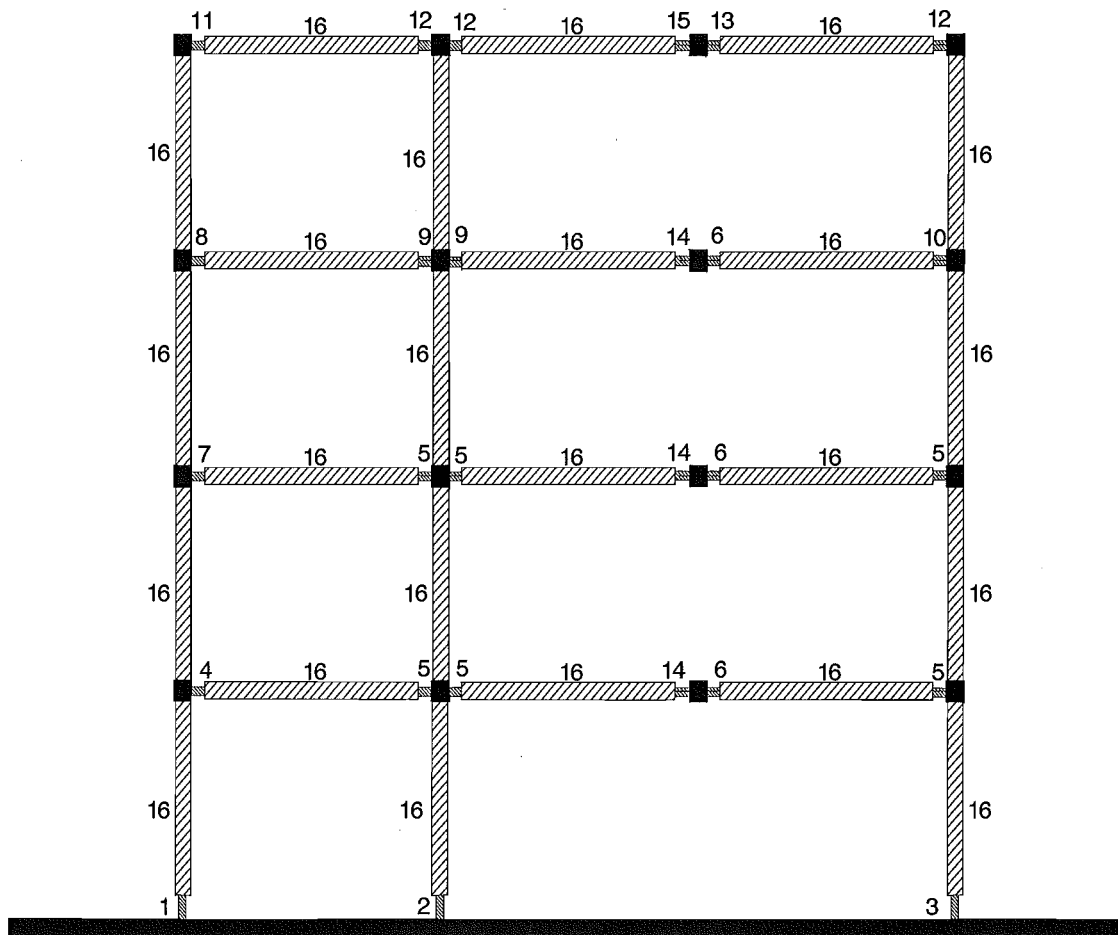


Fig (C-1) Member types.

### Member Properties

Member Number	Member Type	Spring Stiffness (N/m)	Rotational Stiffness (N/m)	Weight/ Unit Length (N)
1	spring	4.0E9	6.0E4	20.48
2	spring	3.5E9	5E4	17.25
3	spring	3.5E9	5E4	17.56
4	spring	5.6E9	2.28E4	26.95
5	spring	9.63E9	3.44E4	46.36
6	spring	1.03E10	3.62E4	49.36
7	spring	4.93E9	2.01E4	23.72
8	spring	3.36E9	1.51E4	16.17
9	spring	8.1E9	3.08E4	38.81
10	spring	8.96E9	3.29E4	43.12
11	spring	1.57E9	7.52E3	7.55
12	spring	7.39E9	2.9E4	35.58
13	spring	1.12E10	3.77E4	53.91
14	spring	1.03E10	3.63E4	49.59
15	spring	1.12E10	3.77E4	53.91

Member Number	Member Type	Cross sectional area ( $m^2$ )	Elastic Modulus (N/ $m^2$ )	Moment of Inertia ( $m^4$ )	Shear Modulus (N/ $m^2$ )	Weight /unit length (N)
16	frame	6.81E-4	2E11	2.29E-7	8.0E10	5.24E1

### Loads

Level	Lumped weight (N)	Static Load (N)
1	3150	4016
2	3150	4016
3	3150	4016
4	3150	4016

### Bending Moment

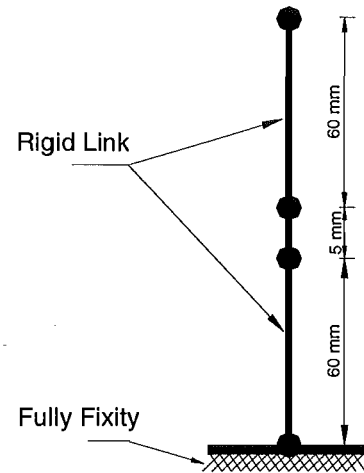
Member Number	Moment (N.m)	
	Positive	Negative
1	1E2	-1E2
2	8E1	-8E1
3	8E1	-8E1
4	1.72E2	-1.72E2
5	2.97E2	-2.97E2
6	3.17E2	-3.17E2
7	1.52E2	-1.52E2
8	1.036E2	-1.036E2
9	2.487E2	-2.487E2
10	2.764E2	-2.764E2
11	4.84E1	-4.84E1
12	2.28E2	-2.28E2
13	3.455E2	-3.455E2

Note: 1E2 means  $1.0 \times 10^2$

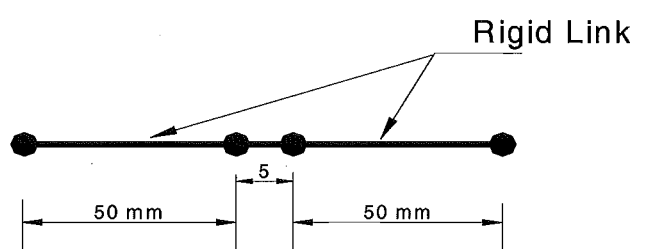
### Steel Hysteresis

Member Number	Dodd-Restrepo Steel Hysteresis [38]			
	Deformation at initiation strain hardening	Deformation at peak load	Force at peak load	Bauschinger effect factor
1	9E-3	3.1E-1	2.0E2	1
2	6E-3	3E-1	1.6E2	1
3	6E-3	3E-1	1.6E2	1
4	8.76E3	3E-1	2.556E2	1
5	1E-2	3E-1	4.39E2	1
6	1.03E-2	3E-1	4.7E2	1
7	8.55E-3	3E-1	2.25E2	1
8	8.15E-3	3E-1	1.53E2	1
9	9.47E-3	3E-1	3.68E2	1
10	9.47E-3	3E-1	4.09E2	1
11	7.7E-3	3E-1	7.16E1	1
12	9.22E-3	3E-1	3.37E2	1
13	1.06E-2	3E-1	5.11E2	1

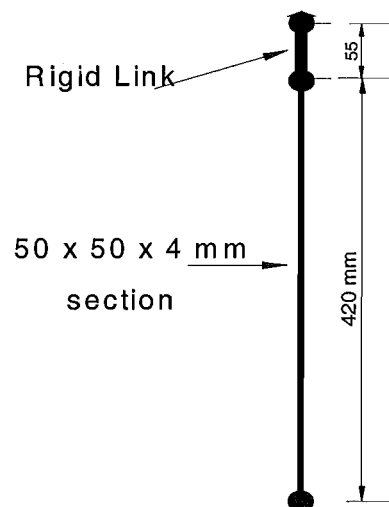
Member properties between inner nodes  
 Elements 1 to 10  
 Ruaumoko spring member



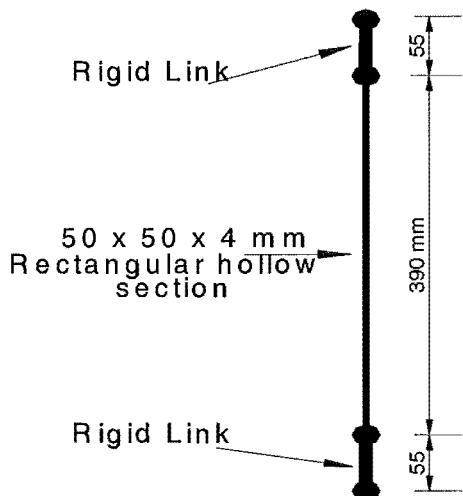
Member properties between inner nodes  
 Elements 1 to 10  
 Ruaumoko spring member



Elements 28 to 30  
 Ruaumoko frame member



Elements 31 to 39  
Ruaumoko frame member



Elements 40 to 51  
Ruaumoko frame member

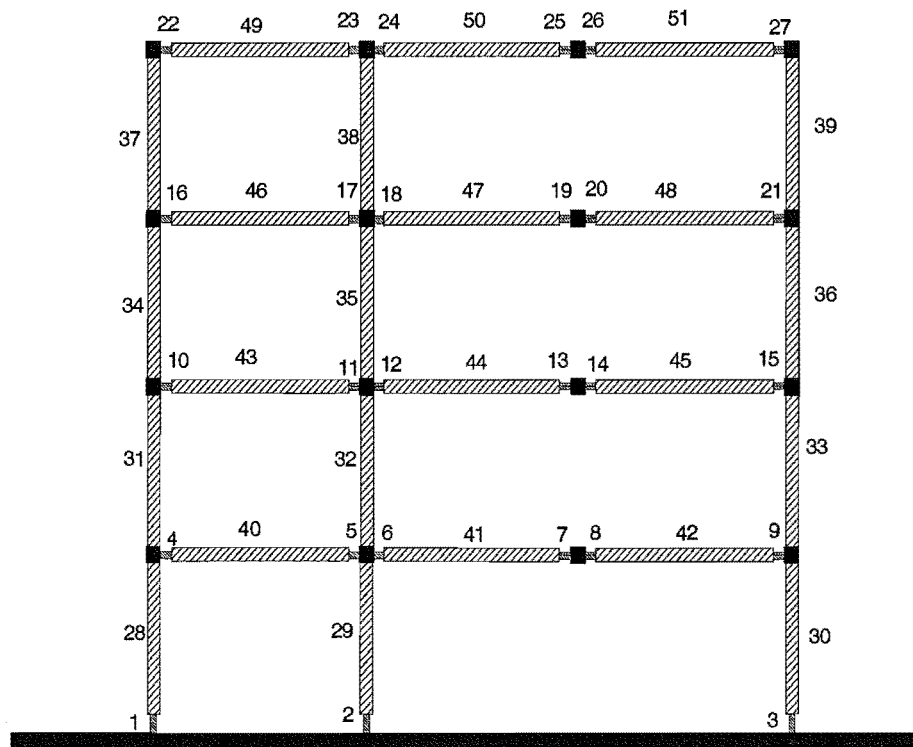
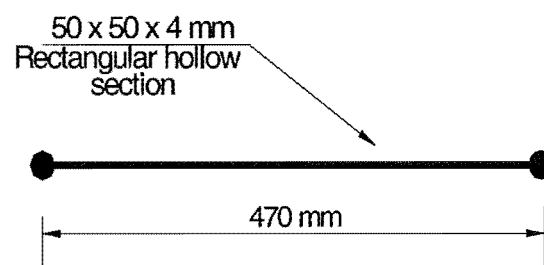


Fig (C-2) Element numbering

## Appendix D

**The twelve-storey, two bay reinforced concrete frame (Modified Jury 1995) [20].**

Data:

Elastic modulus  $E = 25 \times 10^7$  kPa

Shear modulus  $G = 1.04 \times 10^7$  kPa

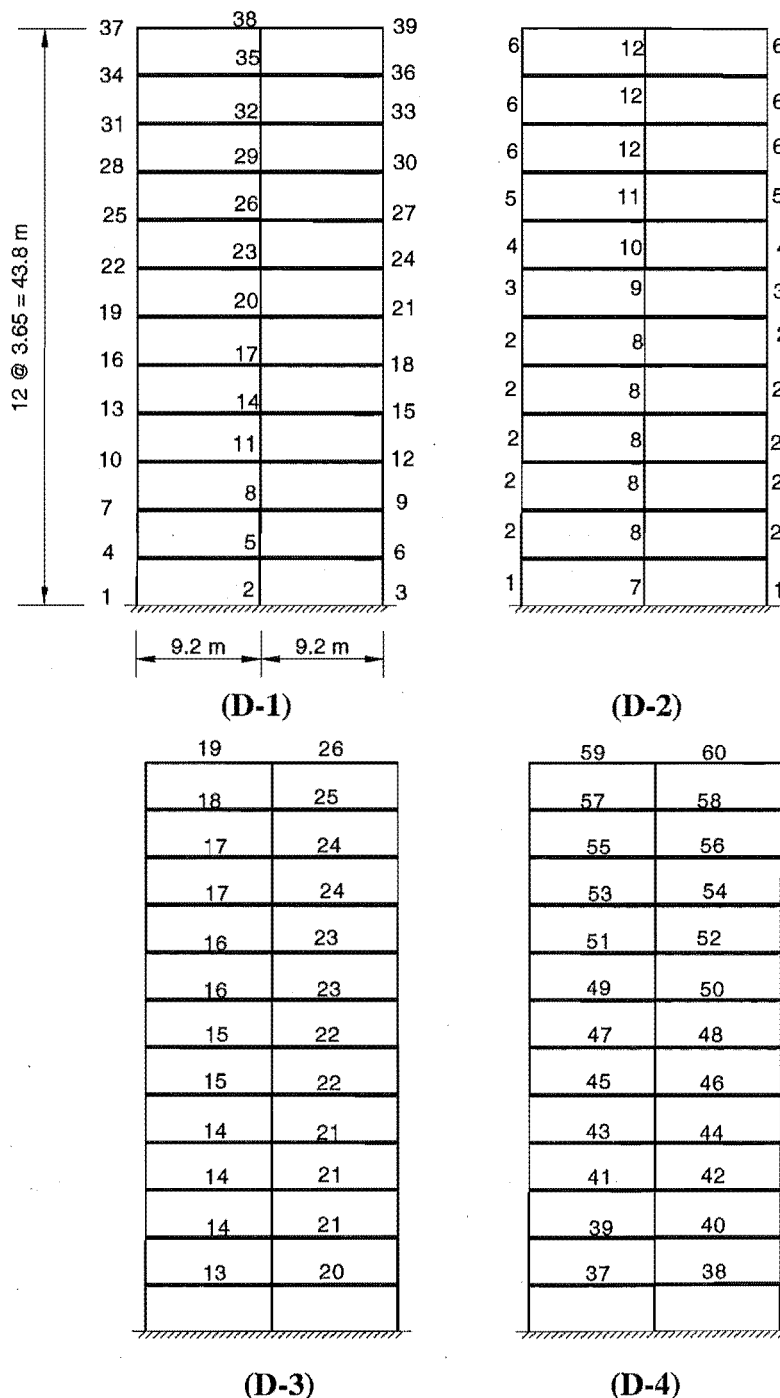


Fig (D-1) Node numbers, Fig (D-2) Column Types, Fig (D-3) Beam Types, Fig (D-4) Beams Numbers.

The weight at each level:

Level	Weight (kN)
1	1625
2	1625
3	1625
4	1625
5	1625
6	1625
7	1597
8	1597
9	1571
10	1571
11	1571
12	1535

### Column Types

	Type	Cross section area ( $m^2$ )	Shear area( $m^2$ )	Moment of inertia( $m^4$ )	End block length(m)	
					Bottom	Top
Exterior columns	1	0.1938	0.1938	0.01455	0	0.45
	2	0.1938	0.1938	0.01455	0.45	0.45
	3	0.175	0.175	0.01079	0.45	0.425
	4	0.175	0.175	0.01079	0.45	0.425
	5	0.1625	0.1625	0.00858	0.425	0.425
	6	0.1625	0.1625	0.00858	0.4	0.4
Interior columns	7	0.32	0.32	0.00265	0	0.45
	8	0.32	0.32	0.0256	0.45	0.45
	9	0.2629	0.2629	0.01727	0.45	0.45
	10	0.2629	0.2629	0.01727	0.425	0.425
	11	0.2278	0.2278	0.01298	0.425	0.4
	12	0.2278	0.2278	0.01298	0.4	0.4

### Beam Types

Beams	Type	Cross section area(m)	Shear area(m)	Moment of inertia(m)	End block length(m)	
					Bottom	Top
	13	0.18	0.18	0.02952	0.388	0.4
	14	0.18	0.18	0.02952	0.388	0.4
	15	0.18	0.18	0.02952	0.388	0.4
	16	0.17	0.17	0.02503	0.35	0.363
	17	0.16	0.16	0.02086	0.35	0.338
	18	0.16	0.16	0.02086	0.325	0.338
	19	0.16	0.16	0.02086	0.325	0.388
	20	0.18	0.18	0.02952	0.4	0.388
	21	0.18	0.18	0.02952	0.4	0.388
	22	0.18	0.18	0.02952	0.4	0.388
	23	0.17	0.17	0.02503	0.363	0.35
	24	0.16	0.16	0.02086	0.338	0.35
	25	0.16	0.16	0.02086	0.338	0.325
	26	0.16	0.16	0.02086	0.338	0.325

### Initial Fixed End Moments and Shears of Beams

Type	M1 (kNm)	M2 (kNm)	V1 (kN)	V2 (KN)
13	-180.1	-179.8	-135.8	135.8
14	-180.1	-179.8	-135.8	135.8
15	-180.1	-179.8	-135.8	135.8
16	-183.7	-182	-133.4	133.4
17	-184.2	-182.6	-131.1	131.1
18	-184.2	-182.6	-131.1	131.1
19	-184.2	-182.6	-131.1	131.1
20	-179.8	-180.1	-135.8	135.8
21	-179.8	-180.1	-135.8	135.8
22	-179.8	-180.1	-135.8	135.8
23	-182	-183.7	-133.4	133.4
24	-182.6	-184.2	-131.1	131.1
25	-182.6	-184.2	-131.1	131.1
26	-182.6	-184.2	-131.1	131.1

### Beam Yield Moments

M1(+) M1(-) M2(+) M2(-)

Type	M1 (kNm)	M2 (kNm)	V1 (kN)	V2 (KN)
13	893	-976	893	-976
14	1047	-1142	1047	-1142
15	887	-988	887	-988
16	762	-833	714	-714
17	559	-631	464	-547
18	307	-369	307	-381
19	307	-307	307	-307
20	893	-976	893	-976
21	1047	-1142	1047	-1142
22	887	-988	887	-988
23	714	-714	833	-762
24	547	-464	631	-559
25	381	-307	369	-307
26	307	-307	307	-307